THE UNIVERSITY OF TULSA

THE GRADUATE SCHOOL

EFFECTIVE PROPERTIES OF RESERVOIR SIMULATOR GRID BLOCKS

by

Yngve Aasum

A dissertation submitted in partial fulfillment of

the requirements for the degree of Doctor of Philosophy

in the Discipline of Petroleum Engineering

The Graduate School

The University of Tulsa

1992

THE UNIVERSITY OF TULSA
THE GRADUATE SCHOOL

EFFECTIVE PROPERTIES OF RESERVOIR SIMULATOR GRID BLOCKS

A DISSERTATION
APPROVED FOR THE DISCIPLINE OF
PETROLEUM ENGINEERING

By Dissertation Committee

Balmohan A Kelkar, Chairperson
Elwyn Harvey, Chairperson
G. Shiv
James C. Young
O. Nitham

ABSTRACT

Yngve Aasum (Doctor of Philosophy in Petroleum Engineering)
Effective Properties of Reservoir Simulator Grid Blocks
(214 pp. – Chapter VI)
Directed by Dr. Balmohan G. Kelkar and Dr. Ekrem Kasap

(203 WORDS)

Computational costs limit large scale reservoir simulations to coarse grid systems. Determination of an effective permeability for a simulation grid block requires a proper scale-up of small scale permeability heterogeneities within that grid block. Conventional scale-up techniques are limited to a diagonal tensor representation of effective permeability. Therefore, such techniques cannot handle general permeability anisotropy (full tensor) exemplified by cross-bedded permeability structures that may be present on a smaller scale.

An analytical method is developed to calculate an effective permeability tensor for a grid block by accounting for small scale heterogeneities within the grid block. The method honors both the location and the orientation of the small scale heterogeneities.

Most commercially available reservoir simulators are not equipped to handle general permeability anisotropy. This work shows in detail how transmissibility coefficients for cases of general permeability anisotropy are developed. These transmissibilities can be readily inserted into point-centered finite difference simulators which accommodate 9-point differencing.

Effective permeability tensors calculated using the analytical method and a numerical method show excellent agreement. Fluid flow simulations, both miscible displacements and waterfloods, show that the effective permeability tensor method

outperforms conventional scale-up techniques when compared to the use of fine scale permeability distribution in cases of general permeability anisotropy.

ACKNOWLEDGEMENTS

I would like to thank my advisor Dr. Balmohan G. Kelkar for his continuous support of me and this work. Special thanks are given to my co-advisor, Dr. Ekrem Kasap, whose contributions "put wind back into the sails" at a critical stage in this project. I am grateful to Dr. Larry C. Young, Reservoir Simulation Research Corporation, for providing access to his simulator, for personal consultation in its use, and for serving on my dissertation committee. My appreciation is also directed to Dr. Gautam S. Shiralkar, Amoco Production Company, for enlightening discussion and for serving on my committee. I wish to thank committee member Dr. Ovadia Shoham for his encouragement and enthusiasm. Also, I would like to thank my professors and fellow graduate students for their help and support.

I wish to thank TUPREP (The University of Tulsa Petroleum Reservoir Exploitation Projects), the Department of Energy, Conoco Inc., and SPE for providing financial support.

Finally, I would like to thank my family Målfrid, Anker, Kirsti, and Dag Rune. Their support has been and will always be important to me.

TABLE OF CONTENTS

Page

TITLE PAGE i

APPROVAL PAGE ii

ABSTRACT iii

ACKNOWLEDGEMENTS v

TABLE OF CONTENTS vi

LIST OF TABLES viii

LIST OF FIGURES viii

CHAPTER I INTRODUCTION 1

CHAPTER II LITERATURE REVIEW 3

Numerical (Simulation) Approach 3

Monte-Carlo Methods 3

Tensor Methods 6

Analytical Approach 8

Streamtube Methods 8

Perturbation Methods 9

Percolation Methods 10

Effective Medium Theory (EMT) 10

Renormalization Techniques 11

Tensor Methods 12

Permeability Anisotropy 13

CHAPTER III DEVELOPMENT OF EFFECTIVE PERMEABILITY TENSOR 15

Analytical Method 15

1. Determine the permeabilities along the principal directions. 17

2. Perform coordinate rotation to obtain the effective permeability tensor. 20

TABLE OF CONTENTS (Continued)

Page

Rationale for dividing the permeability field into four blocks. 22

3. Determine effective permeability tensor for the entire grid block. . . . 24

Numerical Method 38

CHAPTER IV INCORPORATION OF FULL TENSOR PERMEABILITY IN A NUMERICAL RESERVOIR SIMULATOR 41

Method 1 - Based on Finite Element Theory 41

Method 2 - Based on Manipulation of Darcy's Law 60

Relating Methods 1 and 2 67

CHAPTER V RESULTS AND DISCUSSION 70

Comparisons Between Analytical and Numerical Effective Permeabilities . 70

Comparisons Between Results From Fluid Flow Simulations 81

Miscible Displacements 81

Waterfloods 85

CHAPTER VI SUMMARY AND CONCLUSIONS 113

Recommendations for Future Work 115

NOMENCLATURE 116

REFERENCES 120

APPENDIX A – CALCULATION OF PERMEABILITIES ALONG PRINCIPAL DIRECTIONS 127

APPENDIX B – DEVELOPMENT OF PERMEABILITY TENSOR FROM COORDINATE ROTATION 131

APPENDIX C – DEVELOPMENT OF APPARENT PERMEABILITIES 137

APPENDIX D – DEVELOPMENT OF ISOTROPIC "GLOBAL" PRESSURE GRADIENT RATIOS 162

APPENDIX E – DEVELOPMENT OF AVERAGE "GLOBAL" TRANSVERSE PRESSURE DROP 173

TABLE OF CONTENTS (Continued)

Page

APPENDIX F – DEVELOPMENT OF "LOCAL" PRESSURE GRADIENT RATIOS 175

List of Tables

Table — Page

5.1 Flow Rates 87

5.2 Simulation Input Parameters 89

List of Figures

Figure — Page

3.1 **Top:** Cross-Bedded Permeability Distribution (-45° Structure Orientation, Dark Grid Blocks: 20 md, Light Grid Blocks: 1000 md). **Bottom:** Pressure Map Indicating Non-Zero Transverse Pressure Gradient. Boundary Conditions: Closed Horizontal Boundaries; Left Face: Injection; Right Face: Production. 16

3.2 **Top:** Permeability Field with Low Permeability Section (Dark Grid Blocks: 1 md, Light Grid Blocks: 1000 md). **Bottom:** Pressure Map Indicating Non-Zero Transverse Pressure Gradient. Boundary Conditions: Closed Horizontal Boundaries; Left Face: Injection; Right Face: Production. 18

3.3 Field of Small Scale Heterogeneities Divided into Four Quadrants. . . 19

3.4 Directions and Data Points to Consider in Calculating Maximum and Minimum Permeabilities Along 45° and -45° From the Horizontal Axis. 21

3.5 System Containing Four Blocks and Four Permeability Tensors. . . . 23

3.6 Schematic for No Cross-Flow Case; $\hat{k}_{x_{app_{tb}}}$ (Injection Along x-axis). . 26

LIST OF FIGURES (Continued)

		Page
3.7	Schematic for Cross-Flow Case; $\hat{k}_{x_{eff_x}}$ (Injection Along x-axis).	27
3.8	Schematic for Cross-Flow Case; $\hat{k}_{y_{eff_y}}$ (Injection Along y-axis).	29
3.9	Schematic for No Cross-Flow Case; $\hat{k}_{y_{eff_x}}$ (Injection Along y-axis).	30
3.10	Permeability Contrast Yielding a "Global" Non-Zero Transverse Pressure Gradient.	34
3.11	Non-Zero Off-Diagonal Elements in Permeability Tensor of Local Grid Block Yielding "Local" Transverse Pressure Gradient.	35
4.1	Linear Trial Functions in (a) x-direction and (b) y-direction.	43
4.2	Quadrilateral Element With Labeled Transmissibilities.	49
4.3	Element Mesh Superimposed on Point-Centered Grid.[45]	50
4.4	Applied Pressure Drop Along x-axis.	61
4.5	Applied Pressure Drop Along y-axis.	63
5.1	Effective Permeability Tensors Calculated by Analytical and Numerical Methods for Isotropic Local Permeabilities (Units: md).	72
5.2	Effective Permeability Tensors Calculated by Analytical and Numerical Methods for Anisotropic Local Permeabilities (Units: md).	73
5.3	Effective Permeability Tensors Calculated by Analytical and Numerical Methods for Equal Diagonal Elements, but Non-Zero Off-Diagonal Elements in Each Local Permeability Tensor (Units: md).	74
5.4	Effective Permeability Tensors Calculated by Analytical and Numerical Methods for Anisotropic and Full Local Permeability Tensors (Units: md).	76
5.5	Effective Permeability Tensors Calculated by Analytical and Numerical Methods for Cross-Bedded Permeability Distribution (Units: md).	77
5.6	Effective Permeability Tensors Calculated by Analytical and Numerical Methods for Cross-Bedded Stochastic Permeability Distribution (Units: md).	79

LIST OF FIGURES (Continued)

Page

5.7 Effective Permeability Tensors Calculated by Analytical and Numerical Methods for Minipermeameter Measured Permeability Data From the Algerita Outcrop (Units: md). 80

5.8 Initial Permeability Distribution (Dark: 20 md; Light: 1000 md) and 0.5 Concentration Contours After 49.7 Days of Injection Using the Initial Permeability Distribution and the Permeability Distributions Obtained Using Various Upscaling Methods. 82

5.9 Initial Permeability Distribution ($V = 0.7$) and 0.5 Concentration Contours After 94.8 Days of Injection Using the Initial Permeability Distribution and the Permeability Distributions Obtained Using Various Upscaling Methods. 84

5.10 Initial Permeability Distribution ($V = 0.86$) and 0.5 Concentration Contours After 113 Days of Injection Using the Initial Permeability Distribution and the Permeability Distributions Obtained Using Various Upscaling Methods. 86

5.11 Relative Permeability Curves.[9] 90

5.12 Cross-Bedded Permeability Distribution. 91

5.13 Pressure Maps After 0.5 Days of Water Injection Using
(a) the Initial Cross-Bedded Permeability Distribution
(b) the Effective Permeability Tensor and
(c) the Real-Space Renormalized Permeability (Units: psi). 92

5.14 Water Saturation Maps After 0.5 Days of Water Injection Using
(a) the Initial Cross-Bedded Permeability Distribution
(b) the Effective Permeability Tensor and
(c) the Real-Space Renormalized Permeability. 94

LIST OF FIGURES (Continued)

Page

5.15 Water Saturation Maps After 1.0 Days of Water Injection Using
(a) the Initial Cross-Bedded Permeability Distribution
(b) the Effective Permeability Tensor and
(c) the Real-Space Renormalized Permeability. 95

5.16 Water Saturation Maps After 1.5 Days of Water Injection Using
(a) the Initial Cross-Bedded Permeability Distribution
(b) the Effective Permeability Tensor and
(c) the Real-Space Renormalized Permeability. 96

5.17 Cumulative Oil Recovery Versus Time for Rectilinear Waterflood.
Cross-Bedded Initial Permeability Distribution.
Effect of Permeability Upscaling. 98

5.18 Isotropic Stochastic Permeability Distribution.
($\lambda_D = 0.5,\ V = 0.7,$ 40 x 40 Values). 99

5.19 Cumulative Oil Recovery Versus Time for Waterflood in a 1/4 of a 5-Spot.
Isotropic Initial Permeability Distribution.
Effect of Permeability Upscaling. 100

5.20 Anisotropic (Cross-Bedded) Stochastic Permeability Distribution.
($\lambda_{D_\ell} = 1.0,\ \lambda_{D_t} = 0.025,\ V = 0.7,$ 45° Structure Orientation,
64 x 64 Values). 102

5.21 Water Saturation Maps After 20 Days of Water Injection Using
(a) the Initial Permeability Distribution
(b) the Effective Permeability Tensor and
(c) the Geometrically Averaged Permeability. 103

5.22 Cumulative Oil Recovery Versus Pore Volumes Injected for Waterflood in
a 1/4 of a 5-Spot. Anisotropic (Cross-Bedded) Initial Permeability
Distribution. Effect of Permeability Upscaling. 104

LIST OF FIGURES (Continued)

		Page
5.23	Anisotropic (Cross-Bedded) Stochastic Permeability Distribution. ($\lambda_{D_\ell} = 1.0$, $\lambda_{D_t} = 0.016$, $V = 0.7$, 45° Structure Orientation, 63 x 63 Values).	106
5.24	Water Saturation Maps After 8 Days of Water Injection Using (a) the Initial Permeability Distribution (b) the Effective Permeability Tensor and (c) the Geometrically Averaged Permeability.	107
5.25	Cumulative Oil Recovery Versus Pore Volumes Injected for Producing Well P-1 in a 5-Spot Waterflood. Anisotropic (Cross-Bedded) Initial Permeability Distribution. Effect of Permeability Upscaling.	109
5.26	Fractional Flow of Water Versus Pore Volumes Injected for Producing Well P-1 in a 5-Spot Waterflood. Anisotropic (Cross-Bedded) Initial Permeability Distribution. Effect of Permeability Upscaling.	110
5.27	Cumulative Oil Recovery Versus Pore Volumes Injected for Producing Well P-2 in a 5-Spot Waterflood. Anisotropic (Cross-Bedded) Initial Permeability Distribution. Effect of Permeability Upscaling.	111
5.28	Fractional Flow of Water Versus Pore Volumes Injected for Producing Well P-2 in a 5-Spot Waterflood. Anisotropic (Cross-Bedded) Initial Permeability Distribution. Effect of Permeability Upscaling.	112
A-1	Direction Vectors Along the x'-axis.	127
A-2	Direction Vectors Along the y'-axis.	128
B-1	Velocity Vector, $\overline{v}$, in the Simulation Coordinate System (x, y) and in the Coordinate System of the Principal Directions of Permeability (x', y').	131

LIST OF FIGURES (Continued)

		Page
B-2	Transverse to Longitudinal Pressure Gradient Ratio as a Function of Cross-Bedding Angle.	136
C-1	System Containing Four Blocks and Four Permeability Tensors.	137
C-2	Top Layer of Figure C-1 (Injection Along x-axis).	138
C-3	Bottom Layer of Figure C-1 (Injection Along x-axis).	141
C-4	First Column of Figure C-1 (Injection Along x-axis).	144
C-5	Second Column of Figure C-1 (Injection Along x-axis).	146
C-6	Top Layer of Figure C-1 (Injection Along y-axis).	149
C-7	Bottom Layer of Figure C-1 (Injection Along y-axis).	151
C-8	First Column of Figure C-1 (Injection Along y-axis).	154
C-9	Second Column of Figure C-1 (Injection Along y-axis).	157
C-10	Apparent Permeabilities Related to Degree of Cross-Flow. (a) $\hat{k}_{x_{app_{tb}}}$ (No Cross-Flow); (b) $\hat{k}_{x_{app_{fs}}}$ (Cross-Flow); (c) $\hat{k}_{y_{app_{tb}}}$ (Cross-Flow); (d) $\hat{k}_{y_{app_{fs}}}$ (No Cross-Flow).	160
D-1	System Containing Four Blocks and Four Permeability Tensors.	162
D-2	Closed Upper, Middle and Lower Boundaries (Injection Along x-axis).	163
D-3	Closed Left, Middle and Right Boundaries (Injection Along y-axis).	168
E-1	Pressure Versus System Length.	173
F-1	System Cortaining Four Blocks and Four Permeability Tensors.	176
F-2	Top Layer of Figure F-1 (Injection Along x-axis).	177
F-3	Top Layer of Figure F-1 (Injection Along y-axis).	179
F-4	Bottom Layer of Figure F-1 (Injection Along x-axis).	182
F-5	Top and Bottom Layers of Figure F-1 (Injection Along x-axis).	183
F-6	First Column of Figure F-1 (Injection Along x-axis).	186
F-7	Second Column of Figure F-1 (Injection Along x-axis).	188
F-8	First and Second Columns of Figure F-1 (Injection Along x-axis).	189
F-9	First and Second Columns of Figure F-1 (Injection Along y-axis).	191
F-10	First Column of Figure F-1 (Injection Along y-axis).	195

LIST OF FIGURES (Continued)

		Page
F-11	First Column of Figure F-1 (Injection Along x-axis).	197
F-12	Second Column of Figure F-1 (Injection Along y-axis).	201
F-13	First and Second Columns of Figure F-1 (Injection Along y-axis). .	202
F-14	Top Layer of Figure F-1 (Injection Along y-axis).	204
F-15	Bottom Layer of Figure F-1 (Injection Along y-axis).	206
F-16	Top and Bottom Layers of Figure F-1 (Injection Along y-axis). . .	207
F-17	Top and Bottom Layers of Figure F-1 (Injection Along x-axis). . .	209

CHAPTER I
INTRODUCTION

Field development and reservoir management practices require large scale numerical simulations. Although more powerful computers and simulation techniques are continuously being developed, the size of the grid blocks used in field scale fluid flow simulations is too large to explicitly account for the effect of small scale heterogeneities. Such heterogeneities may be comprised of interwell laminations and cross-bedding structures as well as sand/shale sequences. For the large scale simulator grid blocks, the effect of small scale heterogeneities can only be accounted for by calculating an effective permeability. An *effective* permeability preserves the ratio of the fluid flux and the potential drop across a heterogeneous block and an equivalent homogeneous block.[1]

Several methods are presented in the literature for calculating effective permeability. These methods can, in general, be divided into numerical and analytical methods. Numerical methods are used to handle complex heterogeneous systems, whereas analytical methods usually are restricted by simplifying assumptions. Analytical methods, however, tend to be less expensive than numerical methods in terms of computational cost.

In this study, an analytical effective permeability method is developed. This method combines the advantages of numerical and analytical methods. The proposed method is general in that it allows for full tensor representation of effective permeability. Thus, the method allows for complex anisotropic heterogeneities which are not necessarily aligned with the simulation coordinate axes. Also, the effect of the location of the heterogeneities within the grid block to be homogenized is accounted for. The method, in essence, captures the effect of the pressure dis-

tribution within the grid block. A directional search procedure in local areas (four quadrants of the grid block) identifies the principal axes of permeability and their orientation with respect to the simulation coordinate axes. Coordinate rotation yields effective permeability tensors. These tensors are combined into an effective permeability tensor for the entire grid block based on the coupling of cross-flow-averaged and no-cross-flow-averaged effective permeability tensors from the four quadrants. Darcy's law is manipulated throughout this process. Cross-flow-average refers to harmonic or series average of arithmetically averaged block permeabilities in parallel, whereas no-cross-flow-average refers to arithmetic average of harmonically averaged block permeabilities in series. In the homogenization process, transverse pressure gradients are calculated. These transverse pressure gradients result from local coordinate rotations and non-centered heterogeneities within the grid block. Non-zero transverse pressure gradients contribute to non-zero off-diagonal elements of the effective permeability tensor.

The work in this study is presented in the following manner. First, in Chapter II, a literature review is presented on the subject of effective permeability where both numerical and analytical methods are discussed. In Chapter III, a detailed description of the development of an analytical effective permeability tensor method is presented in a step-by-step procedure. Mathematical details are found in the Appendices. For the sake of completion, a description of a numerical method used to verify the analytical method is also presented. Chapter IV gives a description of how to incorporate a full permeability tensor in a numerical simulator. In Chapter V, results are compared between numerical and analytical permeability tensors. Also presented in that chapter are flood fronts, recovery and fractional flow curves, and pressure profiles based on numerical simulation of fluid flow using small scale and upscaled permeability distributions. The final chapter, Chapter VI, presents a summary and conclusions including recommendations for future work.

CHAPTER II
LITERATURE REVIEW

There are generally two approaches for effective permeability determination. The numerical approach generally involves solving the pressure equation and using Darcy's law to back-calculate the effective permeability to be used in a simulator grid block. The analytical approach can be divided into a variety of techniques based on fundamental principles of effective property theory.

Numerical approaches will be presented first, followed by a presentation of studies within main categories of analytical approaches. Finally, a discussion is presented concerning permeability anisotropy.

Numerical (Simulation) Approach

Monte-Carlo Methods

Warren and Price[2], in their frequently referred pioneering study, initiate what has become known as the "Monte-Carlo" technique for determining effective permeability. Their approach is to perform a number of computational experiments using completely random three-dimensional permeability distributions, i.e., spatial correlation is not explicitly modeled. Based on assumptions of steady-state and single-phase flow, finite difference equations are solved for pressure in each computational experiment such that the effective permeability can be solved from the general flow equation.

The results gathered from their stochastic method shows that the geometric mean yields statistically the best effective permeability value, regardless of the type

of permeability distribution investigated. The estimators investigated are harmonic, geometric, and arithmetic mean.

Jensen et al.[3] investigate, also through Monte-Carlo simulations, the quality of effective permeability estimators as the probability distribution function (p.d.f.) of the permeability data changes. The following estimators are investigated with regard to bias and efficiency: arithmetic average, log-normal average, p-normal average and geometric average. An unbiased estimator gives the correct result on the average given a statistically sufficient number of data sets. An efficient estimator has low variability in the estimates. Their results show that the permeability distribution dictates which estimator to use for effective permeability.

Journel et al.[4] realize the limitations of many effective medium approaches. Many methods are restricted to unbounded, statistically isotropic media with specific univariate permeability distributions having relatively small spatial variability. On the basis of geological studies, porous media are highly variant, anisotropic, and spatially correlated. The approach selected is to use an indicator simulation technique to generate binary permeability distributions containing sand and shale. The model is a random permeability function which assumes stationarity and spatial correlation. A Monte-Carlo type approach is then used to study the effect of the volumetric shale proportion on the effective permeability for both horizontal and vertical flows.

A generalized averaging model is used in an attempt to fit the effective permeability curves obtained from a multitude of numerical simulations. This power average model contains an exponent which reduces to harmonic averaging (lower limit) when equal to -1 and arithmetic average (upper limit) when equal to 1. An exponent value of 0 corresponds to geometric averaging.

Horizontal flow in the shale/sand distributions yields an effective permeability between arithmetic and geometric averages. A power average exponent of 0.57 provides the best fit. At large shale proportion, percolation behavior (creeping flow) occurs and the effective permeability drops dramatically, and in the limit the effective permeability approaches the geometric average. For vertical flow, reasonable

fit is obtained using a power averaging exponent of 0.12.

It is evident that this empirical approach is time consuming and not particularly general. For example, a variation in any of the parameters, such as shale aspect ratio, shale frequency, correlation length, etc. will most likely alter the values of the optimal power averaging exponents.

Desbarats[5] performs a numerical study similar to that of Journel et al.,[4] i.e., extending Warren and Price's[2] work to incorporate spatial correlation through variogram analysis and binary sequences of permeability using sand and shale. A stochastic model is applied to the Assakao fluvial sandstone outcropping in Central Sahara.

A comparison of numerical results and analytical model results showed that existing analytical effective permeability models for sand/shale distributions are restricted to particular cases of spatial correlation and shale fractions.

In a similar study, Desbarats[6] applies the numerical Monte-Carlo technique to estimate effective horizontal and vertical permeabilities based on permeability measurements in the lower Stevens formation of the Paloma field in Kern County, California. Univariate (histograms) and spatial (variograms) statistics are honored in generating the small scale permeability distributions within the grid blocks. Desbarats compared the averaged effective permeabilities from the repeated numerical simulations with effective permeability obtained using an analytical perturbation approach. Results show that the analytical model overpredicts horizontal effective permeability and underpredicts vertical effective permeability. Results also indicate that a large nugget (little information on small scale) in the variogram model reduces the effect of long-range spatial correlation structures on effective permeability. However, geometric average is not a good estimator of effective permeability in the presence of long-range spatial correlation structures.

Gómez-Hernández and Gorelick[7] perform a Monte-Carlo simulation study to determine effective hydraulic conductivity in aquifers. They study the effects of factors such as correlation length and conditional simulations on effective hydraulic conductivity. The assumptions involved in the conductivity model are: isotropy,

a given probability distribution, exponential covariance function, and second order stationarity.

Results show that a power averaging exponents of -0.4 and -0.2 yield best fits for unconditional and conditional simulations, respectively. However, it is concluded that factors such as the univariate distribution type, correlation length, anisotropy, discharges, and boundary conditions may alter the value of the best fitting power average exponent.

Deutsch[8] extends Journel et al.'s[4] work to investigate how geometric anisotropy or aspect ratio of the shales influences effective horizontal and vertical permeabilities. Two models are proposed to match the simulation results. The power average model, which is a function of the shale volume and the sand and shale permeabilities, requires the need to determine the value of the power averaging exponent. Empirical relationships relate the power averaging exponent to anisotropy. The other model, based on percolation theory, is deemed impractical because it requires the determination of as many as three parameters in fitting the experimental/numerical effective permeability.

Tensor Methods

White and Horne[9] demonstrate the importance of full tensor representation of grid block scale transmissibility. They present an algorithm to calculate the effective transmissibility tensor based on a small scale permeability field. Pressures and fluxes from several fine scale simulations with different boundary conditions are averaged and summed, respectively, to obtain large scale pressures and fluxes. Large scale transmissibilities are obtained by using the large scale pressures and fluxes in a least square procedure based on the various boundary conditions applied. Thus, a "boundary-condition-averaged" transmissibility tensor is developed.

Samier[10] derives transmissibility tensors using finite element methods based on single-phase flow. A finite element mesh is constructed to be superimposed on an underlying mesh used in a finite volume reservoir simulator such that the nodes of the elements coincide with the grid block centers of the simulator mesh. The

effective permeability tensors are obtained for each element by a selected averaging technique applied to the permeability values of the underlying simulator mesh. Finally, the node to node transmissibilities are computed for the finite element mesh and used for the finite volume simulator. Samier demonstrates the advantages of using a full tensor in horizontal well modeling.

Holden et al.[11] realize the computationally demanding process of numerically computing effective permeability. Based on single-phase, steady-state, incompressible flow, they use an approximation of the pressure solution to estimate the effective permeability. The approximation of the pressure solution is obtained using an iterative solver and stopping before reaching convergence. Off-diagonal values of the permeability tensor is obtained by rotating the grid block and repeating the procedure.

Durlofsky and Chung[12] consider a spatially periodic porous medium and impose periodic boundary conditions in performing finite element numerical simulation on the small scale permeability field. These investigators claim that periodic boundary conditions will circumvent ambiguity with respect to boundary conditions and will always yield a symmetric effective permeability tensor.

Gómez-Hernández and Journel[13] use a least square procedure similar to that of White and Horne[9] to determine the appropriate interface permeability tensors. Several different boundary conditions are applied, but half a grid block away from the boundary of the grid block for which interface permeability tensors are to be determined. Consequently, the pressure distribution of the grid block under consideration has been influenced by the surrounding small scale permeability distribution yielding a more correct, albeit a more computationally expensive, "in-situ" effective permeability tensor.

Gallouët and Guérillot[14] also use the least square approach by minimizing the differences between local and averaged filtration velocities in all selected flow directions. They use a 9-point finite volume technique allowing for non-symmetric off-diagonal elements in the effective permeability tensor.

Analytical Approach

Streamtube Methods

Haldorsen and Lake[15] initiated the use of streamtube models for calculating effective permeability of sand/shale sequences. Their objective is to estimate both horizontal and vertical effective permeabilities. Through manipulation of Darcy's law for a two-component medium (sand and shale), effective permeability is related to the tortuousity of the flow paths through the medium. Steady-state, incompressible, single-phase flow is assumed. In addition, sand permeability is isotropic and shale permeability is zero. Their model requires high aspect ratio grid blocks.

Begg and King[16] present several methods for estimating effective vertical permeability for stochastic sand/shale distributions in both two and three dimensions. In one of the proposed methods, the shales are assumed to be infinitesimally thin and of constant length. The pressure equation is solved analytically within an ellipse surrounding each shale using an elliptic coordinate system in two dimensions. The effective vertical permeability of the ellipse is obtained by replacing the ellipse with a homogeneous medium such that it does not alter the pressure distribution on the surface of the ellipse. It is assumed that each shale is separated enough to ensure independent perturbed flow around it.

Begg and King also modified Haldorsen and Lake's[15] work by removing the constraints on the grid block aspect ratio. They propose two ways of estimating lengths of a sample of streamtubes. One approach is based on an explicit description of the shale distribution and involves streamline tracing. The other approach is statistical and requires a cumulative distribution function (c.d.f.) of the shale lengths as well as the shale density. Shale permeability is assumed zero. Their results indicate that vertical effective permeability is strongly dependent on shale dimensions, density, and facies thickness.

Begg et al.[17] extend Begg and King's[16] statistical streamline method to layered media with different anisotropic sand permeabilities and shale statistics in each layer. In addition to the assumptions made by Begg and King (steady, incom-

pressible, single-phase, unidirectional flow normal to layering), shales are randomly distributed and approximated by rectangles. The method is based on the assumption that tortuousity of streamlines are proportional to the length and frequency of the shales. The required data are frequency and fraction of shales, horizontal and vertical sand permeabilities, and probability distributions/means of shale dimensions.

Begg et al.[18] apply a successive rescaling procedure to determine effective permeability of part of the Sherwood reservoir at Wytch Farm in Dorset, United Kingdom. They present a methodology which involves successive estimation of effective horizontal and vertical rock type permeabilities, then non-shale layer permeabilities based on core plug data, the estimated rock type permeabilities, and statistical spatial distribution information. These first two steps involve numerical simulation methods to estimate effective permeabilities. The effect of shales on vertical permeability is then determined using the streamline method proposed by Begg et al.[17]

Abu-elbashar et al.[19] propose a revision of existing statistical streamtube models for calculating effective horizontal and vertical permeabilities. They suggest incorporating effects of more complex geological features found in sand/shale reservoirs. More specifically, they use statistical information regarding shale convergence and sand compartmentalization to improve Begg and King[16] and Begg et al.'s[17] streamtube models. The statistical information is based on shale data in wells and outcrops which are representative of the reservoir under consideration. Shale permeability is assumed zero.

For sand/shale reservoirs with complex geology, results show that previous methods underpredict effective vertical permeability whereas Haldorsen and Lake's method[15] tend to overestimate effective horizontal permeability.

Perturbation Methods

Perturbation expansion methods are applied to solve mathematical problems which cannot be solved exactly by analytical means.[20] Approximate expressions are

generated in the form of asymptotic series. A truncated series involving two or three terms provide a useful approximation to the original problem.[21]

In the context of effective permeability estimation, permeability is assumed to be approximately constant with only minor deviations from the mean.[22]

King[23] treats the pressure equation for single-phase, steady-state flow as a stochastic differential equation and uses a high-order Taylor series expansion to estimate effective permeability.

Otero et al.[24] use the single-phase transport equation in porous media as a starting point and assume pressure to be a function of a small and a large scale. This pressure is represented in terms of power series in a constant (ϵ) which represents the scale change. The power series representation of pressure is substituted into the transport equation. Eventually a boundary value problem emerges involving a periodic vector function. The effective permeability tensor is obtained via a solution of the boundary value problem and calculation of a tortuousity tensor. The method requires spatial periodicity of the heterogeneous medium.

Rubin and Gómez-Hernández[25] allow for conditioning data in their stochastic approach. Darcy's law and the continuity equation are linked and treated as a stochastic partial differential equation. The coefficient in this P.D.E. corresponds to the point measured conductivity and is treated as a spatial random function. The probability density function for the point conductivity is multinormal. The medium is isotropic, unbounded and of limited conductivity variance.

Percolation Methods

Kirkpatrick[26] uses percolation theory to treat transport phenomena in heterogeneous media. He presents both resistor/conductor network models as well as a foundation for effective medium theory.

Effective Medium Theory (EMT)

McGill et al.[22] describe effective medium theory or mean field theory as follows: Any region of permeability behaves as if embedded within the average medium. The

sum of the permeability regions should reproduce the average medium.

Bernasconi[27] extends Kirkpatrick's[26] effective medium theory to include estimation of conduction in anisotropic heterogeneous networks.

Harris[28] presents a generalized effective medium formulation. It can be applied to networks of arbitrary structural patterns (topology). The formulation is closely linked to Bernasconi's[27] effective medium approach for anisotropic networks. Harris applies the method to fracture networks to obtain fracture network tensor conductance.

Renormalization Techniques

According to King,[29] effective medium theory and perturbation methods yield invalid effective permeability estimates in highly heterogeneous media. He proposes to use a real-space renormalization technique which uses a resistor network as a model for the permeabilities. The method involves a multilevel procedure of estimating the effective conductance or permeability of a gradually smaller number of 2-by-2 resistor networks for each averaging level. In this way, small regions of the permeability field are averaged first. Then, successively larger regions are averaged until, finally, at the last level a single 2-by-2 resistor network is analyzed to yield one effective permeability value for the entire permeability field. The main tool used in this process is the Delta-Star transformation. The process also requires computing the appropriate replacements for resistors in series and parallel. The method may be extended to three dimensions, but without obtaining a closed-form expression.

Jones et al.[30] describe the renormalization approach and its applications. Compared to "truth" case values from numerical simulation methods, the renormalization technique usually produces errors which are less than 10 %. These authors suggest using a large cell approach or combining small cell and multigrid approaches in cases where the small cell approach (real-space renormalization) works less satisfactorily, such as when significant macroscopic flow tortuousity exists.

Williams[31] discusses two schemes for calculating effective properties: small cell methods and large cell methods. The small cell methods described are the

hierarchical method of King[29] and a method which is identical to "no-cross-flow-averaging", i.e., arithmetic average of harmonically averaged permeabilities in series within layers. Williams maintains that large cell methods provide greater accuracy for strongly anisotropic systems, and these methods are not hampered by locally imposed boundary conditions. The large cell method used by Williams is based on an algorithm proposed by Frank and Lobb.[32] This algorithm uses a sequence of propagator transformations which "collapses", in a column by column fashion, the resistors/conductors in a resistor network to arrive at a single effective value of conductance or resistance for the entire network. The algorithm relies heavily on the use of Delta-Star and Star-Delta transformations. This large cell scheme is limited to two-dimensional problems.

Tensor Methods

Most analytical methods are restricted to the estimation of effective permeability which contains only the diagonal elements of the permeability tensor. However, Kasap and Lake[1] propose an analytical method to calculate a full tensor effective block permeability using the geometry, block size, full local tensorial permeabilities and the geology within the block.

Poulisse[33] considers small scale permeability to be a random scalar quantity and solves the continuity equation in conjunction with Darcy's law posed as a random boundary value problem. The solution is then used to construct a transformation between flow quantities on small and large (grid block) scale. Poulisse suggests, in order to speed up convergence, to use the renormalization technique of King[29] first to reduce permeability variations and then apply the proposed method.

Some of the methods presented above allow for full tensor form of the effective permeability. In the next section, permeability anisotropy will be discussed, pointing out the need to treat the effective permeability in its most general form, i.e., as a full tensor.

Permeability Anisotropy

Permeability anisotropy is caused by the orientation and shape of the asymmetric grains in the porous media.[34] There are several aspects related to permeability anisotropy, such as local permeability heterogeneity, periodicity, and scale.[35]

Leung[36] classifies permeability anisotropy in two categories:

1. Simple permeability anisotropy
   (a) anisotropic and homogeneous
   (b) anisotropic and heterogeneous (limited anisotropy)
2. Full/General permeability anisotropy

In the first category, the principal axes of permeability are aligned with the simulation coordinate axes. In case 1(a), the principal permeabilities do not change spatially, whereas in case 1(b) they do. Case 2 represents the most general situation where the principal axes of permeability are not necessarily aligned with the simulation coordinate axes, and both the orientation and magnitude of the principal permeabilities may vary spatially.

If permeability anisotropy exists in its most general form, the direction of the pressure gradient vector at a given point in the anisotropic medium is different from that of the filter velocity vector.[37] Leung[36] shows that serious errors in well response prediction may occur when only a diagonal tensor is used in a complex reservoir with multiple zones of different principal directions of permeability.

Ramey[38] applies interference analysis to anisotropic formations to determine principal axes permeabilities and the orientation angle of the anisotropic structures. The analysis is based on pressure data obtained from observation wells during field water injection. Ramey suggests that this large scale method of estimating effective permeability may become important in planning fluid injection operations.

White and Horne[9] demonstrate, through manipulation of Darcy's law, the need to consider the most general case of anisotropy for calculating effective permeability. Anisotropic small scale heterogeneities, such as laminations, burrows, and

cross-beddings distort local streamlines requiring full tensor representation of permeability at the grid block scale.

In the next chapter, it is shown that there are, in general, two cases which require full tensor effective permeabilities. A method for analytically calculating the effective permeability tensor is presented. The method allows for the possibility of either or both of these cases to be present in the small scale permeability field being scaled up. Also, a description of a numerical method for calculating the effective permeability tensor is presented.

CHAPTER III
DEVELOPMENT OF EFFECTIVE PERMEABILITY TENSOR

This chapter is divided into two main sections: The first section shows the development of an analytical method for calculating an effective permeability tensor. The second section briefly explains how a numerical method to calculate the effective permeability tensor is developed. Effective permeability tensors obtained using both analytical and numerical methods are compared in Chapter V.

Analytical Method

The analytical method proposed here combines the advantages of numerical and analytical methods. Complex permeability heterogeneities are handled at a relatively high computational speed.

The location and size of small scale heterogeneities within a simulator grid block and the orientation of anisotropic permeability structures are accounted for using this method. The method estimates effective coarse scale (macroscale) permeability yielding a tensorial form of effective permeability.

There are generally two situations in which a full permeability tensor is required to correctly account for the effect of the heterogeneities within a simulator grid block:

1. Heterogeneous or homogeneous permeability structures (layers) are anisotropic and oriented at angles other than those parallel and perpendicular to the simulation coordinate axes (general anisotropy). An example is shown in Figure 3.1.

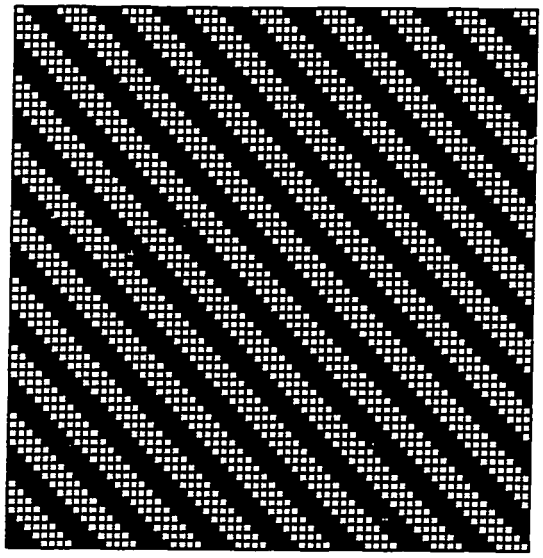

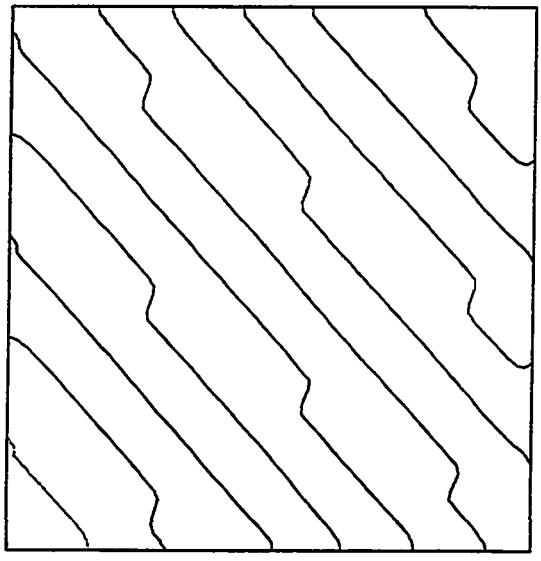

Fig. 3.1: **Top:** Cross-Bedded Permeability Distribution (−45° Structure Orientation, Dark Grid Blocks: 20 md, Light Grid Blocks: 1000 md). **Bottom:** Pressure Map Indicating Non-Zero Transverse Pressure Gradient. Boundary Conditions: Closed Horizontal Boundaries; Left Face: Injection; Right Face: Production.

2. Heterogeneities are not centered in the grid block. An example of this is shown in Figure 3.2.

Figures 3.1 and 3.2 are examples of cases where permeability heterogeneities generate a pressure drop transverse to the direction of applied pressure drop. In both of the cases shown, the applied pressure drop is along the horizontal axis.

The following procedure describes how cross-beddings and laminations (case 1) and location of permeability heterogeneities of high contrast, such as sand and shale (case 2), are considered in the development of an analytical method for calculating an effective permeability tensor.

The first step in this procedure is to divide the grid block containing small scale permeability heterogeneities into four quadrants or local blocks as shown in Figure 3.3. Dividing the grid block into four quadrants is done to capture the effect of the location of heterogeneities within the grid block (case 2). The next step will be to determine the effective permeability tensor in each of the four quadrants. The final step is to obtain the effective permeability tensor for the entire grid block by combining the effective permeability tensors from each of the four quadrants.

Steps 1 and 2 below are performed on <u>each</u> of the four quadrants for cases where permeability structures are anisotropic and not aligned with the simulation coordinate axes:

<u>1. Determine the permeabilities along the principal directions.</u>

The principal directions of permeability are the directions of maximum and minimum permeabilities, k'_{xx} and k'_{yy}, respectively. In this study, it is assumed that, within each quadrant, the principal directions (x' and y') are perpendicular and that k'_{xy} and k'_{yx} are zero. Therefore, if anisotropy exists ($k'_{xx} \neq k'_{yy}$), then the principal directions of permeability must be determined.

The method proposed to determine k'_{xx} and k'_{yy} is explained as follows. The objective is to find the direction which yields the maximum ratio of k'_{xx}/k'_{yy}. A "sweep" is performed in directions between $-90°$ and $90°$ relative to the horizontal x-axis to determine in which direction k'_{xx}/k'_{yy} is largest. As many as forty-nine

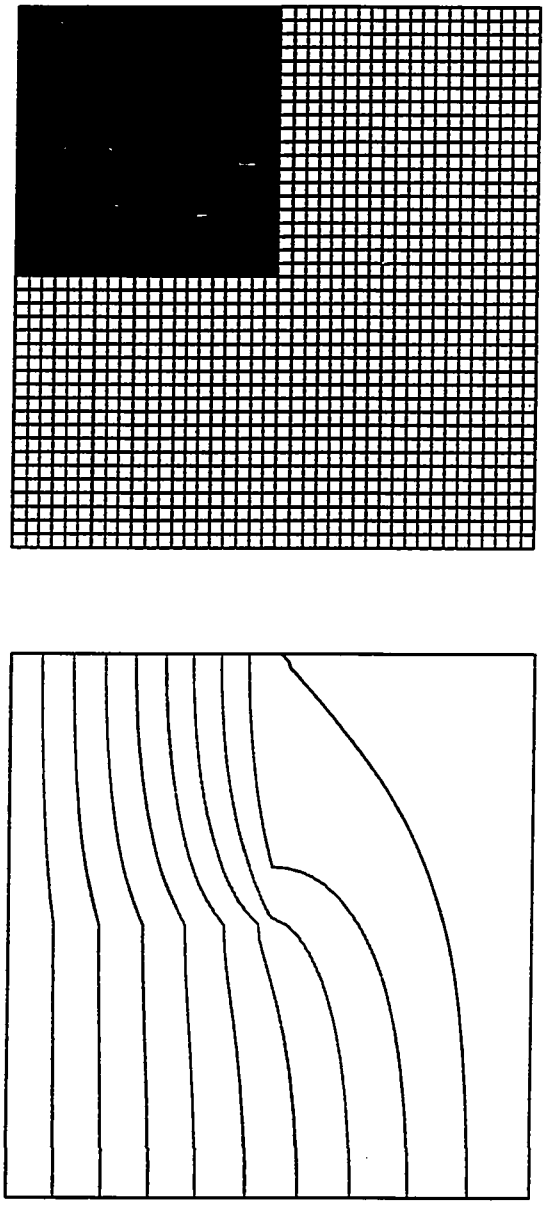

Fig. 3.2: **Top:** Permeability Field with Low Permeability Section (Dark Grid Blocks: 1 md, Light Grid Blocks: 1000 md).
Bottom: Pressure Map Indicating Non-Zero Transverse Pressure Gradient. Boundary Conditions: Closed Horizontal Boundaries; Left Face: Injection; Right Face: Production.

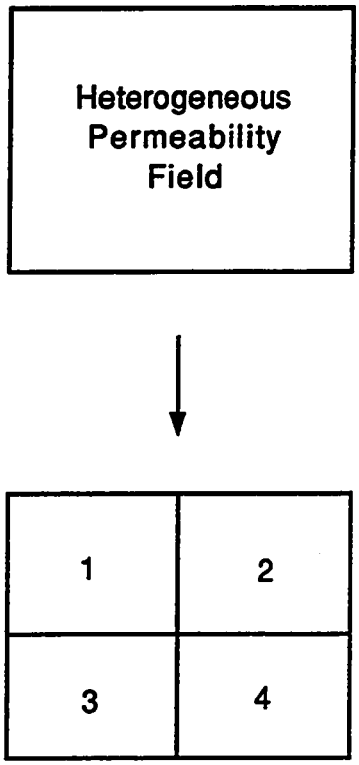

Fig. 3.3: Field of Small Scale Heterogeneities Divided into Four Quadrants.

directions are used to ensure accuracy to within a few degrees. Both k'_{xx} and k'_{yy} are calculated for each direction. k'_{yy} is the permeability in the direction perpendicular to that of k'_{xx}. In addition to k'_{xx} and k'_{yy}, the orientation angle, α, in the direction of maximum k'_{xx}/k'_{yy} is determined and used in Step 2.

Figure 3.4 shows the data points included in the calculation of k'_{xx} and k'_{yy} for the directions 45° and −45° from the horizontal, respectively. k'_{xx} and k'_{yy} are determined by an analytical homogenization procedure of combining arithmetically averaged values in series and harmonically averaged values in parallel. The procedure is similar to that of calculating $\tilde{k}_{x_{app}}$ and $\tilde{k}_{y_{app}}$ which is explained in detail in Appendix C. However, in the calculation of k'_{xx} and k'_{yy}, the number of data values may be extended to more than 2 x 2 values. In Appendix A, a small example is presented to demonstrate how k'_{xx} and k'_{yy} are calculated for an orientation angle of $\alpha = 26.6°$ on a 5×5 grid.

2. Perform coordinate rotation to obtain the effective permeability tensor.

k'_{xx}, k'_{yy}, and the orientation angle, α, were determined in Step 1 above. These parameters are used in a coordinate rotation procedure which yields the following effective permeability tensor for the simulation coordinate system:

$$k_{xx} = (\cos\alpha)^2 k'_{xx} + (\sin\alpha)^2 k'_{yy} \tag{3.1}$$

$$k_{xy} = \sin\alpha\cos\alpha(k'_{xx} - k'_{yy}) \tag{3.2}$$

$$k_{yx} = \sin\alpha\cos\alpha(k'_{xx} - k'_{yy}) \tag{3.3}$$

$$k_{yy} = (\sin\alpha)^2 k'_{xx} + (\cos\alpha)^2 k'_{yy} \tag{3.4}$$

where k_{xx}, k_{xy}, k_{yx}, and k_{yy} are the effective permeability tensor elements in the x,y-coordinate system. α is the angle by which the x',y'-coordinate system deviates from the x,y-coordinate system. The derivations of Eqs. (3.1)-(3.4) are shown in

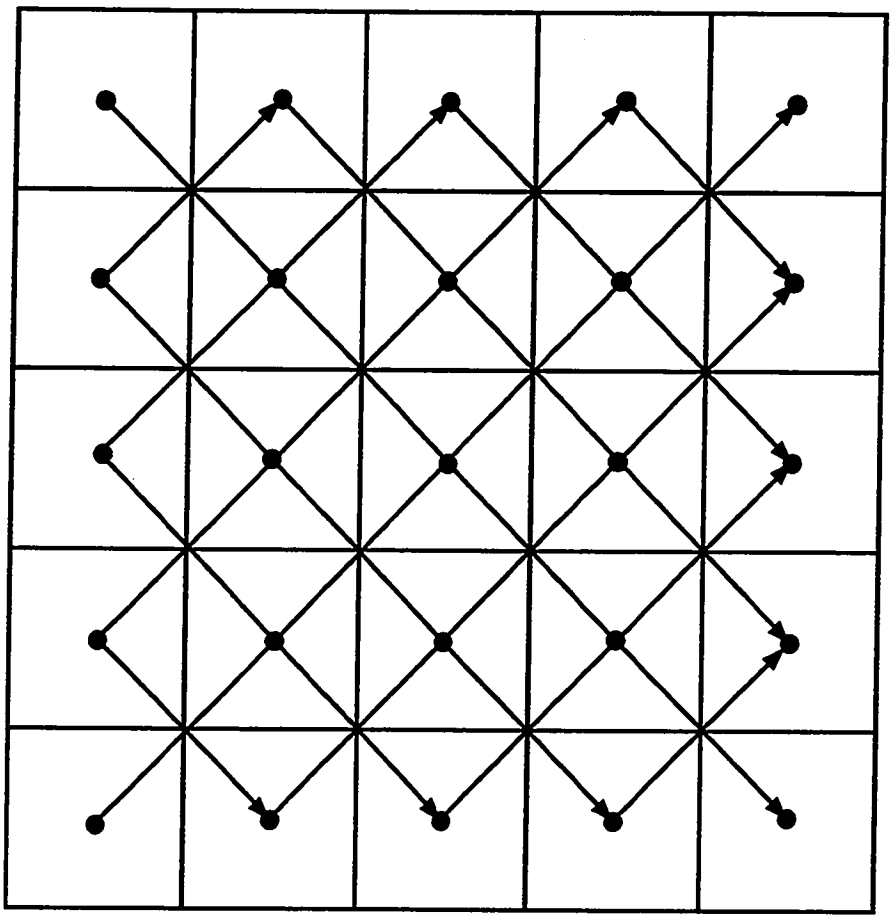

Fig. 3.4: Directions and Data Points to Consider in Calculating Maximum and Minimum Permeabilities Along 45° and −45° From the Horizontal Axis.

detail in Appendix B along with an example showing the translation of the off-diagonal elements into pressure gradient ratios for various orientation angles.

Rationale for dividing the permeability field into four blocks.

At this point an effective permeability tensor has been determined for each of the four quadrants or blocks in the permeability field as illustrated in Figure 3.5. The final step is to calculate the effective permeability tensor for the entire permeability field. Steps 1 and 2 could conceivably be performed on the complete permeability field thereby ensuring symmetric off-diagonal elements of the permeability tensor. Dullien[37] points out that the permeability tensor is always symmetric if the anisotropic medium is "orthotropic". In an orthotropic medium, the principal axes are orthogonal. An effective permeability tensor may, however, have non-symmetric off-diagonal elements.[14,39] This situation may, for example, occur when combining permeability tensors of various magnitude from the various quadrants, reflecting an effectively non-orthotropic medium.

The main reason for dividing the permeability field into four blocks is that transverse pressure gradients, yielding non-zero off-diagonal elements in the permeability tensor, are induced in cases such as the one illustrated in Figure 3.2. In this case, a perturbation (low permeability region, such as a shale) is located in the upper left corner of the system. The location of this perturbation will control the sign of the off-diagonal elements in the effective permeability tensor. For example, the case illustrated in Figure 3.2 yields negative off-diagonal elements (k_{xy} and k_{yx}). If the perturbation were located in the bottom left corner of the permeability field, the off-diagonal elements would be positive. Therefore, the reason for dividing the system into four quadrants is to capture these "global" effects caused by such perturbations and their locations in the permeability field.

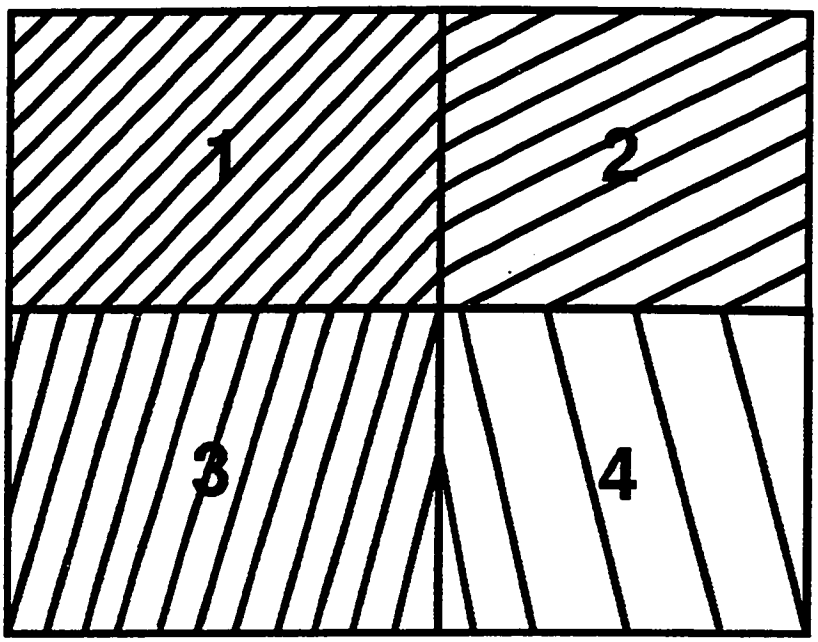

Fig. 3.5: System Containing Four Blocks and Four Permeability Tensors.

3. Determine effective permeability tensor for the entire grid block.

The physical system consists of four grid blocks or quadrants as shown in Figure 3.5. Each of the four blocks may have different, but possibly full ($k_{xy} \neq 0$ and $k_{yx} \neq 0$) permeability tensors obtained from the previous steps. Permeability anisotropy ($k_{xx} \neq k_{yy}$) and varying block sizes are also permitted and accounted for in the determination of the elements of the effective permeability tensor.

The derivation of the overall effective permeability tensor is described next.

The elements of the effective permeability tensor are obtained from the following expressions:

$$\tilde{k}_{xx} = \frac{\tilde{k}_{x_{app}}}{1 - \left(\left[\left(\frac{\partial \tilde{p}}{\partial x} \right)_Y / \left(\frac{\partial \tilde{p}}{\partial y} \right)_Y \right] \times \left[\left(\frac{\partial \tilde{p}}{\partial y} \right)_X / \left(\frac{\partial \tilde{p}}{\partial x} \right)_X \right] \right)} \tag{3.5}$$

$$\tilde{k}_{yy} = \frac{\tilde{k}_{y_{app}}}{1 - \left(\left[\left(\frac{\partial \tilde{p}}{\partial x} \right)_Y / \left(\frac{\partial \tilde{p}}{\partial y} \right)_Y \right] \times \left[\left(\frac{\partial \tilde{p}}{\partial y} \right)_X / \left(\frac{\partial \tilde{p}}{\partial x} \right)_X \right] \right)} \tag{3.6}$$

$$\tilde{k}_{xy} = -\tilde{k}_{xx} \left(\frac{\partial \tilde{p}}{\partial x} \right)_Y \Big/ \left(\frac{\partial \tilde{p}}{\partial y} \right)_Y \tag{3.7}$$

$$\tilde{k}_{yx} = -\tilde{k}_{yy} \left(\frac{\partial \tilde{p}}{\partial y} \right)_X \Big/ \left(\frac{\partial \tilde{p}}{\partial x} \right)_X . \tag{3.8}$$

In Eqs. (3.5)-(3.8), $\tilde{k}_{x_{app}}$ and $\tilde{k}_{y_{app}}$ are the effective *apparent* permeabilities along the x- and y-axis, respectively. *Apparent* permeabilities are used as effective permeabilities if the numerical simulator is not equipped to handle a tensor formulation of permeability. Clearly, $\tilde{k}_{x_{app}}$ reduces to $\tilde{k}_{xx}$ and $\tilde{k}_{y_{app}}$ reduces to $\tilde{k}_{yy}$ whenever the pressure gradient ratios in Eqs. (3.5) and (3.6) are zero. The pressure gradient ratio is defined as the ratio of transverse to longitudinal pressure gradients. $\left(\frac{\partial \tilde{p}}{\partial x} \right)_Y / \left(\frac{\partial \tilde{p}}{\partial y} \right)_Y$ is the pressure gradient ratio induced from injection along

y-axis whereas $\left(\frac{\partial \bar{p}}{\partial y}\right)_X / \left(\frac{\partial \bar{p}}{\partial x}\right)_X$ is the pressure gradient ratio induced from injection along x-axis. In both cases, boundaries transverse to the principal direction of fluid injection are closed. Notice that the pressure gradient ratios are closely linked to the off-diagonal elements of the permeability tensor as can be seen from Eqs. (3.7) and (3.8). Appendix C provides examples of the necessary equations for one- and two-block systems which are extended to a four-block system to obtain Eqs. (3.5)-(3.8).

The apparent permeabilities and the pressure gradient ratios in Eqs. (3.5)-(3-8) must be determined to obtain the elements of the effective permeability tensor, $\tilde{k}_{xx}$, $\tilde{k}_{xy}$, $\tilde{k}_{yx}$, and $\tilde{k}_{yy}$.

$\tilde{k}_{x_{app}}$ and $\tilde{k}_{y_{app}}$ are determined from the following procedure. First, calculate $\hat{k}_{x_{app_{tb}}}$ which is the effective apparent x-direction permeability assuming no cross-flow between the top and the bottom layers (see Figure 3.6):

(i) Isolate the top layer (blocks 1 and 2) in Figure 3.5. Use Darcy's law with full permeability tensor to determine the apparent permeability in the x-direction ($\hat{k}_{x_{app_t}}$) of blocks 1 and 2 combined. Constant pressure drop is applied in the principal direction of flow (x-direction) with closed upper and lower boundaries.

(ii) Isolate the bottom layer (blocks 3 and 4) in Figure 3.5. Use Darcy's law with full permeability tensor to determine the apparent permeability in the x-direction ($\hat{k}_{x_{app_b}}$) of blocks 3 and 4 combined. Constant pressure drop is applied in the principal direction of flow (x-direction) with closed upper and lower boundaries.

(iii) The effective apparent permeability in the x-direction of the top and bottom layers combined ($\hat{k}_{x_{app_{tb}}}$) is a weighted arithmetic average of $\hat{k}_{x_{app_t}}$ and $\hat{k}_{x_{app_b}}$ because these layers are in parallel with respect to the direction of flow.

Next, calculate $\hat{k}_{x_{app_f}}$ which is the effective apparent x-direction permeability assuming cross-flow between top and bottom layers (see Figure 3.7):

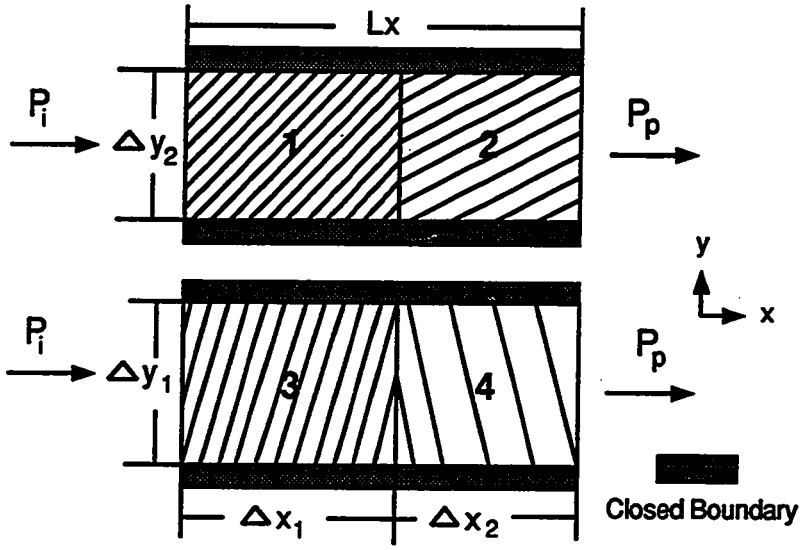

Fig. 3.6: Schematic for No Cross-Flow Case; $\hat{k}_{x_{apptb}}$ (Injection Along x-axis).

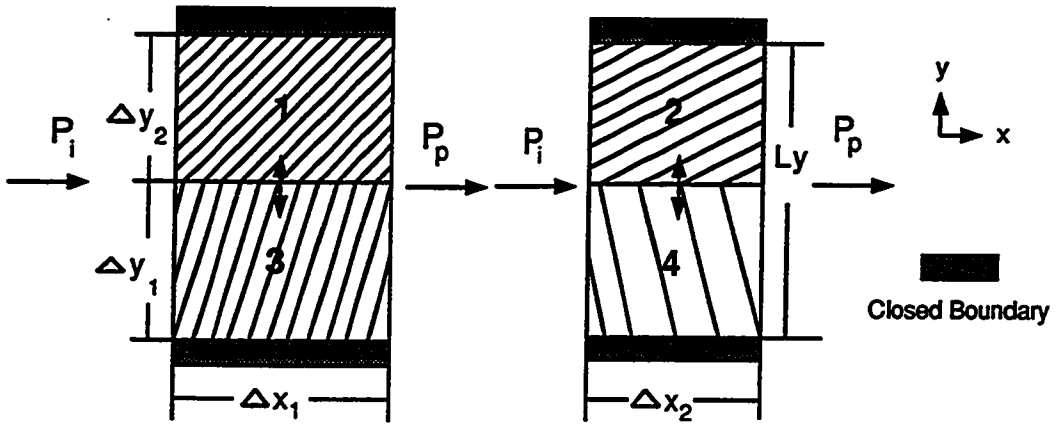

Fig. 3.7: Schematic for Cross-Flow Case; $\hat{k}_{x_{appf_s}}$ (Injection Along x-axis).

(iv) Isolate the first column (blocks 1 and 3) in Figure 3.5. Use Darcy's law with full permeability tensor to determine the apparent permeability in the x-direction ($\hat{k}_{x_{app_f}}$) of blocks 1 and 3 combined. Constant pressure drop is applied in the principal direction of flow (x-direction) with closed upper and lower boundaries.

(v) Isolate the second column (blocks 2 and 4) in Figure 3.5. Use Darcy's law with full permeability tensor to determine the apparent permeability in the x-direction ($\hat{k}_{x_{app_s}}$) of blocks 2 and 4 combined. Constant pressure drop is applied in the principal direction of flow (x-direction) with closed upper and lower boundaries.

(vi) The effective apparent permeability in the x-direction of the first and second columns combined ($\hat{k}_{x_{app_{fs}}}$) is a weighted harmonic average of $\hat{k}_{x_{app_f}}$ and $\hat{k}_{x_{app_s}}$ because these columns are in series with respect to the direction of flow.

Steps (i)-(vi) are repeated to determine the effective apparent permeabilities for cross-flow ($\hat{k}_{y_{app_{tb}}}$) and no cross-flow ($\hat{k}_{y_{app_{fs}}}$) cases along the y-axis. For these cases, injection of fluid is along the y-axis for each of the separate sections: top and bottom layers, and first and second columns. Consequently, the closed boundaries are the left and right vertical boundaries in Figure 3.5 for each case. Figure 3.8 corresponds to a cross-flow case for injection along the y-axis and the calculation of $\hat{k}_{y_{app_{tb}}}$, whereas Figure 3.9 corresponds to a no cross-flow case for injection along the y-axis and the calculation of $\hat{k}_{y_{app_{fs}}}$.

Note that "no cross-flow" refers to no communication and "cross-flow" refers to maximum communication between blocks/layers in the direction transverse to the principal flow direction.

Details regarding calculations of $\hat{k}_{x_{app_{tb}}}$, $\hat{k}_{x_{app_{fs}}}$, $\hat{k}_{y_{app_{tb}}}$, and $\hat{k}_{y_{app_{fs}}}$, can be found in Appendix C. Their final expressions are as follows:

$$\hat{k}_{x_{app_{tb}}} = \frac{\Delta y_2}{L_y}\hat{k}_{x_{app_t}} + \frac{\Delta y_1}{L_y}\hat{k}_{x_{app_b}} \tag{3.9}$$

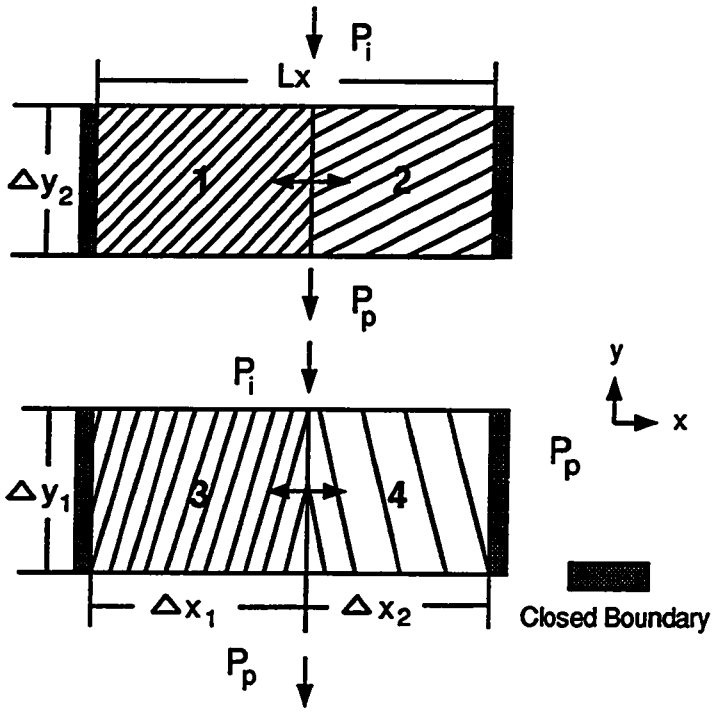

Fig. 3.8: Schematic for Cross-Flow Case; $\hat{k}_{y_{appt_b}}$ (Injection Along y-axis).

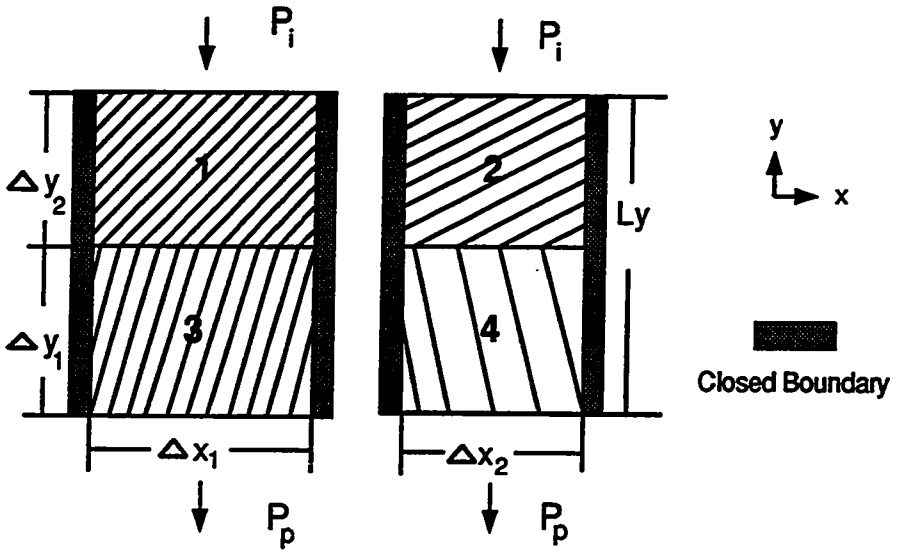

Fig. 3.9: Schematic for No Cross-Flow Case; $\hat{k}_{y_{appf_s}}$ (Injection Along y-axis).

where

$$\hat{k}_{x_{app_t}} = \frac{k_{x_{app_1}} k_{x_{app_2}} L_x}{k_{x_{app_1}} \Delta x_2 + k_{x_{app_2}} \Delta x_1} \tag{3.10}$$

$$\hat{k}_{x_{app_b}} = \frac{k_{x_{app_3}} k_{x_{app_4}} L_x}{k_{x_{app_3}} \Delta x_2 + k_{x_{app_4}} \Delta x_1}. \tag{3.11}$$

The local apparent permeabilities are defined in Appendix C.

$$\hat{k}_{x_{app_{f_s}}} = \frac{\hat{k}_{x_{app_f}} \hat{k}_{x_{app_s}} L_x}{\hat{k}_{x_{app_f}} \Delta x_2 + \hat{k}_{x_{app_s}} \Delta x_1} \tag{3.12}$$

where

$$\hat{k}_{x_{app_f}} = \frac{\Delta y_2}{L_y} k_{x_{app_1}} + \frac{\Delta y_1}{L_y} k_{x_{app_3}} \tag{3.13}$$

$$\hat{k}_{x_{app_s}} = \frac{\Delta y_2}{L_y} k_{x_{app_2}} + \frac{\Delta y_1}{L_y} k_{x_{app_4}}. \tag{3.14}$$

$$\hat{k}_{y_{app_{tb}}} = \frac{\hat{k}_{y_{app_t}} \hat{k}_{y_{app_b}} L_y}{\hat{k}_{y_{app_t}} \Delta y_1 + \hat{k}_{y_{app_b}} \Delta y_2} \tag{3.15}$$

where

$$\hat{k}_{y_{app_t}} = \frac{\Delta x_1}{L_x} k_{y_{app_1}} + \frac{\Delta x_2}{L_x} k_{y_{app_2}} \tag{3.16}$$

$$\hat{k}_{y_{app_b}} = \frac{\Delta x_1}{L_x} k_{y_{app_3}} + \frac{\Delta x_2}{L_x} k_{y_{app_4}}. \tag{3.17}$$

The local apparent permeabilities are defined in Appendix C.

$$\hat{k}_{y_{app_{fs}}} = \frac{\Delta x_1}{L_x}\hat{k}_{y_{app_f}} + \frac{\Delta x_2}{L_x}\hat{k}_{y_{app_s}} \tag{3.18}$$

where

$$\hat{k}_{y_{app_f}} = \frac{k_{y_{app_1}} k_{y_{app_3}} L_y}{k_{y_{app_1}} \Delta y_1 + k_{y_{app_3}} \Delta y_2} \tag{3.19}$$

$$\hat{k}_{y_{app_s}} = \frac{k_{y_{app_2}} k_{y_{app_4}} L_y}{k_{y_{app_2}} \Delta y_1 + k_{y_{app_4}} \Delta y_2}. \tag{3.20}$$

Arithmetic, geometric, and harmonic means may be suggested as options to obtain effective four-block apparent permeabilities. However, it is not clear as to which of these averaging methods would yield the most physically correct result. Therefore, the decision was made to use neither of the above mentioned options and rather use the physical concept of cross-flow in determining effective apparent permeabilities along each of the two coordinate axes.

The apparent permeabilities are determined based on a weighting scheme using apparent permeability anisotropy. It is known[40,41] that the permeability anisotropy to a large degree controls the amount of cross-flow in a system. Therefore, $\tilde{k}_{x_{app}} = f(\hat{k}_{x_{app_{tb}}}, \hat{k}_{x_{app_{fs}}})$ and $\tilde{k}_{y_{app}} = f(\hat{k}_{y_{app_{tb}}}, \hat{k}_{y_{app_{fs}}})$ can be written as:

$$\tilde{k}_{x_{app}} = \frac{\tilde{k}_{x_{app}} \hat{k}_{x_{app_{tb}}} + \tilde{k}_{y_{app}} \hat{k}_{x_{app_{fs}}}}{\tilde{k}_{x_{app}} + \tilde{k}_{y_{app}}} \tag{3.21}$$

$$\tilde{k}_{y_{app}} = \frac{\tilde{k}_{x_{app}} \hat{k}_{y_{app_{tb}}} + \tilde{k}_{y_{app}} \hat{k}_{y_{app_{fs}}}}{\tilde{k}_{x_{app}} + \tilde{k}_{y_{app}}}. \tag{3.22}$$

Eqs. (3.21) and (3.22) are two equations which can be solved for $\tilde{k}_{x_{app}}$ and $\tilde{k}_{y_{app}}$ and subsequently the permeability anisotropy ratio $\frac{\tilde{k}_{x_{app}}}{\tilde{k}_{y_{app}}}$. The derivations of $\tilde{k}_{x_{app}}$ and $\tilde{k}_{y_{app}}$ are shown in detail in Appendix C.

The next step is to determine the effective or overall ratios of transverse to longitudinal pressure gradients which are needed for determining the elements of the effective permeability tensor as seen in Eqs. (3.5)-(3.8). The generalized pressure gradient ratio $\left(\frac{\partial \bar{p}}{\partial t}\right)_L / \left(\frac{\partial \bar{p}}{\partial l}\right)_L$ consists of two components. It was decided to denote the pressure gradient ratio due to permeability contrasts between the four grid blocks the "global" pressure gradient ratio, whereas the "local" pressure gradient ratios evolve from local grid blocks (or quadrants) having non-zero off-diagonal elements of their effective permeability tensors. Figures 3.10 and 3.11 illustrate these concepts.

Details regarding the derivation of the "global" pressure gradient ratios are found in Appendix D. The basic idea for determining "global" pressure gradient ratios in the system is given in the following step-by-step procedure. This particular procedure represents injection along the x-axis:

(i) Isolate the top and bottom layers in Figure 3.5 and determine the magnitude of pressure at the points between blocks 1 and 2, and 3 and 4, respectively, from applying Darcy's law in each layer separately.

(ii) Obtain the maximum transverse pressure by subtracting the expressions for the pressure values obtained in step (i).

(iii) Use the relationship between the total flow rate and the individual layer flow rates to eliminate flow rates from the expression obtained in step (ii).

(iv) Determine the average transverse pressure from geometric analysis as explained in Appendix E.

(v) Obtain the "global" pressure gradient ratio by multiplying the average transverse pressure by $\frac{L_x}{(\Delta p_x L_y)}$. This step eliminates pressure from the pressure gradient ratio expression.

"Local" pressure gradient ratios are calculated for two-block systems in series and parallel which subsequently are combined into parallel and series four-block

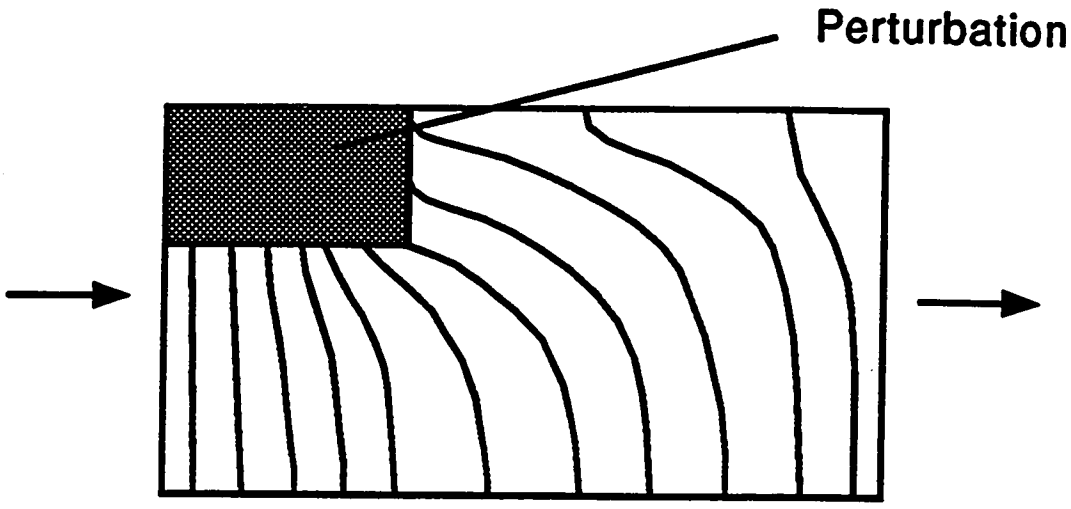

Fig. 3.10: Permeability Contrast Yielding a "Global" Non-Zero Transverse Pressure Gradient.

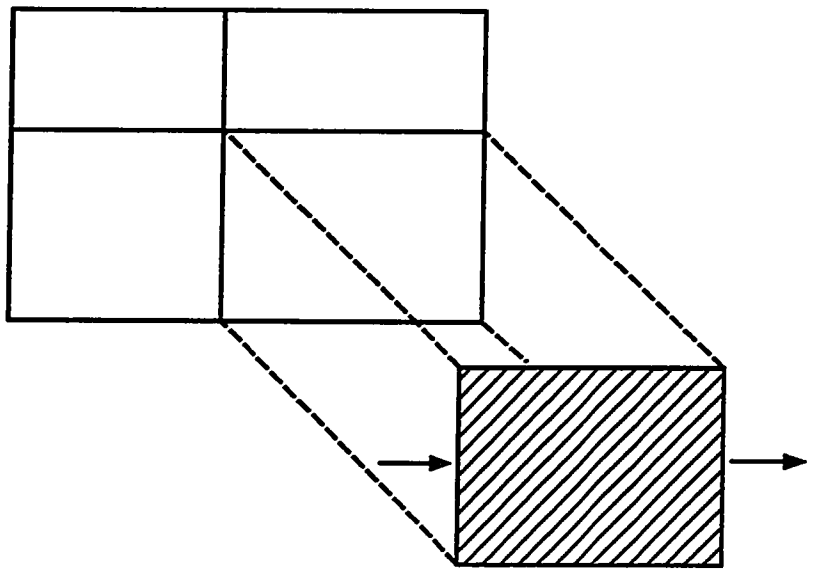

Fig. 3.11: Non-Zero Off-Diagonal Elements in Permeability Tensor of Local Grid Block Yielding "Local" Transverse Pressure Gradient.

"local" pressure gradient ratios, respectively. Details are found in Appendix F where the scenarios are analogous to those for $\tilde{k}_{x_{app}}$ and $\tilde{k}_{y_{app}}$ calculations.

Neither Appendix D nor Appendix F shows the cross-flow corrected "global" and "local" pressure gradient ratios or the combination of these two components. The cross-flow corrections are presented next.

The "global" pressure gradient ratio along the x-axis has the following cross-flow correction:

$$\left[\left(\frac{\partial\tilde{p}}{\partial y}\right)_X \Big/ \left(\frac{\partial\tilde{p}}{\partial x}\right)_X\right]_{global} = \frac{\left[\left(\frac{\partial\tilde{p}}{\partial y}\right)_X \Big/ \left(\frac{\partial\tilde{p}}{\partial x}\right)_X\right]_{iso.global}}{1+\frac{\tilde{k}_{y_{app}}}{\tilde{k}_{x_{app}}}}. \tag{3.23}$$

The isotropic "global" pressure gradient ratio on the right hand side of Eq. (3.23) has the following discrete form (Eq. (D28) in Appendix D):

$$\left[\left(\frac{\partial\tilde{p}}{\partial y}\right)_X \Big/ \left(\frac{\partial\tilde{p}}{\partial x}\right)_X\right]_{iso.global} = \left(\frac{\Delta p_{y_{avg}}}{\Delta p_x}\right)_X \frac{L_x}{L_y}$$

$$= \frac{1}{4\Delta y_2 L_y}\left(\hat{k}_{x_{app_b}}\Delta y_1 - \hat{k}_{x_{app_{tb}}}L_y\right)\left(\frac{\Delta x_2}{k_{x_{app_2}}} - \frac{\Delta x_1}{k_{x_{app_1}}}\right)$$

$$-\frac{1}{4\Delta y_1 L_y}\left(\hat{k}_{x_{app_t}}\Delta y_2 - \hat{k}_{x_{app_{tb}}}L_y\right)\left(\frac{\Delta x_2}{k_{x_{app_4}}} - \frac{\Delta x_1}{k_{x_{app_3}}}\right). \tag{3.24}$$

Similarly, the "global" pressure gradient ratio along the y-axis has the following cross-flow correction:

$$\left[\left(\frac{\partial\tilde{p}}{\partial x}\right)_Y \Big/ \left(\frac{\partial\tilde{p}}{\partial y}\right)_Y\right]_{global} = \frac{\left[\left(\frac{\partial\tilde{p}}{\partial x}\right)_Y \Big/ \left(\frac{\partial\tilde{p}}{\partial y}\right)_Y\right]_{iso.global}}{1+\frac{\tilde{k}_{x_{app}}}{\tilde{k}_{y_{app}}}}. \tag{3.25}$$

The isotropic "global" pressure gradient ratio on the right hand side of Eq. (3.25) has the following discrete form (Eq. (D56) in Appendix D):

$$\left[\left(\frac{\partial \tilde{p}}{\partial x}\right)_Y \Big/ \left(\frac{\partial \tilde{p}}{\partial y}\right)_Y\right]_{iso.global} = \left(\frac{\Delta p_{x_{avg}}}{\Delta p_y}\right)_Y \frac{L_y}{L_x}$$

$$= -\frac{1}{4\Delta x_2 L_x}\left(\hat{k}_{y_{app_f}}\Delta x_1 - \hat{k}_{y_{app_{fs}}}L_x\right)\left(\frac{\Delta y_1}{k_{y_{app_4}}} - \frac{\Delta y_2}{k_{y_{app_2}}}\right)$$

$$+\frac{1}{4\Delta x_1 L_x}\left(\hat{k}_{y_{app_s}}\Delta x_2 - \hat{k}_{y_{app_{fs}}}L_x\right)\left(\frac{\Delta y_1}{k_{y_{app_3}}} - \frac{\Delta y_2}{k_{y_{app_1}}}\right). \qquad (3.26)$$

The "local" pressure gradient ratio along x-axis has the following cross-flow correction:

$$\left[\left(\frac{\partial \tilde{p}}{\partial y}\right)_X \Big/ \left(\frac{\partial \tilde{p}}{\partial x}\right)_X\right]_{local}$$

$$= \frac{\tilde{k}_{x_{app}}\left[\left(\frac{\partial \tilde{p}}{\partial y}\right)_X \Big/ \left(\frac{\partial \tilde{p}}{\partial x}\right)_X\right]_{tb} + \tilde{k}_{y_{app}}\left[\left(\frac{\partial \tilde{p}}{\partial y}\right)_X \Big/ \left(\frac{\partial \tilde{p}}{\partial x}\right)_X\right]_{fs}}{\tilde{k}_{x_{app}} + \tilde{k}_{y_{app}}} \qquad (3.27)$$

where $\left[\left(\frac{\partial \tilde{p}}{\partial y}\right)_X \Big/ \left(\frac{\partial \tilde{p}}{\partial x}\right)_X\right]_{tb}$ and $\left[\left(\frac{\partial \tilde{p}}{\partial y}\right)_X \Big/ \left(\frac{\partial \tilde{p}}{\partial x}\right)_X\right]_{fs}$ are defined in Appendix F.

The "local" pressure gradient ratio along y-axis has the following cross-flow correction:

$$\left[\left(\frac{\partial \tilde{p}}{\partial x}\right)_Y \Big/ \left(\frac{\partial \tilde{p}}{\partial y}\right)_Y\right]_{local}$$

$$= \frac{\tilde{k}_{x_{app}}\left[\left(\frac{\partial \tilde{p}}{\partial x}\right)_Y \Big/ \left(\frac{\partial \tilde{p}}{\partial y}\right)_Y\right]_{fs} + \tilde{k}_{y_{app}}\left[\left(\frac{\partial \tilde{p}}{\partial x}\right)_Y \Big/ \left(\frac{\partial \tilde{p}}{\partial y}\right)_Y\right]_{tb}}{\tilde{k}_{x_{app}} + \tilde{k}_{y_{app}}} \qquad (3.28)$$

where $\left[\left(\frac{\partial \tilde{p}}{\partial x}\right)_Y \Big/ \left(\frac{\partial \tilde{p}}{\partial y}\right)_Y\right]_{fs}$ and $\left[\left(\frac{\partial \tilde{p}}{\partial x}\right)_Y \Big/ \left(\frac{\partial \tilde{p}}{\partial y}\right)_Y\right]_{tb}$ are defined in Appendix F.

Next, the "global" and the "local" contributions are combined to yield the overall or effective pressure gradient ratio:

$$\left(\frac{\partial \tilde{p}}{\partial y}\right)_X \Big/ \left(\frac{\partial \tilde{p}}{\partial x}\right)_X = \left[\left(\frac{\partial \tilde{p}}{\partial y}\right)_X \Big/ \left(\frac{\partial \tilde{p}}{\partial x}\right)_X\right]_{global} + \left[\left(\frac{\partial \tilde{p}}{\partial y}\right)_X \Big/ \left(\frac{\partial \tilde{p}}{\partial x}\right)_X\right]_{local} \tag{3.29}$$

$$\left(\frac{\partial \tilde{p}}{\partial x}\right)_Y \Big/ \left(\frac{\partial \tilde{p}}{\partial y}\right)_Y = \left[\left(\frac{\partial \tilde{p}}{\partial x}\right)_Y \Big/ \left(\frac{\partial \tilde{p}}{\partial y}\right)_Y\right]_{global} + \left[\left(\frac{\partial \tilde{p}}{\partial x}\right)_Y \Big/ \left(\frac{\partial \tilde{p}}{\partial y}\right)_Y\right]_{local}. \tag{3.30}$$

At this point, the apparent permeabilities and the overall pressure gradient ratios have been determined. Eqs. (3.5)-(3.8) can, therefore, be solved for the elements of the effective permeability tensor.

To summarize, the analytical effective permeability tensor method consists of four basic steps:

0. The grid block containing the small scale heterogeneous permeability field is divided into four quadrants or local blocks.

1. Determine the permeabilities along the principal directions and the orientation angle of k'_{xx} in each quadrant by calculating effective permeability along direction vectors between -90 and +90 degrees and deciding which direction results in the largest k'_{xx}/k'_{yy} ratio.

2. Calculate the effective permeability tensor in each quadrant by coordinate rotation.

3. Calculate the effective permeability tensor for the entire permeability field within the grid block by combining the effective permeability tensors obtained from each quadrant.

Numerical Method

To validate the analytical method presented for obtaining an effective permeability tensor, a numerical method is developed. This method is based on the steady-state, single-phase, incompressible version of the continuity equation:

$$\overline{\nabla} \cdot \overline{v} = 0. \tag{3.31}$$

Darcy's law is the constitutive equation used:

$$\overline{v} = -\frac{\mathbf{K}}{\mu} \overline{\nabla} p. \tag{3.32}$$

In Eqs. (3.31) and (3.32), $\overline{\nabla}$ is the divergence operator, $\overline{v}$ is the velocity vector, and $\mathbf{K}$ is the permeability tensor:

$$\mathbf{K} = \begin{pmatrix} k_{xx} & k_{xy} \\ k_{yx} & k_{yy} \end{pmatrix} \tag{3.33}$$

where k_{xx} and k_{yy} are the diagonal elements and k_{xy} and k_{yx} are the off-diagonal elements of the permeability tensor. μ is the fluid viscosity, and p represents pressure. Note that for a two-dimensional Cartesian coordinate system, the divergence operator is of the following form:

$$\overline{\nabla} = \frac{\partial}{\partial x}\bar{i} + \frac{\partial}{\partial y}\bar{j} \tag{3.34}$$

where $\bar{i}$ and $\bar{j}$ are unit vectors.

A finite element simulator[1] is used to solve Eqs. (3.31) and (3.32) for pressure and velocities. Two solutions are required to obtain all the elements of the effective permeability tensor. The first solution is obtained for a full face constant pressure gradient along the horizontal x-axis with closed upper and lower boundaries. The

following version of Eq. (3.32), assuming fluid viscosity of 1.0 cp, represents two equations and four unknowns, k_{xx}, k_{xy}, k_{yx}, and k_{yy}:

$$v_{xX} = -k_{xx}\left(\frac{\partial p}{\partial x}\right)_X - k_{xy}\left(\frac{\partial p}{\partial y}\right)_X \tag{3.35}$$

$$v_{yX} = -k_{yx}\left(\frac{\partial p}{\partial x}\right)_X - k_{yy}\left(\frac{\partial p}{\partial y}\right)_X . \tag{3.36}$$

Two additional equations are required to obtain all the elements of the permeability tensor. Therefore, the second solution is obtained for a constant pressure gradient along the vertical y-axis with closed left and right boundaries:

$$v_{xY} = -k_{xx}\left(\frac{\partial p}{\partial x}\right)_Y - k_{xy}\left(\frac{\partial p}{\partial y}\right)_Y \tag{3.37}$$

$$v_{yY} = -k_{yx}\left(\frac{\partial p}{\partial x}\right)_Y - k_{yy}\left(\frac{\partial p}{\partial y}\right)_Y . \tag{3.38}$$

v_{xX} and v_{xY} are velocity components in the x-direction for injection along x- and y-axis, respectively. v_{yX} and v_{yY} are the corresponding velocity components in the y-direction. $\left(\frac{\partial p}{\partial x}\right)_X$ and $\left(\frac{\partial p}{\partial x}\right)_Y$ are the pressure gradients in the x-direction for injection along x- and y-axis, respectively, whereas $\left(\frac{\partial p}{\partial y}\right)_X$ and $\left(\frac{\partial p}{\partial y}\right)_Y$ are the corresponding gradients in the y-direction.

In summary, effective pressure gradients and velocities are obtained from two solutions on the same small scale permeability field. One solution is obtained from injection along the x-axis and the other solution from injection along the y-axis. Eqs. (3.35)-(3.38) are then solved for the only unknowns, the elements of the effective permeability tensor, k_{xx}, k_{xy}, k_{yx}, and k_{yy}.

To summarize, this chapter showed how full effective permeability tensors can be developed using both analytical and numerical means. The next chapter shows how full tensor permeabilities can be incorporated in a numerical simulator.

CHAPTER IV
INCORPORATION OF FULL TENSOR PERMEABILITY IN A NUMERICAL RESERVOIR SIMULATOR

Most commercially available reservoir simulators are currently restricted to handle limited anisotropy, i.e., only the diagonal elements of the permeability tensor. However, some industry and research simulators have recently incorporated the general anisotropic model.[1,9,10,36,42]

Full tensor permeability can be incorporated in both finite difference and finite element simulators. A 9-point differencing scheme is required when using finite difference methods. The 9-point schemes are more computationally demanding, but reduce grid orientation effects compared to standard 5-point differencing schemes.[36,42,43]

This chapter will describe in some detail how to develop transmissibilities for point-centered 9-point schemes based on full tensor permeability. Finite element theory is used as a basis for this development.[44,45] The material presented in this chapter can, therefore, be useful in the development of both finite element and finite difference techniques that consider the full tensor form of absolute permeability. A second method is also presented. This method is based on satisfying Darcy's law and maximizing the range of positive transmissibilities.[42] The last section of this chapter shows how the two methods can be related.

Method 1 - Based on Finite Element Theory

The method presented in this section is to a large degree based on Young's study[44] which presents a relationship between finite element and finite difference methods. The development shown here extends Young's work to generally anisotropic permeability systems.

Single-phase, steady-state, incompressible flow is assumed as well as fluid viscosity of 1 cp to simplify derivations. The derivations are based on the continuity equation (pressure equation) without boundary conditions:

$$-\overline{\nabla} \cdot (\Lambda \overline{\nabla} p) = 0 \tag{4.1}$$

where

$$\Lambda = \begin{pmatrix} \lambda_{xx} & \lambda_{xy} \\ \lambda_{yx} & \lambda_{yy} \end{pmatrix} = \begin{pmatrix} k_{xx} & k_{xy} \\ k_{yx} & k_{yy} \end{pmatrix} h. \tag{4.2}$$

Λ is the mobility tensor, h is the thickness of the reservoir, k_{xx}, k_{xy}, k_{yx}, and k_{yy} are the elements of the permeability tensor, and p represents pressure.

For a two-dimensional areal Cartesian coordinate system, Eq. (4.1) can be expanded as follows:

$$-\frac{\partial}{\partial x}\left(\lambda_{xx}\frac{\partial p}{\partial x} + \lambda_{xy}\frac{\partial p}{\partial y}\right) - \frac{\partial}{\partial y}\left(\lambda_{yx}\frac{\partial p}{\partial x} + \lambda_{yy}\frac{\partial p}{\partial y}\right) = 0. \tag{4.3}$$

Using finite element theory, pressure can be approximated by a piecewise continuous Lagrange interpolating polynomial:

$$p \approx \sum_{i=1}^{nx}\sum_{j=1}^{ny} u_i(x) w_j(y) p_{ij} \tag{4.4}$$

where $u_i(x)$ and $w_j(y)$ are trial functions. Linear trial functions are shown in Figure 4.1. nx and ny represent the number of nodes or grid points in x- and y-direction, respectively. In the remaining derivations, the parentheses in Eq. (4.4) are dropped for notational convenience.

Differentiating pressure with respect to x and y in Eq. (4.4) yields:

$$\frac{\partial p}{\partial x} \approx \sum_{i=1}^{nx}\sum_{j=1}^{ny} \frac{du_i}{dx} w_j p_{ij} \tag{4.5}$$

$$\frac{\partial p}{\partial y} \approx \sum_{i=1}^{nx}\sum_{j=1}^{ny} u_i \frac{dw_j}{dy} p_{ij}. \tag{4.6}$$

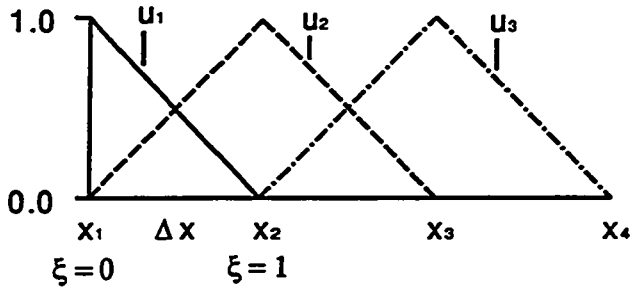

(a)

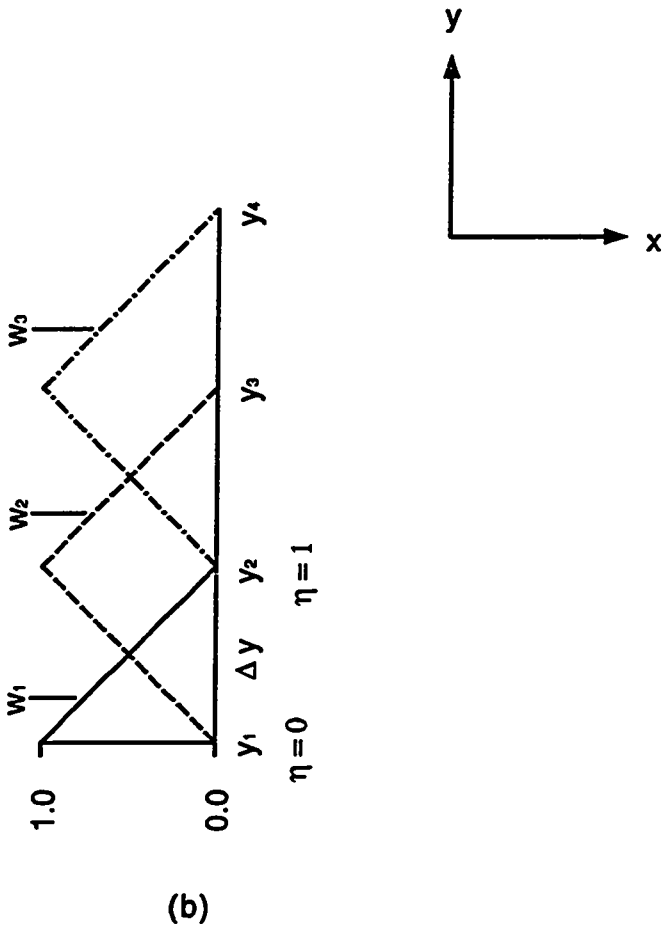

(b)

Fig. 4.1: Linear Trial Functions in (a) x-direction and (b) y-direction.

The first step is to write the residual equation. The residual, R, is the difference between the left hand side and the right hand side of the given equation which in this case is Eq. (4.3). Combining Eqs. (4.3), (4.5), and (4.6), the residual, R, can be written as follows:

$$R = \sum_{i=1}^{nx} \sum_{j=1}^{ny} [R_{xx} + R_{xy} + R_{yx} + R_{yy}] p_{ij} - 0 \tag{4.7}$$

where

$$R_{xx} = -w_j \frac{\partial}{\partial x} \left(\lambda_{xx} \frac{\partial u_i}{\partial x} \right) \tag{4.7b}$$

$$R_{xy} = -\frac{dw_j}{dy} \frac{\partial}{\partial x} (\lambda_{xy} u_i) \tag{4.7c}$$

$$R_{yx} = -\frac{du_i}{dx} \frac{\partial}{\partial y} (\lambda_{yx} w_j) \tag{4.7d}$$

$$R_{yy} = -u_i \frac{\partial}{\partial y} \left(\lambda_{yy} \frac{dw_j}{dy} \right). \tag{4.7e}$$

The Galerkin optimizing criterion is then applied to make R as small as possible for all values of x and y throughout the domain. Using the Galerkin criterion, a weighted average of R over the entire domain is required to be zero.[46] The weighting functions are the trial functions, u_k and w_ℓ:

$$\int_0^{L_y} \int_0^{L_x} u_k w_\ell R dx dy = 0, \quad k = 1, ..., nx; \ \ell = 1, ..., ny \tag{4.8}$$

where L_x and L_y are system lengths in x- and y-directions, respectively. Eq. (4.7) is substituted into Eq. (4.8) to give the following expression:

$$\sum_{i=1}^{nx} \sum_{j=1}^{ny} \int_0^{L_y} \int_0^{L_x} u_k w_\ell [R_{xx} + R_{xy} + R_{yx} + R_{yy}] p_{ij} dx dy = 0,$$
$$k = 1, ..., nx; \ \ell = 1, ..., ny. \tag{4.9}$$

The next step is to integrate by parts. First, apply the "chain rule" for differentiating the product of two functions:

$$-\frac{\partial}{\partial x}\left(\lambda_{xx}\frac{du_i}{dx}\right)u_k = -\left(\frac{\partial}{\partial x}\left(\lambda_{xx}\frac{du_i}{dx}u_k\right) - \left(\lambda_{xx}\frac{du_i}{dx}\right)\frac{du_k}{dx}\right) \tag{4.10}$$

$$-\frac{\partial}{\partial x}(\lambda_{xy}u_i)u_k = -\left(\frac{\partial}{\partial x}(\lambda_{xy}u_iu_k) - (\lambda_{xy}u_i)\frac{du_k}{dx}\right) \tag{4.11}$$

$$-\frac{\partial}{\partial y}(\lambda_{yx}w_j)w_\ell = -\left(\frac{\partial}{\partial y}(\lambda_{yx}w_jw_\ell) - (\lambda_{yx}w_j)\frac{dw_\ell}{dy}\right) \tag{4.12}$$

$$-\frac{\partial}{\partial y}\left(\lambda_{yy}\frac{dw_j}{dy}\right)w_\ell = -\left(\frac{\partial}{\partial y}\left(\lambda_{yy}\frac{dw_j}{dy}w_\ell\right) - \left(\lambda_{yy}\frac{dw_j}{dy}\right)\frac{dw_\ell}{dy}\right). \tag{4.13}$$

Substitute Eqs. (4.10)-(4.13) into Eq. (4.9):

$$\begin{aligned}&\sum_{i=1}^{nx}\sum_{j=1}^{ny}(G_{xx}+G_{xy}+G_{yx}+G_{yy})p_{ij}\\ &-\sum_{i=1}^{nx}\sum_{j=1}^{ny}(G_{xx_b}+G_{xy_b}+G_{yx_b}+G_{yy_b})p_{ij}=0,\\ &\qquad k=1,...,nx;\ \ \ell=1,...,ny\end{aligned} \tag{4.14}$$

where

$$G_{xx} = \int_0^{L_y}\int_0^{L_x}\lambda_{xx}\frac{du_i}{dx}w_j\frac{du_k}{dx}w_\ell dxdy \tag{4.14b}$$

$$G_{xy} = \int_0^{L_y}\int_0^{L_x}\lambda_{xy}u_i\frac{dw_j}{dy}\frac{du_k}{dx}w_\ell dxdy \tag{4.14c}$$

$$G_{yx} = \int_0^{L_y}\int_0^{L_x}\lambda_{yx}\frac{du_i}{dx}w_ju_k\frac{dw_\ell}{dy}dxdy \tag{4.14d}$$

$$G_{yy} = \int_0^{L_y}\int_0^{L_x} \lambda_{yy} u_i \frac{dw_j}{dy} u_k \frac{dw_\ell}{dy} dx dy \tag{4.14e}$$

$$G_{xx_b} = \int_0^{L_y}\int_0^{L_x} w_j w_\ell \frac{\partial}{\partial x}\left(\lambda_{xx}\frac{du_i}{dx}u_k\right) dx dy \tag{4.14f}$$

$$G_{xy_b} = \int_0^{L_y}\int_0^{L_x} \frac{dw_j}{dy} w_\ell \frac{\partial}{\partial x}\left(\lambda_{xy} u_i u_k\right) dx dy \tag{4.14g}$$

$$G_{yx_b} = \int_0^{L_y}\int_0^{L_x} \frac{du_i}{dx} u_k \frac{\partial}{\partial y}\left(\lambda_{yx} w_j w_\ell\right) dx dy \tag{4.14h}$$

$$G_{yy_b} = \int_0^{L_y}\int_0^{L_x} u_i u_k \frac{\partial}{\partial y}\left(\lambda_{yy}\frac{dw_j}{dy}w_\ell\right) dx dy. \tag{4.14i}$$

The second part of Eq. (4.14) can be represented as a line integral around all external and internal (well) boundaries.

Although not directly related to the development of transmissibilities, the development of the line integral term is presented for completeness.

The reduction of the second part of Eq. (4.14) into a line integral is accomplished using the 2-D divergence theorem which is a corollary to Green's theorem for line integrals.[46] For a two-dimensional domain, Ω, the divergence theorem may be written as follows:

$$\int\int_\Omega \overline{\nabla}\cdot\overline{\Psi} dx dy = \oint_{\partial\Omega} \overline{\Psi}\cdot\overline{n} d\Omega. \tag{4.15}$$

If $\overline{\Psi} = F\vec{i} + G\vec{j}$, where $\overline{\Psi}$ is a general vector and F and G are x and y components of the vector, then Eq. (4.15) can be written as:

$$\int\int_\Omega \left(\frac{\partial F}{\partial x} + \frac{\partial G}{\partial y}\right) dx dy = \oint_{\partial\Omega} \left(F n_x + G n_y\right) d\Omega \tag{4.16}$$

where n_x and n_y are the x- and y-components of the outward unit normal vector, $\overline{n}$, of the domain Ω. If Eq. (4.16) is applied to the second part of Eq. (4.14), the following line integral can be written:

$$-\sum_{i=1}^{nx}\sum_{j=1}^{ny}(L_{xx}+L_{xy}+L_{yx}+L_{yy})\,p_{ij}d\Omega, \quad k=1,...,nx;\ \ell=1,...,ny \tag{4.17}$$

where

$$L_{xx}=\oint_{\partial\Omega} w_j w_\ell \lambda_{xx}\frac{du_i}{dx}u_k n_x \tag{4.17b}$$

$$L_{xy}=\oint_{\partial\Omega} \frac{dw_j}{dy}w_\ell \lambda_{xy}u_i u_k n_x \tag{4.17c}$$

$$L_{yx}=\oint_{\partial\Omega} \frac{du_i}{dx}u_k \lambda_{yx}w_j w_\ell n_y \tag{4.17d}$$

$$L_{yy}=\oint_{\partial\Omega} u_i u_k \lambda_{yy}\frac{dw_j}{dy}w_\ell n_y. \tag{4.17e}$$

Eq. (4.17) can be rewritten using Eqs. (4.5) and (4.6):

$$-\oint_{\partial\Omega} u_k w_\ell \left[\left(\lambda_{xx}\frac{\partial p}{\partial x}+\lambda_{xy}\frac{\partial p}{\partial y}\right)n_x+\left(\lambda_{yx}\frac{\partial p}{\partial x}+\lambda_{yy}\frac{\partial p}{\partial y}\right)n_y\right]d\Omega,$$
$$k=1,...,nx;\ \ell=1,...,ny. \tag{4.18}$$

Eq. (4.18) can be condensed as follows:

$$-\oint_{\partial\Omega} u_k w_\ell \left(\Lambda\overline{\nabla}p\right)\cdot\overline{n}d\Omega. \tag{4.19}$$

Using Eq. (4.19), Eq. (4.14) has the following form:

$$\sum_{i=1}^{nx}\sum_{j=1}^{ny}(G_{xx}+G_{xy}+G_{yx}+G_{yy})p_{ij}$$
$$=\oint_{\partial\Omega}u_k w_\ell(\Lambda\overline{\nabla}p)\cdot\overline{n}d\Omega,$$
$$k=1,...,nx;\ \ \ell=1,...,ny. \tag{4.20}$$

Eq. (4.20) is the basis for solving Eq. (4.1) using finite element analysis. The next step in the finite element approach would be to decide on specific expressions for the trial functions. These expressions are dependent on the choice of the finite element regarding shape (triangular or quadrilateral) and number of nodes (type of polynomial; linear, quadratic, etc.). Details about the general procedure of solving an expression like Eq. (4.20) can be found in Reference 46.

The remainder of this chapter deals with the use of Eq. (4.20) in the development of transmissibilities for a 9-point finite difference scheme.

Figure 4.2 shows a quadrilateral element with a node in each corner. This element is labeled with the transmissibilities to be derived. T_{x1}, T_{x2}, T_{y1}, and T_{y2} represent one-sided edge transmissibilities and are added to neighboring element transmissibilities to yield total transmissibility values. T_{xy1} and T_{xy2} are diagonal transmissibilities and represent total values. In Figure 4.3, it is shown how an element mesh is superimposed on a point-centered grid.

For simplicity in subsequent derivations, Eq. (4.4) will be written in terms of trial functions that are based on dimensionless coordinates.[45] For a single element, Eq. (4.4) can be written as follows:

$$p\approx\sum_{i=1}^{2}\sum_{j=1}^{2}U_i(\xi)W_j(\eta)p_{ij} \tag{4.21}$$

where

$$\xi=\frac{x-x_1}{x_2-x_1} \tag{4.22}$$

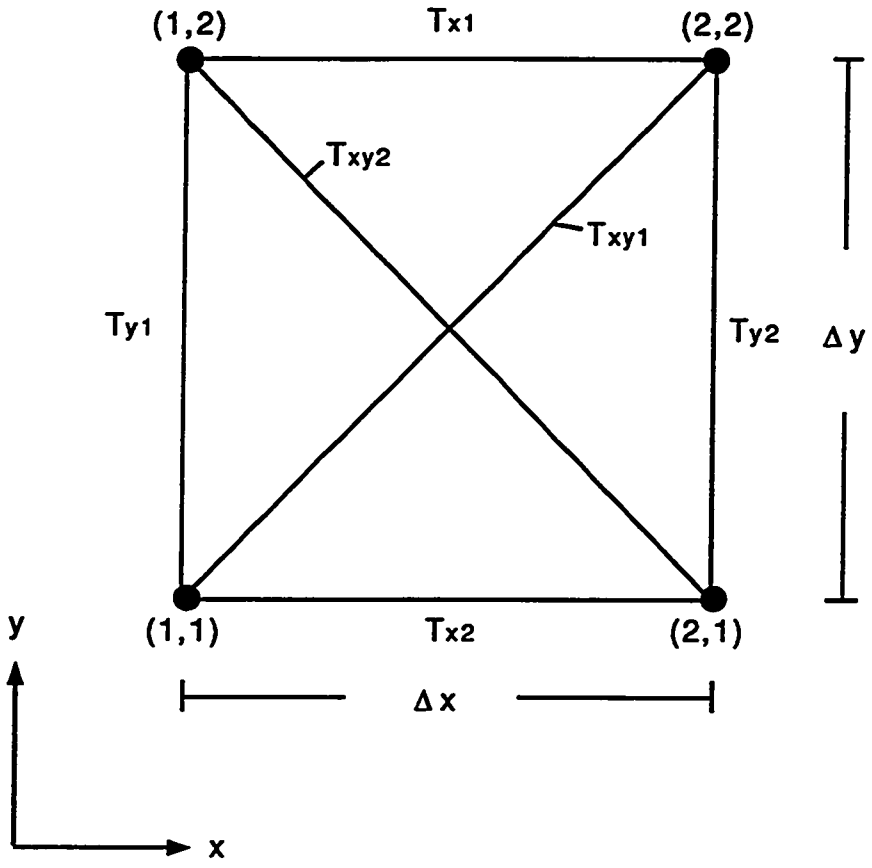

Fig. 4.2: Quadrilateral Element With Labeled Transmissibilities.

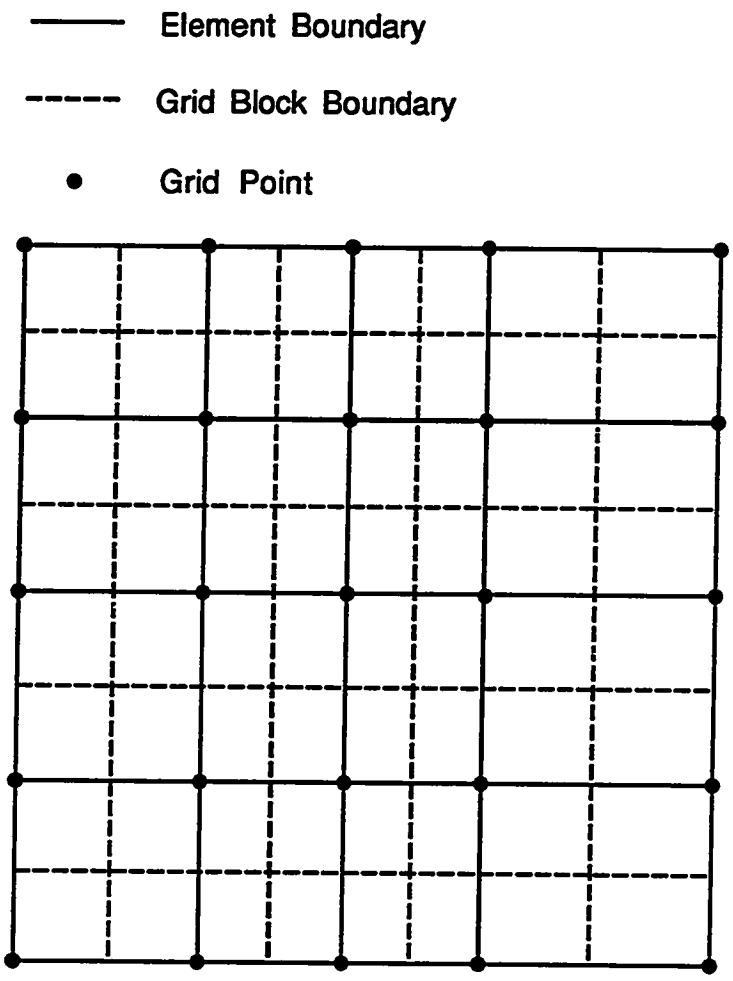

Fig. 4.3: Element Mesh Superimposed on Point-Centered Grid.[45]

$$\eta = \frac{y - y_1}{y_2 - y_1}. \tag{4.23}$$

Differentiating Eqs. (4.22) and (4.23) and rearranging gives the following expressions:

$$dx = (x_2 - x_1)\, d\xi = \Delta x d\xi \tag{4.24}$$

$$dy = (y_2 - y_1)\, d\eta = \Delta y d\eta. \tag{4.25}$$

From analyzing the trial functions in Figure 4.1 for the first element, the corresponding dimensionless trial functions and their first derivatives can be expressed as follows:

$$U_1(\xi) = 1 - \xi \tag{4.26}$$

$$U_2(\xi) = \xi \tag{4.27}$$

$$W_1(\eta) = 1 - \eta \tag{4.28}$$

$$W_2(\eta) = \eta \tag{4.29}$$

$$U_1'(\xi) = -1 \tag{4.30}$$

$$U_2'(\xi) = 1 \tag{4.31}$$

$$W_1'(\eta) = -1 \tag{4.32}$$

$$W_2'(\eta) = 1. \tag{4.33}$$

Using Eqs. (4.24) and (4.25), the derivative of the trial functions can be written as:

$$\frac{du_i}{dx} = \frac{d(U_i(\xi))}{dx} = \frac{d(U_i(\xi))}{\Delta x d\xi} \tag{4.34}$$

$$\frac{dw_j}{dy} = \frac{d(W_j(\eta))}{dy} = \frac{d(W_j(\eta))}{\Delta y d\eta}. \tag{4.35}$$

In Eq. (4.21), it is shown how pressure is represented using bilinear interpolation. The mobility elements (λ_{xx}, λ_{xy}, λ_{yx}, and λ_{yy}) may each be represented in a similar manner:

$$\begin{aligned}\lambda(\xi,\eta) \approx & \sum_{i=1}^{2}\sum_{j=1}^{2} U_i(\xi)W_j(\eta)\lambda_{ij} \\ =& U_1(\xi)W_1(\eta)\lambda_{1,1} + U_2(\xi)W_1(\eta)\lambda_{2,1} + U_1(\xi)W_2(\eta)\lambda_{1,2} + U_2(\xi)W_2(\eta)\lambda_{2,2} \\ =& (1-\xi)(1-\eta)\lambda_{1,1} + \xi(1-\eta)\lambda_{2,1} + (1-\xi)\eta\lambda_{1,2} + \xi\eta\lambda_{2,2}. \end{aligned} \tag{4.36}$$

In substituting Eqs. (4.24), (4.25), (4.34), and (4.35) into Eq. (4.20), the following expression can be obtained representing a general transmissibility coefficient:

$$\begin{aligned} B_{ijkl} =& \frac{\Delta y}{\Delta x}\int_0^1\int_0^1 \lambda_{xx}(\xi,\eta)U_i'(\xi)U_k'(\xi)W_j(\eta)W_l(\eta)d\xi d\eta \\ &+ \int_0^1\int_0^1 \lambda_{xy}(\xi,\eta)U_i(\xi)U_k'(\xi)W_j'(\eta)W_l(\eta)d\xi d\eta \\ &+ \int_0^1\int_0^1 \lambda_{yx}(\xi,\eta)U_i'(\xi)U_k(\xi)W_j(\eta)W_l'(\eta)d\xi d\eta \\ &+ \frac{\Delta x}{\Delta y}\int_0^1\int_0^1 \lambda_{yy}(\xi,\eta)U_i(\xi)U_k(\xi)W_j'(\eta)W_l'(\eta)d\xi d\eta. \end{aligned} \tag{4.37}$$

The following transmissibility coefficients can be written based on Figure 4.2 and Eq. (4.37):

$$T_{x1} = -B_{1222} = -B_{2212} \tag{4.38}$$

$$T_{x2} = -B_{1121} = -B_{2111} \tag{4.39}$$

$$T_{y1} = -B_{1112} = -B_{1211} \tag{4.40}$$

$$T_{y2} = -B_{2122} = -B_{2221} \tag{4.41}$$

$$T_{xy1} = -B_{1122} = -B_{2211} \tag{4.42}$$

$$T_{xy2} = -B_{2112} = -B_{1221}. \tag{4.43}$$

Numerical integration is necessary to evaluate the integrals in Eq. (4.37). The Lobatto integration method is used here. It reduces to the trapezoidal rule for two evaluation points and Simpson's rule for three evaluation points.[44] Reference 47 shows how the weights are determined. A general parameter, ω, can be obtained based on the weights obtained from two- and three-point evaluations. The resulting general formula may be expressed as follows:

$$\int_0^1 f(x)dx = \omega f(\frac{1}{2}) + \frac{1}{2}(1-\omega)\,[f(0) + f(1)] \tag{4.44}$$

where $\omega = 0$ reduces Eq. (4.44) to the trapezoidal rule, $\omega = \frac{2}{3}$ corresponds to Simpson's rule, and $\omega = 1$ yields the midpoint rule. Using Eq. (4.44) and Eqs. (4.26)-(4.33), Eq. (4.37) may be evaluated to obtain the desired transmissibilities. The expressions for these transmissibilities are presented next. The development of

T_{x1} is shown in detail. In the following four equations, each integral in Eq. (4.37) is evaluated separately:

$$B_{1222}^{xx} = \frac{\Delta y}{\Delta x} \int_0^1 W_2(\eta) W_2(\eta) \left[\int_0^1 \lambda_{xx}(\xi, \eta) U_1'(\xi) U_2'(\xi) d\xi \right] d\eta. \qquad (4.45)$$

The integral within the square brackets in Eq. (4.45) can be evaluated using Eqs. (4.36) and (4.44) as follows:

$$\omega \left[\left(\frac{1}{2}(1-\eta)\lambda_{xx_{1,1}} + \frac{1}{2}(1-\eta)\lambda_{xx_{2,1}} + \frac{1}{2}\eta\lambda_{xx_{1,2}} + \frac{1}{2}\eta\lambda_{xx_{2,2}} \right)(-1)(1) \right]$$
$$+\frac{1}{2}(1-\omega)\left[\left((1-\eta)\lambda_{xx_{1,1}} + \eta\lambda_{xx_{1,2}} \right)(-1)(1) + \left((1-\eta)\lambda_{xx_{2,1}} + \eta\lambda_{xx_{2,2}} \right)(-1)(1) \right]$$
$$= -\frac{1}{2}(1-\eta)\lambda_{xx_{1,1}} - \frac{1}{2}\eta\lambda_{xx_{1,2}} - \frac{1}{2}(1-\eta)\lambda_{xx_{2,1}} - \frac{1}{2}\eta\lambda_{xx_{2,2}}. \qquad (4.45b)$$

Substituting Eq. (4.45b) into Eq. (4.45) yields the following intermediate result:

$$B_{1222}^{xx} = -\frac{\Delta y}{\Delta x} \int_0^1 W_2(\eta) W_2(\eta) \left[\frac{1}{2}(1-\eta)(\lambda_{xx_{1,1}} + \lambda_{xx_{2,1}}) + \frac{1}{2}\eta(\lambda_{xx_{1,2}} + \lambda_{xx_{2,2}}) \right] d\eta. \qquad (4.45c)$$

Numerically integrating the integral in Eq. (4.45c) using Eq. (4.44) produces the following expression:

$$\omega \left[\left(-\frac{1}{4}\lambda_{xx_{1,1}} - \frac{1}{4}\lambda_{xx_{2,1}} - \frac{1}{4}\lambda_{xx_{1,2}} - \frac{1}{4}\lambda_{xx_{2,2}} \right)\left(\frac{1}{2}\right)\left(\frac{1}{2}\right) \right]$$
$$+\frac{1}{2}(1-\omega)\left[\left(-\frac{1}{2}\lambda_{xx_{1,1}} - \frac{1}{2}\lambda_{xx_{2,1}} \right)(0)(0) + \left(-\frac{1}{2}\lambda_{xx_{1,2}} - \frac{1}{2}\lambda_{xx_{2,2}} \right)(1)(1) \right]. \qquad (4.45d)$$

Substituting Eq. (4.45d) into Eq. (4.45c) yields the following expression for B_{1222}^{xx}:

$$B_{1222}^{xx} = \frac{1}{4}(\omega-1)(\lambda_{xx_{1,2}} + \lambda_{xx_{2,2}})\frac{\Delta y}{\Delta x} - \frac{1}{16}\omega(\lambda_{xx_{1,1}} + \lambda_{xx_{2,1}} + \lambda_{xx_{1,2}} + \lambda_{xx_{2,2}})\frac{\Delta y}{\Delta x}. \tag{4.45e}$$

The other integrals in Eq. (4.37) are evaluated in a similar manner:

$$\begin{aligned} B_{1222}^{xy} &= \int_0^1 W_2'(\eta)W_2(\eta)\left[\int_0^1 \lambda_{xy}(\xi,\eta)U_1(\xi)U_2'(\xi)d\xi\right]d\eta \\ &= \frac{1}{4}(\frac{1}{2}\omega-1)^2\lambda_{xy_{1,2}} - \frac{1}{8}(\frac{1}{2}\omega-1)\omega(\lambda_{xy_{1,1}} + \lambda_{xy_{2,2}}) + \frac{1}{16}\omega^2\lambda_{xy_{2,1}} \end{aligned} \tag{4.46}$$

$$\begin{aligned} B_{1222}^{yx} &= \int_0^1 W_2(\eta)W_2'(\eta)\left[\int_0^1 \lambda_{yx}(\xi,\eta)U_1'(\xi)U_2(\xi)d\xi\right]d\eta \\ &= -\frac{1}{4}(\frac{1}{2}\omega-1)^2\lambda_{yx_{2,2}} + \frac{1}{8}(\frac{1}{2}\omega-1)\omega(\lambda_{yx_{2,1}} + \lambda_{yx_{1,2}}) - \frac{1}{16}\omega^2\lambda_{yx_{1,1}} \end{aligned} \tag{4.47}$$

$$\begin{aligned} B_{1222}^{yy} &= \frac{\Delta x}{\Delta y}\int_0^1 W_2'(\eta)W_2'(\eta)\left[\int_0^1 \lambda_{yy}(\xi,\eta)U_1(\xi)U_2(\xi)d\xi\right]d\eta \\ &= \frac{1}{16}\omega(\lambda_{yy_{1,1}} + \lambda_{yy_{2,1}} + \lambda_{yy_{1,2}} + \lambda_{yy_{2,2}})\frac{\Delta x}{\Delta y}. \end{aligned} \tag{4.48}$$

Combining Eqs. (4.45e)-(4.48) yields:

$$\begin{aligned} B_{1222} &= B_{1222}^{xx} + B_{1222}^{xy} + B_{1222}^{yx} + B_{1222}^{yy} \\ &= \frac{1}{4}(\omega-1)(\lambda_{xx_{1,2}} + \lambda_{xx_{2,2}})\frac{\Delta y}{\Delta x} - \frac{1}{16}\omega(\lambda_{xx_{1,1}} + \lambda_{xx_{2,1}} + \lambda_{xx_{1,2}} + \lambda_{xx_{2,2}})\frac{\Delta y}{\Delta x} \\ &\quad + \frac{1}{4}(\frac{1}{2}\omega-1)^2\lambda_{xy_{1,2}} - \frac{1}{8}(\frac{1}{2}\omega-1)\omega(\lambda_{xy_{1,1}} + \lambda_{xy_{2,2}}) + \frac{1}{16}\omega^2\lambda_{xy_{2,1}} \\ &\quad - \frac{1}{4}(\frac{1}{2}\omega-1)^2\lambda_{yx_{2,2}} + \frac{1}{8}(\frac{1}{2}\omega-1)\omega(\lambda_{yx_{2,1}} + \lambda_{yx_{1,2}}) - \frac{1}{16}\omega^2\lambda_{yx_{1,1}} \\ &\quad + \frac{1}{16}\omega(\lambda_{yy_{1,1}} + \lambda_{yy_{2,1}} + \lambda_{yy_{1,2}} + \lambda_{yy_{2,2}})\frac{\Delta x}{\Delta y}. \end{aligned} \tag{4.49}$$

The transmissibility coefficient T_{x1} can, therefore, be expressed as follows:

$$
\begin{aligned}
T_{x1} =& - B_{1222} \\
=& - \frac{1}{4}(\omega-1)(\lambda_{xx_{1,2}} + \lambda_{xx_{2,2}})\frac{\Delta y}{\Delta x} + \frac{1}{16}\omega(\lambda_{xx_{1,1}} + \lambda_{xx_{2,1}} + \lambda_{xx_{1,2}} + \lambda_{xx_{2,2}})\frac{\Delta y}{\Delta x} \\
& - \frac{1}{4}(\frac{1}{2}\omega-1)^2\lambda_{xy_{1,2}} + \frac{1}{8}(\frac{1}{2}\omega-1)\omega(\lambda_{xy_{1,1}} + \lambda_{xy_{2,2}}) - \frac{1}{16}\omega^2\lambda_{xy_{2,1}} \\
& + \frac{1}{4}(\frac{1}{2}\omega-1)^2\lambda_{yx_{2,2}} - \frac{1}{8}(\frac{1}{2}\omega-1)\omega(\lambda_{yx_{2,1}} + \lambda_{yx_{1,2}}) + \frac{1}{16}\omega^2\lambda_{yx_{1,1}} \\
& - \frac{1}{16}\omega(\lambda_{yy_{1,1}} + \lambda_{yy_{2,1}} + \lambda_{yy_{1,2}} + \lambda_{yy_{2,2}})\frac{\Delta x}{\Delta y}. \qquad (4.50)
\end{aligned}
$$

The other transmissibility coefficients are derived in a similar manner. their final expressions are as follows:

$$
\begin{aligned}
T_{x2} =& - B_{1121} \\
=& - \frac{1}{4}(\omega-1)(\lambda_{xx_{1,1}} + \lambda_{xx_{2,1}})\frac{\Delta y}{\Delta x} + \frac{1}{16}\omega(\lambda_{xx_{1,1}} + \lambda_{xx_{2,1}} + \lambda_{xx_{1,2}} + \lambda_{xx_{2,2}})\frac{\Delta y}{\Delta x} \\
& + \frac{1}{4}(\frac{1}{2}\omega-1)^2\lambda_{xy_{1,1}} - \frac{1}{8}(\frac{1}{2}\omega-1)\omega(\lambda_{xy_{2,1}} + \lambda_{xy_{1,2}}) + \frac{1}{16}\omega^2\lambda_{xy_{2,2}} \\
& - \frac{1}{4}(\frac{1}{2}\omega-1)^2\lambda_{yx_{2,1}} + \frac{1}{8}(\frac{1}{2}\omega-1)\omega(\lambda_{yx_{1,1}} + \lambda_{yx_{2,2}}) - \frac{1}{16}\omega^2\lambda_{yx_{1,2}} \\
& - \frac{1}{16}\omega(\lambda_{yy_{1,1}} + \lambda_{yy_{2,1}} + \lambda_{yy_{1,2}} + \lambda_{yy_{2,2}})\frac{\Delta x}{\Delta y} \qquad (4.51)
\end{aligned}
$$

$$
\begin{aligned}
T_{y1} =& - B_{1112} \\
=& - \frac{1}{4}(\omega-1)(\lambda_{yy_{1,1}} + \lambda_{yy_{1,2}})\frac{\Delta x}{\Delta y} + \frac{1}{16}\omega(\lambda_{yy_{1,1}} + \lambda_{yy_{2,1}} + \lambda_{yy_{1,2}} + \lambda_{yy_{2,2}})\frac{\Delta x}{\Delta y} \\
& - \frac{1}{4}(\frac{1}{2}\omega-1)^2\lambda_{xy_{1,2}} + \frac{1}{8}(\frac{1}{2}\omega-1)\omega(\lambda_{xy_{1,1}} + \lambda_{xy_{2,2}}) - \frac{1}{16}\omega^2\lambda_{xy_{2,1}} \\
& + \frac{1}{4}(\frac{1}{2}\omega-1)^2\lambda_{yx_{1,1}} - \frac{1}{8}(\frac{1}{2}\omega-1)\omega(\lambda_{yx_{2,1}} + \lambda_{yx_{1,2}}) + \frac{1}{16}\omega^2\lambda_{yx_{2,2}} \\
& - \frac{1}{16}\omega(\lambda_{xx_{1,1}} + \lambda_{xx_{2,1}} + \lambda_{xx_{1,2}} + \lambda_{xx_{2,2}})\frac{\Delta y}{\Delta x} \qquad (4.52)
\end{aligned}
$$

$$
\begin{aligned}
T_{y2} &= -B_{2122} \\
&= -\frac{1}{4}(\omega-1)(\lambda_{yy_{2,1}}+\lambda_{yy_{2,2}})\frac{\Delta x}{\Delta y}+\frac{1}{16}\omega(\lambda_{yy_{1,1}}+\lambda_{yy_{2,1}}+\lambda_{yy_{1,2}}+\lambda_{yy_{2,2}})\frac{\Delta x}{\Delta y} \\
&\quad +\frac{1}{4}(\frac{1}{2}\omega-1)^2\lambda_{xy_{2,2}}-\frac{1}{8}(\frac{1}{2}\omega-1)\omega(\lambda_{xy_{2,1}}+\lambda_{xy_{1,2}})+\frac{1}{16}\omega^2\lambda_{xy_{1,1}} \\
&\quad -\frac{1}{4}(\frac{1}{2}\omega-1)^2\lambda_{yx_{2,1}}+\frac{1}{8}(\frac{1}{2}\omega-1)\omega(\lambda_{yx_{1,1}}+\lambda_{yx_{2,2}})-\frac{1}{16}\omega^2\lambda_{yx_{1,2}} \\
&\quad -\frac{1}{16}\omega(\lambda_{xx_{1,1}}+\lambda_{xx_{2,1}}+\lambda_{xx_{1,2}}+\lambda_{xx_{2,2}})\frac{\Delta y}{\Delta x} \qquad (4.53)
\end{aligned}
$$

$$
\begin{aligned}
T_{xy1} &= -B_{1122} \\
&= \frac{1}{16}\omega(\lambda_{xx_{1,1}}+\lambda_{xx_{2,1}}+\lambda_{xx_{1,2}}+\lambda_{xx_{2,2}})\frac{\Delta y}{\Delta x} \\
&\quad +\frac{1}{4}(\frac{1}{2}\omega-1)^2\lambda_{xy_{1,2}}-\frac{1}{8}(\frac{1}{2}\omega-1)\omega(\lambda_{xy_{1,1}}+\lambda_{xy_{2,2}})+\frac{1}{16}\omega^2\lambda_{xy_{2,1}} \\
&\quad +\frac{1}{4}(\frac{1}{2}\omega-1)^2\lambda_{yx_{2,1}}-\frac{1}{8}(\frac{1}{2}\omega-1)\omega(\lambda_{yx_{1,1}}+\lambda_{yx_{2,2}})+\frac{1}{16}\omega^2\lambda_{yx_{1,2}} \\
&\quad +\frac{1}{16}\omega(\lambda_{yy_{1,1}}+\lambda_{yy_{2,1}}+\lambda_{yy_{1,2}}+\lambda_{yy_{2,2}})\frac{\Delta x}{\Delta y} \qquad (4.54)
\end{aligned}
$$

$$
\begin{aligned}
T_{xy2} &= -B_{2112} \\
&= \frac{1}{16}\omega(\lambda_{xx_{1,1}}+\lambda_{xx_{2,1}}+\lambda_{xx_{1,2}}+\lambda_{xx_{2,2}})\frac{\Delta y}{\Delta x} \\
&\quad -\frac{1}{4}(\frac{1}{2}\omega-1)^2\lambda_{xy_{2,2}}+\frac{1}{8}(\frac{1}{2}\omega-1)\omega(\lambda_{xy_{2,1}}+\lambda_{xy_{1,2}})-\frac{1}{16}\omega^2\lambda_{xy_{1,1}} \\
&\quad -\frac{1}{4}(\frac{1}{2}\omega-1)^2\lambda_{yx_{1,1}}+\frac{1}{8}(\frac{1}{2}\omega-1)\omega(\lambda_{yx_{2,1}}+\lambda_{yx_{1,2}})-\frac{1}{16}\omega^2\lambda_{yx_{2,2}} \\
&\quad +\frac{1}{16}\omega(\lambda_{yy_{1,1}}+\lambda_{yy_{2,1}}+\lambda_{yy_{1,2}}+\lambda_{yy_{2,2}})\frac{\Delta x}{\Delta y}. \qquad (4.55)
\end{aligned}
$$

Transmissibilities calculated for the opposite directions to those listed above are as follows:

$$
\begin{aligned}
T_{x1} &= -B_{2212} \\
&= -\frac{1}{4}(\omega-1)(\lambda_{xx_{1,2}}+\lambda_{xx_{2,2}})\frac{\Delta y}{\Delta x}+\frac{1}{16}\omega(\lambda_{xx_{1,1}}+\lambda_{xx_{2,1}}+\lambda_{xx_{1,2}}+\lambda_{xx_{2,2}})\frac{\Delta y}{\Delta x} \\
&\quad +\frac{1}{4}(\frac{1}{2}\omega-1)^2\lambda_{xy_{2,2}}-\frac{1}{8}(\frac{1}{2}\omega-1)\omega(\lambda_{xy_{2,1}}+\lambda_{xy_{1,2}})+\frac{1}{16}\omega^2\lambda_{xy_{1,1}} \\
&\quad -\frac{1}{4}(\frac{1}{2}\omega-1)^2\lambda_{yx_{1,2}}+\frac{1}{8}(\frac{1}{2}\omega-1)\omega(\lambda_{yx_{1,1}}+\lambda_{yx_{2,2}})-\frac{1}{16}\omega^2\lambda_{yx_{2,1}} \\
&\quad -\frac{1}{16}\omega(\lambda_{yy_{1,1}}+\lambda_{yy_{2,1}}+\lambda_{yy_{1,2}}+\lambda_{yy_{2,2}})\frac{\Delta x}{\Delta y}
\end{aligned}
\tag{4.56}
$$

$$
\begin{aligned}
T_{x2} &= -B_{2111} \\
&= -\frac{1}{4}(\omega-1)(\lambda_{xx_{1,1}}+\lambda_{xx_{2,1}})\frac{\Delta y}{\Delta x}+\frac{1}{16}\omega(\lambda_{xx_{1,1}}+\lambda_{xx_{2,1}}+\lambda_{xx_{1,2}}+\lambda_{xx_{2,2}})\frac{\Delta y}{\Delta x} \\
&\quad -\frac{1}{4}(\frac{1}{2}\omega-1)^2\lambda_{xy_{2,1}}+\frac{1}{8}(\frac{1}{2}\omega-1)\omega(\lambda_{xy_{1,1}}+\lambda_{xy_{2,2}})-\frac{1}{16}\omega^2\lambda_{xy_{1,2}} \\
&\quad +\frac{1}{4}(\frac{1}{2}\omega-1)^2\lambda_{yx_{1,1}}-\frac{1}{8}(\frac{1}{2}\omega-1)\omega(\lambda_{yx_{2,1}}+\lambda_{yx_{1,2}})+\frac{1}{16}\omega^2\lambda_{yx_{2,2}} \\
&\quad -\frac{1}{16}\omega(\lambda_{yy_{1,1}}+\lambda_{yy_{2,1}}+\lambda_{yy_{1,2}}+\lambda_{yy_{2,2}})\frac{\Delta x}{\Delta y}
\end{aligned}
\tag{4.57}
$$

$$
\begin{aligned}
T_{y1} &= -B_{1211} \\
&= -\frac{1}{4}(\omega-1)(\lambda_{yy_{1,1}}+\lambda_{yy_{1,2}})\frac{\Delta x}{\Delta y}+\frac{1}{16}\omega(\lambda_{yy_{1,1}}+\lambda_{yy_{2,1}}+\lambda_{yy_{1,2}}+\lambda_{yy_{2,2}})\frac{\Delta x}{\Delta y} \\
&\quad +\frac{1}{4}(\frac{1}{2}\omega-1)^2\lambda_{xy_{1,1}}-\frac{1}{8}(\frac{1}{2}\omega-1)\omega(\lambda_{xy_{2,1}}+\lambda_{xy_{1,2}})+\frac{1}{16}\omega^2\lambda_{xy_{2,2}} \\
&\quad -\frac{1}{4}(\frac{1}{2}\omega-1)^2\lambda_{yx_{1,2}}+\frac{1}{8}(\frac{1}{2}\omega-1)\omega(\lambda_{yx_{1,1}}+\lambda_{yx_{2,2}})-\frac{1}{16}\omega^2\lambda_{yx_{2,1}} \\
&\quad -\frac{1}{16}\omega(\lambda_{xx_{1,1}}+\lambda_{xx_{2,1}}+\lambda_{xx_{1,2}}+\lambda_{xx_{2,2}})\frac{\Delta y}{\Delta x}
\end{aligned}
\tag{4.58}
$$

$$
\begin{aligned}
T_{y2} &= -B_{2221} \\
&= -\frac{1}{4}(\omega-1)(\lambda_{yy_{2,1}}+\lambda_{yy_{2,2}})\frac{\Delta x}{\Delta y}+\frac{1}{16}\omega(\lambda_{yy_{1,1}}+\lambda_{yy_{2,1}}+\lambda_{yy_{1,2}}+\lambda_{yy_{2,2}})\frac{\Delta x}{\Delta y} \\
&\quad -\frac{1}{4}(\frac{1}{2}\omega-1)^2\lambda_{xy_{2,1}}+\frac{1}{8}(\frac{1}{2}\omega-1)\omega(\lambda_{xy_{1,1}}+\lambda_{xy_{2,2}})-\frac{1}{16}\omega^2\lambda_{xy_{1,2}}
\end{aligned}
$$

$$+\frac{1}{4}(\frac{1}{2}\omega-1)^2\lambda_{yx_{2,2}}-\frac{1}{8}(\frac{1}{2}\omega-1)\omega(\lambda_{yx_{2,1}}+\lambda_{yx_{1,2}})+\frac{1}{16}\omega^2\lambda_{yx_{1,1}}$$
$$-\frac{1}{16}\omega(\lambda_{xx_{1,1}}+\lambda_{xx_{2,1}}+\lambda_{xx_{1,2}}+\lambda_{xx_{2,2}})\frac{\Delta y}{\Delta x} \tag{4.59}$$

$$\begin{aligned}T_{xy1} &= -B_{2211}\\ &= \frac{1}{16}\omega(\lambda_{xx_{1,1}}+\lambda_{xx_{2,1}}+\lambda_{xx_{1,2}}+\lambda_{xx_{2,2}})\frac{\Delta y}{\Delta x}\\ &\quad+\frac{1}{4}(\frac{1}{2}\omega-1)^2\lambda_{xy_{2,1}}-\frac{1}{8}(\frac{1}{2}\omega-1)\omega(\lambda_{xy_{1,1}}+\lambda_{xy_{2,2}})+\frac{1}{16}\omega^2\lambda_{xy_{1,2}}\\ &\quad+\frac{1}{4}(\frac{1}{2}\omega-1)^2\lambda_{yx_{1,2}}-\frac{1}{8}(\frac{1}{2}\omega-1)\omega(\lambda_{yx_{1,1}}+\lambda_{yx_{2,2}})+\frac{1}{16}\omega^2\lambda_{yx_{2,1}}\\ &\quad+\frac{1}{16}\omega(\lambda_{yy_{1,1}}+\lambda_{yy_{2,1}}+\lambda_{yy_{1,2}}+\lambda_{yy_{2,2}})\frac{\Delta x}{\Delta y}\end{aligned} \tag{4.60}$$

$$\begin{aligned}T_{xy2} &= -B_{1221}\\ &= \frac{1}{16}\omega(\lambda_{xx_{1,1}}+\lambda_{xx_{2,1}}+\lambda_{xx_{1,2}}+\lambda_{xx_{2,2}})\frac{\Delta y}{\Delta x}\\ &\quad-\frac{1}{4}(\frac{1}{2}\omega-1)^2\lambda_{xy_{1,1}}+\frac{1}{8}(\frac{1}{2}\omega-1)\omega(\lambda_{xy_{2,1}}+\lambda_{xy_{1,2}})-\frac{1}{16}\omega^2\lambda_{xy_{2,2}}\\ &\quad-\frac{1}{4}(\frac{1}{2}\omega-1)^2\lambda_{yx_{2,2}}+\frac{1}{8}(\frac{1}{2}\omega-1)\omega(\lambda_{yx_{2,1}}+\lambda_{yx_{1,2}})-\frac{1}{16}\omega^2\lambda_{yx_{1,1}}\\ &\quad+\frac{1}{16}\omega(\lambda_{yy_{1,1}}+\lambda_{yy_{2,1}}+\lambda_{yy_{1,2}}+\lambda_{yy_{2,2}})\frac{\Delta x}{\Delta y}.\end{aligned} \tag{4.61}$$

For physically meaningful results in this finite difference framework, the transmissibilities calculated for opposite directions need to be identical. For example, Eqs. (4.50) and (4.56) must be equal. Equating these two equations yields the following equality:

$$\begin{aligned}&\left[\frac{1}{8}(\frac{1}{2}\omega-1)\omega-\frac{1}{16}\omega^2\right]\lambda_{xy_{1,1}}+\left[\frac{1}{8}(\frac{1}{2}\omega-1)\omega-\frac{1}{16}\omega^2\right]\lambda_{xy_{2,1}}\\ &+\left[\frac{1}{8}(\frac{1}{2}\omega-1)\omega-\frac{1}{4}(\frac{1}{2}\omega-1)^2\right]\lambda_{xy_{1,2}}+\left[\frac{1}{8}(\frac{1}{2}\omega-1)\omega-\frac{1}{4}(\frac{1}{2}\omega-1)^2\right]\lambda_{xy_{2,2}}\\ &=\left[\frac{1}{8}(\frac{1}{2}\omega-1)\omega-\frac{1}{16}\omega^2\right]\lambda_{yx_{1,1}}+\left[\frac{1}{8}(\frac{1}{2}\omega-1)\omega-\frac{1}{16}\omega^2\right]\lambda_{yx_{2,1}}\\ &+\left[\frac{1}{8}(\frac{1}{2}\omega-1)\omega-\frac{1}{4}(\frac{1}{2}\omega-1)^2\right]\lambda_{yx_{1,2}}+\left[\frac{1}{8}(\frac{1}{2}\omega-1)\omega-\frac{1}{4}(\frac{1}{2}\omega-1)^2\right]\lambda_{yx_{2,2}}.\end{aligned} \tag{4.62}$$

The equality in Eq. (4.62) is satisfied if $\omega = 1$ (midpoint rule) or if the off-diagonal elements of the tensor are equal (symmetric tensor). Non-symmetric permeability tensors can be made symmetric by arithmetically averaging the off-diagonal elements of the permeability tensor.[14] In the next section, it is shown, based on Eqs. (4.54) and (4.55), that arithmetic averaging of the off-diagonal elements of the mobility tensor, Λ, is appropriate in the context of 9-point finite differencing.

Method 2 - Based on Manipulation of Darcy's Law

The method presented in this section is an alternative to Method 1 presented in the previous section. The transmissibilities derived in that section are consistent and general. However, for highly anisotropic and heterogeneous permeability distributions, negative transmissibilities may occur. Negative transmissibilities may yield model instability, in particular for multiphase flow conditions.[42]

Shiralkar[42] constructs 9-point transmissibilities for a generally anisotropic system (coordinate axes are not necessarily aligned with the principal axes of permeability). These transmissibilities have a large range of positiveness. The following development of "stable" transmissibilities is similar to that of Shiralkar.[42] The major difference is that the transmissibilities developed here are based on developments of the previous section in order to handle non-symmetric permeability tensors.

The basis for the development of the transmissibilities is the following form of Darcy's law also presented in Chapter III:

$$v_x = -k_{xx}\frac{\partial p}{\partial x} - k_{xy}\frac{\partial p}{\partial y} \tag{4.63}$$

$$v_y = -k_{yx}\frac{\partial p}{\partial x} - k_{yy}\frac{\partial p}{\partial y} \tag{4.64}$$

where fluid viscosity is 1 cp. Consider now the element shown in Figure 4.2. If a constant pressure drop is applied along x-axis as shown in Figure 4.4, the general flow direction is from left to right as indicated by the arrows. Integration of Eq. (4.63) yields:

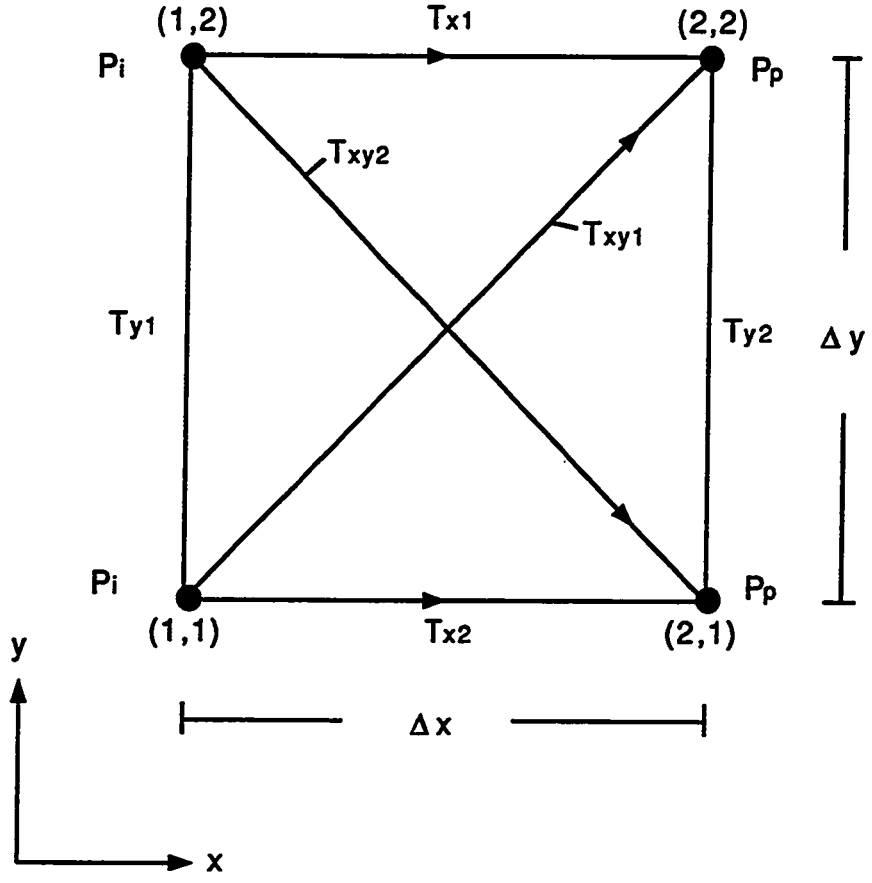

Fig. 4.4: Applied Pressure Drop Along x-axis.

$$(T_{x1} + T_{x2} + T_{xy1} + T_{xy2})\Delta p = \lambda_{xx_a}\Delta y\frac{\Delta p}{\Delta x} \tag{4.65}$$

or

$$T_{x1} + T_{x2} + T_{xy1} + T_{xy2} = \lambda_{xx_a}\frac{\Delta y}{\Delta x} = g_{xx} \tag{4.66}$$

where

$$\lambda_{xx_a} = \frac{(\lambda_{xx})_{1,1} + (\lambda_{xx})_{2,1} + (\lambda_{xx})_{1,2} + (\lambda_{xx})_{2,2}}{4}. \tag{4.67}$$

The pressure gradient applied along x-axis may produce flow along y-axis also, as can be seen from Eq. (4.64) and Figure 4.4. Integration yields:

$$(T_{xy1} - T_{xy2})\Delta p = \lambda_{yx_a}\Delta x\frac{\Delta p}{\Delta x} \tag{4.68}$$

or

$$T_{xy1} - T_{xy2} = \lambda_{yx_a}. \tag{4.69}$$

If a constant pressure drop is applied along y-axis as shown in Figure 4.5, the general flow direction is upwards as indicated by the arrows. Integration of Eq. (4.64) yields:

$$(T_{y1} + T_{y2} + T_{xy1} + T_{xy2})\Delta p = \lambda_{yy_a}\Delta x\frac{\Delta p}{\Delta y} \tag{4.70}$$

or

$$T_{y1} + T_{y2} + T_{xy1} + T_{xy2} = \lambda_{yy_a}\frac{\Delta x}{\Delta y} = g_{yy} \tag{4.71}$$

where

$$\lambda_{yy_a} = \frac{(\lambda_{yy})_{1,1} + (\lambda_{yy})_{2,1} + (\lambda_{yy})_{1,2} + (\lambda_{yy})_{2,2}}{4}. \tag{4.72}$$

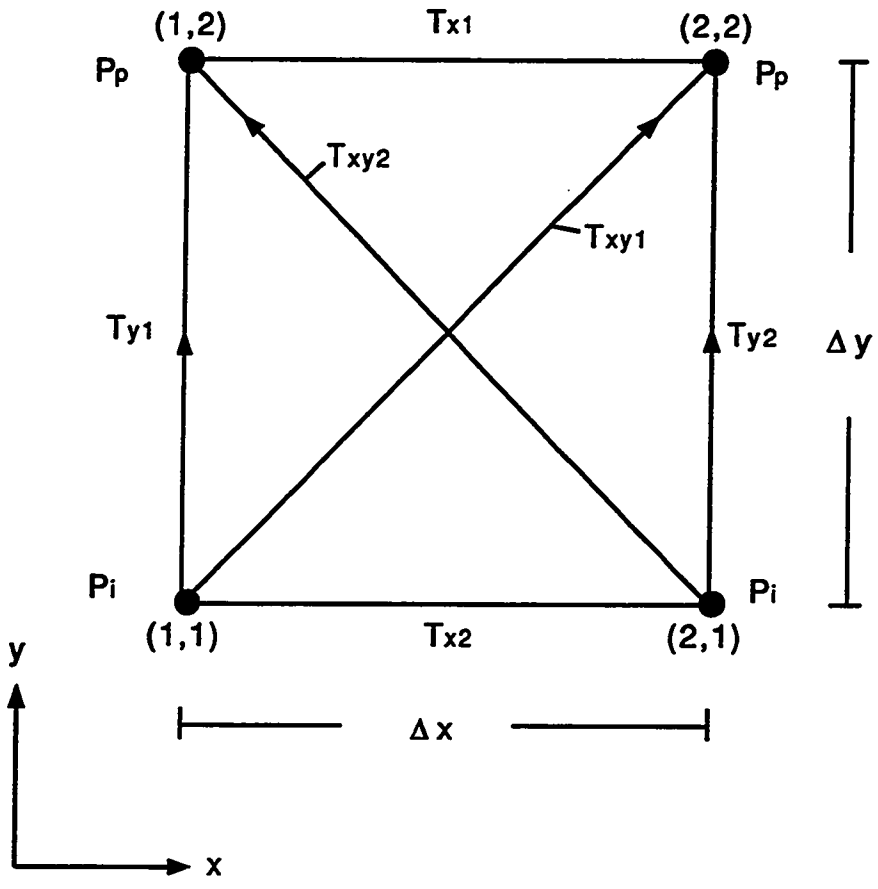

Fig. 4.5: Applied Pressure Drop Along y-axis.

The pressure gradient applied along y-axis produces flow in the x-direction as can be seen from Eq. (4.63) and Figure 4.5. Integration yields:

$$(T_{xy1} - T_{xy2})\,\Delta p = \lambda_{xy_a}\,\Delta y \frac{\Delta p}{\Delta y} \tag{4.73}$$

or

$$T_{xy1} - T_{xy2} = \lambda_{xy_a}. \tag{4.74}$$

The difference between T_{xy1} and T_{xy2} in Eqs. (4.69) and (4.74) translates into flow transverse to the direction of applied pressure gradient. This difference is determined here based on Eqs. (4.54) and (4.55) of the previous section and using the midpoint rule (ω =1). The midpoint rule is appropriate based on the equality in Eq. (4.62). Eq. (4.55) subtracted from Eq. (4.54) becomes:

$$\begin{aligned} T_{xy1} - T_{xy2} =& \frac{1}{8}\left(\lambda_{xy_{1,1}} + \lambda_{xy_{2,1}} + \lambda_{xy_{1,2}} + \lambda_{xy_{2,2}} + \lambda_{yx_{1,1}} + \lambda_{yx_{2,1}} + \lambda_{yx_{1,2}} + \lambda_{yx_{2,2}}\right) \\ =& \frac{1}{4}\left(\frac{\lambda_{xy_{1,1}} + \lambda_{yx_{1,1}}}{2} + \frac{\lambda_{xy_{2,1}} + \lambda_{yx_{2,1}}}{2} + \frac{\lambda_{xy_{1,2}} + \lambda_{yx_{1,2}}}{2} + \frac{\lambda_{xy_{2,2}} + \lambda_{yx_{2,2}}}{2}\right) \\ =& \frac{1}{4}\left(\lambda_{xy_{a1,1}} + \lambda_{xy_{a2,1}} + \lambda_{xy_{a1,2}} + \lambda_{xy_{a2,2}}\right) \\ =& \lambda_{yx_a} = \lambda_{xy_a} = g_{xy_a}. \end{aligned} \tag{4.75}$$

Thus, non-symmetric permeability tensors can be handled using this procedure. From Eq. (4.75), it is clear that g_{xy_a} is a simple arithmetic average of all the off-diagonal elements of the mobility tensor for the particular element (Figure 4.2) being considered.

Edge transmissibilities are define as follows:

$$T_{x_{edge}} = T_{x1} + T_{x2} \tag{4.76}$$

$$T_{y_{edge}} = T_{y1} + T_{y2}. \tag{4.77}$$

Combining Eqs. (4.66) and (4.76), and Eqs. (4.71) and (4.77) produces the following expressions:

$$T_{x_{edge}} = g_{xx} - T_{xy1} - T_{xy2} \tag{4.78}$$

$$T_{y_{edge}} = g_{yy} - T_{xy1} - T_{xy2}. \tag{4.79}$$

To ensure non-negative edge transmissibilities in Eqs. (4.78) and (4.79), the following must be true:

$$g_{xx} \geq T_{xy1} + T_{xy2} \tag{4.80}$$

$$g_{yy} \geq T_{xy1} + T_{xy2}. \tag{4.81}$$

Shiralkar and Stephenson[48] define $T_{xy1} = T_{xy2}$ (limited anisotropy) as follows:

$$T_{xy1} = T_{xy2} = \frac{1}{3}\frac{g_{xx}g_{yy}}{g_{xx} + g_{yy}}. \tag{4.82}$$

In other words, the diagonal transmissibilities are proportional to a series combination of the directional conductances, g_{xx} and g_{yy}. The analogy to Eq. (4.82) for a generally anisotropic system ($T_{xy1} \neq T_{xy2}$) is obtained by subtracting Eq. (4.75) from both sides of Eqs. (4.66) and (4.71):

$$g_{x_{app}} = g_{xx} - g_{xy_a} = T_{x1} + T_{x2} + T_{xy1} + T_{xy2} - (T_{xy1} - T_{xy2}) = T_{x1} + T_{x2} + T_{xy2} + T_{xy2} \tag{4.83}$$

$$g_{y_{app}} = g_{yy} - g_{xy_a} = T_{y1} + T_{y2} + T_{xy1} + T_{xy2} - (T_{xy1} - T_{xy2}) = T_{y1} + T_{y2} + T_{xy2} + T_{xy2}. \tag{4.84}$$

In Eqs. (4.83) and (4.84), $g_{x_{app}}$ and $g_{y_{app}}$ are the apparent directional conductances along the x- and y-axis, respectively. The apparent conductances are analogous to the apparent permeabilities, $\tilde{k}_{x_{app}}$ and $\tilde{k}_{y_{app}}$, described in Chapter III. The simple transformations shown in Eqs. (4.83) and (4.84) effectively make $g_{x_{app}}$ and $g_{y_{app}}$ equivalent to g_{xx} and g_{yy} in Eq. (4.82) which represents limited anisotropy cases. The reason for this equivalence is that both diagonal transmissibilities (northwest-southeast and northeast-southwest) are equal to T_{xy2} in Eqs. (4.83) and (4.84). Therefore, as an analogy to Eq. (4.82), the following equation is used to represent T_{xy2} in cases of general anisotropy:

$$T_{xy2} = \frac{1}{3}\frac{g_{x_{app}} g_{y_{app}}}{g_{x_{app}} + g_{y_{app}}} = \frac{1}{3}\frac{(g_{xx} - g_{xy_a})(g_{yy} - g_{xy_a})}{(g_{xx} - g_{xy_a}) + (g_{yy} - g_{xy_a})}. \tag{4.85}$$

The expression for the other diagonal transmissibility, T_{xy1}, is based on Eq. (4.75):

$$T_{xy1} = \frac{1}{3}\frac{g_{x_{app}} g_{y_{app}}}{g_{x_{app}} + g_{y_{app}}} + g_{xy_a}. \tag{4.86}$$

The remaining transmissibilities are developed from Eqs. (4.76) and (4.77):

$$T_{x_{edge}} = T_{x1} + T_{x2} = \beta_x T_{x_{edge}} + \gamma_x T_{x_{edge}} \tag{4.87}$$

$$T_{y_{edge}} = T_{y1} + T_{y2} = \beta_y T_{y_{edge}} + \gamma_y T_{y_{edge}} \tag{4.88}$$

where

$$\beta_x + \gamma_x = 1.0 \tag{4.89}$$

$$\beta_y + \gamma_y = 1.0. \tag{4.90}$$

The $\beta's$ and the $\gamma's$ are weighting factors based on the conductances along each edge of the element. Using Eqs. (4.87)-(4.90), the horizontal and vertical transmissibilities are defined as:

$$T_{x1} = \beta_x T_{x_{edge}} = \frac{(\lambda_{xx})_{1,2} + (\lambda_{xx})_{2,2}}{4(\lambda_{xx_a})} T_{x_{edge}} \tag{4.91}$$

$$T_{x2} = \gamma_x T_{x_{edge}} = \frac{(\lambda_{xx})_{1,1} + (\lambda_{xx})_{2,1}}{4(\lambda_{xx_a})} T_{x_{edge}} \tag{4.92}$$

$$T_{y1} = \beta_y T_{y_{edge}} = \frac{(\lambda_{yy})_{1,1} + (\lambda_{yy})_{1,2}}{4(\lambda_{yy_a})} T_{y_{edge}} \tag{4.93}$$

$$T_{y2} = \gamma_y T_{y_{edge}} = \frac{(\lambda_{yy})_{2,1} + (\lambda_{yy})_{2,2}}{4(\lambda_{yy_a})} T_{y_{edge}} \tag{4.94}$$

where $T_{x_{edge}}$ and $T_{y_{edge}}$ are calculated from Eqs. (4.78) and (4.79). Eqs. (4.85) and (4.86) are valid for a positive value of g_{xy_a}. For a negative value of g_{xy_a}, the following equations are used:

$$T_{xy2} = \frac{1}{3} \frac{(g_{xx} + g_{xy_a})(g_{yy} + g_{xy_a})}{(g_{xx} + g_{xy_a}) + (g_{yy} + g_{xy_a})} - g_{xy_a} \tag{4.95}$$

$$T_{xy1} = \frac{1}{3} \frac{(g_{xx} + g_{xy_a})(g_{yy} + g_{xy_a})}{(g_{xx} + g_{xy_a}) + (g_{yy} + g_{xy_a})}. \tag{4.96}$$

Note that T_{x1}, T_{x2}, T_{y1}, and T_{y2} are one-sided transmissibilities. They are added to corresponding one-sided transmissibilities of neighboring elements.

Relating Methods 1 and 2

Method 1 which is based on finite element theory, has a strong theoretical basis. A suitable choice of the integration parameter, ω, of Method 1 yields identical transmissibilities for Methods 1 and 2 for a rectangular finite element of homogeneous, but generally anisotropic permeability. The identical transmissibilities ensures the validity of Method 2. Next, it is shown how to determine ω such that each of the individual transmissibilities of the two methods agree.

A value of ω is selected such that T_{xy2} is equal for both methods ($g_{xy_a} > 0$). Based on Eq. (4.75), $\omega = 1$ is used for all the off-diagonal elements of the mobility tensor. Then, T_{xy2} of Method 1 [Eq. (4.55)] set equal to T_{xy2} of Method 2 [Eq. (4.85)] can be expressed as follows:

$$\frac{1}{4}\omega(g_{xx}+g_{yy})-\frac{1}{2}g_{xy_a}=\frac{1}{3}\frac{(g_{xx}-g_{xy_a})(g_{yy}-g_{xy_a})}{(g_{xx}-g_{xy_a})+(g_{yy}-g_{xy_a})}. \tag{4.97}$$

Eq. (4.97) can be solved for ω:

$$\omega=\frac{4}{3}\frac{(g_{xx}-g_{xy_a})(g_{yy}-g_{xy_a})}{[(g_{xx}-g_{xy_a})+(g_{yy}-g_{xy_a})](g_{xx}+g_{yy})}+\frac{2g_{xy_a}}{(g_{xx}+g_{yy})}. \tag{4.98}$$

Using the expression of ω shown in Eq. (4.98) for terms containing the diagonal elements of the mobility tensor and $\omega = 1$ for the off-diagonal elements, the transmissibilities of the two methods become identical for a rectangular finite element with homogeneous, but generally anisotropic permeability.

When $g_{xy_a} < 0$, a value of ω is selected such that T_{xy1} is equal for both methods. Again, $\omega = 1$ is used for all the off-diagonal elements of the mobility tensor. Then, T_{xy1} of Method 1 [Eq. (4.54)] set equal to T_{xy1} of Method 2 [Eq. (4.96)] can be expressed as follows:

$$\frac{1}{4}\omega(g_{xx}+g_{yy})+\frac{1}{2}g_{xy_a}=\frac{1}{3}\frac{(g_{xx}+g_{xy_a})(g_{yy}+g_{xy_a})}{(g_{xx}+g_{xy_a})+(g_{yy}+g_{xy_a})}. \tag{4.99}$$

Eq. (4.99) can be solved for ω:

$$\omega=\frac{4}{3}\frac{(g_{xx}+g_{xy_a})(g_{yy}+g_{xy_a})}{[(g_{xx}+g_{xy_a})+(g_{yy}+g_{xy_a})](g_{xx}+g_{yy})}-\frac{2g_{xy_a}}{(g_{xx}+g_{yy})}. \tag{4.100}$$

In the next chapter, results are presented where effective permeability tensors of analytical and numerical methods are compared. Also shown are results based on simulation of fluid flow through fine scale and upscaled permeability fields. Both finite element and finite difference simulators are used. The transmissibility expressions derived in this chapter are used in calculating transmissibilities to be inserted into a point-centered reservoir simulator[49] for waterflood simulations.

CHAPTER V
RESULTS AND DISCUSSION

This chapter is divided into three sections. In the first section, comparisons are made between effective permeability tensors obtained by the analytical and the numerical methods presented in Chapter III.

In the second section, flood fronts based on single-phase, steady-state, incompressible miscible fluid displacement simulations are shown. Comparisons are made between flood fronts obtained using initial permeability distributions and their upscaled permeability distributions using the analytical effective permeability method, real-space renormalization, geometric average, and harmonic average. To compare results without introducing effects of numerical dispersion associated with the solution of the convection-dispersion equation for coarse grid systems, the same number of grid blocks is used in all of these simulations. For these miscible displacements, only the location of the 0.5 concentration contours are compared.

The last section of this chapter deals with simulation of waterflood performance using initial and upscaled permeability distributions.

Comparisons Between Analytical and Numerical Effective Permeabilities

The first four cases are presented to illustrate the effect on effective permeability of a low permeability region ("perturbation") located off-center in a permeability field. In the following examples, the low permeability region and the remaining permeability field are isotropic, anisotropic and cross-bedded. The degree of complexity generally increases for each case.

Case 1: The four local grid blocks contain isotropic permeabilities with zero off-diagonal elements in their permeability tensors. The block numbering is the same

as in Figure 3.5. Block # 1 has $k_{xx_1} = k_{yy_1} = 1$ md. The remaining blocks have $k_{xx} = k_{yy} = 1000$ md. Figure 5.1 shows the initial permeability distribution, and the analytical and the numerical effective permeability tensors.

From Figure 5.1, it can be observed that the diagonal elements for analytical and numerical methods are practically identical. The off-diagonal elements for the two methods are slightly different; although this difference is not significant based on the relatively small ratio between the off-diagonal and the diagonal tensor elements. The good agreement between the two effective permeability tensors can be demonstrated by comparing the apparent permeabilities. The apparent permeability for the numerical method is 579 md, whereas the apparent permeability for the analytical method is 584 md. They differ by only 0.9 %. The simple weighting scheme used in combining cases of "no cross-flow" and "cross-flow" in Chapter III works satisfactorily in all cases investigated, but works most favorably for systems having an initially anisotropic permeability distribution, which will be demonstrated next.

Case 2: The four local grid blocks contain anisotropic permeabilities with zero off-diagonal elements in their permeability tensors. Block # 1 has $k_{xx_1} = 1$ md and $k_{yy_1} = 0.1$ md. The remaining blocks have $k_{xx} = 1000$ md and $k_{yy} = 100$ md. Figure 5.2 shows the analytical and the numerical effective permeability tensors.

The analytical method shows good agreement with the numerical method. All other anisotropic cases investigated showed similar results.

Case 3: More complexity is introduced in this case. The four local grid blocks each contain equal diagonal elements, but non-zero off-diagonal elements in their permeability tensors. Thus, both "global" and "local" non-zero pressure gradient ratios will exist for this case. The arrangement of the local permeability tensors is shown in Figure 5.3.

The results from both the analytical and the numerical methods indicate that the magnitude of the off-diagonal elements are relatively small compared to the diagonal elements. The relatively small off-diagonal elements are explained by the counteracting effects of the "global" and the "local" pressure gradient ratios. The

1	0	1000	0
0	1	0	1000
1000	0	1000	0
0	1000	0	1000

Analytical Method:	
593	-74
-74	593
Numerical Method:	
592	-89
-89	592

Fig. 5.1: Effective Permeability Tensors Calculated by Analytical and Numerical Methods for Isotropic Local Permeabilities (Units: md).

1	0	1000	0
0	0.1	0	100
1000	0	1000	0
0	100	0	100

Analytical Method:	
523	-14
-14	65
Numerical Method:	
531	-14
-15	65

Fig. 5.2: Effective Permeability Tensors Calculated by Analytical and Numerical Methods for Anisotropic Local Permeabilities (Units: md).

1	0.1	1000	100
0.1	1	100	1000
1000	100	1000	100
100	1000	100	1000

Analytical Method:	
579	-14
-14	579
Numerical Method:	
577	-34
-34	577

Fig. 5.3: Effective Permeability Tensors Calculated by Analytical and Numerical Methods for Equal Diagonal Elements, but Non-Zero Off-Diagonal Elements in Each Local Permeability Tensor (Units: md).

"global' pressure gradient ratio causes negative off-diagonal elements, whereas the pressure gradient ratios within the local blocks creates positive off-diagonal elements. Thus, the magnitude of the effective pressure gradient ratio is reduced.

Case 4: In this case, the local grid blocks contain anisotropic permeabilities with non-zero off-diagonal elements in their permeability tensors. Figure 5.4 shows the arrangement of the local permeability tensors.

Local anisotropy exists and the analytical method yields good prediction of the effective permeability tensor. Notice that the off-diagonal elements of the effective permeability tensor are non-symmetric using both analytical and numerical methods. This phenomena is a result of anisotropic and full local permeability tensors. The two methods agree in both form and existence of non-symmetry of the effective permeability tensors, as shown in Figure 5.4. In the three previous cases, the sign of the off-diagonal elements were negative. However, in this case, the off-diagonal elements are positive. The positive off-diagonal elements are caused by the "local" pressure gradient ratios outweighing the opposing "global" pressure gradient ratio.

The next three cases include a well defined and regular cross-bedded permeability distribution, a simulated stochastic anisotropic permeability distribution, as well as minipermeameter data from the Algerita outcrop in New Mexico.

Case 5: This case is based on the cross-bedded permeability distribution shown in Figure 5.5, where the light and the dark grid blocks initially have isotropic permeabilities of 1000 md and 20 md, respectively.

Figure 5.5 also shows the effective permeability obtained from the numerical and analytical methods. The results agree well. Both methods predict isotropic diagonal elements of the effective permeability tensor, which is correct since the cross-beds are oriented at a $-45°$ angle from the horizontal x-axis. The off-diagonal elements are correctly predicted to be negative and symmetric. For this particular permeability distribution, the exact effective permeability tensor can be obtained through simple coordinate rotation since the permeabilities along the principal axes are simple arithmetic and harmonic averages of the two permeability values in

1	0.1	1000	100
0.1	0.1	100	100
1000	100	1000	100
100	100	100	100

Analytical Method:	
495	36
48	62
Numerical Method:	
501	34
44	61

Fig. 5.4: Effective Permeability Tensors Calculated by Analytical and Numerical Methods for Anisotropic and Full Local Permeability Tensors (Units: md).

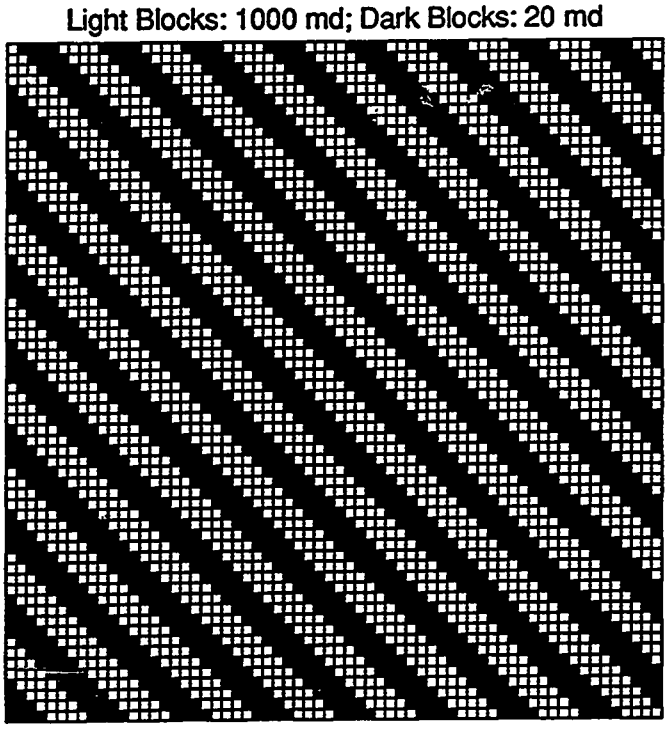

Analytical Method:	
275	-235
-235	275
Numerical Method:	
271	-224
-224	271

Fig. 5.5: Effective Permeability Tensors Calculated by Analytical and Numerical Methods for Cross-Bedded Permeability Distribution (Units: md).

this distribution, 1000 md and 20 md, and the angle of the cross-beds, −45°, is known. The analytical method agrees exactly with the tensor obtained from simple coordinate rotation.

The results show that the directional search for k'_{xx}/k'_{yy} is successful in determining the principal axes of permeability. Therefore, the directional search method may also be a useful tool in detecting permeability structures in minipermeameter measured permeability data from outcrops.

Case 6: The permeability distribution used in this case contains a random component. A Turning Bands program[50] is used to generate a permeability distribution with Dykstra-Parsons coefficient, V, of 0.7 and a dimensionless correlation length of 0.64 along the principal axis of maximum permeability which is at −65° from the horizontal x-axis. The anisotropy ratio of the correlation lengths is 10.

The results indicate that the analytical and the numerical methods agree well even for stochastic systems with cross-bedding structures. In terms of computer time, however, the analytical method is about two orders of magnitude faster than the numerical method. As can be observed from Figure 5.6, both methods predict negative off-diagonal elements of the permeability tensor and k_{yy} larger than k_{xx}. These results along with the results from Case 5 suggest that the analytical effective permeability method works well for both deterministic and stochastic permeability distributions. It will be shown next how this method works on "real" data.

Case 7: In this case, the effective permeability is determined from minipermeameter measured permeability data from a small section of a San Andres carbonate outcrop in Algerita, New Mexico. The distribution of these data is shown in Figure 5.7.

Comparing the permeability distributions of Figures 5.5 and 5.7, it is evident that the permeabilities in Figure 5.7 have less structure or correlation. In Figure 5.5, there are complete high and low permeability layers whereas the outcrop data in Figure 5.7 appear to be more random in their distribution. This observation is supported by the analytical and numerical effective permeabilities calculated for the outcrop data. The off-diagonal elements in the permeability tensors are small

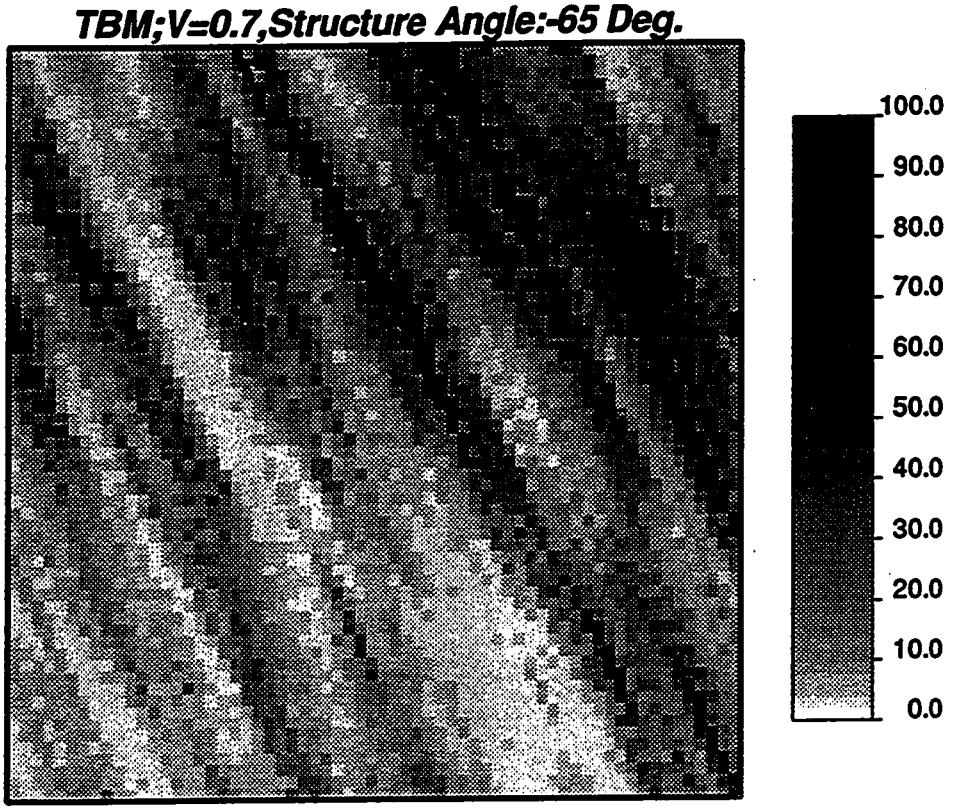

Analytical Method:	
10.3	-2.4
-2.5	12.6
Numerical Method:	
9.7	-1.7
-2.8	13.2

Fig. 5.6: Effective Permeability Tensors Calculated by Analytical and Numerical Methods for Cross-Bedded Stochastic Permeability Distribution (Units: md).

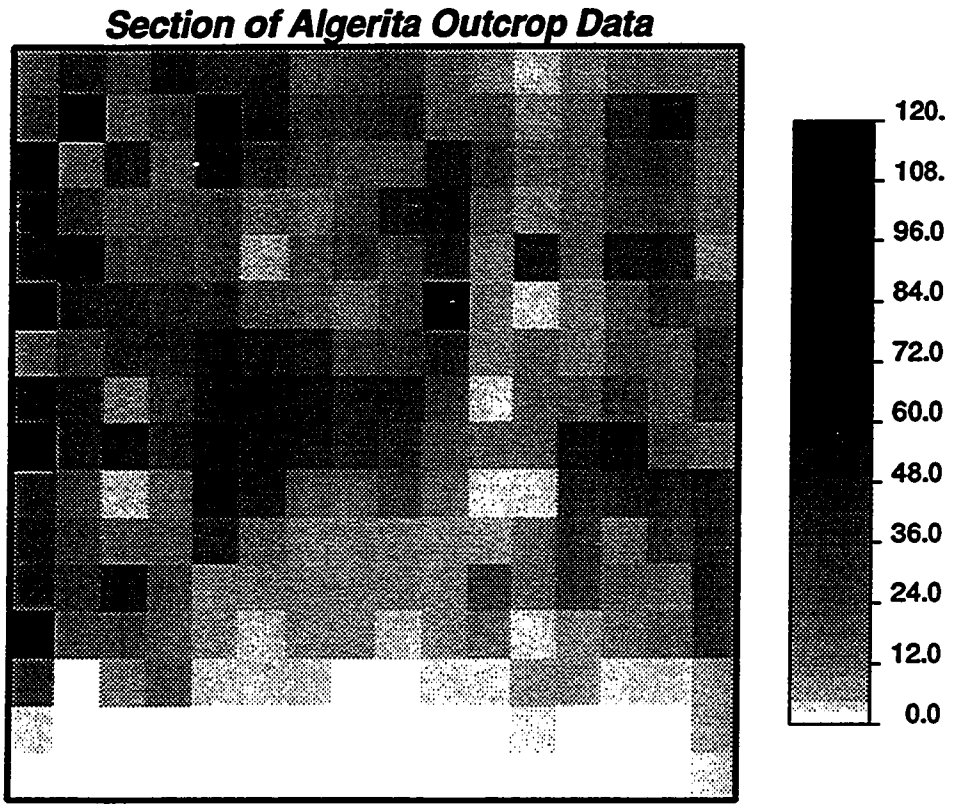

Analytical Method:	
11.9	0.0
0.1	1.7
Numerical Method:	
11.8	0.9
0.1	1.7

Fig. 5.7: Effective Permeability Tensors Calculated by Analytical and Numerical Methods for Minipermeameter Measured Permeability Data From the Algerita Outcrop (Units: md).

compared to their respective diagonal elements. The ratios of k_{xy}/k_{xx} and k_{yx}/k_{yy} are indications of the sizes of the transverse to longitudinal pressure gradient ratios. Both numerical and analytical methods show ratios ranging from about 0.0 to 0.08. In Figure 5.5 however, the ratios are -0.83 and -0.85. In other words, the cross-bedded heterogeneities in Figure 5.5 induce much higher transverse pressure gradients than the more random heterogeneities in Figure 5.7. The relatively small off-diagonal elements and the magnitudes of the diagonal elements indicate that the permeability heterogeneities for all practical purposes are oriented along the x-axis.

There appears to be a difference in the prediction of k_{xy} in Figure 5.7. Numerically k_{xy}=0.9 md and analytically k_{xy}=0.0 md. However, this difference is negligible considering the low pressure gradient ratios obtained both numerically and analytically. The diagonal elements show excellent agreement indicating anisotropy ratios of 7.0 and 6.9 for the analytical and numerical methods, respectively.

Next, results from fluid flow simulations are presented. Comparisons are generally made between microscale simulations, where the initial permeability distributions are used, and simulations using the analytical effective permeability method, geometric average and real-space renormalization.[29]

Comparisons Between Results From Fluid Flow Simulations

Miscible Displacements

In all the following cases, results from unit mobility ratio miscible displacement simulations are presented. The convection-dispersion equation is solved for an incompressible fluid using a finite element simulator.[1] Effects of numerical dispersion are eliminated by using the same number of grid blocks for initial permeability distributions and homogenized permeability distributions.

Case 1: Figure 5.8a shows the permeability distribution used in the simulation. It is essentially the same distribution as in Figure 5.5, except in Figure 5.8a the aspect ratio is 8 to 1 rather than 1 to 1 as in Figure 5.5. The following boundary conditions are used: constant pressure potential of 3.5 atm is specified along the entire left vertical boundary; 1.0 atm is specified along the entire right vertical

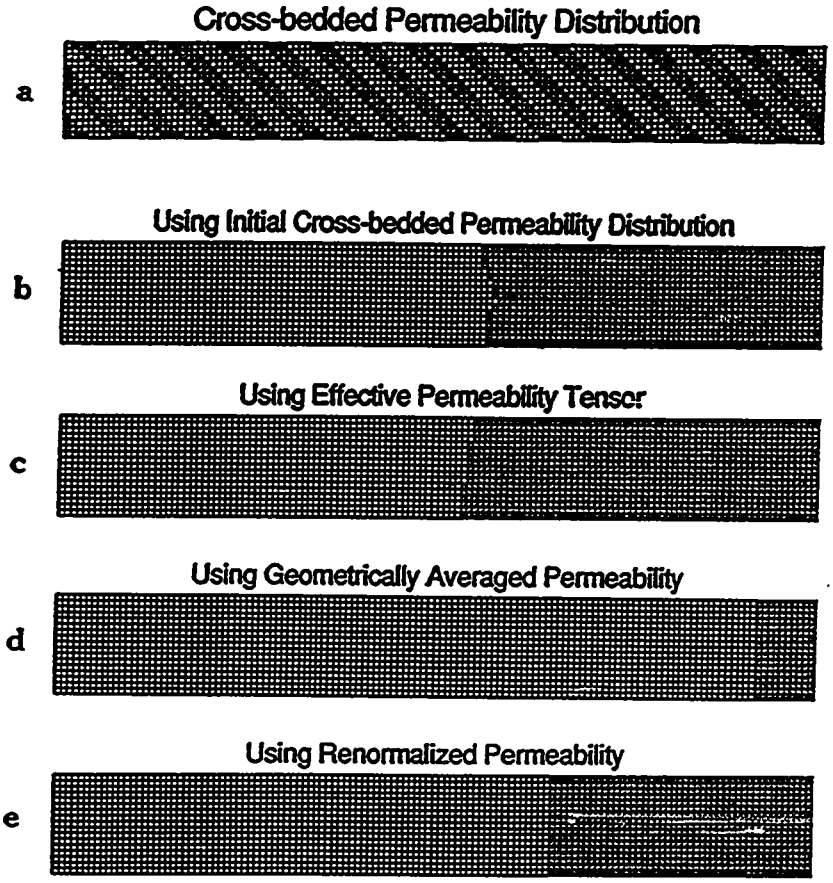

Fig. 5.8: Initial Permeability Distribution (Dark: 20 md; Light: 1000 md) and 0.5 Concentration Contours After 49.7 Days of Injection Using the Initial Permeability Distribution and the Permeability Distributions Obtained Using Various Upscaling Methods.

boundary; both horizontal boundaries are closed to flow.

Figures 5.8b-5.8e show 0.5 concentration contours of the flood fronts after 49.7 days of injection. Figure 5.8b shows the location of the front using the initial permeability distribution. This figure is used as the base case. The analytical effective permeability tensor method (Figure 5.8c) yields the best prediction of the location of the flood front. The geometric mean predicts a flood front which is advancing too fast (Figure 5.8d). Thus, the geometric mean overpredicts the effective permeability. The renormalization method (Figure 5.8e) also predicts a flood front which is advancing too fast, although the overprediction of the effective permeability is not as severe as when using the geometric mean.

Case 2: This case involves a stochastic log-normal permeability distribution. The Dykstra-Parsons coefficient is $V = 0.70$. The angle of the permeability structures is specified to be $-45°$. The dimensionless correlation length along the oriented structures is $\lambda_{D_\ell} = 0.5$ and the dimensionless correlation length transverse to the structures is $\lambda_{D_t} = 0.05$. The permeability distribution is generated using the Turning Bands program. Figure 5.9a shows a map of this permeability distribution. The boundary conditions are identical to those in Case 1.

Figures 5.9b-5.9e show 0.5 concentration contours of the flood fronts after 94.8 days of injection. Figure 5.9b shows the location of the front using the initial stochastic permeability distribution. Both the analytical effective permeability tensor method (Figure 5.9c) and the geometric mean (Figure 5.9d) yield correct flood front matches. The renormalization method (Figure 5.9e), however, predicts a flood front which is advancing too slowly. Thus, the renormalization method underpredicts the effective permeability for this case.

Case 3: This case also involves a stochastic log-normal permeability distribution. However, the Dykstra-Parsons coefficient is $V = 0.86$, which translates into an extremely large permeability variability. The angle of the permeability structures is specified to be $-45°$. The dimensionless correlation length along the oriented structures is $\lambda_{D_\ell} = 1.0$ and the dimensionless correlation length transverse to the

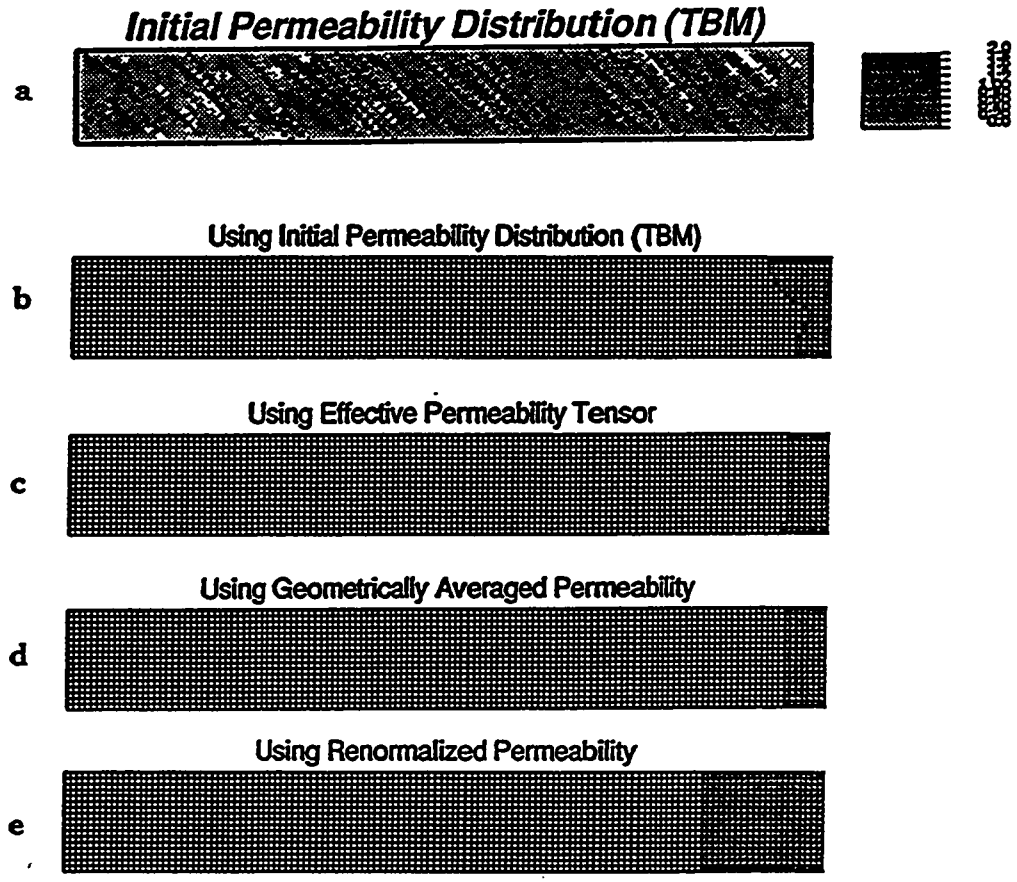

Fig. 5.9: Initial Permeability Distribution ($V = 0.7$) and 0.5 Concentration Contours After 94.8 Days of Injection Using the Initial Permeability Distribution and the Permeability Distributions Obtained Using Various Upscaling Methods.

structures is $\lambda_{D_t} = 0.02$. The Turning Bands program is again used to construct the permeability distribution. Figure 5.10a shows a map of this permeability distribution. The boundary conditions are identical to those in Case 1.

Figures 5.10b-5.10f show 0.5 concentration contours of the flood fronts after 113 days of injection. Figure 5.10b represents the location of the front using the initial stochastic permeability distribution. The analytical effective permeability tensor method (Figure 5.10c) predicts a flood front which is ahead of the base case flood front. The geometric mean (Figure 5.10d) significantly overpredicts effective permeability, whereas the renormalization method (Figure 5.10e) yield a flood front which is the closest to the base case flood front. This result agrees with results obtained from another study[22] which suggests that the renormalization technique works well in cases of extremely high permeability variance. The harmonic mean (Figure 5.10f) severely underpredicts effective permeability based on the location of the flood front.

Considering the high variability of the permeability, which is reflected in the significant difference in the flood fronts for the cases of geometric and harmonic mean, both the analytical effective permeability method and the renormalization method do a remarkable job in estimating the actual effective permeability. This is particularly true for the renormalization method. To give an indication of the variability of the permeability values, the range is from 0.0003 Darcy to 121 Darcy.

Table 5.1 shows the flow rates obtained using the initial and upscaled permeability distributions for Cases 1, 2 and 3.

In the above cases, the analytical effective permeability method has outperformed the other effective permeability methods. These results suggest that the analytical tensor method is more general than the other upscaling methods presented.

Waterfloods

The next cases presented involve comparisons of results from simulating waterfloods using initial permeability distributions and upscaled effective permeability

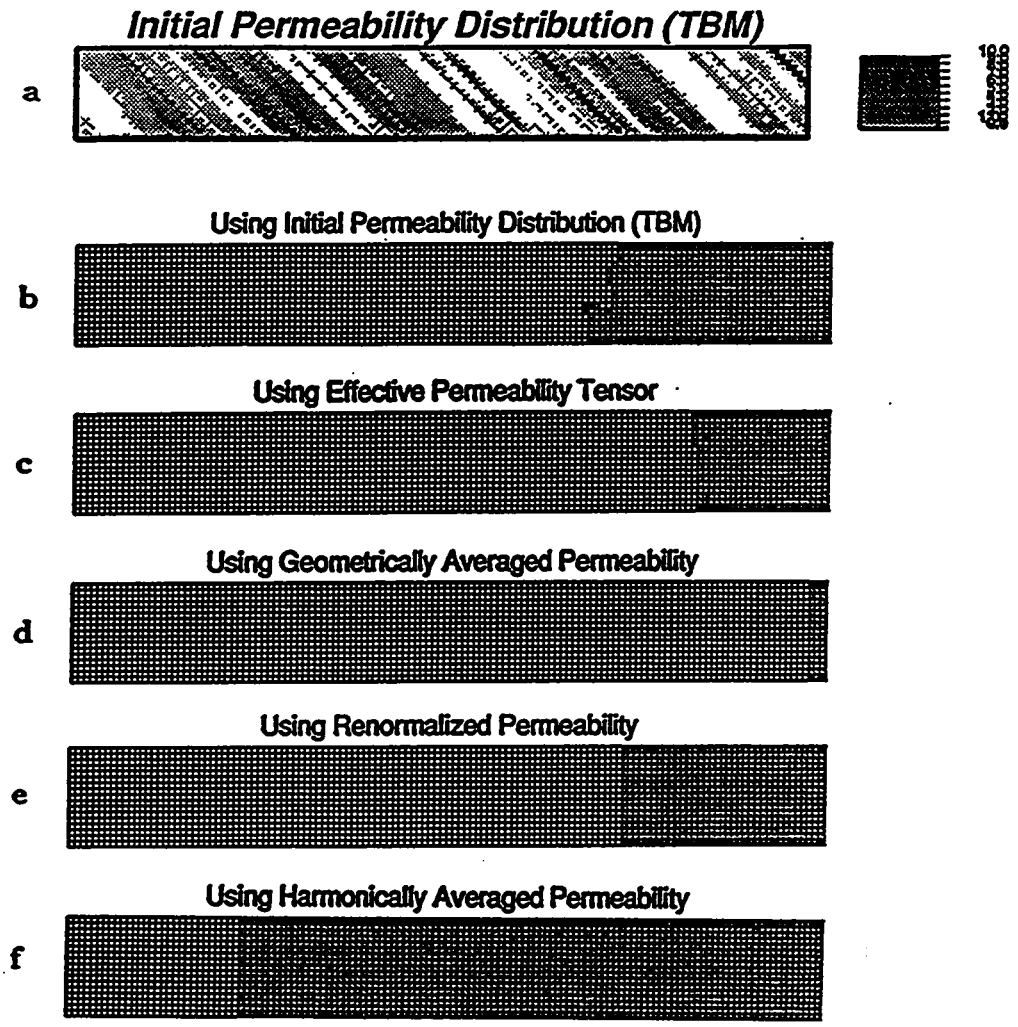

Fig. 5.10: Initial Permeability Distribution ($V = 0.86$) and 0.5 Concentration Contours After 113 Days of Injection Using the Initial Permeability Distribution and the Permeability Distributions Obtained Using Various Upscaling Methods.

Table 5.1	
Flow Rates	
Case 1	q (cm^3/s) x 10^{-2}
Using Initial Permeability Distribution:	2.64
Using Effective Permeability Tensor:	2.48
Using Geometric Average:	4.40
Using Real-Space Renormalization:	2.93
Case 2	q (cm^3/s) x 10^{-2}
Using Initial Permeability Distribution:	2.38
Using Effective Permeability Tensor:	2.37
Using Geometric Average:	2.35
Using Real-Space Renormalization:	2.10
Case 3	q (cm^3/s) x 10^{-2}
Using Initial Permeability Distribution:	1.42
Using Effective Permeability Tensor:	1.71
Using Geometric Average:	2.05
Using Real-Space Renormalization:	1.52
Using Harmonic Average:	0.45

distributions generated based on the analytical effective permeability method, the real-space renormalization technique, and the geometric average. Two-phase oil and water systems are simulated. The simulator used is a point-centered finite difference simulator which has the option of inserting separately computed transmissibilities.[49] Therefore, the 9-point based transmissibility equations developed in Chapter IV are used to compute the transmissibility coefficients to be inserted into the simulator. The initial permeability distributions shown are all in Darcy units. Except for Case 1, permeabilities are scaled (multiplied) by 0.03 before transmissibilities are calculated. Simulator input parameters are listed in Table 5.2. The relative permeability curves are shown in Figure 5.11 and are identical to those used by White and Horne.[9]

Case 1: The first case presented is based on the cross-bedded permeability distribution shown in Figure 5.12. This distribution is identical to that shown in Figure 5.5, except 32x32 grid points are used in Figure 5.12 compared to 64x64 grid points in Figure 5.5. The number of grid points is reduced to minimize simulation time.

Water displaces the in-situ oil by full face injection at the left border, and full face fluid production takes place at the right border of the permeability distribution in Figure 5.12. Constant injection and production rates of 100 bbl/d are used in this case.

Waterflooding is performed using the initial permeability distribution, the analytical effective permeability tensor, and renormalized permeability. Results are compared in terms of pressure maps, water saturation maps at several stages of the waterflood, and oil recovery curves.

The pressure maps after 0.5 days of injection are shown in Figure 5.13. The pressure map for the initial permeability distribution (Figure 5.13a) shows that there is clearly a transverse component of the pressure gradient since the isopotential lines have a general orientation of decreasing pressure from southwest to northeast. Notice, however, the effect of the high permeability layers, within which pressure is decreasing from northwest to southeast. Such detail can not be retained

Table 5.2	
Simulation Input Parameters	
μ_o	1.0 cp
μ_w	1.0 cp
ρ_o	62.4 lbm/ft^3
ρ_w	62.4 lbm/ft^3
c_o	1.0 x E-10 psi^{-1}
c_w	1.0 x E-6 psi^{-1}
L_x	600 ft
L_y	600 ft
h	10 ft
ϕ	0.20
$P_{initial}$	1000 psi

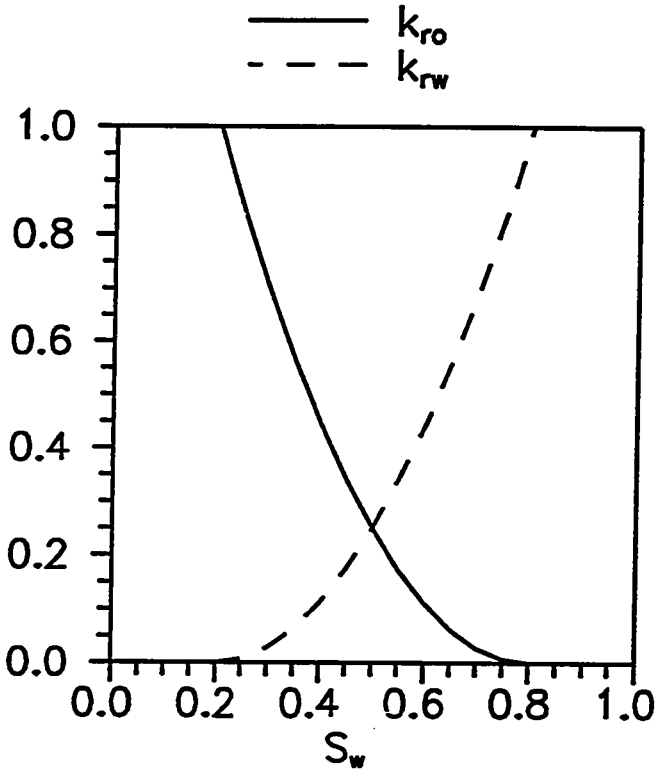

Fig. 5.11: Relative Permeability Curves.[9]

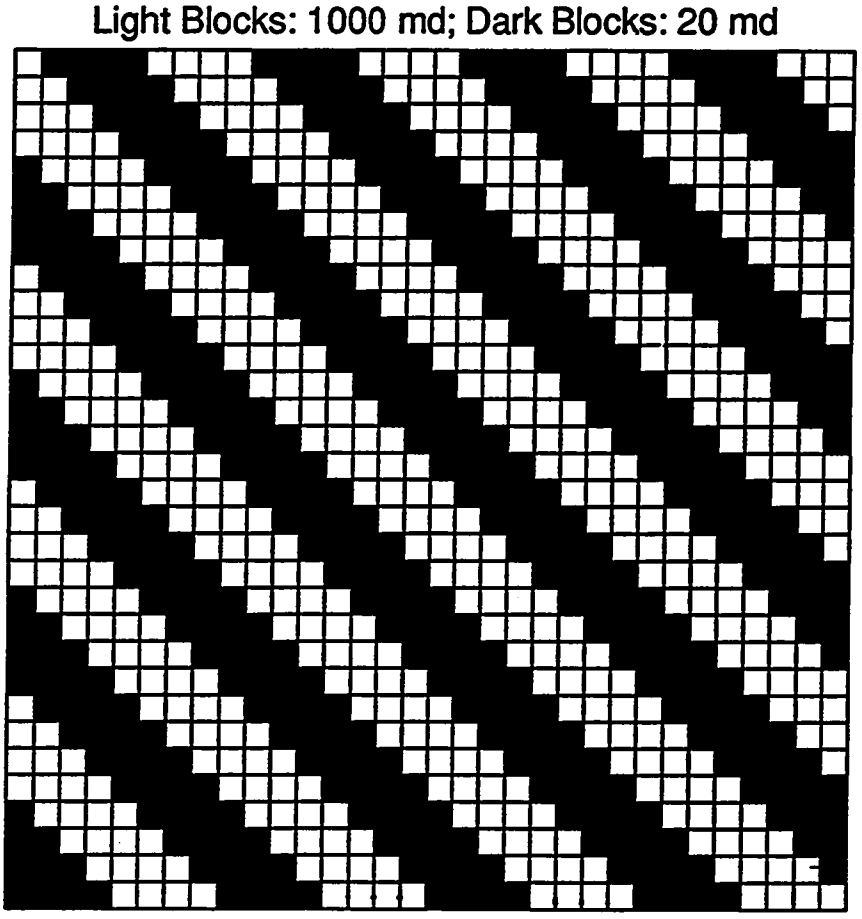

Fig. 5.12: Cross-Bedded Permeability Distribution.

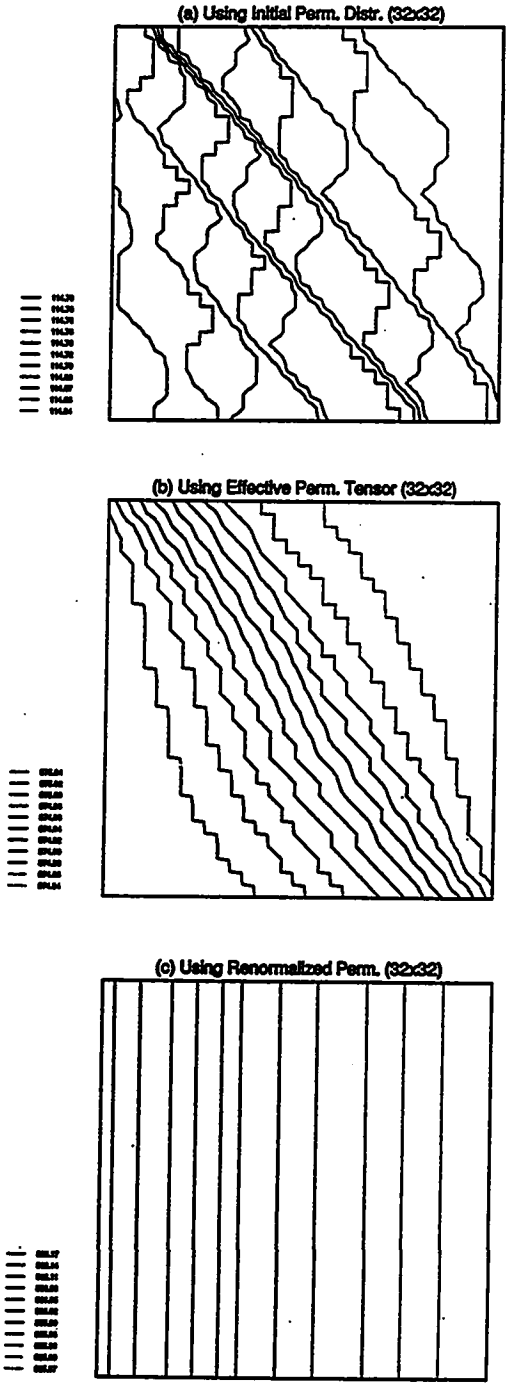

Fig. 5.13: Pressure Maps After 0.5 Days of Water Injection Using (a) the Initial Cross-Bedded Permeability Distribution (b) the Effective Permeability Tensor and (c) the Real-Space Renormalized Permeability (Units: psi).

for pressure maps related to the upscaled permeability distribution. However, the effective permeability tensor produces a permeability map which preserves the general trend of decreasing pressure from southwest to northeast as can be observed from Figure 5.13b. Thus, the main effects of the cross-bedded permeability structures are maintained through the upscaling process. Using real-space renormalization of permeability, however, the characteristics of the pressure map from using the initial permeability distribution are lost as can be observed from Figure 5.13c.

Water saturation maps after 0.5, 1.0, and 1.5 days of water injection are shown in Figures 5.14, 5.15, and 5.16, respectively. Figure 5.14a shows the water saturation map after 0.5 days of water injection using the initial cross-bedded permeability distribution. The injected water flows locally along the high permeability layers, but the non-uniform shape of the overall water saturation front is controlled by the net transverse pressure drop being almost perpendicular to the alternating high and low permeability layers as shown in Figure 5.13a. Even though the effects of some of the details of the initial permeability distribution are lost, the water saturation front after 0.5 days of injection using the effective permeability tensor is very similar in shape as can be seen in Figure 5.14b. However, using the renormalized permeability, the water saturation front after 0.5 days of injection (Figure 5.14c) does not show any of the characteristics of the water saturation front obtained using the initial permeability distribution. Water is uniformly sweeping the oil as can be seen in Figure 5.14c.

Figure 5.15a shows the water saturation map after 1.0 days of injection using the initial permeability distribution. More of the high permeability layers have been flooded, and water breakthrough is soon to occur in the lower portion of the east boundary. Using the effective permeability tensor, water breakthrough has just occurred in the lower portion of the east boundary as can be seen from Figure 5.15b. Loss of detail in upscaling the initial permeability distribution accounts for the slightly earlier water breakthrough obtained using the effective permeability tensor. The high permeability layers in the initial permeability distribution contribute to stabilizing the water saturation front somewhat and to some degree improving the

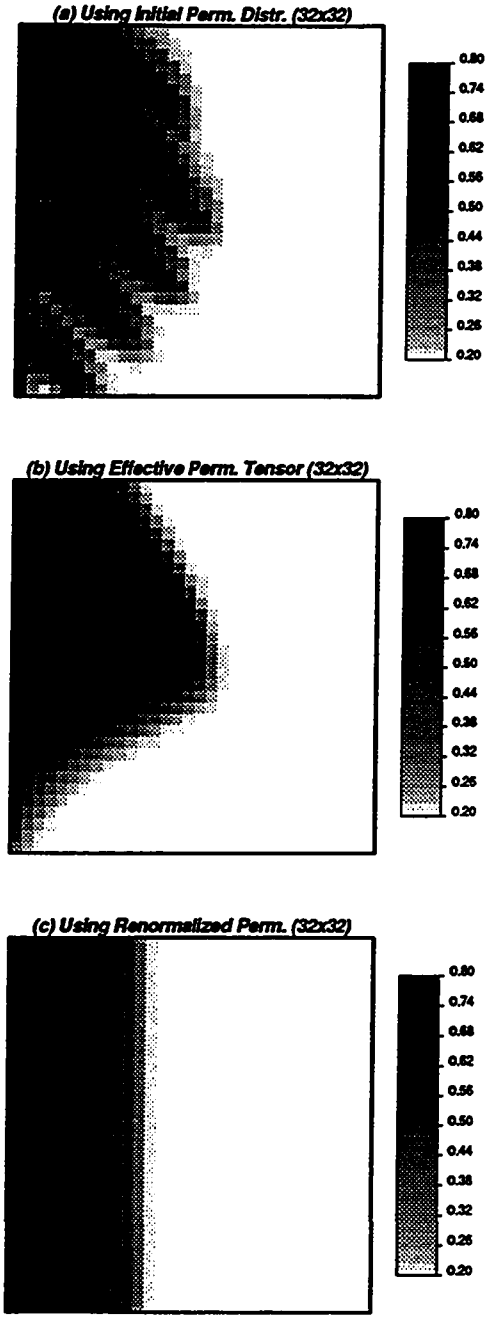

Fig. 5.14: Water Saturation Maps After 0.5 Days of Water Injection Using (a) the Initial Cross-Bedded Permeability Distribution (b) the Effective Permeability Tensor and (c) the Real-Space Renormalized Permeability.

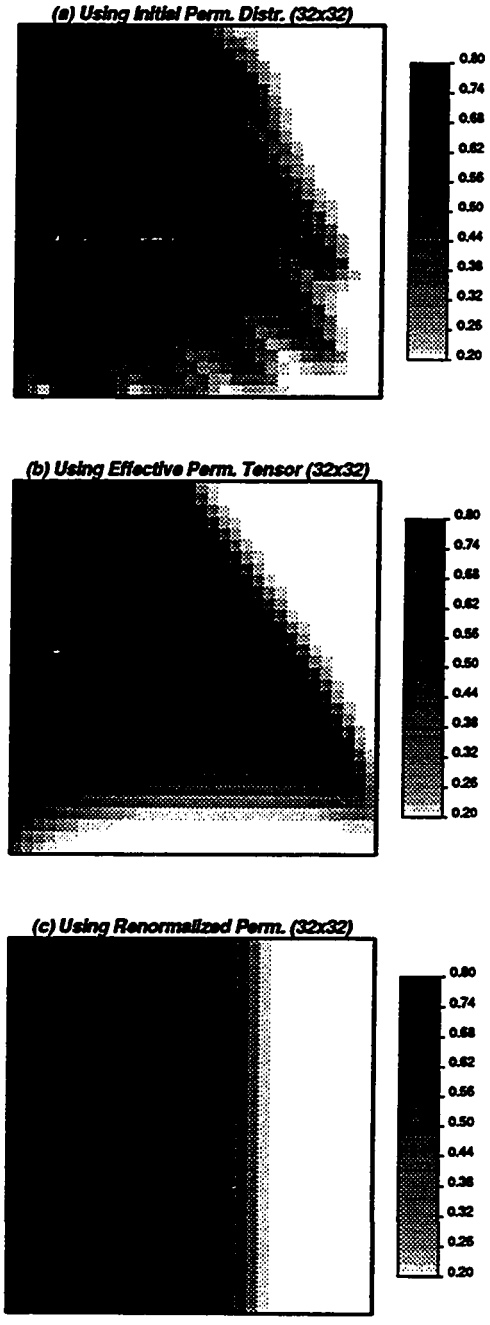

Fig. 5.15: Water Saturation Maps After 1.0 Days of Water Injection Using (a) the Initial Cross-Bedded Permeability Distribution (b) the Effective Permeability Tensor and (c) the Real-Space Renormalized Permeability.

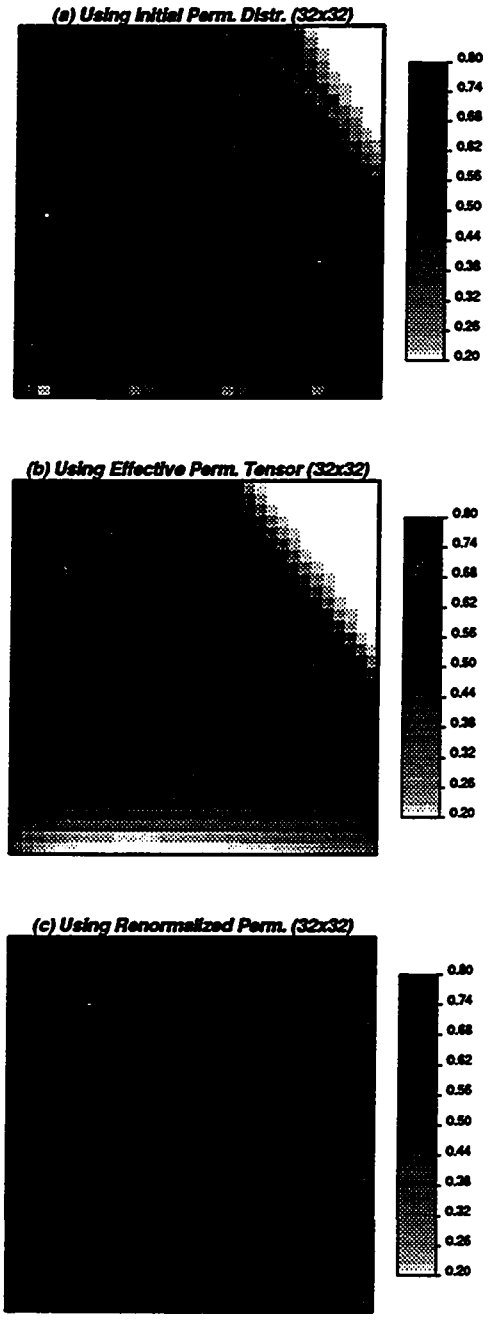

Fig. 5.16: Water Saturation Maps After 1.5 Days of Water Injection Using (a) the Initial Cross-Bedded Permeability Distribution (b) the Effective Permeability Tensor and (c) the Real-Space Renormalized Permeability.

sweep efficiency. Using the renormalized permeability, however, the water saturation front after 1.0 days of injection is far from breaking through and yields an overly optimistic sweep efficiency as can be observed from Figure 5.15c.

After 1.5 days of injection, water breakthrough has occurred using both the initial permeability distribution and the upscaled permeabilities (Figure 5.16). Both using the initial permeability distribution (Figure 5.16a) and the effective permeability tensor (Figure 5.16b) oil is left behind in the upper northeast corner of the field, even to a larger degree so using the effective permeability tensor. Also, in both these cases, an incomplete sweep of the oil takes place in the extreme lower part of the field, but again most clearly so using the effective permeability tensor. The water saturation front obtained using the renormalized permeability is uniform and show optimistic sweep efficiency as can be seen in Figure 5.16c.

The sweep efficiencies may be compared from the oil recovery curves shown in Figure 5.17 where cumulative oil recovery is plotted as a function of elapsed time of water injection. The effective permeability tensor underestimates the sweep efficiency based on the lower recovery curve, whereas renormalized permeability clearly overestimates the sweep efficiency based on the higher recovery curve.

Case 2: The permeability distribution used in this case is shown in Figure 5.18. This isotropic permeability distribution is generated using the Turning Bands method.[50] Statistical input parameters are: isotropic dimensionless correlation length of 0.5 and Dykstra-Parsons coefficient, $V = 0.7$. 40x40 grid points are used. Water is injected at 100 bbl/d from the southwest corner and fluid is produced (100 bbl/d) at the northeast corner of the field in a quarter of a 5-spot pattern.

For this case and the remaining cases presented, the geometric average are used rather than the real-space renormalization technique. The real-space renormalization formulation presented in Reference 29 is restricted to $2^{2i}, i = 1, 2, ...$ permeability values in a multilevel application.

Figure 5.19 shows cumulative oil produced as a function of injection time for the initial (microscale) permeability distribution, the effective permeability tensor,

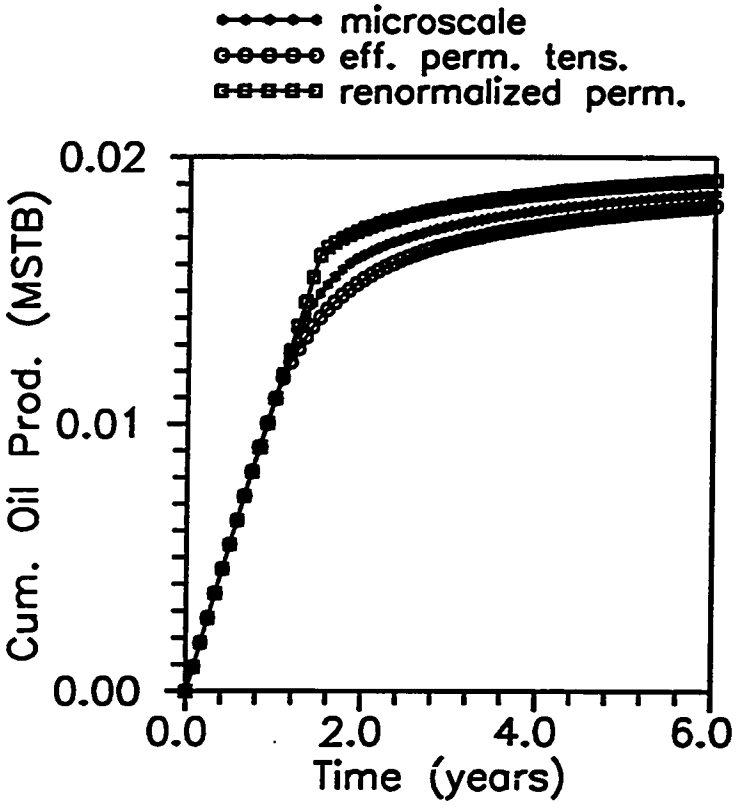

Fig. 5.17: Cumulative Oil Recovery Versus Time for Rectilinear Waterflood. Cross-Bedded Initial Permeability Distribution. Effect of Permeability Upscaling.

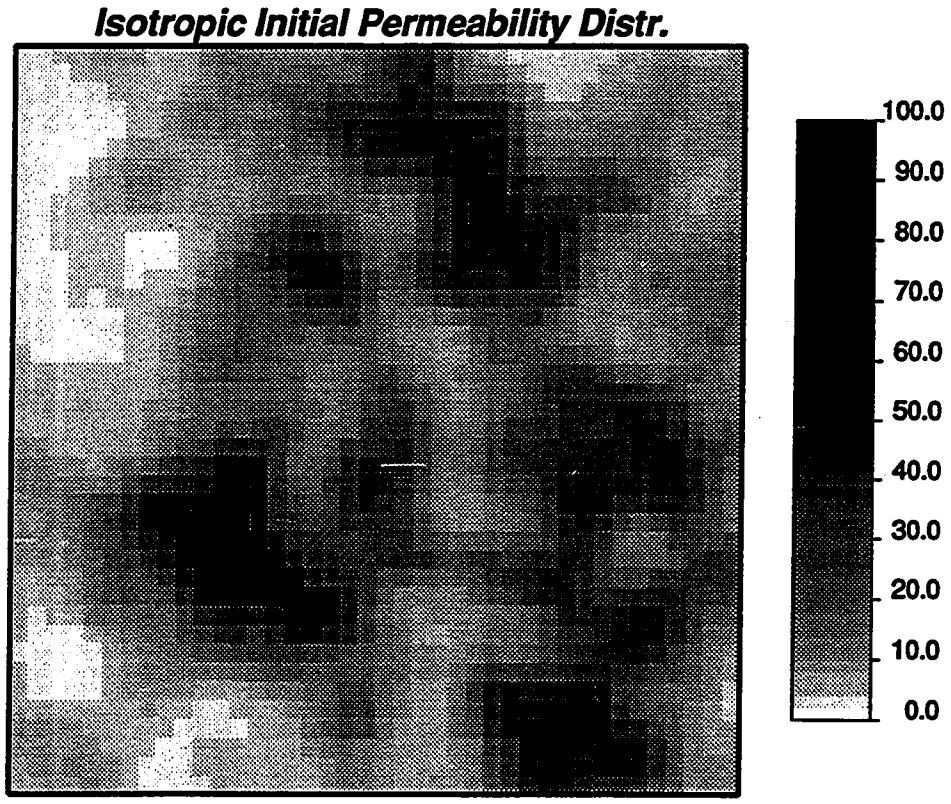

Fig. 5.18: Isotropic Stochastic Permeability Distribution.
($\lambda_D = 0.5$, $V = 0.7$, 40 x 40 Values).

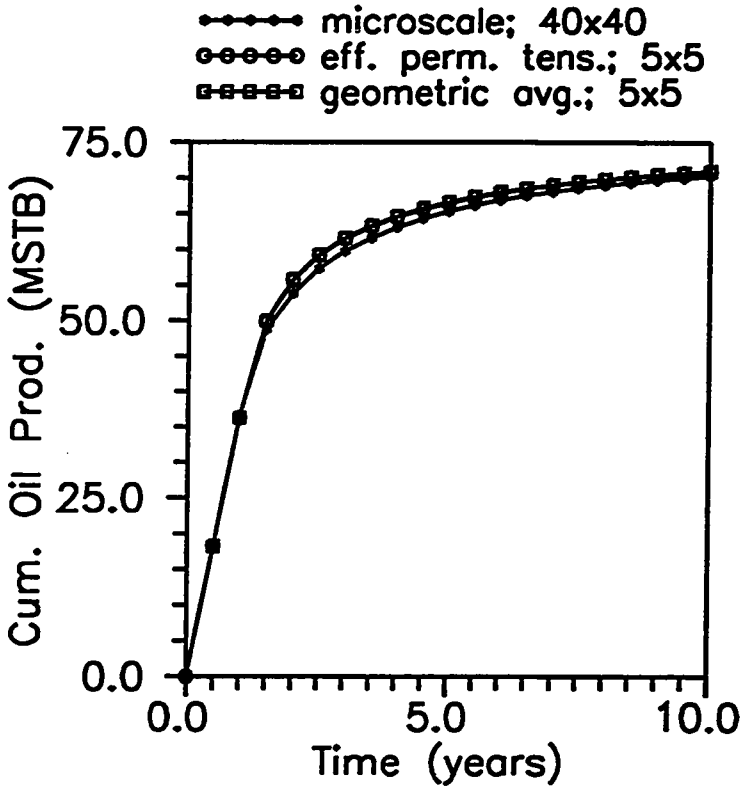

Fig. 5.19: Cumulative Oil Recovery Versus Time for Waterflood in a 1/4 of a 5-Spot. Isotropic Initial Permeability Distribution. Effect of Permeability Upscaling.

and the geometric average of the initial permeability distribution. The upscaled distributions are scaled from 40x40 to 5x5 permeability values. For this isotropic microscale permeability distribution, the effect of permeability upscaling is small and not sensitive to the upscaling technique used. The recovery curves obtained using upscaled permeability are indistinguishable from one another and do not differ much from the recovery curve using the initial permeability distribution.

Case 3: This case also represents waterflooding in a quarter of a 5-spot pattern. However, in this case, the permeability distribution is anisotropic and oriented at a 45° angle from the horizontal x-axis. In other words, the orientation of the anisotropic permeability structures are parallel to the general flow direction from the injector in the southwest corner and the producer in the northeast corner of the field. The dimensionless correlation lengths are $\lambda_{D_\ell} = 1.0$ and $\lambda_{D_t} = 0.025$ along the layers and transverse to the layers, respectively. The Dykstra-Parsons coefficient is $V = 0.7$. There are 64x64 permeability values in the initial permeability distribution shown in Figure 5.20. Injection pressure is 3000 psi and production pressure is 100 psi.

The water saturation fronts after 20 days of injection are shown in Figure 5.21. Figure 5.21a shows the water saturation front using the initial, generally anisotropic permeability distribution. Water breakthrough has already occurred because of the preferential flow paths created by the cross-bedded arrangement of the permeability values in the field. The microscale permeability distribution is upscaled or homogenized from 64x64 to 8x8 permeability values. Comparing Figures 5.21b and 5.21c, it is evident that using the effective permeability tensor, the water saturation front agrees better in terms of shape and amount of water broken through (Figure 5.21b) than using the geometric average of the permeability values (Figure 5.21c). The geometric average method is not able to capture the anisotropic nature of the initial permeability distribution.

In Figure 5.22, the cumulative oil recovery is plotted as a function of pore volumes of water injected for waterflooding through the microscale and the upscaled

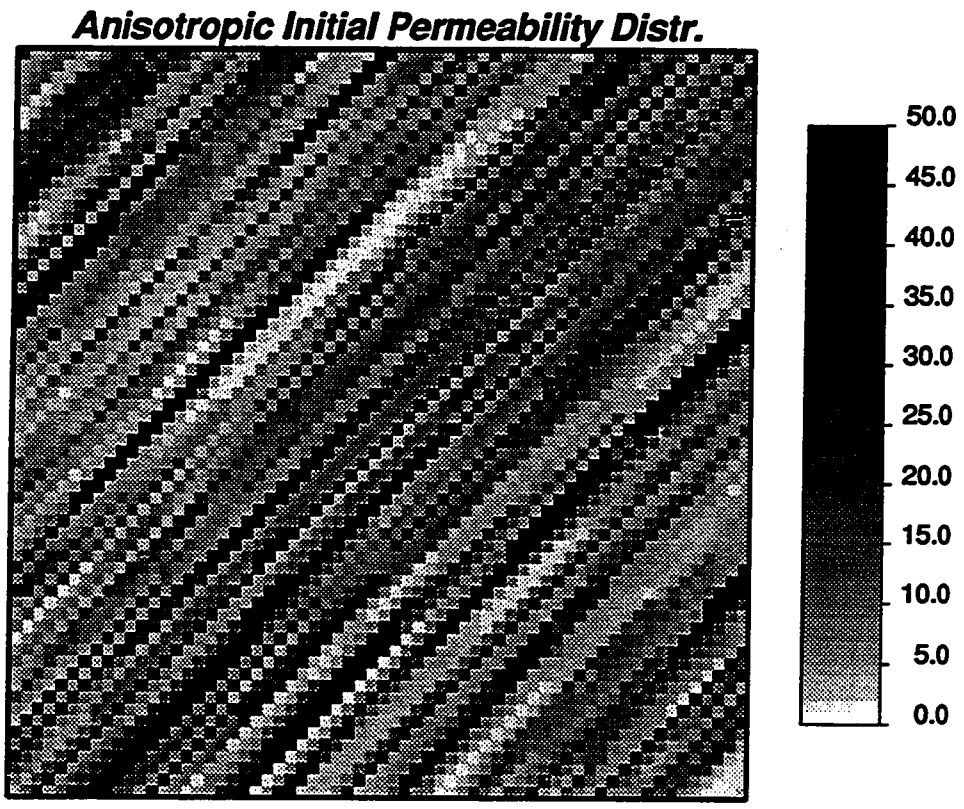

Fig. 5.20: Anisotropic (Cross-Bedded) Stochastic Permeability Distribution. ($\lambda_{D_\ell} = 1.0$, $\lambda_{D_t} = 0.025$, $V = 0.7$, 45° Structure Orientation, 64 x 64 Values).

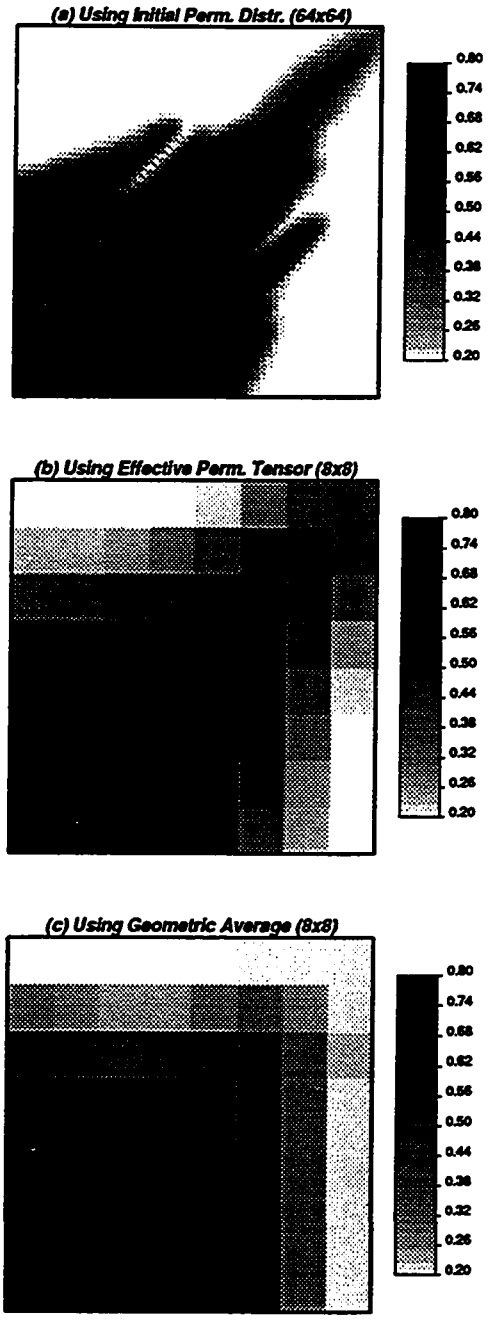

Fig. 5.21: Water Saturation Maps After 20 Days of Water Injection Using (a) the Initial Permeability Distribution (b) the Effective Permeability Tensor and (c) the Geometrically Averaged Permeability.

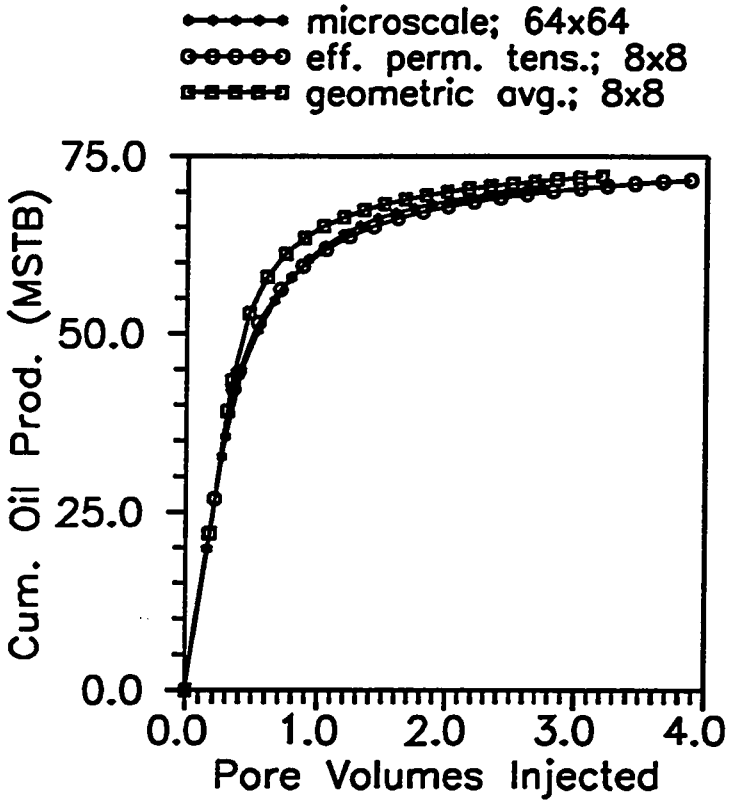

Fig. 5.22: Cumulative Oil Recovery Versus Pore Volumes Injected for Waterflood in a 1/4 of a 5-Spot. Anisotropic (Cross-Bedded) Initial Permeability Distribution. Effect of Permeability Upscaling.

permeability distributions. From this figure, it can be observed that the recovery curve related to the effective permeability tensor shows excellent agreement with the recovery curve associated with the initial microscale permeability distribution. The recovery curve associated with the geometric average of the initial permeability distribution is too optimistic.

Case 4: The final case represents waterflooding in a 5-spot pattern. An injector is located in the middle of the field and injecting water at 3000 psi. Four producers, one in each corner of the field, are producing fluid at 100 psi. The main difference from the permeability distribution used in Case 3 is the use of 63x63 permeability values. An odd number of grid points along each axis are necessary to place the injector in the very middle of the field. In addition, the dimensionless correlation length transverse to the layers is $\lambda_{D_t} = 0.016$. Dykstra-Parsons coefficient is $V = 0.7$. The distribution of the initial microscale permeability values are shown in Figure 5.23. The system is coarsened to 9x9 grid points using the effective permeability tensor and the geometric average. The simulations of the coarsened permeability distributions (9x9 grid points) are approximately 800 times faster than the simulation of the initial permeability distribution.

Figure 5.24 shows the water saturation maps after 8 days of injection. Using the initial permeability distribution, water has broken through in all of the four producing wells (Figure 5.24a). However, the wells with the highest water saturation are located in the southwest (P-3) and the northeast (P-2) corners of the field. This response agrees with the expected response based on the orientation of the permeability streaks. Figure 5.24b shows the water saturation map which is based on the use of the effective permeability tensor. The water saturation distribution agrees well with that observed in Figure 5.24a in terms of the distribution of the major portion of the injected water along the southwest-northeast diagonal. The water saturation map based on using the geometric average of permeability does not indicate any particular direction of preferential fluid flow, as can be seen in Figure 5.24c. An approximately equal amount of water has broken through in each

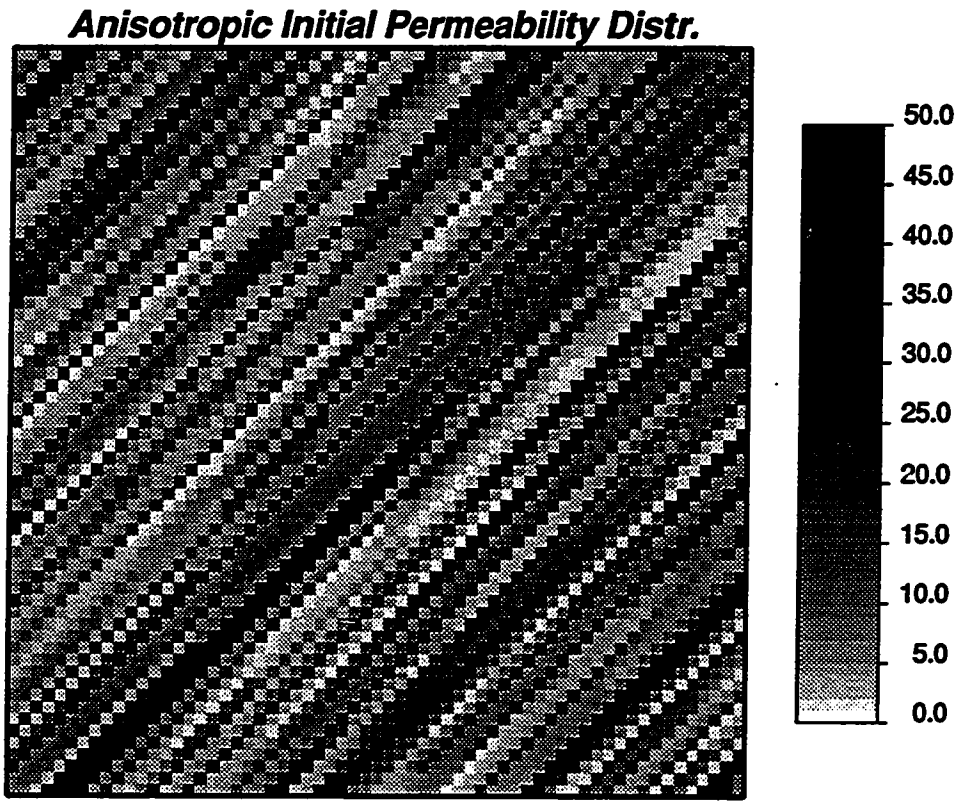

Fig. 5.23: Anisotropic (Cross-Bedded) Stochastic Permeability Distribution. ($\lambda_{D_t} = 1.0$, $\lambda_{D_t} = 0.016$, $V = 0.7$, 45° Structure Orientation, 63 x 63 Values).

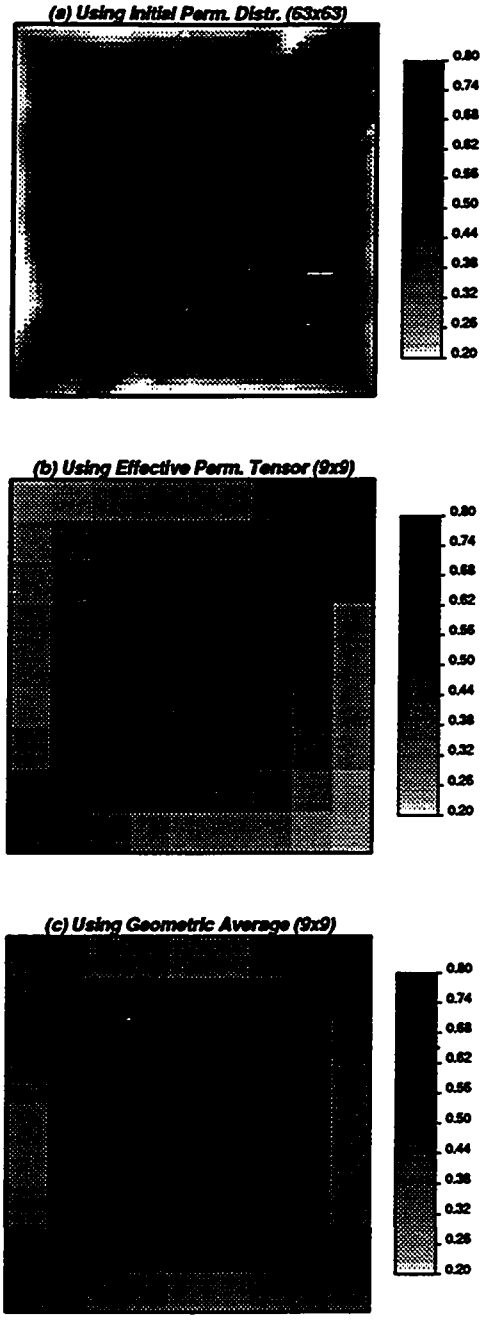

Fig. 5.24: Water Saturation Maps After 8 Days of Water Injection Using (a) the Initial Permeability Distribution (b) the Effective Permeability Tensor and (c) the Geometrically Averaged Permeability.

of the four producing wells after 8 days of water injection. Clearly, the geometric averaging process is not able to capture the effect of the anisotropic nature of the permeability distribution, whereas the effective permeability tensor is able to capture the existence of permeability anisotropy and the effect of the orientation of the permeability structures.

Figure 5.25 shows the cumulative oil recovered as a function of pore volumes of water injected for producer number one (P-1) located in the northwest corner of the field. Based on the recovery curves, there appears to be no distinct advantage of using the effective permeability tensor method in favor of the geometric average method since both recovery curves underpredicts the oil recovery to some degree. However, Figure 5.26 which shows the fractional flow of water as a function of pore volumes of water injected, indicates that water breakthrough is more accurately predicted using the effective permeability tensor.

Cumulative oil recoveries for producing well number two (P-2) are shown in Figure 5.27 as a function of pore volumes of water injected. A significantly better prediction of the oil recovery is realized using the effective permeability tensor compared to using the geometric average. This observation is closely linked to the water saturation map using the geometric average which shows a fairly uniform water distribution (Figure 5.24c). Consequently, oil recovery is too optimistic at well P-2 which receives a substantial portion of the injected water according to the waterfloods through the initial permeability distribution (Figure 5.24a) and using the effective permeability tensor (Figure 5.24b). Figure 5.28 supports this observation. Water breaks through later in well P-2 using the geometric average of permeability than when using the microscale distribution and the effective permeability tensor.

In summary, the results presented in this chapter demonstrate that the effective permeability tensors obtained by the analytical and numerical methods agree well. In addition, results from miscible displacement and waterflood simulations show that the effective permeability tensor method outperforms standard permeability averaging methods for generally anisotropic permeability distributions.

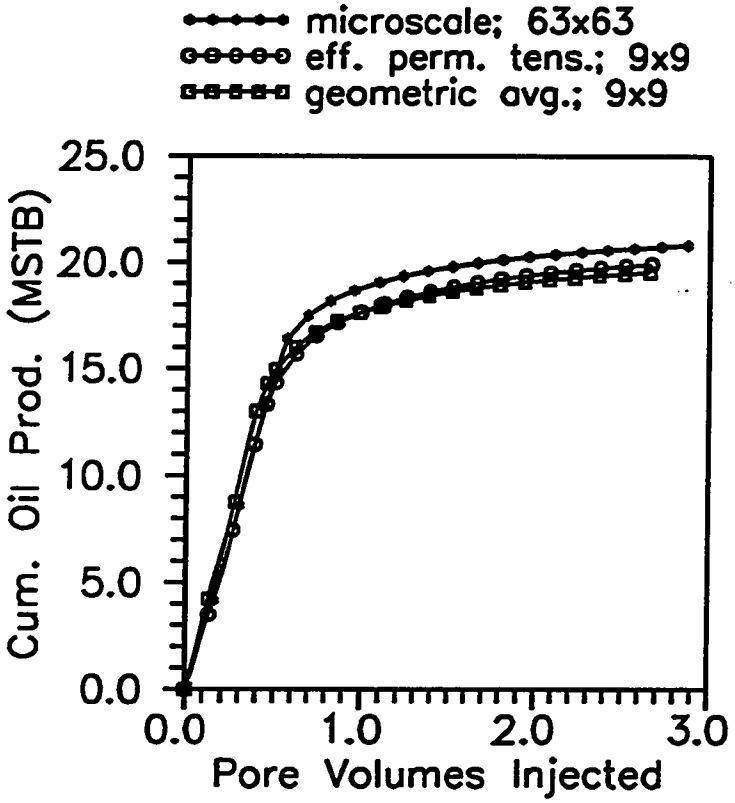

Fig. 5.25: Cumulative Oil Recovery Versus Pore Volumes Injected for Producing Well P-1 in a 5-Spot Waterflood. Anisotropic (Cross-Bedded) Initial Permeability Distribution. Effect of Permeability Upscaling.

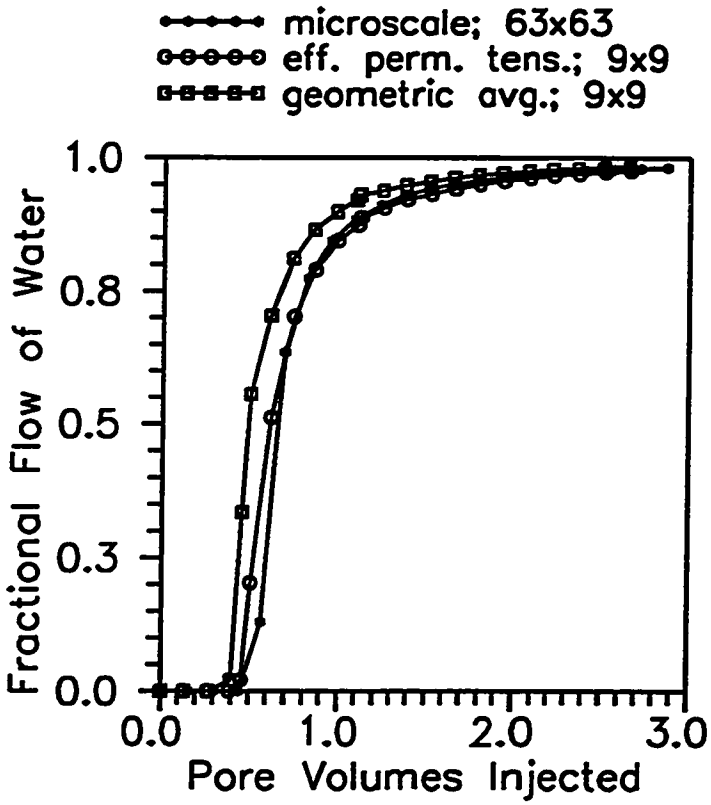

Fig. 5.26: Fractional Flow of Water Versus Pore Volumes Injected for Producing Well P-1 in a 5-Spot Waterflood. Anisotropic (Cross-Bedded) Initial Permeability Distribution. Effect of Permeability Upscaling.

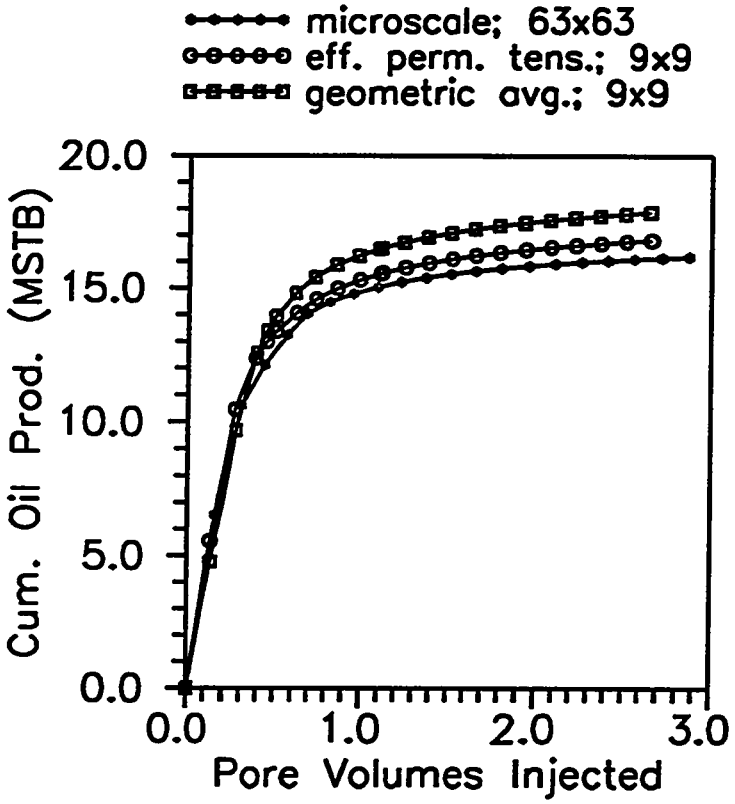

Fig. 5.27: Cumulative Oil Recovery Versus Pore Volumes Injected for Producing Well P-2 in a 5-Spot Waterflood. Anisotropic (Cross-Bedded) Initial Permeability Distribution. Effect of Permeability Upscaling.

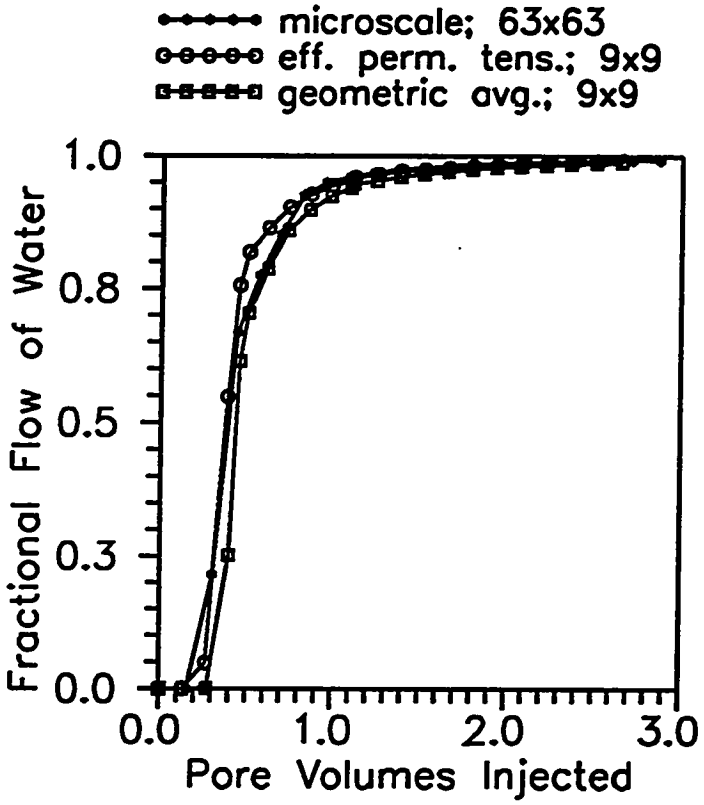

Fig. 5.28: Fractional Flow of Water Versus Pore Volumes Injected for Producing Well P-2 in a 5-Spot Waterflood. Anisotropic (Cross-Bedded) Initial Permeability Distribution. Effect of Permeability Upscaling.

CHAPTER VI
SUMMARY AND CONCLUSIONS

The objective of this study has been to develop an analytical method for calculating effective permeability of a simulator grid block. The motivation for developing an effective permeability method is to improve the computational efficiency in reservoir simulation by reducing the number of grid blocks required and at the same time properly account for local permeability heterogeneities and their effects on fluid flow.

A variety of effective permeability methods are available in the literature, and these methods can generally be divided into two types: numerical and analytical. Numerical methods have the advantage of handling complex heterogeneities, but may be computationally demanding. Analytical methods are generally restricted by simplifying assumptions with respect to the permeability heterogeneities. However, analytical methods are usually more computationally efficient than numerical methods, which require solving the continuity equation for the pressure distribution and Darcy's law for the velocity vectors in order to back-calculate the effective permeability of the medium. Several analytical methods have been proposed, such as streamtube methods for shale/sand sequences, perturbation methods, and effective medium theory and real-space renormalization techniques related to percolation theory. A limited number of methods allow for full tensor representation of effective permeability.

Permeability heterogeneities are often anisotropic in nature, and the anisotropic permeability structures are not necessarily aligned with the simulation coordinate axes. Full tensor methods are required to properly account for general permeability anisotropy.

The first part of this study deals with the development of an effective permeability method. It is an analytical, full tensor, effective permeability method which combines the advantages of numerical and analytical methods. Complex permeability heterogeneities are handled at a relatively low computational cost. The method honors both the location and the orientation of small scale permeability heterogeneities within the grid block.

The second part of this study handles the development of transmissibilities for cases of generally anisotropic permeability. Reservoir simulators have traditionally been restricted to handle only the diagonal elements of the permeability tensor. However, some simulators have recently been developed to accommodate a full tensor formulation of permeability. Two methods are presented for calculating transmissibilities that honor full tensor permeability. These two methods are extensions and parallels to methods presented in the literature.

The last part of this study includes results from comparisons of effective permeability tensors as well as comparisons of results from fluid flow simulations. Effective permeability is calculated for various heterogeneous permeability fields, and effective permeability tensors obtained by the analytical and a numerical methods show good agreement. The analytical method, however, requires less computational cost.

Steady-state, single-phase, incompressible, unit mobility ratio miscible displacements are simulated using a finite element simulator. Initial cross-bedded permeability distributions of deterministic and stochastic nature and their respective upscaled permeability distributions are used in the simulations. Several standard upscaling methods and the tensor method are investigated. For the rectilinear fluid flow cases considered, using the analytical effective permeability tensor method generally yields the best prediction of the location of the flood front.

A point-centered finite difference simulator is used to simulate waterflooding in two-dimensional, two-phase oil and water systems. Transmissibilities calculated by the methods presented in the second part of the study are inserted into the simulator. The effect of permeability upscaling on fluid displacement is investigated. Results are compared using the initial permeability distribution, the effective perme-

ability tensor method, and standard averaging techniques. The basis for comparison are pressure maps, water saturation maps, oil recovery curves and fractional flow curves. For generally anisotropic permeability systems, the results obtained using the effective permeability tensor show the best agreement with results obtained using the original permeability distribution.

Recommendations for Future Work

All of the work presented is based on two-dimensional permeability distributions. The analytical method presented to calculate effective permeability as a tensor may be extended to handle three-dimensional permeability distributions, although this extension adds another degree of complexity to the problem.

The cases presented in this study are simplified. Factors such as gravity, adverse mobility ratio, relative permeability, dispersivity, and capillary pressure often play an important role in fluid displacements in porous media. Effects of these factors may be accounted for by developing pseudofunctions[51] which are averaging functions that adjust a transport property from one scale to another. The effective permeability method developed here is itself a pseudofunction and a first step along the way to developing other pseudofunctions.

Loss of detail is inevitable in any averaging process. The greater the degree of averaging, the more detail is lost. The displacement of fluids through coarsened permeability fields generally yields prediction of overly optimistic results. Compared to the initial heterogeneous permeability field, the upscaled permeability field is more homogeneous, usually resulting in overprediction of sweep efficiency. Although an effective permeability tensor method may preserve much of the characteristics of the initial permeability field, there is still a need for a practical guideline indicating how much averaging is acceptable. An acceptable degree of averaging may vary from one permeability field to another. For example, relatively homogeneous permeability fields may be coarsened more than highly heterogeneous permeability fields. Therefore, an averaging guideline should be a function of the heterogeneity of the system. A study establishing such a guideline should be conducted.

NOMENCLATURE

Symbol

A_A = area of triangle A, L^2

A_B = area of triangle B, L^2

$B_{ijk\ell}$ = general transmissibility coefficient, L^3

C = apparent anisotropy ratio

c = compressibility, $\left(\frac{M}{LT^2}\right)^{-1}$

F = x-component of general vector

G = y-component of general vector

g = conductance, L^3

h = formation thickness, L

$\bar{i}$ = unit vector (x-axis)

$\bar{j}$ = unit vector (y-axis)

$\mathbf{K}$ = permeability tensor, L^2

k = permeability, L^2

L = system length, L

l = spatial dimension parallel to direction of fluid injection, L

$\bar{n}$ = outward unit normal vector

n_x = x-component of outward unit normal vector

n_y = y-component of outward unit normal vector

nx = number of nodes along x-axis

ny = number of nodes along y-axis

p = pressure, $\frac{M}{LT^2}$

p_i = injection pressure, $\frac{M}{LT^2}$

p_p = production pressure, $\frac{M}{LT^2}$

q = flow rate, $\frac{L^3}{T}$

$\mathbf{R}$ = rotation matrix

R = residual (finite element theory)

T_{x1} = edge transmissibility along x-axis (north), L^3

T_{x2} = edge transmissibility along x-axis (south), L^3

$T_{x_{edge}}$ = sum of T_{x1} and T_{x2}, L^3

T_{xy1} = diagonal transmissibility (ne-sw), L^3

T_{xy2} = diagonal transmissibility (nw-se), L^3

T_{y1} = edge transmissibility along y-axis (west), L^3

T_{y2} = edge transmissibility along y-axis (east), L^3

$T_{y_{edge}}$ = sum of T_{y1} and T_{y2}, L^3

t = spatial dimension transverse to direction of fluid injection, L

U = trial function based on dimensionless coordinate ξ

u = trial function (x-axis)

V = Dykstra-Parsons coefficient

v = Darcy velocity, $\frac{L}{T}$

W = trial function based on dimensionless coordinate η

w = trial function (y-axis)

Δx = length of system block in the x-direction, L

Δy = length of system block in the y-direction, L

α = angle representing direction of k'_{xx}, degrees

β = weighting factor

ϵ = constant representing scale change

η = dimensionless coordinate along y-axis

γ = weighting factor

$\mathbf{\Lambda}$ = mobility tensor, L^3

λ = mobility, L^3

λ_{D_l} = dimensionless correlation length along permeability structures

λ_{D_t} = dimensionless correlation length transverse to permeability structures

μ = fluid viscosity, $\frac{M}{LT}$

Ω = two-dimensional domain

ω = general weighting parameter

$\overline{\Psi}$ = general vector

ϕ = porosity, %

ρ = fluid density, $\frac{M}{L^3}$

ξ = dimensionless coordinate along x-axis

Subscripts

1 = block 1

2 = block 2

3 = block 3

4 = block 4

a = arithmetic

app = apparent

avg = average

b = bottom layer

f = first column

fs = first and second columns combined

$global$ = related to "global" pressure gradient ratio

h = harmonic

i = related to x-axis

$iso.$ = isotropic

j = related to y-axis

k = related to x-axis

ℓ = related to y-axis

L = injection along l-axis

$local$ = related to "local" pressure gradient ratio

max = maximum

nc = no cross-flow

o = oil

s = second column

t = top layer

tb = top and bottom layers combined

ve = cross-flow

w = water

X = injection along x-axis

x = x-direction

xx = diagonal element of permeability/mobility tensor in x-direction

xy = off-diagonal element of permeability/mobility tensor

Y = injection along y-axis

y = y-direction

yx = off-diagonal element of permeability/mobility tensor

yy = diagonal element of permeability/mobility tensor in y-direction

Superscript

$'$ = related to principal axes

$\bar{}$ = indicates vector property

$\tilde{}$ = effective system property

$\hat{}$ = effective property of part of system

$*$ = layer pressure between blocks

o = layer pressure between blocks

REFERENCES

1. Kasap, E. and Lake, L.W.: "Calculating the Effective Permeability Tensor of a Gridblock," *SPEFE* (June 1990) 192-200.

2. Warren, J.E. and Price, H.S.: "Flow in Heterogeneous Porous Media," *SPEJ* (Sept. 1961) 153-169.

3. Jensen, J.L., Lake, L.W. and Hinkley, D.V.: "A Statistical Study of Reservoir Permeability: Distributions, Correlations, and Averages," *SPEFE* (Dec. 1987) 461-468.

4. Journel, A.G., Deutsch, C. and Desbarats, A.J.: "Power Averaging for Block Effective Permeability," *Reservoir Characterization II*, Lake, L.W., Carrol, Jr., H.B., Wesson, T.C. (editors), Academic Press, Inc., San Diego (1991) 149-154.

5. Desbarats, A.J.: "Numerical Estimation of Effective Permeability in Sand-Shale Formations," *Water Res. Res.* (Feb. 1987) 273-286.

6. Desbarats, A.: "Estimation of Effective Permeabilities in the Lower Stevens Formation of the Paloma Field, San Joaquin Valley, California," *SPERE* (Nov. 1988) 1301-1307.

7. Gómez-Hernández, J.J. and Gorelick, S.M.: "Effective Groundwater Model Parameter Values: Influence of Spatial Variability of Hydraulic Conductivity, Leakance, and Recharge," *Water Res. Res.* (March 1989) 405-419.

8. Deutsch, C.: "Calculating Effective Absolute Permeability in Sandstone/Shale Sequences," *SPEFE* (Sept. 1989) 343-348.

9. White, C.D. and Horne, R.N.: "Computing Absolute Transmissibility in the Presence of Fine-Scale Heterogeneity," paper SPE 16011 presented at the 1987 SPE Symposium on Reservoir Simulation, San Antonio, Feb. 1-4.

10. Samier, P.: "A Finite Element Method for Calculating Transmissibilities in N-point Difference Equations Using a Non-Diagonal Permeability Tensor," paper presented at the 1990 2nd European Conference on the Mathematics of Oil Recovery, Arles, France, Sept. 11-14, 121-130.

11. Holden, L., Høiberg, J. and Lia, O.: "An Estimator for the Effective Permeability," paper presented at the 1990 2nd European Conference on the Mathematics of Oil Recovery, Arles, France, Sept. 11-14, 287-290.

12. Durlofsky, L.J. and Chung, E.Y.: "Effective Permeability of Heterogeneous Reservoir Regions," paper presented at the 1990 2nd European Conference on the Mathematics of Oil Recovery, Arles, France, Sept. 11-14, 57-64.

13. Gómez-Hernández, J.J. and Journel, A.G.: "Stochastic Characterization of Grid-Block Permeabilities: from Point Values to Block Tensors," paper presented at the 1990 2nd European Conference on the Mathematics of Oil Recovery, Arles, France, Sept. 11-14, 83-90.

14. Gallouët, T. and Guérillot, D.: "An Optimal Method for Averaging the Absolute Permeability," poster presented at the 1991 3rd International Reservoir Characterization Technical Conference, Tulsa, OK, Nov. 3-5.

15. Haldorsen, H.H. and Lake, L.W.: "A New Approach to Shale Management in

Field-Scale Models," *SPEJ* (Aug. 1984) 447-457.

16. Begg, S.H. and King, P.R.: "Modelling the Effects of Shales on Reservoir Performance: Calculation of Effective Vertical Permeability," paper SPE 13529 presented at the 1985 SPE Symposium on Reservoir Simulation, Dallas, Feb. 10-13.

17. Begg, S.H., Chang, D.M. and Haldorsen, H.H.: "A Simple Statistical Method for Calculating the Effective Vertical Permeability of a Reservoir Containing Discontinuous Shales," paper SPE 14271 presented at the 1985 SPE Annual Technical Conference and Exhibition, Las Vegas, Sept. 22-25.

18. Begg, S.H., Carter, R.R. and Dranfield, P.: "Assigning Effective Values to Simulator Gridblock Parameters for Heterogeneous Reservoirs," *SPERE* (Nov. 1989) 455-463.

19. Abu-elbashar, O.B., Daltaban, T.S., Wall, C.G. and Archer, J.S.: "Statistical and Experimental Calculation of Effective Permeabilities in Presence of Oblique Shales," *The Mathematics of Oil Recovery*, King, P.R. (editor), Oxford University Press, New York (1992) 597-615.

20. Nayfeh, A.H.: *Introduction to Perturbation Techniques*, John Wiley & Sons, Inc., New York (1981).

21. Bush, A.W.: *Perturbation Methods for Engineers and Scientists*, CRC Press, Inc., Boca Raton (1992).

22. McGill, C., King, P. and Williams, J.: "Estimating Effective Permeability: A Comparison of Techniques," poster presented at the 1991 3rd International Reservoir Characterization Technical Conference, Tulsa, OK, Nov. 3-5.

23. King, P.R.: "The use of Field Theoretic Methods for the Study of Flow in a Heterogeneous Porous Medium," *J. Phys. A: Math. Gen.* **20** (1987) 3935-3947.

24. Otero, C., Sáez, A.E. and Rusinek, I.: "Effective Permeabilities for Model Heterogeneous Porous Media," *In Situ* (Sept. 1990) 229-244.

25. Rubin, Y. and Gómez-Hernández, J.J.: "A Stochastic Approach to the Problem of Upscaling of Conductivity in Disordered Media: Theory and Unconditional Numerical Simulations," *Water Res. Res.* (April 1990) 691-701.

26. Kirkpatrick, S.: "Percolation and Conduction," *Rev. Mod. Phys.* (Oct. 1973) 574-588.

27. Bernasconi, J.: "Conduction in Anisotropic Disordered Systems: Effective-Medium Theory," *Phys. Rev. B* (May 1974) 4575-4579.

28. Harris, C.K.: "Application of Generalised Effective-Medium Theory To Transport in Porous Media," *Transport in Porous Media* (Oct. 1990) 517-542.

29. King, P.R.: "The use of Renormalization for Calculating Effective Permeability," *Transport in Porous Media* (Feb. 1989) 37-58.

30. Jones, A., King, P., McGill, C. and Williams, J.: "Renormalization: A Multilevel Methodology for Upscaling," poster presented at the 1991 3rd International Reservoir Characterization Technical Conference, Tulsa, OK, Nov. 3-5.

31. Williams, J.K.: "Simple Renormalization Schemes for Calculating Effective Properties of Heterogeneous Reservoirs," *The Mathematics of Oil Recovery*, King, P.R. (editor), Oxford University Press, New York (1992) 281-298.

32. Frank, D.J. and Lobb, C.J.: "Highly Efficient Algorithm for Percolative Trans-

port Studies in Two Dimensions," *Phys. Rev. B* (Jan. 1988) 302-307.

33. Poulisse, H.N.J.: "Effective Absolute Permeability in the Presence of Sub-Grid Heterogeneities: An Analytical Approach," *The Mathematics of Oil Recovery*, King, P.R. (editor), Oxford University Press, New York (1992) 699-720.

34. Rice, P.A., Fontugne, D.J., Latini, R.G. and Barduhn, A.J.: "Anisotropic Permeability in Porous Media," *Flow Through Porous Media*, Nunge, R. (editor), American Chemical Society, Washington, D.C. (1970) 48-56.

35. Lake, L.W.: "The Origins of Anisotropy," *JPT* (April 1988) 395-396.

36. Leung, W.F.: "A Tensor Model for Anisotropic and Heterogeneous Reservoirs With Variable Directional Permeabilities," paper SPE 15134 presented at the 1986 SPE California Regional Meeting, Oakland, April 2-4.

37. Dullien, F.A.L.: *Porous Media, Fluid Transport and Pore Structure*, Academic Press, New York (1979).

38. Ramey, H.J. Jr.: "Interference Analysis for Anisotropic Formations - A Case History," *JPT* (Oct. 1975) 1290-1298.

39. Aasum, Y., Kasap, E. and Kelkar, M.: "Scale-Up of Tensorial Effective Permeability to Detect Anisotropy Through MFP Measurements," poster presented at the 1991 3rd International Reservoir Characterization Technical Conference, Tulsa, OK, Nov. 3-5.

40. Goddin, C.S., Craig, F.F. Jr., Wilkes, J.O. and Tek, M.R.: "A Numerical Study of Waterflood Performance in a Stratified System With Crossflow," *JPT* (June 1966) 765-771.

41. Zapata, V.J. and Lake, L.W.: "A Theoretical Analysis of Viscous Crossflow," paper SPE 10111 presented at the 1981 SPE Annual Technical Conference and Exhibition, San Antonio, October 5-7.

42. Shiralkar, G.S.: "Reservoir Simulation of Generally Anisotropic Systems," *SPERE* (Aug. 1990) 409-414.

43. Yanosik, J.L. and McCracken, T.A.: "A Nine-Point, Finite-Difference Reservoir Simulator for Realistic Prediction of Adverse Mobility Ratio Displacements," *SPEJ* (Aug. 1979) 253-262.

44. Young, L.C.: "A Finite-Element Method for Reservoir Simulation," *SPEJ* (Feb. 1981) 115-128.

45. Young, L.C.: Personal Communication, June 1992.

46. Burnett, D.S.: *Finite Element Analysis, From Concepts to Applications*, Addison-Wesley Publishing Company, Reading, Massachusetts (1987).

47. Jain, M.K., Iyengar, S.R.K. and Jain, R.K.: *Numerical Methods for Scientific and Engineering Computation*, John Wiley & Sons, Inc., New York (1985).

48. Shiralkar, G.S. and Stephenson, R.E.: "A General Formulation for Simulating Physical Dispersion and a New Nine-Point Scheme," *SPERE* (Feb. 1991) 115-120.

49. M.O.R.E. simulator, Black-Oil Version, Reservoir Simulation Research Corporation, Tulsa, May 1992.

50. Yang, A.-P.: "Turning Bands Method to Generate 2-D Random Field with Autocorrelation," University of Texas at Austin (April 1987).

51. Lake, L.W., Kasap, E. and Shook, M.: "Pseudofunctions - The Key to Practical Use of Reservoir Description," paper presented at the 2nd North Sea Oil and Gas Reservoirs Conference, Trondheim, Norway, May 1989, 297-308.

APPENDIX A
CALCULATION OF PERMEABILITIES ALONG PRINCIPAL DIRECTIONS

This section shows, using a small example (5×5 grid cells), how the permeabilities along the principal directions, k'_{xx} and k'_{yy}, are calculated. The orientation angle relating the x- and x'-axes is 26.6°. Figures A-1 and A-2 show the individual grid cells with their respective numbering. Each cell contains a permeability value and the solid lines connecting grid cells indicate the direction vectors used in the calculation procedure.

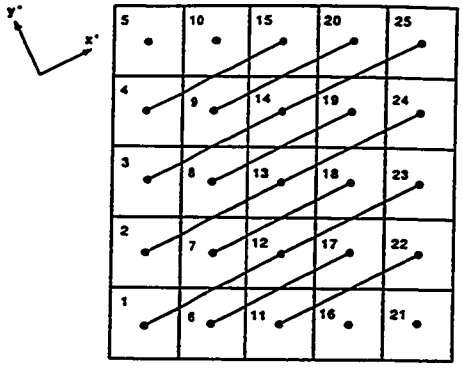

Fig. A-1: Direction Vectors Along the x'-axis.

First, calculate the no cross-flow permeability, $k'_{xx_{nc}}$ along x'-axis. In other words, perform a weighted arithmetic average of the "layer" permeabilities which are obtained using harmonic average since these values are in series with respect to the direction of the x'-axis. Figure A-1 shows the direction vectors and cell values used:

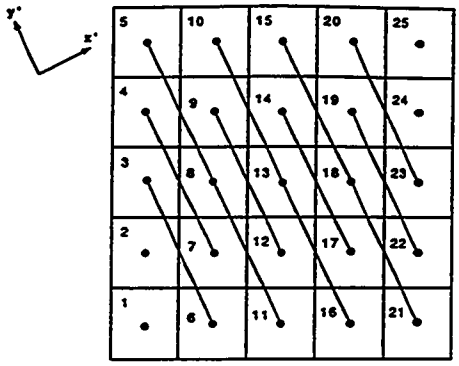

Fig. A-2: Direction Vectors Along the y'-axis.

$$k'_{xx_{nc}} =$$

$$\frac{(3k_{x_{h1}} + 3k_{x_{h2}} + 3k_{x_{h3}} + 2k_{x_{h4}} + k_{x_{h5}} + 2k_{x_{h6}} + 2k_{x_{h7}} + 2k_{x_{h8}} + 2k_{x_{h9}} + k_{x_{h10}} + 2k_{x_{h11}} + k_{x_{h16}} + k_{x_{h21}})}{25} \qquad (A1)$$

where

$$k_{x_{h1}} = \frac{3}{\frac{1}{k_1}+\frac{1}{k_{12}}+\frac{1}{k_{23}}}; \quad k_{x_{h2}} = \frac{3}{\frac{1}{k_2}+\frac{1}{k_{13}}+\frac{1}{k_{24}}}; \quad k_{x_{h3}} = \frac{3}{\frac{1}{k_3}+\frac{1}{k_{14}}+\frac{1}{k_{25}}};$$
$$k_{x_{h4}} = \frac{2}{\frac{1}{k_4}+\frac{1}{k_{15}}}; \quad k_{x_{h5}} = \frac{1}{\frac{1}{k_5}} = k_5; \quad k_{x_{h6}} = \frac{2}{\frac{1}{k_6}+\frac{1}{k_{17}}};$$
$$k_{x_{h7}} = \frac{2}{\frac{1}{k_7}+\frac{1}{k_{18}}}; \quad k_{x_{h8}} = \frac{2}{\frac{1}{k_8}+\frac{1}{k_{19}}}; \quad k_{x_{h9}} = \frac{2}{\frac{1}{k_9}+\frac{1}{k_{20}}};$$
$$k_{x_{h10}} = \frac{1}{\frac{1}{k_{10}}} = k_{10}; \quad k_{x_{h11}} = \frac{2}{\frac{1}{k_{11}}+\frac{1}{k_{22}}}; \quad k_{x_{h16}} = \frac{1}{\frac{1}{k_{16}}} = k_{16};$$
$$k_{x_{h21}} = \frac{1}{\frac{1}{k_{21}}} = k_{21}.$$

Second, calculate the cross-flow permeability, $k'_{xx_{vc}}$ along x'-axis. This case will correspond to injection along x'-axis in Figure A-2. More specifically, perform a weighted harmonic average of the "layer" or "column" permeabilities which are obtained using arithmetic average since the values within each "column" are in parallel with respect to the direction of the x'-axis:

$$k'_{xx_{vc}} =$$

$$25 \Big/ \left(\frac{1}{k_{x_{a1}}} + \frac{1}{k_{x_{a2}}} + \frac{2}{k_{x_{a3}}} + \frac{2}{k_{x_{a4}}} + \frac{3}{k_{x_{a5}}} + \frac{2}{k_{x_{a9}}} + \frac{3}{k_{x_{a10}}} + \frac{2}{k_{x_{a14}}} + \frac{3}{k_{x_{a15}}} + \frac{2}{k_{x_{a19}}} + \frac{2}{k_{x_{a20}}} + \frac{1}{k_{x_{a24}}} + \frac{1}{k_{x_{a25}}}\right) \qquad (A2)$$

where

$$k_{x_{a1}} = k_1; \quad k_{x_{a2}} = k_2; \quad k_{x_{a3}} = \frac{k_3+k_6}{2}; \quad k_{x_{a4}} = \frac{k_4+k_7}{2};$$
$$k_{x_{a5}} = \frac{k_5+k_8+k_{11}}{3}; \quad k_{x_{a9}} = \frac{k_9+k_{12}}{2}; \quad k_{x_{a10}} = \frac{k_{10}+k_{13}+k_{16}}{3}; \quad k_{x_{a14}} = \frac{k_{14}+k_{17}}{2};$$
$$k_{x_{a15}} = \frac{k_{15}+k_{18}+k_{21}}{3}; \quad k_{x_{a19}} = \frac{k_{19}+k_{22}}{2}; \quad k_{x_{a20}} = \frac{k_{20}+k_{23}}{2}; \quad k_{x_{a24}} = k_{24};$$
$$k_{x_{a25}} = k_{25}.$$

Third, calculate the cross-flow permeability, $k'_{yy_{vc}}$ along y'-axis. This case will correspond to injection along y'-axis in Figure A-1. More specifically, perform a weighted harmonic average of the "layer" or "column" permeabilities which are obtained using arithmetic average since the values within each "column" are in parallel with respect to the direction of the y'-axis:

$$k'_{yy_{vc}} =$$

$$25 \Big/ \left(\frac{3}{k_{y_{a1}}} + \frac{3}{k_{y_{a2}}} + \frac{3}{k_{y_{a3}}} + \frac{2}{k_{y_{a4}}} + \frac{1}{k_{y_{a5}}} + \frac{2}{k_{y_{a6}}} + \frac{2}{k_{y_{a7}}} + \frac{2}{k_{y_{a8}}} + \frac{2}{k_{y_{a9}}} + \frac{1}{k_{y_{a10}}} + \frac{2}{k_{y_{a11}}} + \frac{1}{k_{y_{a16}}} + \frac{1}{k_{y_{a21}}}\right) \qquad (A3)$$

where

$$k_{y_{a1}} = \frac{k_1+k_{12}+k_{23}}{3}; \quad k_{y_{a2}} = \frac{k_2+k_{13}+k_{24}}{3}; \quad k_{y_{a3}} = \frac{k_3+k_{14}+k_{25}}{3}; \quad k_{y_{a4}} = \frac{k_4+k_{15}}{2};$$
$$k_{y_{a5}} = k_5; \quad k_{y_{a6}} = \frac{k_6+k_{17}}{2}; \quad k_{y_{a7}} = \frac{k_7+k_{18}}{2}; \quad k_{y_{a8}} = \frac{k_8+k_{19}}{2};$$
$$k_{y_{a9}} = \frac{k_9+k_{20}}{2}; \quad k_{y_{a10}} = k_{10}; \quad k_{y_{a11}} = \frac{k_{11}+k_{22}}{2}; \quad k_{y_{a16}} = k_{16};$$
$$k_{y_{a21}} = k_{21}.$$

Fourth, calculate the no cross-flow permeability, $k'_{yy_{nc}}$ along y'-axis. In other words, perform a weighted arithmetic average of the "layer" permeabilities which

are obtained using harmonic average since these values are in series with respect to the direction of the y'-axis. Figure A-2 shows the direction vectors and cell values used:

$$k'_{yy_{nc}} = \frac{(k_{y_{h1}} + k_{y_{h2}} + 2k_{y_{h3}} + 2k_{y_{h4}} + 3k_{y_{h5}} + 2k_{y_{h9}} + 3k_{y_{h10}} + 2k_{y_{h14}} + 3k_{y_{h15}} + 2k_{y_{h19}} + 2k_{y_{h20}} + k_{y_{h24}} + k_{y_{h25}})}{25} \tag{A4}$$

where

$$k_{y_{h1}} = \frac{1}{\frac{1}{k_1}} = k_1; \quad k_{y_{h2}} = \frac{1}{\frac{1}{k_2}} = k_2; \quad k_{y_{h3}} = \frac{2}{\frac{1}{k_3}+\frac{1}{k_6}};$$
$$k_{y_{h4}} = \frac{2}{\frac{1}{k_4}+\frac{1}{k_7}}; \quad k_{y_{h5}} = \frac{3}{\frac{1}{k_5}+\frac{1}{k_8}+\frac{1}{k_{11}}}; \quad k_{y_{h9}} = \frac{2}{\frac{1}{k_9}+\frac{1}{k_{12}}};$$
$$k_{y_{h10}} = \frac{3}{\frac{1}{k_{10}}+\frac{1}{k_{13}}+\frac{1}{k_{16}}}; \quad k_{y_{h14}} = \frac{2}{\frac{1}{k_{14}}+\frac{1}{k_{17}}}; \quad k_{y_{h15}} = \frac{3}{\frac{1}{k_{15}}+\frac{1}{k_{18}}+\frac{1}{k_{21}}};$$
$$k_{y_{h19}} = \frac{2}{\frac{1}{k_{19}}+\frac{1}{k_{22}}}; \quad k_{y_{h20}} = \frac{2}{\frac{1}{k_{20}}+\frac{1}{k_{23}}}; \quad k_{y_{h24}} = \frac{1}{\frac{1}{k_{24}}} = k_{24};$$
$$k_{y_{h25}} = \frac{1}{\frac{1}{k_{25}}} = k_{25}.$$

Finally, $k'_{xx_{nc}}$, $k'_{xx_{vc}}$, $k'_{yy_{vc}}$, and $k'_{yy_{nc}}$ are combined using a permeability anisotropy weighting procedure similar to that shown in Chapter III to yield k'_{xx} and k'_{yy}:

$$k'_{xx} = \frac{k'_{xx}k'_{xx_{nc}} + k'_{yy}k'_{xx_{vc}}}{k'_{xx} + k'_{yy}} \tag{A5}$$

$$k'_{yy} = \frac{k'_{xx}k'_{yy_{vc}} + k'_{yy}k'_{yy_{nc}}}{k'_{xx} + k'_{yy}}. \tag{A6}$$

Equations (A5) and (A6) are solved for the two unknowns, k'_{xx} and k'_{yy}.

APPENDIX B
DEVELOPMENT OF PERMEABILITY TENSOR FROM COORDINATE ROTATION

This section describes the coordinate rotation procedure to obtain the elements of the permeability tensor for the simulation coordinates (x,y).

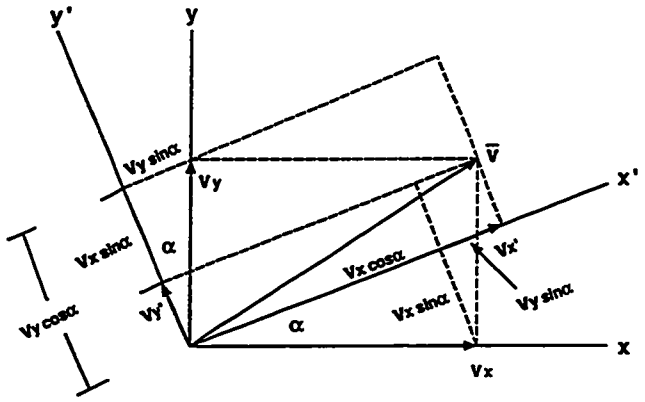

Fig. B-1: Velocity Vector, $\bar{v}$, in the Simulation Coordinate System (x, y) and in the Coordinate System of the Principal Directions of Permeability (x', y').

The objective of this procedure is to obtain the elements of the permeability tensor from the following equations of the velocity components in the simulation coordinates (x,y), where fluid viscosity is 1.0 cp:

$$v_x = -k_{xx}\left(\frac{\partial p}{\partial x}\right) - k_{xy}\left(\frac{\partial p}{\partial y}\right) \qquad (B1)$$

$$v_y = -k_{yx}\left(\frac{\partial p}{\partial x}\right) - k_{yy}\left(\frac{\partial p}{\partial y}\right). \qquad (B2)$$

The goal is to obtain the following permeability tensor:

$$\mathbf{K} = \begin{pmatrix} k_{xx} & k_{xy} \\ k_{yx} & k_{yy} \end{pmatrix}. \tag{B3}$$

For the coordinate system of the principal direction of permeability, the velocity components are given as follows:

$$v'_x = -k'_{xx}\left(\frac{\partial p}{\partial x}\right)' - k'_{xy}\left(\frac{\partial p}{\partial y}\right)' \tag{B4}$$

$$v'_y = -k'_{yx}\left(\frac{\partial p}{\partial x}\right)' - k'_{yy}\left(\frac{\partial p}{\partial y}\right)' \tag{B5}$$

and the permeability tensor for the principal axes is, in general, as follows:

$$\mathbf{K}' = \begin{pmatrix} k'_{xx} & k'_{xy} \\ k'_{yx} & k'_{yy} \end{pmatrix}. \tag{B6}$$

A rotational matrix, $\mathbf{R}$, may be used to relate the velocity vectors of the two coordinate systems:

$$\begin{pmatrix} v'_x \\ v'_y \end{pmatrix} = \mathbf{R}\begin{pmatrix} v_x \\ v_y \end{pmatrix}. \tag{B7}$$

Based on Fig. B-1, Eq. (B7) can be rewritten as follows:

$$\begin{pmatrix} v'_x \\ v'_y \end{pmatrix} = \begin{pmatrix} \cos\alpha & \sin\alpha \\ -\sin\alpha & \cos\alpha \end{pmatrix}\begin{pmatrix} v_x \\ v_y \end{pmatrix}. \tag{B8}$$

The pressure gradients can be related in the same way:

$$\begin{pmatrix} \left(\frac{\partial p}{\partial x}\right)' \\ \left(\frac{\partial p}{\partial y}\right)' \end{pmatrix} = \mathbf{R}\begin{pmatrix} \left(\frac{\partial p}{\partial x}\right) \\ \left(\frac{\partial p}{\partial y}\right) \end{pmatrix} \tag{B9}$$

$$\begin{pmatrix} \left(\frac{\partial p}{\partial x}\right)' \\ \left(\frac{\partial p}{\partial y}\right)' \end{pmatrix} = \begin{pmatrix} \cos\alpha & \sin\alpha \\ -\sin\alpha & \cos\alpha \end{pmatrix}\begin{pmatrix} \left(\frac{\partial p}{\partial x}\right) \\ \left(\frac{\partial p}{\partial y}\right) \end{pmatrix}. \tag{B10}$$

Notice that Eqs. (B4) and (B5) can be written more concisely as:

$$\begin{pmatrix} v_x' \\ v_y' \end{pmatrix} = -\mathbf{K}' \begin{pmatrix} \left(\frac{\partial p}{\partial x}\right)' \\ \left(\frac{\partial p}{\partial y}\right)' \end{pmatrix}. \qquad (B11)$$

Using Eqs. (B7) and (B9), Eq. (B11) can be rewritten as:

$$\mathbf{R}\begin{pmatrix} v_x \\ v_y \end{pmatrix} = -\mathbf{K}'\mathbf{R} \begin{pmatrix} \left(\frac{\partial p}{\partial x}\right) \\ \left(\frac{\partial p}{\partial y}\right) \end{pmatrix}. \qquad (B12)$$

Premultiplying both sides of Eq. (B12) by the inverse of the rotation matrix, $\mathbf{R}^{-1}$, yields:

$$\begin{pmatrix} v_x \\ v_y \end{pmatrix} = -\mathbf{R}^{-1}\mathbf{K}'\mathbf{R} \begin{pmatrix} \left(\frac{\partial p}{\partial x}\right) \\ \left(\frac{\partial p}{\partial y}\right) \end{pmatrix}. \qquad (B13)$$

Based on Eqs. (B1)-(B3) and Eq. (B13), the following expression for $\mathbf{K}$ can be written:

$$\mathbf{K} = \mathbf{R}^{-1}\mathbf{K}'\mathbf{R}. \qquad (B14)$$

We know that the inverse of a 2-by-2 matrix is relatively easy to compute. It is, in general, given as:

$$\begin{pmatrix} a & b \\ c & d \end{pmatrix}^{-1} = \frac{1}{ad-bc}\begin{pmatrix} d & -b \\ -c & a \end{pmatrix}. \qquad (B15)$$

Using Eq. (B15) and referring to Eqs. (B7) and (B8), $\mathbf{R}^{-1}$ can be written as:

$$\mathbf{R}^{-1} = \begin{pmatrix} \cos\alpha & -\sin\alpha \\ \sin\alpha & \cos\alpha \end{pmatrix}. \qquad (B16)$$

Equation (B14) can, therefore, be written as:

$$\mathbf{K} = \begin{pmatrix} \cos\alpha & -\sin\alpha \\ \sin\alpha & \cos\alpha \end{pmatrix}\begin{pmatrix} k_{xx}' & k_{xy}' \\ k_{yx}' & k_{yy}' \end{pmatrix}\begin{pmatrix} \cos\alpha & \sin\alpha \\ -\sin\alpha & \cos\alpha \end{pmatrix}. \qquad (B17)$$

After performing the matrix-matrix multiplications in Eq. (B17) and combining terms, the elements of K can be written as:

$$k_{xx} = (\cos\alpha)^2 k'_{xx} - \sin\alpha\cos\alpha(k'_{xy} + k'_{yx}) + (\sin\alpha)^2 k'_{yy}$$

$$k_{xy} = \sin\alpha\cos\alpha(k'_{xx} - k'_{yy}) + (\cos\alpha)^2 k'_{xy} - (\sin\alpha)^2 k'_{yx}$$

$$k_{yx} = \sin\alpha\cos\alpha(k'_{xx} - k'_{yy}) + (\cos\alpha)^2 k'_{yx} - (\sin\alpha)^2 k'_{xy}$$

$$k_{yy} = (\sin\alpha)^2 k'_{xx} + \sin\alpha\cos\alpha(k'_{yx} + k'_{xy}) + (\cos\alpha)^2 k'_{yy}. \qquad (B18)$$

Assuming the off-diagonal elements k'_{xy} and k'_{yx} are zero for the coordinate system of principal direction of permeability, the permeability tensor, K, can be simplified to:

$$\mathrm{K} = \begin{pmatrix} (\cos\alpha)^2 k'_{xx} + (\sin\alpha)^2 k'_{yy} & \sin\alpha\cos\alpha(k'_{xx} - k'_{yy}) \\ \sin\alpha\cos\alpha(k'_{xx} - k'_{yy}) & (\sin\alpha)^2 k'_{xx} + (\cos\alpha)^2 k'_{yy} \end{pmatrix}. \qquad (B19)$$

Thus, the elements of the permeability tensor for the simulation coordinates are:

$$k_{xx} = (\cos\alpha)^2 k'_{xx} + (\sin\alpha)^2 k'_{yy}$$

$$k_{xy} = k_{yx} = \sin\alpha\cos\alpha(k'_{xx} - k'_{yy})$$

$$k_{yy} = (\sin\alpha)^2 k'_{xx} + (\cos\alpha)^2 k'_{yy}. \qquad (B20)$$

Using Eq. (B20), the pressure gradient ratios for cases where the boundaries parallel to the principal direction of flow are closed (global transverse velocity component is zero) can be calculated as follows:

$$\frac{\left(\frac{\partial p}{\partial y}\right)}{\left(\frac{\partial p}{\partial x}\right)} = -\frac{k_{yx}}{k_{yy}} = -\frac{\sin\alpha\cos\alpha(k'_{xx} - k'_{yy})}{(\sin\alpha)^2 k'_{xx} + (\cos\alpha)^2 k'_{yy}} = -\frac{\tan\alpha(k'_{xx} - k'_{yy})}{(\tan\alpha)^2 k'_{xx} + k'_{yy}} \qquad (B21)$$

$$\frac{\left(\frac{\partial p}{\partial x}\right)}{\left(\frac{\partial p}{\partial y}\right)} = -\frac{k_{xy}}{k_{xx}} = -\frac{\sin\alpha\cos\alpha(k'_{xx} - k'_{yy})}{(\cos\alpha)^2 k'_{xx} + (\sin\alpha)^2 k'_{yy}} = -\frac{\tan\alpha(k'_{xx} - k'_{yy})}{k'_{xx} + (\tan\alpha)^2 k'_{yy}}. \qquad (B22)$$

Based on Eqs. (B21) and (B22), a plot can be made of the ratio of the transverse to longitudinal pressure gradient ratios for various orientation angles of cross-beds. Figure B-2 shows such a plot for a case where the ratio of maximum to minimum permeability is 13. In this "butterfly" plot, the pressure gradient ratios along both x-axis and y-axis are plotted for orientation angles ranging from −90° to 90°. From this plot, it is clear that the pressure gradient ratios are all zero when the bedding planes are either parallel or perpendicular to the simulation coordinate axes; in other words, when cross-bedding angles are 0° or 90° (−90°). For cross-bedding orientations of −45° and 45°, the pressure gradient ratios along both axes are identical.

Notice also that the absolute value of the pressure gradient ratio may exceed one. In this plot, there are four peak values. These maximum pressure gradient ratios occur at −75°, −15°, 15°, and 75° for this particular anisotropy ratio of 13. Other anisotropy ratios, however, will generally show different orientation angles with peak pressure gradient ratios.

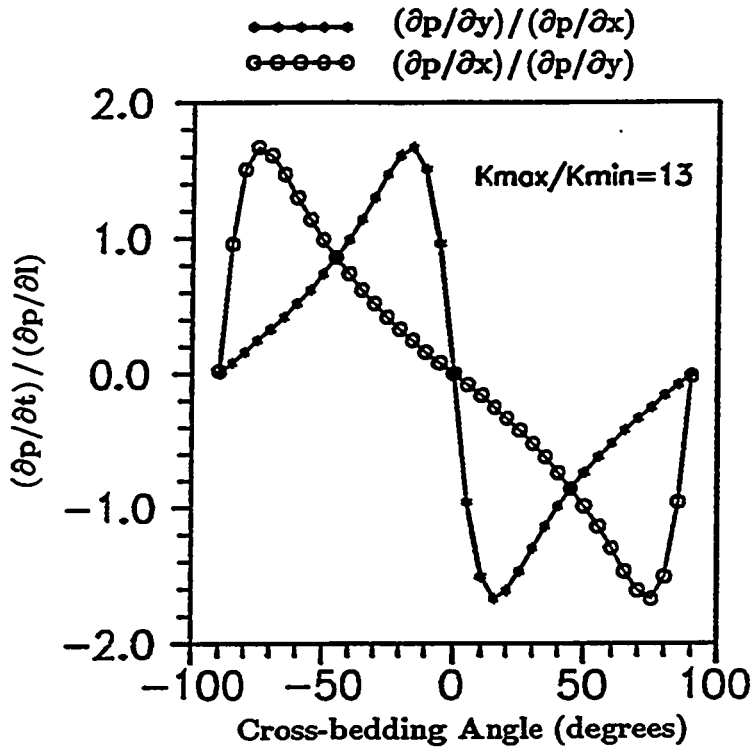

Fig. B-2: Transverse to Longitudinal Pressure Gradient Ratio as a Function of Cross-Bedding Angle.

APPENDIX C
DEVELOPMENT OF APPARENT PERMEABILITIES

The derivations shown in this Appendix are based on a similar approach taken by Kasap and Lake.[1] These investigators used open boundary conditions and tensorial local permeabilities. However, in the following derivations, closed boundary conditions with tensorial local permeabilities are assumed. Moreover, derivations of $\tilde{k}_{x_{app}}$ and $\tilde{k}_{y_{app}}$ are based on cross-flow correction rather than power averaging.

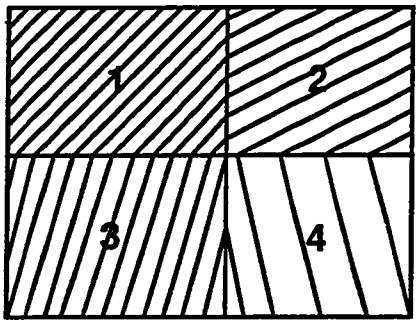

Fig. C-1: System Containing Four Blocks and Four Permeability Tensors.

Determination of $\hat{k}_{x_{app_{tb}}}$ and $\hat{k}_{x_{app_{fs}}}$, and $\hat{k}_{y_{app_{tb}}}$ and $\hat{k}_{y_{app_{fs}}}$.

Figure C-1 is used in the determination of the single or apparent permeabilities, $\hat{k}_{x_{app_{tb}}}$ and $\hat{k}_{x_{app_{fs}}}$, and $\hat{k}_{y_{app_{tb}}}$ and $\hat{k}_{y_{app_{fs}}}$. In all the following cases, unit thickness of the system is assumed.

I. $\hat{k}_{x_{app_{tb}}}$ and $\hat{k}_{x_{app_{fs}}}$:

$\hat{k}_{x_{app_{tb}}}$ is determined from combining the apparent permeability of the top ($\hat{k}_{x_{app_t}}$) and bottom ($\hat{k}_{x_{app_b}}$) layers. Both of these two-block apparent permeabilities

are obtained assuming closed upper and lower boundaries and injection along the x-axis. The two-block permeabilities are then combined to yield $\hat{k}_{x_{appt_b}}$.

1. Isolate the top layer or section of Figure C-1 as shown in Figure C-2.

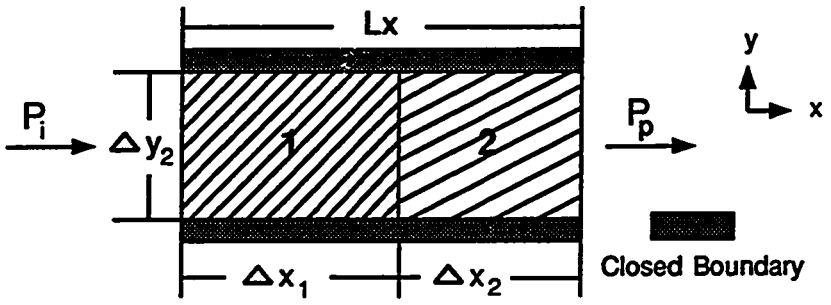

Fig. C-2: Top Layer of Figure C-1 (Injection Along x-axis).

Velocity components along the x-axis for blocks 1 and 2:

$$v_{x_1} = -\frac{1}{\mu}\left(k_{xx_1}\left(\frac{\partial p}{\partial x}\right)_1 + k_{xy_1}\left(\frac{\partial p}{\partial y}\right)_1\right) \qquad (C1)$$

$$v_{x_2} = -\frac{1}{\mu}\left(k_{xx_2}\left(\frac{\partial p}{\partial x}\right)_2 + k_{xy_2}\left(\frac{\partial p}{\partial y}\right)_2\right). \qquad (C2)$$

Velocity component along the x-axis for blocks 1 and 2 combined:

$$\hat{v}_{x_t} = -\frac{1}{\mu}\left(\hat{k}_{xx_t}\left(\frac{\partial \hat{p}}{\partial x}\right)_t + \hat{k}_{xy_t}\left(\frac{\partial \hat{p}}{\partial y}\right)_t\right). \qquad (C3)$$

Velocity components along the y-axis for blocks 1 and 2 are zero because of closed upper and lower boundaries:

$$v_{y_1} = -\frac{1}{\mu}\left(k_{yx_1}\left(\frac{\partial p}{\partial x}\right)_1 + k_{yy_1}\left(\frac{\partial p}{\partial y}\right)_1\right) = 0 \qquad (C4)$$

$$v_{y_2} = -\frac{1}{\mu}\left(k_{yx_2}\left(\frac{\partial p}{\partial x}\right)_2 + k_{yy_2}\left(\frac{\partial p}{\partial y}\right)_2\right) = 0. \qquad (C5)$$

Velocity component along the y-axis for blocks 1 and 2 combined is zero because of closed upper and lower boundaries:

$$\hat{v}_{y_t} = -\frac{1}{\mu}\left(\hat{k}_{yx_t}\left(\frac{\partial \hat{p}}{\partial x}\right)_t + \hat{k}_{yy_t}\left(\frac{\partial \hat{p}}{\partial y}\right)_t\right) = 0. \qquad (C6)$$

Rearrange Eqs. (C4)-(C6):

$$\left(\frac{\partial p}{\partial y}\right)_1 = -\frac{k_{yx_1}}{k_{yy_1}}\left(\frac{\partial p}{\partial x}\right)_1 \qquad (C7)$$

$$\left(\frac{\partial p}{\partial y}\right)_2 = -\frac{k_{yx_2}}{k_{yy_2}}\left(\frac{\partial p}{\partial x}\right)_2 \qquad (C8)$$

$$\left(\frac{\partial \hat{p}}{\partial y}\right)_t = -\frac{\hat{k}_{yx_t}}{\hat{k}_{yy_t}}\left(\frac{\partial \hat{p}}{\partial x}\right)_t. \qquad (C9)$$

Insert Eqs. (C7)-(C9) into Eqs. (C1)-(C3):

$$v_{x_1} = -\frac{1}{\mu}\left(k_{xx_1} - \frac{k_{xy_1}k_{yx_1}}{k_{yy_1}}\right)\left(\frac{\partial p}{\partial x}\right)_1 \qquad (C10)$$

$$v_{x_2} = -\frac{1}{\mu}\left(k_{xx_2} - \frac{k_{xy_2}k_{yx_2}}{k_{yy_2}}\right)\left(\frac{\partial p}{\partial x}\right)_2 \qquad (C11)$$

$$\hat{v}_{x_t} = -\frac{1}{\mu}\left(\hat{k}_{xx_t} - \frac{\hat{k}_{xy_t}\hat{k}_{yx_t}}{\hat{k}_{yy_t}}\right)\left(\frac{\partial \hat{p}}{\partial x}\right)_t. \qquad (C12)$$

Solve Eqs. (C10)-(C12) for the pressure gradients:

$$\left(\frac{\partial p}{\partial x}\right)_1 = \frac{v_{x_1}}{-\frac{1}{\mu}\left(k_{xx_1} - \frac{k_{xy_1}k_{yx_1}}{k_{yy_1}}\right)} \qquad (C13)$$

$$\left(\frac{\partial p}{\partial x}\right)_2 = \frac{v_{x_2}}{-\frac{1}{\mu}\left(k_{xx_2} - \frac{k_{xy_2}k_{yx_2}}{k_{yy_2}}\right)} \qquad (C14)$$

$$\left(\frac{\partial \hat{p}}{\partial x}\right)_t = \frac{\hat{v}_{x_t}}{-\frac{1}{\mu}\left(\hat{k}_{xx_t} - \frac{\hat{k}_{xy_t}\hat{k}_{yx_t}}{\hat{k}_{yy_t}}\right)}. \qquad (C15)$$

The total pressure gradient can be expressed as:

$$\left(\frac{\partial \hat{p}}{\partial x}\right)_t = \frac{\Delta x_1}{L_x}\left(\frac{\partial p}{\partial x}\right)_1 + \frac{\Delta x_2}{L_x}\left(\frac{\partial p}{\partial x}\right)_2. \qquad (C16)$$

Since the total pressure drop is constant:

$$\hat{v}_{x_t} = v_{x_1} = v_{x_2}. \qquad (C17)$$

Use Eqs. (C13)-(C15) and Eq. (C17) in Eq. (C16):

$$\frac{1}{\left(\hat{k}_{xx_t} - \frac{\hat{k}_{xy_t}\hat{k}_{yx_t}}{\hat{k}_{yy_t}}\right)} = \frac{\Delta x_1}{L_x\left(k_{xx_1} - \frac{k_{xy_1}k_{yx_1}}{k_{yy_1}}\right)} + \frac{\Delta x_2}{L_x\left(k_{xx_2} - \frac{k_{xy_2}k_{yx_2}}{k_{yy_2}}\right)}. \qquad (C18)$$

Rearrange Eq. (C18):

$$\left(\hat{k}_{xx_t} - \frac{\hat{k}_{xy_t}\hat{k}_{yx_t}}{\hat{k}_{yy_t}}\right) = \frac{L_x}{\frac{\Delta x_1}{\left(k_{xx_1} - \frac{k_{xy_1}k_{yx_1}}{k_{yy_1}}\right)} + \frac{\Delta x_2}{\left(k_{xx_2} - \frac{k_{xy_2}k_{yx_2}}{k_{yy_2}}\right)}}. \qquad (C19)$$

Let $\hat{k}_{x_{app_t}} = \left(\hat{k}_{xx_t} - \frac{\hat{k}_{xy_t}\hat{k}_{yx_t}}{\hat{k}_{yy_t}}\right)$ and simplify Eq. (C19):

$$\hat{k}_{x_{app_t}} = \frac{L_x k_{x_{app_1}} k_{x_{app_2}}}{\Delta x_1 k_{x_{app_2}} + \Delta x_2 k_{x_{app_1}}} \qquad (C20)$$

where

$$k_{x_{app_1}} = k_{xx_1} - \frac{k_{xy_1}k_{yx_1}}{k_{yy_1}} \qquad (C21)$$

$$k_{x_{app_2}} = k_{xx_2} - \frac{k_{xy_2}k_{yx_2}}{k_{yy_2}}. \qquad (C22)$$

Notice that $\hat{k}_{x_{app_t}}$ is a weighted harmonic average of the local $k_{x_{app_1}}$ and $k_{x_{app_2}}$.

2. Isolate the bottom layer or section of Figure C-1 as shown in Figure C-3.

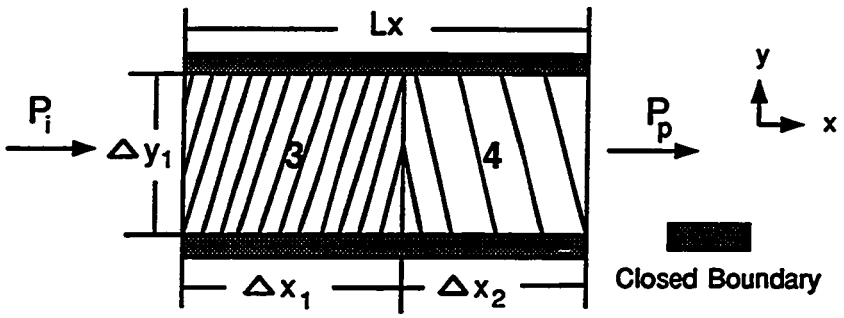

Fig. C-3: Bottom Layer of Figure C-1 (Injection Along x-axis).

Velocity components along the x-axis for blocks 3 and 4:

$$v_{x_3} = -\frac{1}{\mu}\left(k_{xx_3}\left(\frac{\partial p}{\partial x}\right)_3 + k_{xy_3}\left(\frac{\partial p}{\partial y}\right)_3\right) \qquad (C23)$$

$$v_{x_4} = -\frac{1}{\mu}\left(k_{xx_4}\left(\frac{\partial p}{\partial x}\right)_4 + k_{xy_4}\left(\frac{\partial p}{\partial y}\right)_4\right). \qquad (C24)$$

Velocity component along the x-axis for blocks 3 and 4 combined:

$$\hat{v}_{x_b} = -\frac{1}{\mu}\left(\hat{k}_{xx_b}\left(\frac{\partial \hat{p}}{\partial x}\right)_b + \hat{k}_{xy_b}\left(\frac{\partial \hat{p}}{\partial y}\right)_b\right). \qquad (C25)$$

Velocity components along the y-axis for blocks 3 and 4 are zero because of closed upper and lower boundaries:

$$v_{y_3} = -\frac{1}{\mu}\left(k_{yx_3}\left(\frac{\partial p}{\partial x}\right)_3 + k_{yy_3}\left(\frac{\partial p}{\partial y}\right)_3\right) = 0 \qquad (C26)$$

$$v_{y_4} = -\frac{1}{\mu}\left(k_{yx_4}\left(\frac{\partial p}{\partial x}\right)_4 + k_{yy_4}\left(\frac{\partial p}{\partial y}\right)_4\right) = 0. \qquad (C27)$$

Velocity component along the y-axis for blocks 3 and 4 combined is zero because of closed upper and lower boundaries:

$$\hat{v}_{y_b} = -\frac{1}{\mu}\left(\hat{k}_{yx_b}\left(\frac{\partial \hat{p}}{\partial x}\right)_b + \hat{k}_{yy_b}\left(\frac{\partial \hat{p}}{\partial y}\right)_b\right) = 0. \qquad (C28)$$

Rearrange Eqs. (C26)-(C28):

$$\left(\frac{\partial p}{\partial y}\right)_3 = -\frac{k_{yx_3}}{k_{yy_3}}\left(\frac{\partial p}{\partial x}\right)_3 \tag{C29}$$

$$\left(\frac{\partial p}{\partial y}\right)_4 = -\frac{k_{yx_4}}{k_{yy_4}}\left(\frac{\partial p}{\partial x}\right)_4 \tag{C30}$$

$$\left(\frac{\partial \hat{p}}{\partial y}\right)_b = -\frac{\hat{k}_{yx_b}}{\hat{k}_{yy_b}}\left(\frac{\partial \hat{p}}{\partial x}\right)_b. \tag{C31}$$

Insert Eqs. (C29)-(C31) into Eqs. (C23)-(C25):

$$v_{x_3} = -\frac{1}{\mu}\left(k_{xx_3} - \frac{k_{xy_3}k_{yx_3}}{k_{yy_3}}\right)\left(\frac{\partial p}{\partial x}\right)_3 \tag{C32}$$

$$v_{x_4} = -\frac{1}{\mu}\left(k_{xx_4} - \frac{k_{xy_4}k_{yx_4}}{k_{yy_4}}\right)\left(\frac{\partial p}{\partial x}\right)_4 \tag{C33}$$

$$\hat{v}_{x_b} = -\frac{1}{\mu}\left(\hat{k}_{xx_b} - \frac{\hat{k}_{xy_b}\hat{k}_{yx_b}}{\hat{k}_{yy_b}}\right)\left(\frac{\partial \hat{p}}{\partial x}\right)_b. \tag{C34}$$

Solve Eqs. (C32)-(C34) for the pressure gradients:

$$\left(\frac{\partial p}{\partial x}\right)_3 = \frac{v_{x_3}}{-\frac{1}{\mu}\left(k_{xx_3} - \frac{k_{xy_3}k_{yx_3}}{k_{yy_3}}\right)} \tag{C35}$$

$$\left(\frac{\partial p}{\partial x}\right)_4 = \frac{v_{x_4}}{-\frac{1}{\mu}\left(k_{xx_4} - \frac{k_{xy_4}k_{yx_4}}{k_{yy_4}}\right)} \tag{C36}$$

$$\left(\frac{\partial \hat{p}}{\partial x}\right)_b = \frac{\hat{v}_{x_b}}{-\frac{1}{\mu}\left(\hat{k}_{xx_b} - \frac{\hat{k}_{xy_b}\hat{k}_{yx_b}}{\hat{k}_{yy_b}}\right)}. \tag{C37}$$

The total pressure gradient can be expressed as:

$$\left(\frac{\partial \hat{p}}{\partial x}\right)_b = \frac{\Delta x_1}{L_x}\left(\frac{\partial p}{\partial x}\right)_3 + \frac{\Delta x_2}{L_x}\left(\frac{\partial p}{\partial x}\right)_4. \tag{C38}$$

Since the total pressure drop is constant:

$$\hat{v}_{x_b} = v_{x_3} = v_{x_4}. \tag{C39}$$

Use Eqs. (C35)-(C37) and Eq. (C39) in Eq. (C38):

$$\frac{1}{\left(\hat{k}_{xx_b} - \frac{\hat{k}_{xy_b}\hat{k}_{yx_b}}{\hat{k}_{yy_b}}\right)} = \frac{\Delta x_1}{L_x\left(k_{xx_3} - \frac{k_{xy_3}k_{yx_3}}{k_{yy_3}}\right)} + \frac{\Delta x_2}{L_x\left(k_{xx_4} - \frac{k_{xy_4}k_{yx_4}}{k_{yy_4}}\right)}. \tag{C40}$$

Rearrange Eq. (C40):

$$\left(\hat{k}_{xx_b} - \frac{\hat{k}_{xy_b}\hat{k}_{yx_b}}{\hat{k}_{yy_b}}\right) = \frac{L_x}{\frac{\Delta x_1}{\left(k_{xx_3} - \frac{k_{xy_3}k_{yx_3}}{k_{yy_3}}\right)} + \frac{\Delta x_2}{\left(k_{xx_4} - \frac{k_{xy_4}k_{yx_4}}{k_{yy_4}}\right)}}. \tag{C41}$$

Let $\hat{k}_{x_{app_b}} = \left(\hat{k}_{xx_b} - \frac{\hat{k}_{xy_b}\hat{k}_{yx_b}}{\hat{k}_{yy_b}}\right)$ and simplify Eq. (C41):

$$\hat{k}_{x_{app_b}} = \frac{L_x k_{x_{app_3}} k_{x_{app_4}}}{\Delta x_1 k_{x_{app_4}} + \Delta x_2 k_{x_{app_3}}} \tag{C42}$$

where

$$k_{x_{app_3}} = k_{xx_3} - \frac{k_{xy_3}k_{yx_3}}{k_{yy_3}} \tag{C43}$$

$$k_{x_{app_4}} = k_{xx_4} - \frac{k_{xy_4}k_{yx_4}}{k_{yy_4}}. \tag{C44}$$

Notice that $\hat{k}_{x_{app_b}}$ is a weighted harmonic average of the local $k_{x_{app_3}}$ and $k_{x_{app_4}}$.

3. Since the top and bottom layers are parallel with respect to the direction of flow, the effective apparent permeability, $\hat{k}_{x_{app_{tb}}}$, from combining $\hat{k}_{x_{app_t}}$ and $\hat{k}_{x_{app_b}}$ is the following weighted arithmetic average:

$$\hat{k}_{x_{app_{tb}}} = \frac{\Delta y_2}{L_y}\hat{k}_{x_{app_t}} + \frac{\Delta y_1}{L_y}\hat{k}_{x_{app_b}}. \tag{C45}$$

$\hat{k}_{x_{app_{f_s}}}$ is determined from combining the apparent permeability of the first ($\hat{k}_{x_{app_f}}$) and second ($\hat{k}_{x_{app_s}}$) columns. Both of these two-block apparent permeabilities are obtained assuming closed upper and lower boundaries and injection along the x-axis. The two-block permeabilities are then combined to yield $\hat{k}_{x_{app_{f_s}}}$.

4. Isolate the first column of Figure C-1, i.e., combine blocks 1 and 3 as shown in Figure C-4.

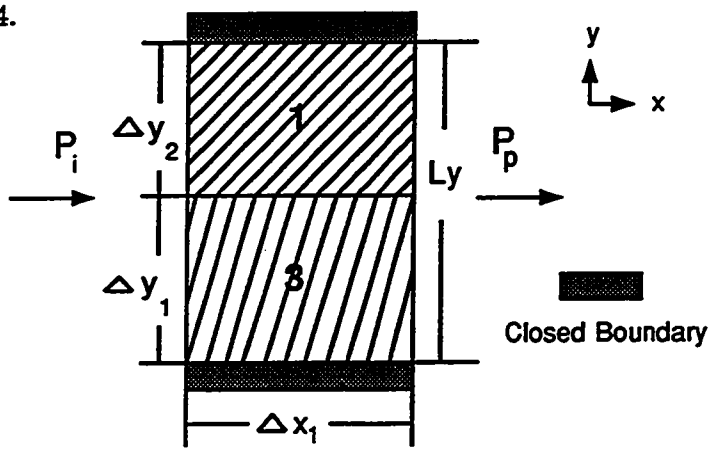

Fig. C-4: First Column of Figure C-1 (Injection Along x-axis).

Velocity components along the x-axis for blocks 1 and 3:

$$v_{x_1} = -\frac{1}{\mu}\left(k_{xx_1}\left(\frac{\partial p}{\partial x}\right)_1 + k_{xy_1}\left(\frac{\partial p}{\partial y}\right)_1\right) \qquad (C46)$$

$$v_{x_3} = -\frac{1}{\mu}\left(k_{xx_3}\left(\frac{\partial p}{\partial x}\right)_3 + k_{xy_3}\left(\frac{\partial p}{\partial y}\right)_3\right). \qquad (C47)$$

Velocity component along the x-axis for blocks 1 and 3 combined:

$$\hat{v}_{x_f} = -\frac{1}{\mu}\left(\hat{k}_{xx_f}\left(\frac{\partial \hat{p}}{\partial x}\right)_f + \hat{k}_{xy_f}\left(\frac{\partial \hat{p}}{\partial y}\right)_f\right). \qquad (C48)$$

Velocity components along the y-axis for blocks 1 and 3 are zero because of closed upper and lower boundaries:

$$v_{y_1} = -\frac{1}{\mu}\left(k_{yx_1}\left(\frac{\partial p}{\partial x}\right)_1 + k_{yy_1}\left(\frac{\partial p}{\partial y}\right)_1\right) = 0 \qquad (C49)$$

$$v_{y_3} = -\frac{1}{\mu}\left(k_{yx_3}\left(\frac{\partial p}{\partial x}\right)_3 + k_{yy_3}\left(\frac{\partial p}{\partial y}\right)_3\right) = 0. \qquad (C50)$$

Velocity component along the y-axis for blocks 1 and 3 combined is zero because of closed upper and lower boundaries:

$$\hat{v}_{y_f} = -\frac{1}{\mu}\left(\hat{k}_{yx_f}\left(\frac{\partial \hat{p}}{\partial x}\right)_f + \hat{k}_{yy_f}\left(\frac{\partial \hat{p}}{\partial y}\right)_f\right) = 0. \qquad (C51)$$

Rearrange Eqs. (C49)-(C51):

$$\left(\frac{\partial p}{\partial y}\right)_1 = -\frac{k_{yx_1}}{k_{yy_1}}\left(\frac{\partial p}{\partial x}\right)_1 \qquad (C52)$$

$$\left(\frac{\partial p}{\partial y}\right)_3 = -\frac{k_{yx_3}}{k_{yy_3}}\left(\frac{\partial p}{\partial x}\right)_3 \qquad (C53)$$

$$\left(\frac{\partial \hat{p}}{\partial y}\right)_f = -\frac{\hat{k}_{yx_f}}{\hat{k}_{yy_f}}\left(\frac{\partial \hat{p}}{\partial x}\right)_f. \qquad (C54)$$

Insert Eqs. (C52)-(C54) into Eqs. (C46)-(C48):

$$v_{x_1} = -\frac{1}{\mu}k_{x_{app_1}}\left(\frac{\partial p}{\partial x}\right)_1 \qquad (C55)$$

$$v_{x_3} = -\frac{1}{\mu}k_{x_{app_3}}\left(\frac{\partial p}{\partial x}\right)_3 \qquad (C56)$$

$$\hat{v}_{x_f} = -\frac{1}{\mu}\left(\hat{k}_{xx_f} - \frac{\hat{k}_{xy_f}\hat{k}_{yx_f}}{\hat{k}_{yy_f}}\right)\left(\frac{\partial \hat{p}}{\partial x}\right)_f. \qquad (C57)$$

$\hat{v}_{x_f}$ is expressed in terms of local velocities as:

$$\hat{v}_{x_f} = \frac{\Delta y_2}{L_y}v_{x_1} + \frac{\Delta y_1}{L_y}v_{x_3}. \qquad (C58)$$

The total pressure gradient is the same as for each of the two blocks separately:

$$\left(\frac{\partial \hat{p}}{\partial x}\right)_f = \left(\frac{\partial p}{\partial x}\right)_1 = \left(\frac{\partial p}{\partial x}\right)_3. \qquad (C59)$$

Use Eqs. (C55)-(C57) and Eq. (C59) in Eq. (C58):

$$\left(\hat{k}_{xx_f} - \frac{\hat{k}_{xy_f}\hat{k}_{yx_f}}{\hat{k}_{yy_f}}\right) = \frac{\Delta y_2}{L_y} k_{x_{app_1}} + \frac{\Delta y_1}{L_y} k_{x_{app_3}}. \qquad (C60)$$

Let $\hat{k}_{x_{app_f}} = \left(\hat{k}_{xx_f} - \frac{\hat{k}_{xy_f}\hat{k}_{yx_f}}{\hat{k}_{yy_f}}\right)$ in Eq. (C60):

$$\hat{k}_{x_{app_f}} = \frac{\Delta y_2}{L_y} k_{x_{app_1}} + \frac{\Delta y_1}{L_y} k_{x_{app_3}}. \qquad (C61)$$

Notice that $\hat{k}_{x_{app_f}}$ is a weighted arithmetic average of the local $k_{x_{app_1}}$ and $k_{x_{app_3}}$.

5. Isolate the second column of Figure C-1, i.e., combine blocks 2 and 4 as shown in Figure C-5.

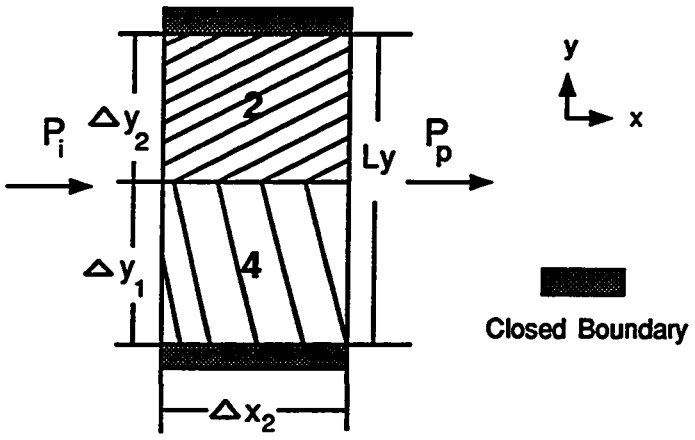

Fig. C-5: Second Column of Figure C-1 (Injection Along x-axis).

Velocity components along the x-axis for blocks 2 and 4:

$$v_{x_2} = -\frac{1}{\mu}\left(k_{xx_2}\left(\frac{\partial p}{\partial x}\right)_2 + k_{xy_2}\left(\frac{\partial p}{\partial y}\right)_2\right) \qquad (C62)$$

$$v_{x_4} = -\frac{1}{\mu}\left(k_{xx_4}\left(\frac{\partial p}{\partial x}\right)_4 + k_{xy_4}\left(\frac{\partial p}{\partial y}\right)_4\right). \qquad (C63)$$

Velocity component along the x-axis for blocks 2 and 4 combined:

$$\hat{v}_{x_s} = -\frac{1}{\mu}\left(\hat{k}_{xx_s}\left(\frac{\partial \hat{p}}{\partial x}\right)_s + \hat{k}_{xy_s}\left(\frac{\partial \hat{p}}{\partial y}\right)_s\right). \qquad (C64)$$

Velocity components along the y-axis for blocks 2 and 4 are zero because of closed upper and lower boundaries:

$$v_{y_2} = -\frac{1}{\mu}\left(k_{yx_2}\left(\frac{\partial p}{\partial x}\right)_2 + k_{yy_2}\left(\frac{\partial p}{\partial y}\right)_2\right) = 0 \qquad (C65)$$

$$v_{y_4} = -\frac{1}{\mu}\left(k_{yx_4}\left(\frac{\partial p}{\partial x}\right)_4 + k_{yy_4}\left(\frac{\partial p}{\partial y}\right)_4\right) = 0. \qquad (C66)$$

Velocity component along the y-axis for blocks 2 and 4 combined is zero because of closed upper and lower boundaries:

$$\hat{v}_{y_s} = -\frac{1}{\mu}\left(\hat{k}_{yx_s}\left(\frac{\partial \hat{p}}{\partial x}\right)_s + \hat{k}_{yy_s}\left(\frac{\partial \hat{p}}{\partial y}\right)_s\right) = 0. \qquad (C67)$$

Rearrange Eqs. (C65)-(C67):

$$\left(\frac{\partial p}{\partial y}\right)_2 = -\frac{k_{yx_2}}{k_{yy_2}}\left(\frac{\partial p}{\partial x}\right)_2 \qquad (C68)$$

$$\left(\frac{\partial p}{\partial y}\right)_4 = -\frac{k_{yx_4}}{k_{yy_4}}\left(\frac{\partial p}{\partial x}\right)_4 \qquad (C69)$$

$$\left(\frac{\partial \hat{p}}{\partial y}\right)_s = -\frac{\hat{k}_{yx_s}}{\hat{k}_{yy_s}}\left(\frac{\partial \hat{p}}{\partial x}\right)_s. \qquad (C70)$$

Insert Eqs. (C68)-(C70) into Eqs. (C62)-(C64):

$$v_{x_2} = -\frac{1}{\mu}k_{x_{eff2}}\left(\frac{\partial p}{\partial x}\right)_2 \qquad (C71)$$

$$v_{x_4} = -\frac{1}{\mu} k_{x_{app_4}} \left(\frac{\partial p}{\partial x}\right)_4 \tag{C72}$$

$$\hat{v}_{x_s} = -\frac{1}{\mu}\left(\hat{k}_{xx_s} - \frac{\hat{k}_{xy_s}\hat{k}_{yx_s}}{\hat{k}_{yy_s}}\right)\left(\frac{\partial \hat{p}}{\partial x}\right)_s . \tag{C73}$$

$\hat{v}_{x_s}$ is expressed in terms of local velocities as:

$$\hat{v}_{x_s} = \frac{\Delta y_2}{L_y} v_{x_2} + \frac{\Delta y_1}{L_y} v_{x_4} . \tag{C74}$$

The total pressure gradient is the same as for each of the two blocks separately:

$$\left(\frac{\partial \hat{p}}{\partial x}\right)_s = \left(\frac{\partial p}{\partial x}\right)_2 = \left(\frac{\partial p}{\partial x}\right)_4 . \tag{C75}$$

Use Eqs. (C71)-(C73) and Eq. (C75) in Eq. (C74):

$$\left(\hat{k}_{xx_s} - \frac{\hat{k}_{xy_s}\hat{k}_{yx_s}}{\hat{k}_{yy_s}}\right) = \frac{\Delta y_2}{L_y} k_{x_{app_2}} + \frac{\Delta y_1}{L_y} k_{x_{app_4}} . \tag{C76}$$

Let $\hat{k}_{x_{app_s}} = \left(\hat{k}_{xx_s} - \frac{\hat{k}_{xy_s}\hat{k}_{yx_s}}{\hat{k}_{yy_s}}\right)$ in Eq. (C76):

$$\hat{k}_{x_{app_s}} = \frac{\Delta y_2}{L_y} k_{x_{app_2}} + \frac{\Delta y_1}{L_y} k_{x_{app_4}} . \tag{C77}$$

Notice that $\hat{k}_{x_{app_s}}$ is a weighted arithmetic average of the local $k_{x_{app_2}}$ and $k_{x_{app_4}}$.

6. Since the two columns of blocks are in series with respect to the direction of flow, the effective apparent permeability, $\hat{k}_{x_{app_{fs}}}$, from combining $\hat{k}_{x_{app_f}}$ and $\hat{k}_{x_{app_s}}$ is the following weighted harmonic average:

$$\hat{k}_{x_{app_{fs}}} = \frac{\hat{k}_{x_{app_f}} \hat{k}_{x_{app_s}} L_x}{\hat{k}_{x_{app_f}} \Delta x_2 + \hat{k}_{x_{app_s}} \Delta x_1} . \tag{C78}$$

II. $\hat{k}_{y_{app_{tb}}}$ and $\hat{k}_{y_{app_{tb}}}$:

$\hat{k}_{y_{app_{tb}}}$ is determined from combining the apparent permeability of the top ($\hat{k}_{y_{app_t}}$) and bottom ($\hat{k}_{y_{app_b}}$) layers. Both of these two-block apparent permeabilities are obtained assuming closed left and right boundaries and injection along the y-axis. The two-block permeabilities are then combined to yield $\hat{k}_{y_{app_{tb}}}$.

1. Isolate the top layer or section of Figure C-1 as shown in Figure C-6.

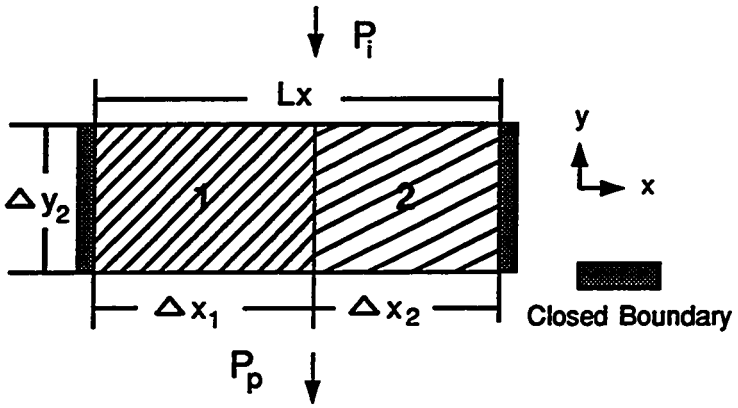

Fig. C-6: Top Layer of Figure C-1 (Injection Along y-axis).

Velocity components along the x-axis for blocks 1 and 2 are zero because of closed left and right boundaries:

$$v_{x_1} = -\frac{1}{\mu}\left(k_{xx_1}\left(\frac{\partial p}{\partial x}\right)_1 + k_{xy_1}\left(\frac{\partial p}{\partial y}\right)_1\right) = 0 \qquad (C79)$$

$$v_{x_2} = -\frac{1}{\mu}\left(k_{xx_2}\left(\frac{\partial p}{\partial x}\right)_2 + k_{xy_2}\left(\frac{\partial p}{\partial y}\right)_2\right) = 0. \qquad (C80)$$

Velocity component along the x-axis for blocks 1 and 2 combined:

$$\hat{v}_{x_t} = -\frac{1}{\mu}\left(\hat{k}_{xx_t}\left(\frac{\partial \hat{p}}{\partial x}\right)_t + \hat{k}_{xy_t}\left(\frac{\partial \hat{p}}{\partial y}\right)_t\right) = 0. \qquad (C81)$$

Velocity components along the y-axis for blocks 1 and 2:

$$v_{y_1} = -\frac{1}{\mu}\left(k_{yx_1}\left(\frac{\partial p}{\partial x}\right)_1 + k_{yy_1}\left(\frac{\partial p}{\partial y}\right)_1\right) \qquad (C82)$$

$$v_{y_2} = -\frac{1}{\mu}\left(k_{yx_2}\left(\frac{\partial p}{\partial x}\right)_2 + k_{yy_2}\left(\frac{\partial p}{\partial y}\right)_2\right). \qquad (C83)$$

Velocity component along the y-axis for blocks 1 and 2 combined:

$$\hat{v}_{y_t} = -\frac{1}{\mu}\left(\hat{k}_{yx_t}\left(\frac{\partial \hat{p}}{\partial x}\right)_t + \hat{k}_{yy_t}\left(\frac{\partial \hat{p}}{\partial y}\right)_t\right). \qquad (C84)$$

Rearrange Eqs. (C79)-(C81):

$$\left(\frac{\partial p}{\partial x}\right)_1 = -\frac{k_{xy_1}}{k_{xx_1}}\left(\frac{\partial p}{\partial y}\right)_1 \qquad (C85)$$

$$\left(\frac{\partial p}{\partial x}\right)_2 = -\frac{k_{xy_2}}{k_{xx_2}}\left(\frac{\partial p}{\partial y}\right)_2 \qquad (C86)$$

$$\left(\frac{\partial \hat{p}}{\partial x}\right)_t = -\frac{\hat{k}_{xy_t}}{\hat{k}_{xx_t}}\left(\frac{\partial \hat{p}}{\partial y}\right)_t. \qquad (C87)$$

Insert Eqs. (C85)-(C87) into Eqs. (C82)-(C84):

$$v_{y_1} = -\frac{1}{\mu}\left(k_{yy_1} - \frac{k_{xy_1}k_{yx_1}}{k_{xx_1}}\right)\left(\frac{\partial p}{\partial y}\right)_1 \qquad (C88)$$

$$v_{y_2} = -\frac{1}{\mu}\left(k_{yy_2} - \frac{k_{xy_2}k_{yx_2}}{k_{xx_2}}\right)\left(\frac{\partial p}{\partial y}\right)_2 \qquad (C89)$$

$$\hat{v}_{y_t} = -\frac{1}{\mu}\left(\hat{k}_{yy_t} - \frac{\hat{k}_{xy_t}\hat{k}_{yx_t}}{\hat{k}_{xx_t}}\right)\left(\frac{\partial \hat{p}}{\partial y}\right)_t. \qquad (C90)$$

$\hat{v}_{y_t}$ is expressed in terms of local velocities as:

$$\hat{v}_{y_t} = \frac{\Delta x_1}{L_x}v_{y_1} + \frac{\Delta x_2}{L_x}v_{y_2}. \qquad (C91)$$

The total pressure gradient is the same as for each of the two blocks separately:

$$\left(\frac{\partial \hat{p}}{\partial y}\right)_t = \left(\frac{\partial p}{\partial y}\right)_1 = \left(\frac{\partial p}{\partial y}\right)_2. \qquad (C92)$$

Use Eqs. (C88)-(C90) and Eq. (C92) in Eq. (C91):

$$\left(\hat{k}_{yy_t} - \frac{\hat{k}_{xy_t}\hat{k}_{yx_t}}{\hat{k}_{xx_t}}\right) = \frac{\Delta x_1}{L_x}\left(k_{yy_1} - \frac{k_{xy_1}k_{yx_1}}{k_{xx_1}}\right) + \frac{\Delta x_2}{L_x}\left(k_{yy_2} - \frac{k_{xy_2}k_{yx_2}}{k_{xx_2}}\right). \quad (C93)$$

Let $\hat{k}_{y_{app_t}} = \left(\hat{k}_{yy_t} - \frac{\hat{k}_{xy_t}\hat{k}_{yx_t}}{\hat{k}_{xx_t}}\right)$ in Eq. (C93):

$$\hat{k}_{y_{app_t}} = \frac{\Delta x_1}{L_x}k_{y_{app_1}} + \frac{\Delta x_2}{L_x}k_{y_{app_2}} \quad (C94)$$

where

$$k_{y_{app_1}} = k_{yy_1} - \frac{k_{xy_1}k_{yx_1}}{k_{xx_1}} \quad (C95)$$

$$k_{y_{app_2}} = k_{yy_2} - \frac{k_{xy_2}k_{yx_2}}{k_{xx_2}}. \quad (C96)$$

Notice that $\hat{k}_{y_{app_t}}$ is a weighted arithmetic average of the local $k_{y_{app_1}}$ and $k_{y_{app_2}}$.

2. Isolate the bottom layer or section of Figure C-1 as shown in Figure C-7.

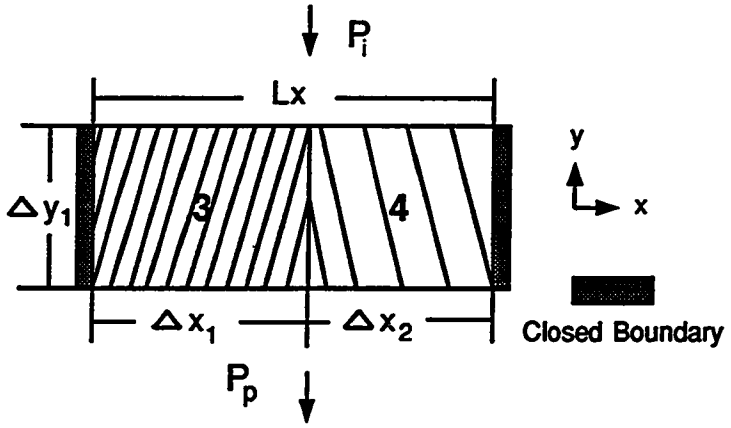

Fig. C-7: Bottom Layer of Figure C-1 (Injection Along y-axis).

Velocity components along the x-axis for blocks 3 and 4 are zero because of closed left and right boundaries:

$$v_{x_3} = -\frac{1}{\mu}\left(k_{xx_3}\left(\frac{\partial p}{\partial x}\right)_3 + k_{xy_3}\left(\frac{\partial p}{\partial y}\right)_3\right) = 0 \qquad (C97)$$

$$v_{x_4} = -\frac{1}{\mu}\left(k_{xx_4}\left(\frac{\partial p}{\partial x}\right)_4 + k_{xy_4}\left(\frac{\partial p}{\partial y}\right)_4\right) = 0. \qquad (C98)$$

Velocity component along the x-axis for blocks 3 and 4 combined:

$$\hat{v}_{x_b} = -\frac{1}{\mu}\left(\hat{k}_{xx_b}\left(\frac{\partial \hat{p}}{\partial x}\right)_b + \hat{k}_{xy_b}\left(\frac{\partial \hat{p}}{\partial y}\right)_b\right) = 0. \qquad (C99)$$

Velocity components along the y-axis for blocks 3 and 4:

$$v_{y_3} = -\frac{1}{\mu}\left(k_{yx_3}\left(\frac{\partial p}{\partial x}\right)_3 + k_{yy_3}\left(\frac{\partial p}{\partial y}\right)_3\right) \qquad (C100)$$

$$v_{y_4} = -\frac{1}{\mu}\left(k_{yx_4}\left(\frac{\partial p}{\partial x}\right)_4 + k_{yy_4}\left(\frac{\partial p}{\partial y}\right)_4\right). \qquad (C101)$$

Velocity component along the y-axis for blocks 3 and 4 combined:

$$\hat{v}_{y_b} = -\frac{1}{\mu}\left(\hat{k}_{yx_b}\left(\frac{\partial \hat{p}}{\partial x}\right)_b + \hat{k}_{yy_b}\left(\frac{\partial \hat{p}}{\partial y}\right)_b\right). \qquad (C102)$$

Rearrange Eqs. (C97)-(C99):

$$\left(\frac{\partial p}{\partial x}\right)_3 = -\frac{k_{xy_3}}{k_{xx_3}}\left(\frac{\partial p}{\partial y}\right)_3 \qquad (C103)$$

$$\left(\frac{\partial p}{\partial x}\right)_4 = -\frac{k_{xy_4}}{k_{xx_4}}\left(\frac{\partial p}{\partial y}\right)_4 \qquad (C104)$$

$$\left(\frac{\partial \hat{p}}{\partial x}\right)_b = -\frac{\hat{k}_{xy_b}}{\hat{k}_{xx_b}}\left(\frac{\partial \hat{p}}{\partial y}\right)_b. \qquad (C105)$$

Insert Eqs. (C103)-(C105) into Eqs. (C100)-(C102):

$$v_{y_3} = -\frac{1}{\mu}\left(k_{yy_3} - \frac{k_{xy_3}k_{yx_3}}{k_{xx_3}}\right)\left(\frac{\partial p}{\partial y}\right)_3 \qquad (C106)$$

$$v_{y_4} = -\frac{1}{\mu}\left(k_{yy_4} - \frac{k_{xy_4}k_{yx_4}}{k_{xx_4}}\right)\left(\frac{\partial p}{\partial y}\right)_4 \qquad (C107)$$

$$\hat{v}_{y_b} = -\frac{1}{\mu}\left(\hat{k}_{yy_b} - \frac{\hat{k}_{xy_b}\hat{k}_{yx_b}}{\hat{k}_{xx_b}}\right)\left(\frac{\partial \hat{p}}{\partial y}\right)_b. \qquad (C108)$$

$\hat{v}_{y_b}$ is expressed in terms of local velocities as:

$$\hat{v}_{y_b} = \frac{\Delta x_1}{L_x}v_{y_3} + \frac{\Delta x_2}{L_x}v_{y_4}. \qquad (C109)$$

The total pressure gradient is the same as for each of the two blocks separately:

$$\left(\frac{\partial \hat{p}}{\partial y}\right)_b = \left(\frac{\partial p}{\partial y}\right)_3 = \left(\frac{\partial p}{\partial y}\right)_4. \qquad (C110)$$

Use Eqs. (C106)-(C108) and Eq. (C110) in Eq. (C109):

$$\left(\hat{k}_{yy_b} - \frac{\hat{k}_{xy_b}\hat{k}_{yx_b}}{\hat{k}_{xx_b}}\right) = \frac{\Delta x_1}{L_x}\left(k_{yy_3} - \frac{k_{xy_3}k_{yx_3}}{k_{xx_3}}\right) + \frac{\Delta x_2}{L_x}\left(k_{yy_4} - \frac{k_{xy_4}k_{yx_4}}{k_{xx_4}}\right). \qquad (C111)$$

Let $\hat{k}_{y_{app_b}} = \left(\hat{k}_{yy_b} - \frac{\hat{k}_{xy_b}\hat{k}_{yx_b}}{\hat{k}_{xx_b}}\right)$ in Eq. (C111):

$$\hat{k}_{y_{app_b}} = \frac{\Delta x_1}{L_x}k_{y_{app_3}} + \frac{\Delta x_2}{L_x}k_{y_{app_4}} \qquad (C112)$$

where

$$k_{y_{app_3}} = k_{yy_3} - \frac{k_{xy_3}k_{yx_3}}{k_{xx_3}} \qquad (C113)$$

$$k_{y_{app_4}} = k_{yy_4} - \frac{k_{xy_4}k_{yx_4}}{k_{xx_4}}. \qquad (C114)$$

Notice that $\hat{k}_{y_{app_b}}$ is a weighted arithmetic average of the local $k_{y_{app_3}}$ and $k_{y_{app_4}}$.

3. Since the top and bottom layers are in series with respect to the direction of flow, the effective apparent permeability, $\hat{k}_{y_{app_{tb}}}$, from combining $\hat{k}_{y_{app_t}}$ and $\hat{k}_{y_{app_b}}$ is the following weighted harmonic average:

$$\hat{k}_{y_{app_{tb}}} = \frac{\hat{k}_{y_{app_t}} \hat{k}_{y_{app_b}} L_y}{\hat{k}_{y_{app_t}} \Delta y_1 + \hat{k}_{y_{app_b}} \Delta y_2}. \qquad (C115)$$

$\hat{k}_{y_{app_f}}$ is determined from combining the apparent permeability of the first ($\hat{k}_{y_{app_f}}$) and second ($\hat{k}_{y_{app_s}}$) columns. Both of these two-block apparent permeabilities are obtained assuming closed left and right boundaries and injection along the y-axis. The two-block permeabilities are then combined to yield $\hat{k}_{y_{app_f}}$.

4. Isolate the first column of Figure C-1, i.e., combine blocks 1 and 3 as shown in Figure C-8.

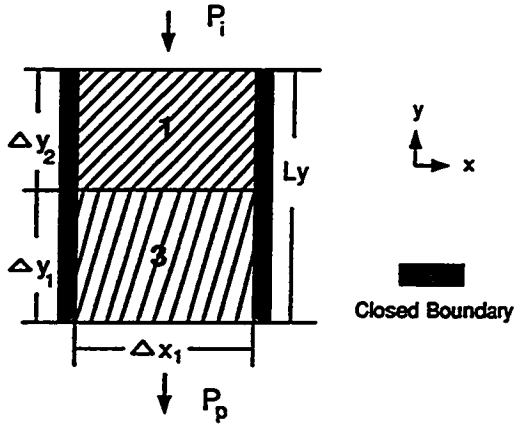

Fig. C-8: First Column of Figure C-1 (Injection Along y-axis).

Velocity components along the x-axis for blocks 1 and 3 are zero because of closed left and right boundaries:

$$v_{x_1} = -\frac{1}{\mu}\left(k_{xx_1}\left(\frac{\partial p}{\partial x}\right)_1 + k_{xy_1}\left(\frac{\partial p}{\partial y}\right)_1\right) = 0 \qquad (C116)$$

$$v_{x_3} = -\frac{1}{\mu}\left(k_{xx_3}\left(\frac{\partial p}{\partial x}\right)_3 + k_{xy_3}\left(\frac{\partial p}{\partial y}\right)_3\right) = 0. \qquad (C117)$$

Velocity component along the x-axis for blocks 1 and 3 combined:

$$\hat{v}_{x_f} = -\frac{1}{\mu}\left(\hat{k}_{xx_f}\left(\frac{\partial \hat{p}}{\partial x}\right)_f + \hat{k}_{xy_f}\left(\frac{\partial \hat{p}}{\partial y}\right)_f\right) = 0. \qquad (C118)$$

Velocity components along the y-axis for blocks 1 and 3:

$$v_{y_1} = -\frac{1}{\mu}\left(k_{yx_1}\left(\frac{\partial p}{\partial x}\right)_1 + k_{yy_1}\left(\frac{\partial p}{\partial y}\right)_1\right) \qquad (C119)$$

$$v_{y_3} = -\frac{1}{\mu}\left(k_{yx_3}\left(\frac{\partial p}{\partial x}\right)_3 + k_{yy_3}\left(\frac{\partial p}{\partial y}\right)_3\right). \qquad (C120)$$

Velocity component along the y-axis for blocks 1 and 3 combined:

$$\hat{v}_{y_f} = -\frac{1}{\mu}\left(\hat{k}_{yx_f}\left(\frac{\partial \hat{p}}{\partial x}\right)_f + \hat{k}_{yy_f}\left(\frac{\partial \hat{p}}{\partial y}\right)_f\right). \qquad (C121)$$

Rearrange Eqs. (C116)-(C118):

$$\left(\frac{\partial p}{\partial x}\right)_1 = -\frac{k_{xy_1}}{k_{xx_1}}\left(\frac{\partial p}{\partial y}\right)_1 \qquad (C122)$$

$$\left(\frac{\partial p}{\partial x}\right)_3 = -\frac{k_{xy_3}}{k_{xx_3}}\left(\frac{\partial p}{\partial y}\right)_3 \qquad (C123)$$

$$\left(\frac{\partial \hat{p}}{\partial x}\right)_f = -\frac{\hat{k}_{xy_f}}{\hat{k}_{xx_f}}\left(\frac{\partial \hat{p}}{\partial y}\right)_f. \qquad (C124)$$

Insert Eqs. (C122)-(C124) into Eqs. (C119)-(C121):

$$v_{y_1} = -\frac{1}{\mu}k_{y_{eff_1}}\left(\frac{\partial p}{\partial y}\right)_1 \qquad (C125)$$

$$v_{y_3} = -\frac{1}{\mu}k_{y_{eff_3}}\left(\frac{\partial p}{\partial y}\right)_3 \qquad (C126)$$

$$\hat{v}_{y_f} = -\frac{1}{\mu}\left(\hat{k}_{yy_f} - \frac{\hat{k}_{xy_f}\hat{k}_{yx_f}}{\hat{k}_{xx_f}}\right)\left(\frac{\partial \hat{p}}{\partial y}\right)_f. \qquad (C127)$$

Solve Eqs. (C125)-(C127) for the pressure gradients:

$$\left(\frac{\partial p}{\partial y}\right)_1 = \frac{v_{y_1}}{-\frac{1}{\mu}k_{y_{app_1}}} \qquad (C128)$$

$$\left(\frac{\partial p}{\partial y}\right)_3 = \frac{v_{y_3}}{-\frac{1}{\mu}k_{y_{app_3}}} \qquad (C129)$$

$$\left(\frac{\partial \hat{p}}{\partial y}\right)_f = \frac{\hat{v}_{y_f}}{-\frac{1}{\mu}\left(\hat{k}_{yy_f} - \frac{\hat{k}_{xy_f}\hat{k}_{yx_f}}{\hat{k}_{xx_f}}\right)}. \qquad (C130)$$

The total pressure gradient can be expressed as:

$$\left(\frac{\partial \hat{p}}{\partial y}\right)_f = \frac{\Delta y_2}{L_y}\left(\frac{\partial p}{\partial y}\right)_1 + \frac{\Delta y_1}{L_y}\left(\frac{\partial p}{\partial y}\right)_3. \qquad (C131)$$

Since the total pressure drop is constant:

$$\hat{v}_{y_f} = v_{y_1} = v_{y_3}. \qquad (C132)$$

Use Eqs. (C128)-(C130) and Eq. (C132) in Eq. (C131):

$$\frac{1}{\left(\hat{k}_{yy_f} - \frac{\hat{k}_{xy_f}\hat{k}_{yx_f}}{\hat{k}_{xx_f}}\right)} = \frac{\Delta y_2}{L_y k_{y_{app_1}}} + \frac{\Delta y_1}{L_y k_{y_{app_3}}}. \qquad (C133)$$

Rearrange Eq. (C133):

$$\left(\hat{k}_{yy_f} - \frac{\hat{k}_{xy_f}\hat{k}_{yx_f}}{\hat{k}_{xx_f}}\right) = \frac{L_y}{\frac{\Delta y_2}{k_{y_{app_1}}} + \frac{\Delta y_1}{k_{y_{app_3}}}}. \qquad (C134)$$

Let $\hat{k}_{y_{app_f}} = \left(\hat{k}_{yy_f} - \frac{\hat{k}_{xy_f}\hat{k}_{yx_f}}{\hat{k}_{xx_f}}\right)$ and simplify Eq. (C134):

$$\hat{k}_{y_{appf}} = \frac{L_y k_{y_{app1}} k_{y_{app3}}}{\Delta y_2 k_{y_{app3}} + \Delta y_1 k_{y_{app1}}}. \qquad (C135)$$

Notice that $\hat{k}_{y_{appf}}$ is a weighted harmonic average of the local $k_{y_{app1}}$ and $k_{y_{app3}}$.

5. Isolate the second column of Figure C-1, i.e., combine blocks 2 and 4 as shown in Figure C-9.

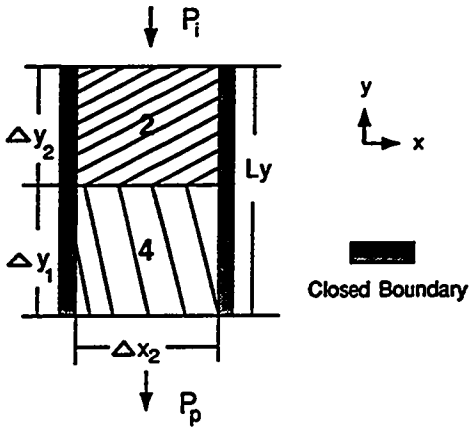

Fig. C-9: Second Column of Figure C-1 (Injection Along y-axis).

Velocity components along the x-axis for blocks 2 and 4 are zero because of closed left and right boundaries:

$$v_{x_2} = -\frac{1}{\mu}\left(k_{xx_2}\left(\frac{\partial p}{\partial x}\right)_2 + k_{xy_2}\left(\frac{\partial p}{\partial y}\right)_2\right) = 0 \qquad (C136)$$

$$v_{x_4} = -\frac{1}{\mu}\left(k_{xx_4}\left(\frac{\partial p}{\partial x}\right)_4 + k_{xy_4}\left(\frac{\partial p}{\partial y}\right)_4\right) = 0. \qquad (C137)$$

Velocity component along the x-axis for blocks 2 and 4 combined:

$$\hat{v}_{x_s} = -\frac{1}{\mu}\left(\hat{k}_{xx_s}\left(\frac{\partial \hat{p}}{\partial x}\right)_s + \hat{k}_{xy_s}\left(\frac{\partial \hat{p}}{\partial y}\right)_s\right) = 0. \qquad (C138)$$

Velocity components along the y-axis for blocks 2 and 4:

$$v_{y_2} = -\frac{1}{\mu}\left(k_{yx_2}\left(\frac{\partial p}{\partial x}\right)_2 + k_{yy_2}\left(\frac{\partial p}{\partial y}\right)_2\right) \qquad (C139)$$

$$v_{y_4} = -\frac{1}{\mu}\left(k_{yx_4}\left(\frac{\partial p}{\partial x}\right)_4 + k_{yy_4}\left(\frac{\partial p}{\partial y}\right)_4\right). \qquad (C140)$$

Velocity component along the y-axis for blocks 2 and 4 combined:

$$\hat{v}_{y_s} = -\frac{1}{\mu}\left(\hat{k}_{yx_s}\left(\frac{\partial \hat{p}}{\partial x}\right)_s + \hat{k}_{yy_s}\left(\frac{\partial \hat{p}}{\partial y}\right)_s\right). \qquad (C141)$$

Rearrange Eqs. (C136)-(C138):

$$\left(\frac{\partial p}{\partial x}\right)_2 = -\frac{k_{xy_2}}{k_{xx_2}}\left(\frac{\partial p}{\partial y}\right)_2 \qquad (C142)$$

$$\left(\frac{\partial p}{\partial x}\right)_4 = -\frac{k_{xy_4}}{k_{xx_4}}\left(\frac{\partial p}{\partial y}\right)_4 \qquad (C143)$$

$$\left(\frac{\partial \hat{p}}{\partial x}\right)_s = -\frac{\hat{k}_{xy_s}}{\hat{k}_{xx_s}}\left(\frac{\partial \hat{p}}{\partial y}\right)_s. \qquad (C144)$$

Insert Eqs. (C142)-(C144) into Eqs. (C139)-(C141):

$$v_{y_2} = -\frac{1}{\mu}k_{y_{app_2}}\left(\frac{\partial p}{\partial y}\right)_2 \qquad (C145)$$

$$v_{y_4} = -\frac{1}{\mu}k_{y_{app_4}}\left(\frac{\partial p}{\partial y}\right)_4 \qquad (C146)$$

$$\hat{v}_{y_s} = -\frac{1}{\mu}\left(\hat{k}_{yy_s} - \frac{\hat{k}_{xy_s}\hat{k}_{yx_s}}{\hat{k}_{xx_s}}\right)\left(\frac{\partial \hat{p}}{\partial y}\right)_s. \qquad (C147)$$

Solve Eqs. (C145)-(C147) for the pressure gradients:

$$\left(\frac{\partial p}{\partial y}\right)_2 = \frac{v_{y_2}}{-\frac{1}{\mu}k_{y_{app_2}}} \qquad (C148)$$

$$\left(\frac{\partial p}{\partial y}\right)_4 = \frac{v_{y_4}}{-\frac{1}{\mu}k_{y_{app_4}}} \qquad (C149)$$

$$\left(\frac{\partial \hat{p}}{\partial y}\right)_s = \frac{\hat{v}_{y_s}}{-\frac{1}{\mu}\left(\hat{k}_{yy_s} - \frac{\hat{k}_{xy_s}\hat{k}_{yx_s}}{\hat{k}_{xx_s}}\right)}. \qquad (C150)$$

The total pressure gradient can be expressed as:

$$\left(\frac{\partial \hat{p}}{\partial y}\right)_s = \frac{\Delta y_2}{L_y}\left(\frac{\partial p}{\partial y}\right)_2 + \frac{\Delta y_1}{L_y}\left(\frac{\partial p}{\partial y}\right)_4. \qquad (C151)$$

Since the total pressure drop is constant:

$$\hat{v}_{y_s} = v_{y_2} = v_{y_4}. \qquad (C152)$$

Use Eqs. (C148)-(C150) and Eq. (C152) in Eq. (C151):

$$\frac{1}{\left(\hat{k}_{yy_s} - \frac{\hat{k}_{xy_s}\hat{k}_{yx_s}}{\hat{k}_{xx_s}}\right)} = \frac{\Delta y_2}{L_y k_{y_{app_2}}} + \frac{\Delta y_1}{L_y k_{y_{app_4}}}. \qquad (C153)$$

Rearrange Eq. (C153):

$$\left(\hat{k}_{yy_s} - \frac{\hat{k}_{xy_s}\hat{k}_{yx_s}}{\hat{k}_{xx_s}}\right) = \frac{L_y}{\frac{\Delta y_2}{k_{y_{app_2}}} + \frac{\Delta y_1}{k_{y_{app_4}}}}. \qquad (C154)$$

Let $\hat{k}_{y_{app_s}} = \left(\hat{k}_{yy_s} - \frac{\hat{k}_{xy_s}\hat{k}_{yx_s}}{\hat{k}_{xx_s}}\right)$ and simplify Eq. (C154):

$$\hat{k}_{y_{app_s}} = \frac{L_y k_{y_{app_2}} k_{y_{app_4}}}{\Delta y_2 k_{y_{app_4}} + \Delta y_1 k_{y_{app_2}}}. \qquad (C155)$$

Notice that $\hat{k}_{y_{app_s}}$ is a weighted harmonic average of the local $k_{y_{app_2}}$ and $k_{y_{app_4}}$.

6. Since the two columns of blocks are in parallel with respect to the direction of flow, the effective apparent permeability, $\hat{k}_{y_{app_{fs}}}$, from combining $\hat{k}_{y_{app_f}}$ and $\hat{k}_{y_{app_s}}$ is the following weighted arithmetic average:

$$\hat{k}_{y_{app_{fs}}} = \frac{\Delta x_1}{L_x}\hat{k}_{y_{app_f}} + \frac{\Delta x_2}{L_x}\hat{k}_{y_{app_s}}. \qquad (C156)$$

Next, it is shown how to arrive at $\tilde{k}_{x_{app}}$ using $\hat{k}_{x_{app_{tb}}}$ and $\hat{k}_{x_{app_{fs}}}$, and $\tilde{k}_{y_{app}}$ using $\hat{k}_{y_{app_{tb}}}$ and $\hat{k}_{y_{app_{fs}}}$.

Derivation of $\tilde{k}_{x_{app}}$ and $\tilde{k}_{y_{app}}$ based on degree of cross-flow:

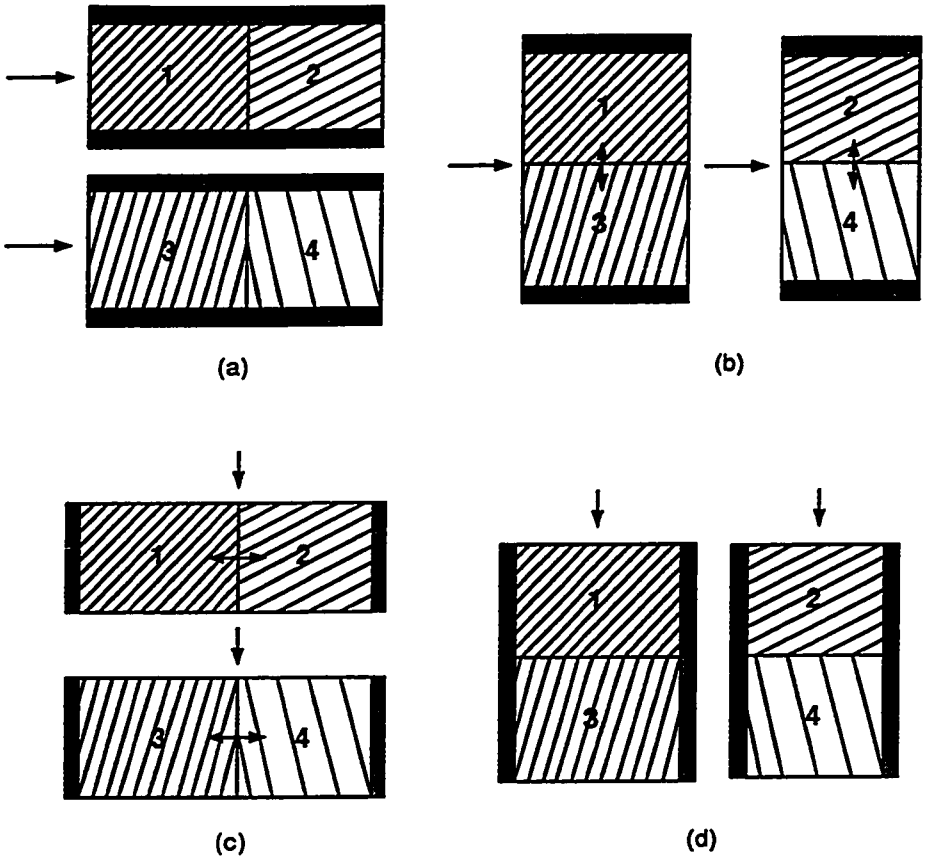

Fig. C-10: Apparent Permeabilities Related to Degree of Cross-Flow.
(a) $\hat{k}_{x_{app_{tb}}}$ (No Cross-Flow); (b) $\hat{k}_{x_{app_{fs}}}$ (Cross-Flow);
(c) $\hat{k}_{y_{app_{tb}}}$ (Cross-Flow); (d) $\hat{k}_{y_{app_{fs}}}$ (No Cross-Flow).

The apparent permeabilities are weighted according to the amount of cross-flow present, which is directly related to the permeability anisotropy ratio. The following weighted average can therefore be written to express $\tilde{k}_{x_{app}}$ and $\tilde{k}_{y_{app}}$:

$$\tilde{k}_{x_{app}} = \frac{\tilde{k}_{x_{app}} \hat{k}_{x_{app_{tb}}} + \tilde{k}_{y_{app}} \hat{k}_{x_{app_{fs}}}}{\tilde{k}_{x_{app}} + \tilde{k}_{y_{app}}} \qquad (C157)$$

$$\tilde{k}_{y_{app}} = \frac{\tilde{k}_{x_{app}}\hat{k}_{y_{app_{tb}}} + \tilde{k}_{y_{app}}\hat{k}_{y_{app_{fs}}}}{\tilde{k}_{x_{app}} + \tilde{k}_{y_{app}}}. \qquad (C158)$$

Let

$$C = \frac{\tilde{k}_{x_{app}}}{\tilde{k}_{y_{app}}}. \qquad (C159)$$

Substitute Eqs. (C157)-(C158) in Eq. (C159):

$$C = \frac{\tilde{k}_{x_{app}}\hat{k}_{x_{app_{tb}}} + \tilde{k}_{y_{app}}\hat{k}_{x_{app_{fs}}}}{\tilde{k}_{x_{app}}\hat{k}_{y_{app_{tb}}} + \tilde{k}_{y_{app}}\hat{k}_{y_{app_{fs}}}}. \qquad (C160)$$

Divide numerator and denominator in Eq. (C160) by $\tilde{k}_{y_{app}}$:

$$C = \frac{C\hat{k}_{x_{app_{tb}}} + \hat{k}_{x_{app_{fs}}}}{C\hat{k}_{y_{app_{tb}}} + \hat{k}_{y_{app_{fs}}}}. \qquad (C161)$$

Eq. (C161) can be rearranged as follows:

$$\hat{k}_{y_{app_{tb}}}C^2 + \left(\hat{k}_{y_{app_{fs}}} - \hat{k}_{x_{app_{tb}}}\right)C - \hat{k}_{x_{app_{fs}}} = 0. \qquad (C162)$$

The apparent anisotropy ratio, C, can be obtained from solving the quadratic equation (C162):

$$C = \frac{-\left(\hat{k}_{y_{app_{fs}}} - \hat{k}_{x_{app_{tb}}}\right) \pm \sqrt{\left(\hat{k}_{y_{app_{fs}}} - \hat{k}_{x_{app_{tb}}}\right)^2 + 4\hat{k}_{y_{app_{tb}}}\hat{k}_{x_{app_{fs}}}}}{2\hat{k}_{y_{app_{tb}}}}. \qquad (C163)$$

Since C must be positive, the plus sign in front of the square root sign in Eq. (C163) must be used. Once C is determined, $\tilde{k}_{x_{app}}$ and $\tilde{k}_{y_{app}}$ are obtained as follows:

$$\tilde{k}_{x_{app}} = \frac{C\hat{k}_{x_{app_{tb}}} + \hat{k}_{x_{app_{fs}}}}{C+1} \qquad (C164)$$

$$\tilde{k}_{y_{app}} = \frac{C\hat{k}_{y_{app_{tb}}} + \hat{k}_{y_{app_{fs}}}}{C+1}. \qquad (C165)$$

APPENDIX D
DEVELOPMENT OF ISOTROPIC "GLOBAL" PRESSURE GRADIENT RATIOS

Figure D-1 is used in the determination of the isotropic "global" pressure gradient ratios. Isotropic "global" pressure gradient ratios are not cross-flow corrected. Such corrections are shown in Chapter III of this study. The "global" pressure gradient ratios are necessary components of the total pressure gradient ratios which in turn are required for determining the elements of the effective permeability tensor. In all the following cases, unit thickness of the system is assumed.

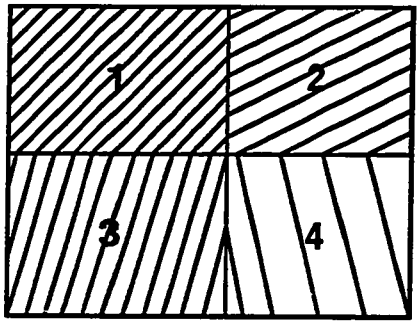

Fig. D-1: System Containing Four Blocks and Four Permeability Tensors.

$\left[\left(\frac{\partial \bar{p}}{\partial y}\right)_X / \left(\frac{\partial \bar{p}}{\partial x}\right)_X\right]_{iso.global}$, the isotropic "global" pressure gradient ratio for injection along the x-axis, is obtained from Figure D-1 assuming closed upper and lower boundaries and injection along the x-axis. In addition, it is assumed that there is no cross-flow between the top and bottom layers in the derivation in order to determine the pressure difference between the two layers. Once an average pressure difference has been obtained between the two layers, the transverse pressure gradient and the transverse to longitudinal pressure gradient ratio can be calculated.

$\left[\left(\frac{\partial \tilde{p}}{\partial x}\right)_Y / \left(\frac{\partial \tilde{p}}{\partial y}\right)_Y\right]_{iso.global}$, the isotropic "global" pressure gradient ratio for injection along the y-axis, is obtained from Figure D-1 in a similar manner. However, since injection for this case occurs along the y-axis, the following boundaries are closed: the left, the right, and the boundary between columns 1 and 2. Column 1 consists of blocks 1 and 3, whereas column 2 consists of blocks 2 and 4. Once an average pressure difference has been obtained between the two columns, the transverse pressure gradient and the transverse to longitudinal pressure gradient ratio can be obtained.

I. $\left[\left(\frac{\partial \tilde{p}}{\partial y}\right)_X / \left(\frac{\partial \tilde{p}}{\partial x}\right)_X\right]_{iso.global}$:

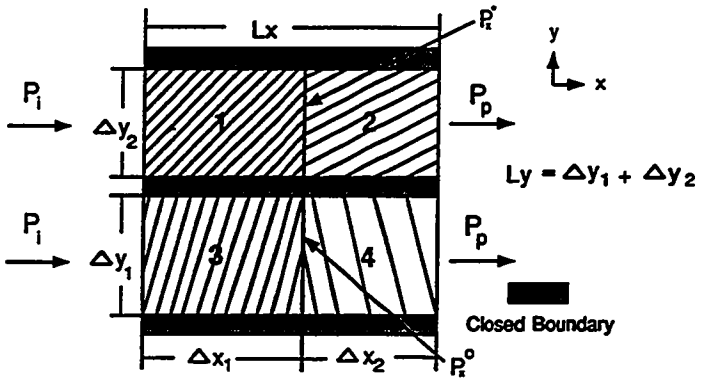

Fig. D-2: Closed Upper, Middle and Lower Boundaries (Injection Along x-axis).

1. Top Layer of Figure D-2:

The flow rates for blocks 1 and 2 are given by Darcy's law as:

$$q_{x_1} = -\frac{k_{x_{app_1}} \Delta y_2}{\mu} \frac{(p_x^* - p_i)}{\Delta x_1} \qquad (D1)$$

$$q_{x_2} = -\frac{k_{x_{app_2}} \Delta y_2}{\mu} \frac{(p_p - p_x^*)}{\Delta x_2}. \qquad (D2)$$

The effective flow rate for the top layer is given by Darcy's law as:

$$\hat{q}_{x_t} = -\frac{\hat{k}_{x_{app_t}} \Delta y_2}{\mu} \frac{(p_p - p_i)}{L_x} \qquad (D3)$$

where $\hat{k}_{x_{app_t}}$ is the weighted harmonic average of the local $k_{x_{app}}$'s in the top layer (see Appendix C).

Eqs. (D1) and (D2) can be rewritten as follows:

$$-\frac{q_{x_1}\mu\Delta x_1}{k_{x_{app_1}}\Delta y_2} = p_x^* - p_i \tag{D4}$$

$$\frac{q_{x_2}\mu\Delta x_2}{k_{x_{app_2}}\Delta y_2} = p_x^* - p_p. \tag{D5}$$

As a result of the law of conservation of mass,

$$\hat{q}_{x_t} = q_{x_1} = q_{x_2}. \tag{D6}$$

Add Eqs. (D4) and (D5) and use Eq. (D6):

$$\frac{\hat{q}_{x_t}\mu}{\Delta y_2}\left(\frac{\Delta x_2}{k_{x_{app_2}}} - \frac{\Delta x_1}{k_{x_{app_1}}}\right) = 2p_x^* - (p_i + p_p). \tag{D7}$$

Solve Eq. (D7) for p_x^*:

$$p_x^* = \frac{\hat{q}_{x_t}\mu}{2\Delta y_2}\left(\frac{\Delta x_2}{k_{x_{app_2}}} - \frac{\Delta x_1}{k_{x_{app_1}}}\right) + \left(\frac{p_i + p_p}{2}\right). \tag{D8}$$

2. Bottom Layer of Figure D-2:

The flow rates for blocks 3 and 4 are given by Darcy's law as:

$$q_{x_3} = -\frac{k_{x_{app_3}}\Delta y_1}{\mu}\frac{(p_x^o - p_i)}{\Delta x_1} \tag{D9}$$

$$q_{x_4} = -\frac{k_{x_{app_4}}\Delta y_1}{\mu}\frac{(p_p - p_x^o)}{\Delta x_2}. \tag{D10}$$

The effective flow rate for the bottom layer is given by Darcy's law as:

$$\hat{q}_{x_b} = -\frac{\hat{k}_{x_{app_b}}\Delta y_1}{\mu}\frac{(p_p - p_i)}{L_x} \tag{D11}$$

where $\hat{k}_{x_{app_b}}$ is the weighted harmonic average of the local $k_{x_{app}}$'s in the bottom layer (see Appendix C).

Eqs. (D9) and (D10) can be rewritten as follows:

$$-\frac{q_{x_3}\mu\Delta x_1}{k_{x_{app_3}}\Delta y_1} = p_x^o - p_i \tag{D12}$$

$$\frac{q_{x_4}\mu\Delta x_2}{k_{x_{app_4}}\Delta y_1} = p_x^o - p_p. \tag{D13}$$

Using the law of conservation of mass:

$$\hat{q}_{x_b} = q_{x_3} = q_{x_4}. \tag{D14}$$

Add Eqs. (D12) and (D13) and use Eq. (D14):

$$\frac{\hat{q}_{x_b}\mu}{\Delta y_1}\left(\frac{\Delta x_2}{k_{x_{app_4}}} - \frac{\Delta x_1}{k_{x_{app_3}}}\right) = 2p_x^o - (p_i + p_p). \tag{D15}$$

Solve Eq. (D15) for p_x^o:

$$p_x^o = \frac{\hat{q}_{x_b}\mu}{2\Delta y_1}\left(\frac{\Delta x_2}{k_{x_{app_4}}} - \frac{\Delta x_1}{k_{x_{app_3}}}\right) + \left(\frac{p_i + p_p}{2}\right). \tag{D16}$$

The maximum possible pressure drop in the direction transverse to flow for the total system is the difference between p_x^* and p_x^o:

$$\begin{aligned}\Delta p_{y_{max}} =& p_x^* - p_x^o \\ =& \frac{\hat{q}_{x_t}\mu}{2\Delta y_2}\left(\frac{\Delta x_2}{k_{x_{app_2}}} - \frac{\Delta x_1}{k_{x_{app_1}}}\right) + \left(\frac{p_i + p_p}{2}\right) \\ & - \frac{\hat{q}_{x_b}\mu}{2\Delta y_1}\left(\frac{\Delta x_2}{k_{x_{app_4}}} - \frac{\Delta x_1}{k_{x_{app_3}}}\right) - \left(\frac{p_i + p_p}{2}\right).\end{aligned} \tag{D17}$$

Eq. (D17) can be simplified:

$$\Delta p_{y_{max}} = \frac{\hat{q}_{x_t}\mu}{2\Delta y_2}\left(\frac{\Delta x_2}{k_{x_{app_2}}} - \frac{\Delta x_1}{k_{x_{app_1}}}\right) - \frac{\hat{q}_{x_b}\mu}{2\Delta y_1}\left(\frac{\Delta x_2}{k_{x_{app_4}}} - \frac{\Delta x_1}{k_{x_{app_3}}}\right). \qquad (D18)$$

Next, separate equations for $\hat{q}_{x_t}\mu$ and $\hat{q}_{x_b}\mu$ are derived based on:

$$\tilde{q}_x = \hat{q}_{x_t} + \hat{q}_{x_b} \qquad (D19)$$

and

$$\tilde{q}_x = -\frac{\hat{k}_{x_{app_{tb}}} L_y}{\mu}\frac{\Delta p_x}{L_x} \qquad (D20)$$

where $\hat{k}_{x_{app_{tb}}}$ is the effective apparent permeability of the top and bottom layers in Figure D-2 when the layers are parallel to the flow direction (see Appendix C).

Rearrange Eq. (D19) and use Eqs. (D11) and (D20):

$$\hat{q}_{x_t} = \tilde{q}_x - \hat{q}_{x_b} = -\frac{\hat{k}_{x_{app_{tb}}} L_y}{\mu}\frac{\Delta p_x}{L_x} - \left(-\frac{\hat{k}_{x_{app_b}} \Delta y_1}{\mu}\frac{\Delta p_x}{L_x}\right). \qquad (D21)$$

Rearrange Eq. (D21):

$$\hat{q}_{x_t}\mu = \frac{\Delta p_x}{L_x}\left(\hat{k}_{x_{app_b}} \Delta y_1 - \hat{k}_{x_{app_{tb}}} L_y\right). \qquad (D22)$$

Again, rearrange Eq. (D19) and use Eqs. (D3) and (D20):

$$\hat{q}_{x_b} = \tilde{q}_x - \hat{q}_{x_t} = -\frac{\hat{k}_{x_{app_{tb}}} L_y}{\mu}\frac{\Delta p_x}{L_x} - \left(-\frac{\hat{k}_{x_{app_t}} \Delta y_2}{\mu}\frac{\Delta p_x}{L_x}\right). \qquad (D23)$$

Rearrange Eq. (D23):

$$\hat{q}_{x_b}\mu = \frac{\Delta p_x}{L_x}\left(\hat{k}_{x_{app_t}} \Delta y_2 - \hat{k}_{x_{app_{tb}}} L_y\right). \qquad (D24)$$

Insert Eqs. (D22) and (D24) into Eq. (D18):

$$\Delta p_{y_{max}} = \frac{\Delta p_x}{2L_x\Delta y_2}\left(\hat{k}_{x_{app_b}}\Delta y_1 - \hat{k}_{x_{app_{tb}}}L_y\right)\left(\frac{\Delta x_2}{k_{x_{app_2}}} - \frac{\Delta x_1}{k_{x_{app_1}}}\right)$$
$$-\frac{\Delta p_x}{2L_x\Delta y_1}\left(\hat{k}_{x_{app_t}}\Delta y_2 - \hat{k}_{x_{app_{tb}}}L_y\right)\left(\frac{\Delta x_2}{k_{x_{app_4}}} - \frac{\Delta x_1}{k_{x_{app_3}}}\right). \quad (D25)$$

In Appendix E it is shown that

$$\Delta p_{y_{avg}} = \frac{1}{2}\Delta p_{y_{max}}. \quad (D26)$$

Using Eq. (D26) in Eq. (D25), $\Delta p_{y_{avg}}$ becomes:

$$\Delta p_{y_{avg}} = \frac{\Delta p_x}{4L_x\Delta y_2}\left(\hat{k}_{x_{app_b}}\Delta y_1 - \hat{k}_{x_{app_{tb}}}L_y\right)\left(\frac{\Delta x_2}{k_{x_{app_2}}} - \frac{\Delta x_1}{k_{x_{app_1}}}\right)$$
$$-\frac{\Delta p_x}{4L_x\Delta y_1}\left(\hat{k}_{x_{app_t}}\Delta y_2 - \hat{k}_{x_{app_{tb}}}L_y\right)\left(\frac{\Delta x_2}{k_{x_{app_4}}} - \frac{\Delta x_1}{k_{x_{app_3}}}\right). \quad (D27)$$

Multiplying Eq. (D27) by $L_x/(\Delta p_x L_y)$ gives the ratio of the transverse pressure gradient to that of the longitudinal pressure gradient:

$$\left[\left(\frac{\partial\tilde{p}}{\partial y}\right)_X \Big/ \left(\frac{\partial\tilde{p}}{\partial x}\right)_X\right]_{iso.global} = \left(\frac{\Delta p_{y_{avg}}}{\Delta p_x}\right)_X \frac{L_x}{L_y}$$
$$= \frac{1}{4\Delta y_2 L_y}\left(\hat{k}_{x_{app_b}}\Delta y_1 - \hat{k}_{x_{app_{tb}}}L_y\right)\left(\frac{\Delta x_2}{k_{x_{app_2}}} - \frac{\Delta x_1}{k_{x_{app_1}}}\right)$$
$$-\frac{1}{4\Delta y_1 L_y}\left(\hat{k}_{x_{app_t}}\Delta y_2 - \hat{k}_{x_{app_{tb}}}L_y\right)\left(\frac{\Delta x_2}{k_{x_{app_4}}} - \frac{\Delta x_1}{k_{x_{app_3}}}\right). \quad (D28)$$

Notice that Eq. (D28) is valid for any local permeability value of the 4 blocks. Also, the sign of Eq. (D28) changes depending on the relative location and magnitude of the local permeability values.

Eq. (D28) is not corrected for cross-flow. This correction is shown in Chapter III of this study.

II. $\left[\left(\frac{\partial \tilde{p}}{\partial x}\right)_Y \Big/ \left(\frac{\partial \tilde{p}}{\partial y}\right)_Y\right]_{iso.global}$:

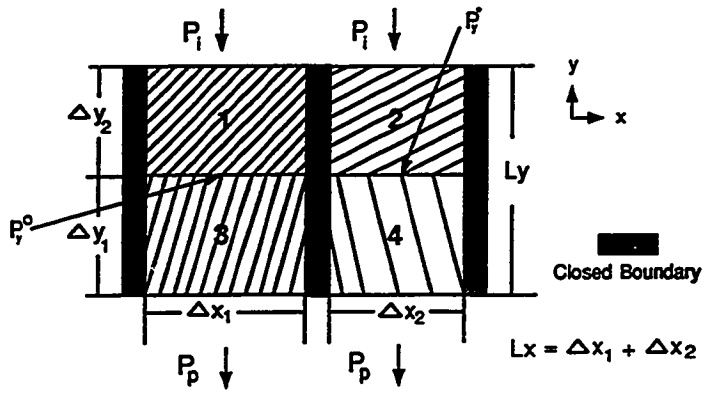

Fig. D-3: Closed Left, Middle and Right Boundaries (Injection Along y-axis).

1. First Column of Figure D-3:

The flow rates for blocks 1 and 3 are given by Darcy's law as:

$$q_{y_1} = -\frac{k_{y_{app_1}} \Delta x_1}{\mu} \frac{(p_y^o - p_i)}{\Delta y_2} \qquad (D29)$$

$$q_{y_3} = -\frac{k_{y_{app_3}} \Delta x_1}{\mu} \frac{(p_p - p_y^o)}{\Delta y_1}. \qquad (D30)$$

The effective flow rate for the first column is given by Darcy's law as:

$$\hat{q}_{y_f} = -\frac{\hat{k}_{y_{app_f}} \Delta x_1}{\mu} \frac{(p_p - p_i)}{L_y}. \qquad (D31)$$

where $\hat{k}_{y_{app_f}}$ is the weighted harmonic average of the local $k_{y_{app}}$'s in the first column, i.e., in blocks 1 and 3 (see Appendix C).

Eqs. (D29) and (D30) can be rewritten as follows:

$$-\frac{q_{y_1} \mu \Delta y_2}{k_{y_{app_1}} \Delta x_1} = p_y^o - p_i \qquad (D32)$$

$$\frac{q_{y_3}\mu\Delta y_1}{k_{y_{app_3}}\Delta x_1} = p_y^o - p_p. \tag{D33}$$

As a result of the law of conservation of mass,

$$\hat{q}_{y_f} = q_{y_1} = q_{y_3}. \tag{D34}$$

Add Eqs. (D32) and (D33) and use Eq. (D34):

$$\frac{\hat{q}_{y_f}\mu}{\Delta x_1}\left(\frac{\Delta y_1}{k_{y_{app_3}}} - \frac{\Delta y_2}{k_{y_{app_1}}}\right) = 2p_y^o - (p_i + p_p). \tag{D35}$$

Solve Eq. (D35) for p_y^o:

$$p_y^o = \frac{\hat{q}_{y_f}\mu}{2\Delta x_1}\left(\frac{\Delta y_1}{k_{y_{app_3}}} - \frac{\Delta y_2}{k_{y_{app_1}}}\right) + \left(\frac{p_i + p_p}{2}\right). \tag{D36}$$

2. Second Column of Figure D-3:

The flow rates for blocks 2 and 4 are given by Darcy's law as:

$$q_{y_2} = -\frac{k_{y_{app_2}}\Delta x_2}{\mu}\frac{(p_y^* - p_i)}{\Delta y_2} \tag{D37}$$

$$q_{y_4} = -\frac{k_{y_{app_4}}\Delta x_2}{\mu}\frac{(p_p - p_y^*)}{\Delta y_1}. \tag{D38}$$

The effective flow rate for the second column is given by Darcy's law as:

$$\hat{q}_{y_s} = -\frac{\hat{k}_{y_{app_s}}\Delta x_2}{\mu}\frac{(p_p - p_i)}{L_y} \tag{D39}$$

where $\hat{k}_{y_{app_s}}$ is the weighted harmonic average of the local $k_{y_{app}}$'s in the second column (see Appendix C).

Eqs. (D37) and (D38) can be rewritten as follows:

$$-\frac{q_{y_2}\mu\Delta y_2}{k_{y_{app_2}}\Delta x_2} = p_y^* - p_i \tag{D40}$$

$$\frac{q_{y_4}\mu\Delta y_1}{k_{y_{app_4}}\Delta x_2} = p_y^* - p_p. \tag{D41}$$

Using the law of conservation of mass:

$$\hat{q}_{y_s} = q_{y_2} = q_{y_4}. \tag{D42}$$

Add Eqs. (D40) and (D41) and use Eq. (D42):

$$\frac{\hat{q}_{y_s}\mu}{\Delta x_2}\left(\frac{\Delta y_1}{k_{y_{app_4}}} - \frac{\Delta y_2}{k_{y_{app_2}}}\right) = 2p_y^* - (p_i + p_p). \tag{D43}$$

Solve Eq. (D43) for p_y^*:

$$p_y^* = \frac{\hat{q}_{y_s}\mu}{2\Delta x_2}\left(\frac{\Delta y_1}{k_{y_{app_4}}} - \frac{\Delta y_2}{k_{y_{app_2}}}\right) + \left(\frac{p_i + p_p}{2}\right). \tag{D44}$$

The maximum possible pressure drop in the direction transverse to flow for the total system is the difference between p_y^* and p_y^o:

$$\begin{aligned}\Delta p_{x_{max}} =& p_y^* - p_y^o \\ =& \frac{\hat{q}_{y_s}\mu}{2\Delta x_2}\left(\frac{\Delta y_1}{k_{y_{app_4}}} - \frac{\Delta y_2}{k_{y_{app_2}}}\right) + \left(\frac{p_i + p_p}{2}\right) \\ & - \frac{\hat{q}_{y_f}\mu}{2\Delta x_1}\left(\frac{\Delta y_1}{k_{y_{app_3}}} - \frac{\Delta y_2}{k_{y_{app_1}}}\right) - \left(\frac{p_i + p_p}{2}\right).\end{aligned} \tag{D45}$$

Eq. (D45) can be simplified:

$$\Delta p_{x_{max}} = \frac{\hat{q}_{y_s}\mu}{2\Delta x_2}\left(\frac{\Delta y_1}{k_{y_{app_4}}} - \frac{\Delta y_2}{k_{y_{app_2}}}\right) - \frac{\hat{q}_{y_f}\mu}{2\Delta x_1}\left(\frac{\Delta y_1}{k_{y_{app_3}}} - \frac{\Delta y_2}{k_{y_{app_1}}}\right). \tag{D46}$$

Next, separate equations for $\hat{q}_{y_s}\mu$ and $\hat{q}_{y_f}\mu$ are derived based on:

$$\tilde{q}_y = \hat{q}_{y_f} + \hat{q}_{y_s} \tag{D47}$$

and

$$\tilde{q}_y = -\frac{\hat{k}_{y_{app_{f_s}}} L_x}{\mu} \frac{\Delta p_y}{L_y} \tag{D48}$$

where $\hat{k}_{y_{app_{f_s}}}$ is the effective permeability of the first and second columns in Figure D-3 when the columns are parallel to the flow direction (see Appendix C).

Rearrange Eq. (D47) and use Eqs. (D39) and (D48):

$$\hat{q}_{y_f} = \tilde{q}_y - \hat{q}_{y_s} = -\frac{\hat{k}_{y_{app_{f_s}}} L_x}{\mu} \frac{\Delta p_y}{L_y} - \left(-\frac{\hat{k}_{y_{app_s}} \Delta x_2}{\mu} \frac{\Delta p_y}{L_y} \right). \tag{D49}$$

Rearrange Eq. (D49):

$$\hat{q}_{y_f} \mu = \frac{\Delta p_y}{L_y} \left(\hat{k}_{y_{app_s}} \Delta x_2 - \hat{k}_{y_{app_{f_s}}} L_x \right). \tag{D50}$$

Again, rearrange Eq. (D47) and use Eqs. (D31) and (D48):

$$\hat{q}_{y_s} = \tilde{q}_y - \hat{q}_{y_f} = -\frac{\hat{k}_{y_{app_{f_s}}} L_x}{\mu} \frac{\Delta p_y}{L_y} - \left(-\frac{\hat{k}_{y_{app_f}} \Delta x_1}{\mu} \frac{\Delta p_y}{L_y} \right). \tag{D51}$$

Rearrange Eq. (D51):

$$\hat{q}_{y_s} \mu = \frac{\Delta p_y}{L_y} \left(\hat{k}_{y_{app_f}} \Delta x_1 - \hat{k}_{y_{app_{f_s}}} L_x \right). \tag{D52}$$

Insert Eqs. (D50) and (D52) into Eq. (D46):

$$\begin{aligned} \Delta p_{x_{max}} = & \frac{\Delta p_y}{2 L_y \Delta x_2} \left(\hat{k}_{y_{app_f}} \Delta x_1 - \hat{k}_{y_{app_{f_s}}} L_x \right) \left(\frac{\Delta y_1}{k_{y_{app_4}}} - \frac{\Delta y_2}{k_{y_{app_2}}} \right) \\ & - \frac{\Delta p_y}{2 L_y \Delta x_1} \left(\hat{k}_{y_{app_s}} \Delta x_2 - \hat{k}_{y_{app_{f_s}}} L_x \right) \left(\frac{\Delta y_1}{k_{y_{app_3}}} - \frac{\Delta y_2}{k_{y_{app_1}}} \right). \end{aligned} \tag{D53}$$

Using a procedure similar to the one given in Appendix E to find $\Delta p_{y_{avg}}$, it can be shown that:

$$\Delta p_{x_{avg}} = -\frac{1}{2}\Delta p_{x_{max}}. \qquad (D54)$$

Using Eq. (D54) in Eq. (D53), $\Delta p_{x_{avg}}$ becomes:

$$\Delta p_{x_{avg}} = -\frac{\Delta p_y}{4L_y\Delta x_2}\left(\hat{k}_{y_{appf}}\Delta x_1 - \hat{k}_{y_{appf_e}}L_x\right)\left(\frac{\Delta y_1}{k_{y_{app4}}} - \frac{\Delta y_2}{k_{y_{app2}}}\right)$$

$$+\frac{\Delta p_y}{4L_y\Delta x_1}\left(\hat{k}_{y_{app_e}}\Delta x_2 - \hat{k}_{y_{appf_e}}L_x\right)\left(\frac{\Delta y_1}{k_{y_{app3}}} - \frac{\Delta y_2}{k_{y_{app1}}}\right). \qquad (D55)$$

Multiplying Eq. (D55) by $L_y/(\Delta p_y L_x)$ gives the ratio of the transverse pressure gradient to that of the longitudinal pressure gradient:

$$\left[\left(\frac{\partial\tilde{p}}{\partial x}\right)_Y \Big/ \left(\frac{\partial\tilde{p}}{\partial y}\right)_Y\right]_{iso.global} = \left(\frac{\Delta p_{x_{avg}}}{\Delta p_y}\right)_Y \frac{L_y}{L_x}$$

$$= -\frac{1}{4\Delta x_2 L_x}\left(\hat{k}_{y_{appf}}\Delta x_1 - \hat{k}_{y_{appf_e}}L_x\right)\left(\frac{\Delta y_1}{k_{y_{app4}}} - \frac{\Delta y_2}{k_{y_{app2}}}\right)$$

$$+\frac{1}{4\Delta x_1 L_x}\left(\hat{k}_{y_{app_e}}\Delta x_2 - \hat{k}_{y_{appf_e}}L_x\right)\left(\frac{\Delta y_1}{k_{y_{app3}}} - \frac{\Delta y_2}{k_{y_{app1}}}\right). \qquad (D56)$$

Notice that Eq. (D56) is valid for any local permeability value of the 4 blocks. Also, the sign of Eq. (D56) changes depending on the relative location and magnitude of the local permeabilities.

Eq. (D56) is not corrected for cross-flow. This correction is shown in Chapter III of this study.

APPENDIX E
DEVELOPMENT OF AVERAGE "GLOBAL" TRANSVERSE PRESSURE DROP

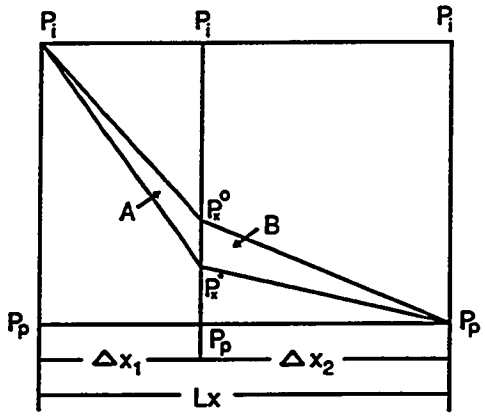

Fig. E-1: Pressure Versus System Length.

Show that: $\Delta p_{y_{avg}} = \frac{1}{2}\Delta p_{y_{max}} = \frac{1}{2}(p_x^* - p_x^o)$.

1. Determine the Area (A_A) of Triangle A:

$$A_A = \frac{1}{2}(p_x^* - p_i)\Delta x_1 - \frac{1}{2}(p_x^o - p_i)\Delta x_1. \qquad (E1)$$

Eq. (E1) can be reduced to:

$$A_A = \frac{1}{2}(p_x^* - p_x^o)\Delta x_1. \qquad (E2)$$

2. Determine the Area (A_B) of Triangle B:

$$A_B = \frac{1}{2}(p_p - p_x^o)\,\Delta x_2 - \frac{1}{2}(p_p - p_x^*)\,\Delta x_2. \qquad (E3)$$

Eq. (E3) can be reduced to:

$$A_B = \frac{1}{2}(p_x^* - p_x^o)\,\Delta x_1. \qquad (E4)$$

3. Determine $\Delta p_{y_{avg}}$ as the weighted average of A_A and A_B:

$$\Delta p_{y_{avg}} = \frac{(A_A + A_B)}{L_x}$$

$$= \frac{\frac{1}{2}(p_x^* - p_x^o)\,\Delta x_1 + \frac{1}{2}(p_x^* - p_x^o)\,\Delta x_2}{L_x}$$

$$= \frac{1}{2}(p_x^* - p_x^o). \qquad (E5)$$

A similar derivation can be performed to obtain $\Delta p_{x_{avg}}$.

APPENDIX F

DEVELOPMENT OF "LOCAL" PRESSURE GRADIENT RATIOS

The "local" transverse to longitudinal pressure gradient ratios are necessary components of the total pressure gradient ratios which in turn are required for determining the elements of the effective permeability tensor. Derivations of two-block pressure gradient ratios $\left(\left(\frac{\partial \hat{p}}{\partial y}\right)_{tb} / \left(\frac{\partial \hat{p}}{\partial x}\right)_{tb}, \left(\frac{\partial \hat{p}}{\partial y}\right)_{fs} / \left(\frac{\partial \hat{p}}{\partial x}\right)_{fs}, \left(\frac{\partial \hat{p}}{\partial x}\right)_{fs} / \left(\frac{\partial \hat{p}}{\partial y}\right)_{fs}, \text{and } \left(\frac{\partial \hat{p}}{\partial x}\right)_{tb} / \left(\frac{\partial \hat{p}}{\partial y}\right)_{tb}\right)$ are shown. Cross-flow corrected four-block "local" pressure gradient ratios are shown in Chapter III of this study. In all the following cases, unit thickness of the system is assumed.

The following "local" pressure gradient ratios are derived next:

I. "Local" pressure gradient ratios for injection along the x-axis:

1. $\frac{\left(\frac{\partial \hat{p}}{\partial y}\right)_t}{\left(\frac{\partial \hat{p}}{\partial x}\right)_t}$ **(top layer)**
2. $\frac{\left(\frac{\partial \hat{p}}{\partial y}\right)_b}{\left(\frac{\partial \hat{p}}{\partial x}\right)_b}$ **(bottom layer)**
3. $\frac{\left(\frac{\partial \hat{p}}{\partial y}\right)_{tb}}{\left(\frac{\partial \hat{p}}{\partial x}\right)_{tb}}$ **(top and bottom layers combined)**
4. $\frac{\left(\frac{\partial \hat{p}}{\partial y}\right)_f}{\left(\frac{\partial \hat{p}}{\partial x}\right)_f}$ **(first column)**
5. $\frac{\left(\frac{\partial \hat{p}}{\partial y}\right)_s}{\left(\frac{\partial \hat{p}}{\partial x}\right)_s}$ **(second column)**
6. $\frac{\left(\frac{\partial \hat{p}}{\partial y}\right)_{fs}}{\left(\frac{\partial \hat{p}}{\partial x}\right)_{fs}}$ **(first and second columns combined).**

II. "Local" pressure gradient ratios for injection along the y-axis:

1. $\frac{\left(\frac{\partial \hat{p}}{\partial x}\right)_f}{\left(\frac{\partial \hat{p}}{\partial y}\right)_f}$ **(first column)**

2. $\frac{\left(\frac{\partial p}{\partial x}\right)_a}{\left(\frac{\partial p}{\partial y}\right)_a}$ **(second column)**

3. $\frac{\left(\frac{\partial p}{\partial x}\right)_{ab}}{\left(\frac{\partial p}{\partial y}\right)_{ab}}$ **(first and second columns combined)**

4. $\frac{\left(\frac{\partial p}{\partial x}\right)_t}{\left(\frac{\partial p}{\partial y}\right)_t}$ **(top layer)**

5. $\frac{\left(\frac{\partial p}{\partial x}\right)_b}{\left(\frac{\partial p}{\partial y}\right)_b}$ **(bottom layer)**

6. $\frac{\left(\frac{\partial p}{\partial x}\right)_{tb}}{\left(\frac{\partial p}{\partial y}\right)_{tb}}$ **(top and bottom layers combined).**

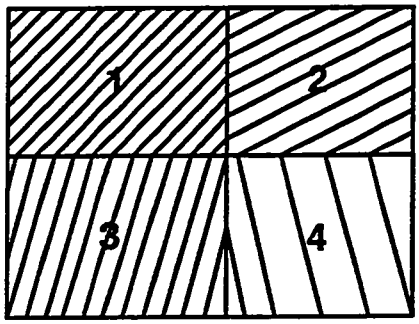

Fig. F-1: System Containing Four Blocks and Four Permeability Tensors.

Figure F-1 is used as a basis in the determination "local" pressure gradient ratios.

I. "Local" pressure gradient ratios for injection along the x-axis:

Determination of $\frac{\left(\frac{\partial p}{\partial y}\right)_t}{\left(\frac{\partial p}{\partial x}\right)_t}$:

1. Isolate the top layer or section of Figure F-1 as shown in Figure F-2.

   Velocity components along the x-axis for blocks 1 and 2:

$$v_{x_1} = -\frac{1}{\mu}\left(k_{xx_1}\left(\frac{\partial p}{\partial x}\right)_1 + k_{xy_1}\left(\frac{\partial p}{\partial y}\right)_1\right) \qquad (F1)$$

$$v_{x_2} = -\frac{1}{\mu}\left(k_{xx_2}\left(\frac{\partial p}{\partial x}\right)_2 + k_{xy_2}\left(\frac{\partial p}{\partial y}\right)_2\right). \qquad (F2)$$

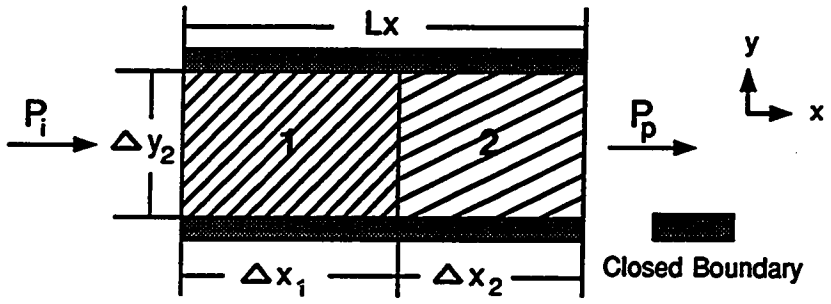

Fig. F-2: Top Layer of Figure F-1 (Injection Along x-axis).

Velocity component along the x-axis for blocks 1 and 2 combined:

$$\hat{v}_{x_t} = -\frac{1}{\mu}\left(\hat{k}_{xx_t}\left(\frac{\partial \hat{p}}{\partial x}\right)_t + \hat{k}_{xy_t}\left(\frac{\partial \hat{p}}{\partial y}\right)_t\right). \qquad (F3)$$

Velocity components along the y-axis for blocks 1 and 2 are zero because of closed upper and lower boundaries:

$$v_{y_1} = -\frac{1}{\mu}\left(k_{yx_1}\left(\frac{\partial p}{\partial x}\right)_1 + k_{yy_1}\left(\frac{\partial p}{\partial y}\right)_1\right) = 0 \qquad (F4)$$

$$v_{y_2} = -\frac{1}{\mu}\left(k_{yx_2}\left(\frac{\partial p}{\partial x}\right)_2 + k_{yy_2}\left(\frac{\partial p}{\partial y}\right)_2\right) = 0. \qquad (F5)$$

Velocity component along the y-axis for blocks 1 and 2 combined is zero because of closed upper and lower boundaries:

$$\hat{v}_{y_t} = -\frac{1}{\mu}\left(\hat{k}_{yx_t}\left(\frac{\partial \hat{p}}{\partial x}\right)_t + \hat{k}_{yy_t}\left(\frac{\partial \hat{p}}{\partial y}\right)_t\right) = 0. \qquad (F6)$$

Rearrange Eqs. (F1)-(F3):

$$\left(\frac{\partial p}{\partial x}\right)_1 = -\frac{v_{x_1}\mu}{k_{xx_1}} - \frac{k_{xy_1}}{k_{xx_1}}\left(\frac{\partial p}{\partial y}\right)_1 \qquad (F7)$$

$$\left(\frac{\partial p}{\partial x}\right)_2 = -\frac{v_{x_2}\mu}{k_{xx_2}} - \frac{k_{xy_2}}{k_{xx_2}}\left(\frac{\partial p}{\partial y}\right)_2 \qquad (F8)$$

$$\left(\frac{\partial \hat{p}}{\partial x}\right)_t = -\frac{\hat{v}_{x_t}\mu}{\hat{k}_{xx_t}} - \frac{\hat{k}_{xy_t}}{\hat{k}_{xx_t}}\left(\frac{\partial \hat{p}}{\partial y}\right)_t. \tag{F9}$$

The total pressure gradient along the x-axis is expressed as:

$$\left(\frac{\partial \hat{p}}{\partial x}\right)_t = \frac{\Delta x_1}{L_x}\left(\frac{\partial p}{\partial x}\right)_1 + \frac{\Delta x_2}{L_x}\left(\frac{\partial p}{\partial x}\right)_2 \tag{F10}$$

and

$$\hat{v}_{x_t} = v_{x_1} = v_{x_2}. \tag{F11}$$

Use Eq. (F11) in Eqs. (F7)-(F9) which are substituted into Eq. (F10):

$$\begin{aligned}\frac{\hat{v}_{x_t}\mu}{\hat{k}_{xx_t}} + \frac{\hat{k}_{xy_t}}{\hat{k}_{xx_t}}\left(\frac{\partial \hat{p}}{\partial y}\right)_t =& \frac{\Delta x_1}{L_x}\left(\frac{\hat{v}_{x_t}\mu}{k_{xx_1}} + \frac{k_{xy_1}}{k_{xx_1}}\left(\frac{\partial p}{\partial y}\right)_1\right) \\ &+ \frac{\Delta x_2}{L_x}\left(\frac{\hat{v}_{x_t}\mu}{k_{xx_2}} + \frac{k_{xy_2}}{k_{xx_2}}\left(\frac{\partial p}{\partial y}\right)_2\right).\end{aligned} \tag{F12}$$

Rearrange Eq. (F12):

$$\begin{aligned}\frac{\hat{k}_{xy_t}}{\hat{k}_{xx_t}}\left(\frac{\partial \hat{p}}{\partial y}\right)_t =& \hat{v}_{x_t}\mu\left[\frac{\Delta x_1}{L_x k_{xx_1}} + \frac{\Delta x_2}{L_x k_{xx_2}} - \frac{1}{\hat{k}_{xx_t}}\right] \\ &+ \frac{\Delta x_1}{L_x}\frac{k_{xy_1}}{k_{xx_1}}\left(\frac{\partial p}{\partial y}\right)_1 + \frac{\Delta x_2}{L_x}\frac{k_{xy_2}}{k_{xx_2}}\left(\frac{\partial p}{\partial y}\right)_2.\end{aligned} \tag{F13}$$

No off-diagonal elements of the permeability tensor exist within the square brackets in Eq. (F13). From Eq. (C20) in Appendix C, it is seen that in the absence of off-diagonal terms of the permeability tensors, Eq. (C20) reduces to:

$$\hat{k}_{xx_t} = \frac{L_x k_{xx_1} k_{xx_2}}{\Delta x_1 k_{xx_2} + \Delta x_2 k_{xx_1}}. \tag{F14}$$

Using Eq. (F14), the expression within the square brackets in Eq. (F13) is zero and Eq. (F13) can be simplified to:

$$\frac{\hat{k}_{xy_t}}{\hat{k}_{xx_t}}\left(\frac{\partial \hat{p}}{\partial y}\right)_t = \frac{\Delta x_1}{L_x}\frac{k_{xy_1}}{k_{xx_1}}\left(\frac{\partial p}{\partial y}\right)_1 + \frac{\Delta x_2}{L_x}\frac{k_{xy_2}}{k_{xx_2}}\left(\frac{\partial p}{\partial y}\right)_2. \qquad (F15)$$

An expression for $\frac{\hat{k}_{xy_t}}{\hat{k}_{xx_t}}$ in Eq. (F15) in terms of local elements of the permeability tensors and system geometry is determined next.

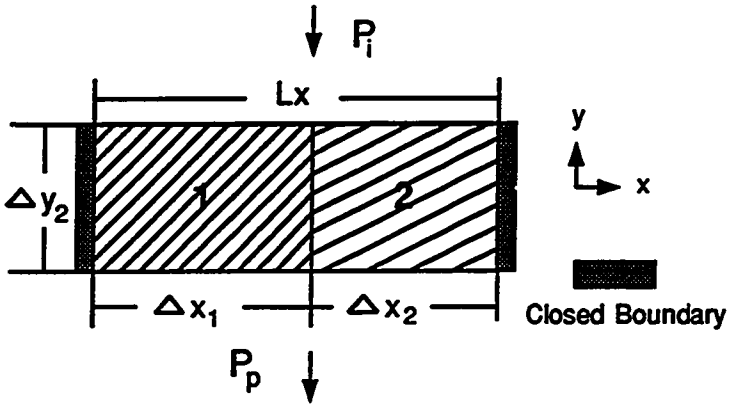

Fig. F-3: Top Layer of Figure F-1 (Injection Along y-axis).

From injection along the y-axis as in Figure F-3:

$$v_{x_1} = -\frac{1}{\mu}\left(k_{xx_1}\left(\frac{\partial p}{\partial x}\right)_1 + k_{xy_1}\left(\frac{\partial p}{\partial y}\right)_1\right) = 0 \qquad (F16)$$

$$v_{x_2} = -\frac{1}{\mu}\left(k_{xx_2}\left(\frac{\partial p}{\partial x}\right)_2 + k_{xy_2}\left(\frac{\partial p}{\partial y}\right)_2\right) = 0 \qquad (F17)$$

$$\hat{v}_{x_t} = -\frac{1}{\mu}\left(\hat{k}_{xx_t}\left(\frac{\partial \hat{p}}{\partial x}\right)_t + \hat{k}_{xy_t}\left(\frac{\partial \hat{p}}{\partial y}\right)_t\right) = 0. \qquad (F18)$$

Rearrange Eqs. (F16)-(F18):

$$\left(\frac{\partial p}{\partial x}\right)_1 = -\frac{k_{xy_1}}{k_{xx_1}}\left(\frac{\partial p}{\partial y}\right)_1 \qquad (F19)$$

$$\left(\frac{\partial p}{\partial x}\right)_2 = -\frac{k_{xy_2}}{k_{xx_2}}\left(\frac{\partial p}{\partial y}\right)_2 \qquad (F20)$$

$$\left(\frac{\partial \hat{p}}{\partial x}\right)_t = -\frac{\hat{k}_{xy_t}}{\hat{k}_{xx_t}}\left(\frac{\partial \hat{p}}{\partial y}\right)_t. \qquad (F21)$$

The total pressure gradient along x-axis is:

$$\left(\frac{\partial \hat{p}}{\partial x}\right)_t = \frac{\Delta x_1}{L_x}\left(\frac{\partial p}{\partial x}\right)_1 + \frac{\Delta x_2}{L_x}\left(\frac{\partial p}{\partial x}\right)_2. \qquad (F22)$$

Substitute Eqs. (F19)-(F21) into Eq. (F22):

$$-\frac{\hat{k}_{xy_t}}{\hat{k}_{xx_t}}\left(\frac{\partial \hat{p}}{\partial y}\right)_t = \frac{\Delta x_1}{L_x}\left(-\frac{k_{xy_1}}{k_{xx_1}}\left(\frac{\partial p}{\partial y}\right)_1\right) + \frac{\Delta x_2}{L_x}\left(-\frac{k_{xy_2}}{k_{xx_2}}\left(\frac{\partial p}{\partial y}\right)_2\right). \qquad (F23)$$

Since

$$\left(\frac{\partial \hat{p}}{\partial y}\right)_t = \left(\frac{\partial p}{\partial y}\right)_1 = \left(\frac{\partial p}{\partial y}\right)_2, \qquad (F24)$$

Eq. (F23) can be expressed as follows:

$$\frac{\hat{k}_{xy_t}}{\hat{k}_{xx_t}} = \frac{\Delta x_1}{L_x}\frac{k_{xy_1}}{k_{xx_1}} + \frac{\Delta x_2}{L_x}\frac{k_{xy_2}}{k_{xx_2}}. \qquad (F25)$$

Note that the sum of the coefficients of the local transverse pressure gradients in Eq. (F15) is equal to the right hand side of Eq. (F25).

Rearrange Eq. (F25) and substitute the rearranged equation into Eq. (F15):

$$\left(\frac{\Delta x_1 k_{xy_1} k_{xx_2} + \Delta x_2 k_{xy_2} k_{xx_1}}{L_x k_{xx_1} k_{xx_2}}\right)\left(\frac{\partial \hat{p}}{\partial y}\right)_t = \frac{\Delta x_1}{L_x}\frac{k_{xy_1}}{k_{xx_1}}\left(\frac{\partial p}{\partial y}\right)_1 + \frac{\Delta x_2}{L_x}\frac{k_{xy_2}}{k_{xx_2}}\left(\frac{\partial p}{\partial y}\right)_2. \qquad (F26)$$

Solve Eq. (F26) for $\left(\frac{\partial \hat{p}}{\partial y}\right)_t$:

$$\left(\frac{\partial \hat{p}}{\partial y}\right)_t = \left(\frac{\Delta x_1 k_{xy_1} k_{xx_2}}{\Delta x_1 k_{xy_1} k_{xx_2} + \Delta x_2 k_{xy_2} k_{xx_1}}\right)\left(\frac{\partial p}{\partial y}\right)_1 + \left(\frac{\Delta x_2 k_{xy_2} k_{xx_1}}{\Delta x_1 k_{xy_1} k_{xx_2} + \Delta x_2 k_{xy_2} k_{xx_1}}\right)\left(\frac{\partial p}{\partial y}\right)_2 . \qquad (F27)$$

Based on Figure F-2, $v_{x_1} = v_{x_2}$. Thus, set Eq. (F1) equal to Eq. (F2):

$$k_{xx_1}\left(\frac{\partial p}{\partial x}\right)_1 + k_{xy_1}\left(\frac{\partial p}{\partial y}\right)_1 = k_{xx_2}\left(\frac{\partial p}{\partial x}\right)_2 + k_{xy_2}\left(\frac{\partial p}{\partial y}\right)_2 . \qquad (F28)$$

Eqs. (F4) and (F5) can be solved for $\left(\frac{\partial p}{\partial y}\right)_1$ and $\left(\frac{\partial p}{\partial y}\right)_2$, respectively, and substituted into Eq. (F28):

$$k_{xx_1}\left(\frac{\partial p}{\partial x}\right)_1 + k_{xy_1}\left(-\frac{k_{yx_1}}{k_{yy_1}}\right)\left(\frac{\partial p}{\partial x}\right)_1 = k_{xx_2}\left(\frac{\partial p}{\partial x}\right)_2 + k_{xy_2}\left(-\frac{k_{yx_2}}{k_{yy_2}}\right)\left(\frac{\partial p}{\partial x}\right)_2 . \qquad (F29)$$

Rearrange Eq. (F29) to solve for $\left(\frac{\partial p}{\partial x}\right)_2$:

$$\left(\frac{\partial p}{\partial x}\right)_2 = \frac{\hat{k}_{x_{app_1}}}{\hat{k}_{x_{app_2}}}\left(\frac{\partial p}{\partial x}\right)_1 \qquad (F30)$$

where

$$\hat{k}_{x_{app_1}} = \left(k_{xx_1} - \frac{k_{xy_1} k_{yx_1}}{k_{yy_1}}\right) \qquad (F31)$$

$$\hat{k}_{x_{app_2}} = \left(k_{xx_2} - \frac{k_{xy_2} k_{yx_2}}{k_{yy_2}}\right). \qquad (F32)$$

Substitute Eq. (F30) into Eq. (F10):

$$\left(\frac{\partial \hat{p}}{\partial x}\right)_t = \frac{\Delta x_1}{L_x}\left(\frac{\partial p}{\partial x}\right)_1 + \frac{\Delta x_2}{L_x}\frac{\hat{k}_{x_{app_1}}}{\hat{k}_{x_{app_2}}}\left(\frac{\partial p}{\partial x}\right)_1 = \left(\frac{\Delta x_1}{L_x} + \frac{\Delta x_2}{L_x}\frac{\hat{k}_{x_{app_1}}}{\hat{k}_{x_{app_2}}}\right)\left(\frac{\partial p}{\partial x}\right)_1 . \qquad (F33)$$

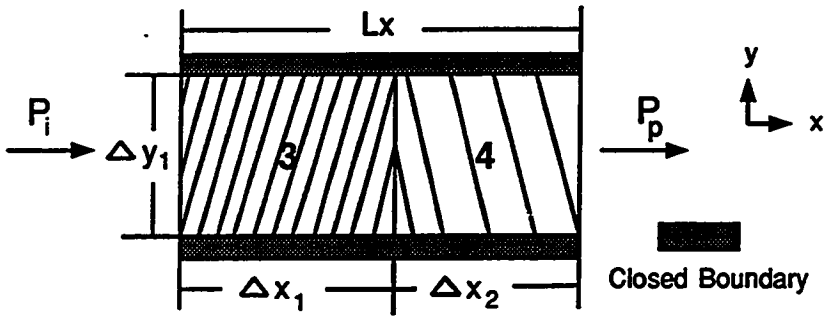

Fig. F-4: Bottom Layer of Figure F-1 (Injection Along x-axis).

Substitute the expressions used in Eq. (F29) for $\left(\frac{\partial p}{\partial y}\right)_1$ and $\left(\frac{\partial p}{\partial y}\right)_2$ and Eq. (F30) into Eq. (F27):

$$\left(\frac{\partial \hat{p}}{\partial y}\right)_t = \left(\frac{\Delta x_1 k_{xy_1} k_{xx_2}}{\Delta x_1 k_{xy_1} k_{xx_2} + \Delta x_2 k_{xy_2} k_{xx_1}}\right)\left[-\frac{k_{yx_1}}{k_{yy_1}}\left(\frac{\partial p}{\partial x}\right)_1\right] + \left(\frac{\Delta x_2 k_{xy_2} k_{xx_1}}{\Delta x_1 k_{xy_1} k_{xx_2} + \Delta x_2 k_{xy_2} k_{xx_1}}\right)\left[-\frac{k_{yx_2}}{k_{yy_2}}\frac{\hat{k}_{x_{app_1}}}{\hat{k}_{x_{app_2}}}\left(\frac{\partial p}{\partial x}\right)_1\right]. \quad (F34)$$

Divide Eq. (F34) by Eq. (F33) to yield:

$$\frac{\left(\frac{\partial \hat{p}}{\partial y}\right)_t}{\left(\frac{\partial \hat{p}}{\partial x}\right)_t} = \frac{-w1t\frac{k_{yx_1}}{k_{yy_1}} - w2t\left(\frac{\hat{k}_{x_{app_1}}}{\hat{k}_{x_{app_2}}}\right)\frac{k_{yx_2}}{k_{yy_2}}}{\left(\frac{\Delta x_1}{L_x} + \frac{\Delta x_2}{L_x}\frac{\hat{k}_{x_{app_1}}}{\hat{k}_{x_{app_2}}}\right)} \quad (F35)$$

where

$$w1t = \frac{\Delta x_1 k_{xy_1} k_{xx_2}}{\Delta x_1 k_{xy_1} k_{xx_2} + \Delta x_2 k_{xy_2} k_{xx_1}} \quad (F36)$$

$$w2t = \frac{\Delta x_2 k_{xy_2} k_{xx_1}}{\Delta x_1 k_{xy_1} k_{xx_2} + \Delta x_2 k_{xy_2} k_{xx_1}}. \quad (F37)$$

Determination of $\frac{\left(\frac{\partial \hat{p}}{\partial y}\right)_b}{\left(\frac{\partial \hat{p}}{\partial x}\right)_b}$:

2. Isolate the bottom layer or section of Figure F-1 as shown in Figure F-4.

The derivation of $\frac{\left(\frac{\partial \hat{p}}{\partial y}\right)_b}{\left(\frac{\partial \hat{p}}{\partial x}\right)_b}$ is directly analogous to the derivation of $\frac{\left(\frac{\partial \hat{p}}{\partial y}\right)_t}{\left(\frac{\partial \hat{p}}{\partial x}\right)_t}$. Therefore, only the final expression is presented:

$$\frac{\left(\frac{\partial \hat{p}}{\partial y}\right)_b}{\left(\frac{\partial \hat{p}}{\partial x}\right)_b} = \frac{-w1b\frac{k_{yx_2}}{k_{yy_3}} - w2b\left(\frac{\hat{k}_{x_{app_3}}}{\hat{k}_{x_{app_4}}}\right)\frac{k_{yx_4}}{k_{yy_4}}}{\left(\frac{\Delta x_1}{L_x} + \frac{\Delta x_2}{L_x}\frac{\hat{k}_{x_{app_3}}}{\hat{k}_{x_{app_4}}}\right)} \qquad (F38)$$

where

$$w1b = \frac{\Delta x_1 k_{xy_3} k_{xx_4}}{\Delta x_1 k_{xy_3} k_{xx_4} + \Delta x_2 k_{xy_4} k_{xx_3}} \qquad (F39)$$

$$w2b = \frac{\Delta x_2 k_{xy_4} k_{xx_3}}{\Delta x_1 k_{xy_3} k_{xx_4} + \Delta x_2 k_{xy_4} k_{xx_3}}. \qquad (F40)$$

Determination of $\frac{\left(\frac{\partial \hat{p}}{\partial y}\right)_{tb}}{\left(\frac{\partial \hat{p}}{\partial x}\right)_{tb}}$:

3. Since the top and bottom layers are parallel with respect to the direction of flow, $\frac{\left(\frac{\partial \hat{p}}{\partial y}\right)_{tb}}{\left(\frac{\partial \hat{p}}{\partial x}\right)_{tb}}$ can be obtained from the following analysis using Figure F-5:

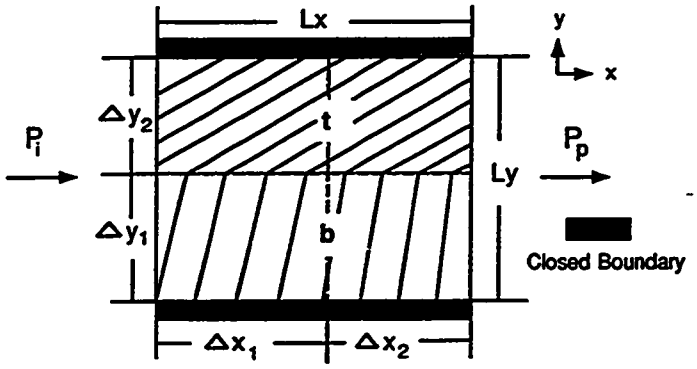

Fig. F-5: Top and Bottom Layers of Figure F-1 (Injection Along x-axis).

Velocity components along the x-axis for the top and bottom layers:

$$\hat{v}_{x_t} = -\frac{1}{\mu}\left(\hat{k}_{xx_t}\left(\frac{\partial \hat{p}}{\partial x}\right)_t + \hat{k}_{xy_t}\left(\frac{\partial \hat{p}}{\partial y}\right)_t\right) \qquad (F41)$$

$$\hat{v}_{x_b} = -\frac{1}{\mu}\left(\hat{k}_{xx_b}\left(\frac{\partial \hat{p}}{\partial x}\right)_b + \hat{k}_{xy_b}\left(\frac{\partial \hat{p}}{\partial y}\right)_b\right). \qquad (F42)$$

Velocity component along the x-axis for top and bottom layers combined:

$$\hat{v}_{x_{tb}} = -\frac{1}{\mu}\left(\hat{k}_{xx_{tb}}\left(\frac{\partial \hat{p}}{\partial x}\right)_{tb} + \hat{k}_{xy_{tb}}\left(\frac{\partial \hat{p}}{\partial y}\right)_{tb}\right). \qquad (F43)$$

Velocity components along the y-axis for top and bottom layers are zero because of closed upper and lower boundaries:

$$\hat{v}_{y_t} = -\frac{1}{\mu}\left(\hat{k}_{yx_t}\left(\frac{\partial \hat{p}}{\partial x}\right)_t + \hat{k}_{yy_t}\left(\frac{\partial \hat{p}}{\partial y}\right)_t\right) = 0 \qquad (F44)$$

$$\hat{v}_{y_b} = -\frac{1}{\mu}\left(\hat{k}_{yx_b}\left(\frac{\partial \hat{p}}{\partial x}\right)_b + \hat{k}_{yy_b}\left(\frac{\partial \hat{p}}{\partial y}\right)_b\right) = 0. \qquad (F45)$$

Velocity component along the y-axis for top and bottom layers combined is zero because of closed upper and lower boundaries:

$$\hat{v}_{y_{tb}} = -\frac{1}{\mu}\left(\hat{k}_{yx_{tb}}\left(\frac{\partial \hat{p}}{\partial x}\right)_{tb} + \hat{k}_{yy_{tb}}\left(\frac{\partial \hat{p}}{\partial y}\right)_{tb}\right) = 0. \qquad (F46)$$

Rearrange Eqs. (F44)-(F46):

$$\left(\frac{\partial \hat{p}}{\partial y}\right)_t = -\frac{\hat{k}_{yx_t}}{\hat{k}_{yy_t}}\left(\frac{\partial \hat{p}}{\partial x}\right)_t \qquad (F47)$$

$$\left(\frac{\partial \hat{p}}{\partial y}\right)_b = -\frac{\hat{k}_{yx_b}}{\hat{k}_{yy_b}}\left(\frac{\partial \hat{p}}{\partial x}\right)_b \qquad (F48)$$

$$\left(\frac{\partial \hat{p}}{\partial y}\right)_{tb} = -\frac{\hat{k}_{yx_{tb}}}{\hat{k}_{yy_{tb}}}\left(\frac{\partial \hat{p}}{\partial x}\right)_{tb}. \qquad (F49)$$

The total pressure gradient along the y-axis is expressed as:

$$\left(\frac{\partial \hat{p}}{\partial y}\right)_{tb} = \frac{\Delta y_2}{L_y}\left(\frac{\partial \hat{p}}{\partial y}\right)_t + \frac{\Delta y_1}{L_y}\left(\frac{\partial \hat{p}}{\partial y}\right)_b. \qquad (F50)$$

Substitute Eqs. (F47)-(F49) into Eq. (F50):

$$-\frac{\hat{k}_{yx_{tb}}}{\hat{k}_{yy_{tb}}}\left(\frac{\partial\hat{p}}{\partial x}\right)_{tb}=\frac{\Delta y_2}{L_y}\left(-\frac{\hat{k}_{yx_t}}{\hat{k}_{yy_t}}\left(\frac{\partial\hat{p}}{\partial x}\right)_t\right)+\frac{\Delta y_1}{L_y}\left(-\frac{\hat{k}_{yx_b}}{\hat{k}_{yy_b}}\left(\frac{\partial\hat{p}}{\partial x}\right)_b\right). \qquad (F51)$$

The total pressure gradient along the x-axis is expressed as:

$$\left(\frac{\partial\hat{p}}{\partial x}\right)_{tb}=\left(\frac{\partial\hat{p}}{\partial x}\right)_t=\left(\frac{\partial\hat{p}}{\partial x}\right)_b. \qquad (F52)$$

Substitute Eq. (F52) into Eq. (F51) and cancel the pressure gradients:

$$-\frac{\hat{k}_{yx_{tb}}}{\hat{k}_{yy_{tb}}}=-\frac{\Delta y_2}{L_y}\frac{\hat{k}_{yx_t}}{\hat{k}_{yy_t}}-\frac{\Delta y_1}{L_y}\frac{\hat{k}_{yx_b}}{\hat{k}_{yy_b}}. \qquad (F53)$$

Eq. (F49) can be rearranged as follows:

$$\frac{\left(\frac{\partial\hat{p}}{\partial y}\right)_{tb}}{\left(\frac{\partial\hat{p}}{\partial x}\right)_{tb}}=-\frac{\hat{k}_{yx_{tb}}}{\hat{k}_{yy_{tb}}}. \qquad (F54)$$

Substitute Eq. (F54) into Eq. (F53):

$$\frac{\left(\frac{\partial\hat{p}}{\partial y}\right)_{tb}}{\left(\frac{\partial\hat{p}}{\partial x}\right)_{tb}}=-\frac{\Delta y_2}{L_y}\frac{\hat{k}_{yx_t}}{\hat{k}_{yy_t}}-\frac{\Delta y_1}{L_y}\frac{\hat{k}_{yx_b}}{\hat{k}_{yy_b}} \qquad (F55)$$

where $-\frac{\hat{k}_{yx_t}}{\hat{k}_{yy_t}}=\frac{\left(\frac{\partial\hat{f}}{\partial y}\right)_t}{\left(\frac{\partial\hat{f}}{\partial x}\right)_t}$ and $-\frac{\hat{k}_{yx_b}}{\hat{k}_{yy_b}}=\frac{\left(\frac{\partial\hat{f}}{\partial y}\right)_b}{\left(\frac{\partial\hat{f}}{\partial x}\right)_b}$ are given by Eqs. (F35) and (F38).

Determination of $\frac{\left(\frac{\partial\hat{p}}{\partial y}\right)_t}{\left(\frac{\partial\hat{p}}{\partial x}\right)_t}$:

4. Isolate the first column of Figure F-1, i.e., combine blocks 1 and 3 as shown in Figure F-6.

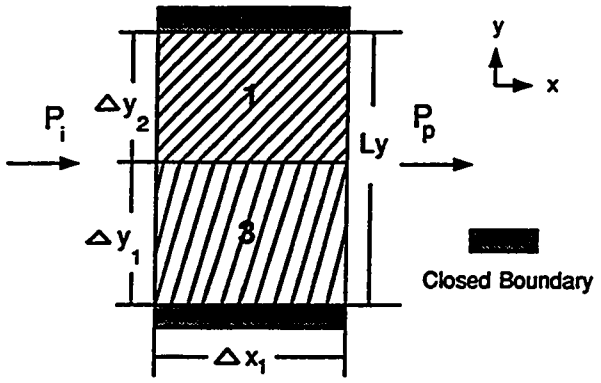

Fig. F-6: First Column of Figure F-1 (Injection Along x-axis).

Velocity components along the x-axis for blocks 1 and 3:

$$v_{x_1} = -\frac{1}{\mu}\left(k_{xx_1}\left(\frac{\partial p}{\partial x}\right)_1 + k_{xy_1}\left(\frac{\partial p}{\partial y}\right)_1\right) \qquad (F56)$$

$$v_{x_3} = -\frac{1}{\mu}\left(k_{xx_3}\left(\frac{\partial p}{\partial x}\right)_3 + k_{xy_3}\left(\frac{\partial p}{\partial y}\right)_3\right). \qquad (F57)$$

Velocity component along the x-axis for blocks 1 and 3 combined:

$$\hat{v}_{x_f} = -\frac{1}{\mu}\left(\hat{k}_{xx_f}\left(\frac{\partial \hat{p}}{\partial x}\right)_f + \hat{k}_{xy_f}\left(\frac{\partial \hat{p}}{\partial y}\right)_f\right). \qquad (F58)$$

Velocity components along the y-axis for blocks 1 and 3 are zero because of closed upper and lower boundaries:

$$v_{y_1} = -\frac{1}{\mu}\left(k_{yx_1}\left(\frac{\partial p}{\partial x}\right)_1 + k_{yy_1}\left(\frac{\partial p}{\partial y}\right)_1\right) = 0 \qquad (F59)$$

$$v_{y_3} = -\frac{1}{\mu}\left(k_{yx_3}\left(\frac{\partial p}{\partial x}\right)_3 + k_{yy_3}\left(\frac{\partial p}{\partial y}\right)_3\right) = 0. \qquad (F60)$$

Velocity component along the y-axis for blocks 1 and 3 combined is zero because of closed upper and lower boundaries:

$$\hat{v}_{y_f} = -\frac{1}{\mu}\left(\hat{k}_{yx_f}\left(\frac{\partial \hat{p}}{\partial x}\right)_f + \hat{k}_{yy_f}\left(\frac{\partial \hat{p}}{\partial y}\right)_f\right) = 0. \qquad (F61)$$

Rearrange Eqs. (F59)-(F61):

$$\left(\frac{\partial p}{\partial y}\right)_1 = -\frac{k_{yx_1}}{k_{yy_1}}\left(\frac{\partial p}{\partial x}\right)_1 \tag{F62}$$

$$\left(\frac{\partial p}{\partial y}\right)_3 = -\frac{k_{yx_3}}{k_{yy_3}}\left(\frac{\partial p}{\partial x}\right)_3 \tag{F63}$$

$$\left(\frac{\partial \hat{p}}{\partial y}\right)_f = -\frac{\hat{k}_{yx_f}}{\hat{k}_{yy_f}}\left(\frac{\partial \hat{p}}{\partial x}\right)_f. \tag{F64}$$

The total pressure gradient along the y-axis is expressed as:

$$\left(\frac{\partial \hat{p}}{\partial y}\right)_f = \frac{\Delta y_2}{L_y}\left(\frac{\partial p}{\partial y}\right)_1 + \frac{\Delta y_1}{L_y}\left(\frac{\partial p}{\partial y}\right)_3. \tag{F65}$$

Substitute Eqs. (F62)-(F64) into Eq. (F65):

$$-\frac{\hat{k}_{yx_f}}{\hat{k}_{yy_f}}\left(\frac{\partial \hat{p}}{\partial x}\right)_f = \frac{\Delta y_2}{L_y}\left(-\frac{k_{yx_1}}{k_{yy_1}}\left(\frac{\partial p}{\partial x}\right)_1\right) + \frac{\Delta y_1}{L_y}\left(-\frac{k_{yx_3}}{k_{yy_3}}\left(\frac{\partial p}{\partial x}\right)_3\right). \tag{F66}$$

The total pressure gradient along the x-axis is expressed as:

$$\left(\frac{\partial \hat{p}}{\partial x}\right)_f = \left(\frac{\partial p}{\partial x}\right)_1 = \left(\frac{\partial p}{\partial x}\right)_3. \tag{F67}$$

Substitute Eq. (F67) into Eq. (F66) and cancel the pressure gradients:

$$-\frac{\hat{k}_{yx_f}}{\hat{k}_{yy_f}} = -\frac{\Delta y_2}{L_y}\frac{k_{yx_1}}{k_{yy_1}} - \frac{\Delta y_1}{L_y}\frac{k_{yx_3}}{k_{yy_3}}. \tag{F68}$$

Eq. (F64) can be rearranged as follows:

$$\frac{\left(\frac{\partial \hat{p}}{\partial y}\right)_f}{\left(\frac{\partial \hat{p}}{\partial x}\right)_f} = -\frac{\hat{k}_{yx_f}}{\hat{k}_{yy_f}}. \tag{F69}$$

Substitute Eq. (F69) into Eq. (F68):

$$\frac{\left(\frac{\partial \hat{p}}{\partial y}\right)_f}{\left(\frac{\partial \hat{p}}{\partial x}\right)_f} = -\frac{\Delta y_2}{L_y}\frac{k_{yx_1}}{k_{yy_1}} - \frac{\Delta y_1}{L_y}\frac{k_{yx_3}}{k_{yy_3}}. \qquad (F70)$$

Determination of $\frac{\left(\frac{\partial \hat{p}}{\partial y}\right)_s}{\left(\frac{\partial \hat{p}}{\partial x}\right)_s}$:

5. Isolate the second column of Figure F-1, i.e., combine blocks 2 and 4 as shown in Figure F-7.

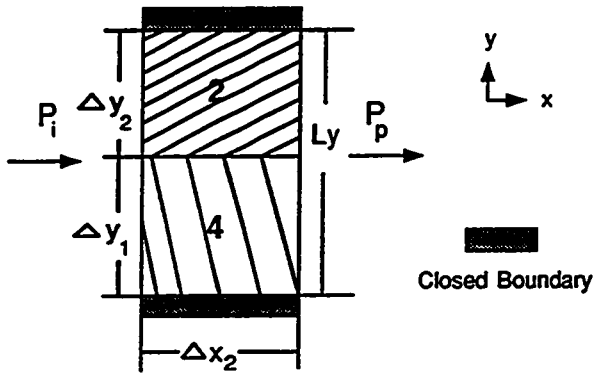

Fig. F-7: Second Column of Figure F-1 (Injection Along x-axis).

The derivation of $\frac{\left(\frac{\partial \hat{p}}{\partial y}\right)_s}{\left(\frac{\partial \hat{p}}{\partial x}\right)_s}$ is directly analogous to the derivation of $\frac{\left(\frac{\partial \hat{p}}{\partial y}\right)_f}{\left(\frac{\partial \hat{p}}{\partial x}\right)_f}$. Therefore, only the final expression is presented:

$$\frac{\left(\frac{\partial \hat{p}}{\partial y}\right)_s}{\left(\frac{\partial \hat{p}}{\partial x}\right)_s} = -\frac{\Delta y_2}{L_y}\frac{k_{yx_2}}{k_{yy_2}} - \frac{\Delta y_1}{L_y}\frac{k_{yx_4}}{k_{yy_4}}. \qquad (F71)$$

Determination of $\frac{\left(\frac{\partial \hat{p}}{\partial y}\right)_{fs}}{\left(\frac{\partial \hat{p}}{\partial x}\right)_{fs}}$:

6. Since the first and second columns are in series with respect to the direction of flow, $\frac{\left(\frac{\partial \hat{p}}{\partial y}\right)_{fs}}{\left(\frac{\partial \hat{p}}{\partial x}\right)_{fs}}$ can be obtained from the following analysis using Figure F-8:

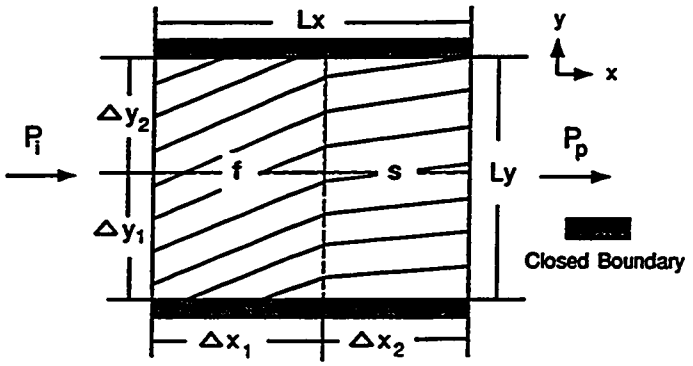

Fig. F-8: First and Second Columns of Figure F-1 (Injection Along x-axis).

Velocity components along the x-axis for first and second columns:

$$\hat{v}_{x_f} = -\frac{1}{\mu}\left(\hat{k}_{xx_f}\left(\frac{\partial \hat{p}}{\partial x}\right)_f + \hat{k}_{xy_f}\left(\frac{\partial \hat{p}}{\partial y}\right)_f\right) \qquad (F72)$$

$$\hat{v}_{x_s} = -\frac{1}{\mu}\left(\hat{k}_{xx_s}\left(\frac{\partial \hat{p}}{\partial x}\right)_s + \hat{k}_{xy_s}\left(\frac{\partial \hat{p}}{\partial y}\right)_s\right). \qquad (F73)$$

Velocity component along the x-axis for first and second columns combined:

$$\hat{v}_{x_{fs}} = -\frac{1}{\mu}\left(\hat{k}_{xx_{fs}}\left(\frac{\partial \hat{p}}{\partial x}\right)_{fs} + \hat{k}_{xy_{fs}}\left(\frac{\partial \hat{p}}{\partial y}\right)_{fs}\right). \qquad (F74)$$

Velocity components along the y-axis for first and second columns are zero because of closed upper and lower boundaries:

$$\hat{v}_{y_f} = -\frac{1}{\mu}\left(\hat{k}_{yx_f}\left(\frac{\partial \hat{p}}{\partial x}\right)_f + \hat{k}_{yy_f}\left(\frac{\partial \hat{p}}{\partial y}\right)_f\right) = 0 \qquad (F75)$$

$$\hat{v}_{y_s} = -\frac{1}{\mu}\left(\hat{k}_{yx_s}\left(\frac{\partial \hat{p}}{\partial x}\right)_s + \hat{k}_{yy_s}\left(\frac{\partial \hat{p}}{\partial y}\right)_s\right) = 0. \qquad (F76)$$

Velocity component along the y-axis for first and second columns combined is zero because of closed upper and lower boundaries:

$$\hat{v}_{y_{fs}} = -\frac{1}{\mu}\left(\hat{k}_{yx_{fs}}\left(\frac{\partial \hat{p}}{\partial x}\right)_{fs} + \hat{k}_{yy_{fs}}\left(\frac{\partial \hat{p}}{\partial y}\right)_{fs}\right) = 0. \qquad (F77)$$

Rearrange Eqs. (F72)-(F74):

$$\left(\frac{\partial \hat{p}}{\partial x}\right)_f = -\frac{\hat{v}_{x_f}\mu}{\hat{k}_{xx_f}} - \frac{\hat{k}_{xy_f}}{\hat{k}_{xx_f}}\left(\frac{\partial \hat{p}}{\partial y}\right)_f \tag{F78}$$

$$\left(\frac{\partial \hat{p}}{\partial x}\right)_s = -\frac{\hat{v}_{x_s}\mu}{\hat{k}_{xx_s}} - \frac{\hat{k}_{xy_s}}{\hat{k}_{xx_s}}\left(\frac{\partial \hat{p}}{\partial y}\right)_s \tag{F79}$$

$$\left(\frac{\partial \hat{p}}{\partial x}\right)_{fs} = -\frac{\hat{v}_{x_{fs}}\mu}{\hat{k}_{xx_{fs}}} - \frac{\hat{k}_{xy_{fs}}}{\hat{k}_{xx_{fs}}}\left(\frac{\partial \hat{p}}{\partial y}\right)_{fs}. \tag{F80}$$

The total pressure gradient along the x-axis is expressed as:

$$\left(\frac{\partial \hat{p}}{\partial x}\right)_{fs} = \frac{\Delta x_1}{L_x}\left(\frac{\partial \hat{p}}{\partial x}\right)_f + \frac{\Delta x_2}{L_x}\left(\frac{\partial \hat{p}}{\partial x}\right)_s \tag{F81}$$

and

$$\hat{v}_{x_{fs}} = \hat{v}_{x_f} = \hat{v}_{x_s}. \tag{F82}$$

Use Eq. (F82) in Eqs. (F78)-(F80) which are substituted into Eq. (F81):

$$\begin{aligned}\frac{\hat{v}_{x_{fs}}\mu}{\hat{k}_{xx_{fs}}} + \frac{\hat{k}_{xy_{fs}}}{\hat{k}_{xx_{fs}}}\left(\frac{\partial \hat{p}}{\partial y}\right)_{fs} =& \frac{\Delta x_1}{L_x}\left(\frac{\hat{v}_{x_{fs}}\mu}{\hat{k}_{xx_f}} + \frac{\hat{k}_{xy_f}}{\hat{k}_{xx_f}}\left(\frac{\partial \hat{p}}{\partial y}\right)_f\right) \\ &+ \frac{\Delta x_2}{L_x}\left(\frac{\hat{v}_{x_{fs}}\mu}{\hat{k}_{xx_s}} + \frac{\hat{k}_{xy_s}}{\hat{k}_{xx_s}}\left(\frac{\partial \hat{p}}{\partial y}\right)_s\right).\end{aligned} \tag{F83}$$

Rearrange Eq. (F83):

$$\begin{aligned}\frac{\hat{k}_{xy_{fs}}}{\hat{k}_{xx_{fs}}}\left(\frac{\partial \hat{p}}{\partial y}\right)_{fs} =& \hat{v}_{x_{fs}}\mu\left[\frac{\Delta x_1}{L_x\hat{k}_{xx_f}} + \frac{\Delta x_2}{L_x\hat{k}_{xx_s}} - \frac{1}{\hat{k}_{xx_{fs}}}\right] \\ &+ \frac{\Delta x_1}{L_x}\frac{\hat{k}_{xy_f}}{\hat{k}_{xx_f}}\left(\frac{\partial \hat{p}}{\partial y}\right)_f + \frac{\Delta x_2}{L_x}\frac{\hat{k}_{xy_s}}{\hat{k}_{xx_s}}\left(\frac{\partial \hat{p}}{\partial y}\right)_s.\end{aligned} \tag{F84}$$

No off-diagonal elements of the permeability tensors exist within the square brackets of Eq. (F84). It can be shown that in the absence of off-diagonal

elements, the two first terms within the square bracket in Eq. (F84) are equal to $\frac{1}{\hat{k}_{xx_{fs}}}$. Thus, Eq. (F84) can be reduced to:

$$\frac{\hat{k}_{xy_{fs}}}{\hat{k}_{xx_{fs}}}\left(\frac{\partial \hat{p}}{\partial y}\right)_{fs} = \frac{\Delta x_1}{L_x}\frac{\hat{k}_{xy_f}}{\hat{k}_{xx_f}}\left(\frac{\partial \hat{p}}{\partial y}\right)_f + \frac{\Delta x_2}{L_x}\frac{\hat{k}_{xy_s}}{\hat{k}_{xx_s}}\left(\frac{\partial \hat{p}}{\partial y}\right)_s . \qquad (F85)$$

An expression for $\frac{\hat{k}_{xy_{fs}}}{\hat{k}_{xx_{fs}}}$ in Eq. (F85) in terms of local elements of the permeability tensors and system geometry is determined next.

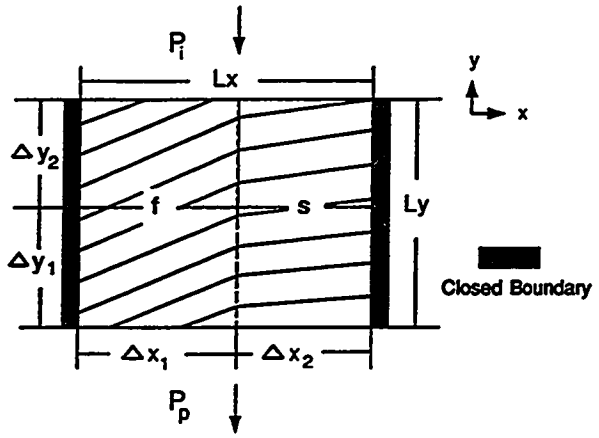

Fig. F-9: First and Second Columns of Figure F-1 (Injection Along y-axis).

From injection along the y-axis as in Figure F-9:

$$\hat{v}_{x_f} = -\frac{1}{\mu}\left(\hat{k}_{xx_f}\left(\frac{\partial \hat{p}}{\partial x}\right)_f + \hat{k}_{xy_f}\left(\frac{\partial \hat{p}}{\partial y}\right)_f\right) = 0 \qquad (F86)$$

$$\hat{v}_{x_s} = -\frac{1}{\mu}\left(\hat{k}_{xx_s}\left(\frac{\partial \hat{p}}{\partial x}\right)_s + \hat{k}_{xy_s}\left(\frac{\partial \hat{p}}{\partial y}\right)_s\right) = 0 \qquad (F87)$$

$$\hat{v}_{x_{fs}} = -\frac{1}{\mu}\left(\hat{k}_{xx_{fs}}\left(\frac{\partial \hat{p}}{\partial x}\right)_{fs} + \hat{k}_{xy_{fs}}\left(\frac{\partial \hat{p}}{\partial y}\right)_{fs}\right) = 0. \qquad (F88)$$

Rearrange Eqs. (F86)-(F88):

$$\left(\frac{\partial \hat{p}}{\partial x}\right)_f = -\frac{\hat{k}_{xy_f}}{\hat{k}_{xx_f}}\left(\frac{\partial \hat{p}}{\partial y}\right)_f \qquad (F89)$$

$$\left(\frac{\partial \hat{p}}{\partial x}\right)_s = -\frac{\hat{k}_{xy_s}}{\hat{k}_{xx_s}}\left(\frac{\partial \hat{p}}{\partial y}\right)_s \tag{F90}$$

$$\left(\frac{\partial \hat{p}}{\partial x}\right)_{fs} = -\frac{\hat{k}_{xy_{fs}}}{\hat{k}_{xx_{fs}}}\left(\frac{\partial \hat{p}}{\partial y}\right)_{fs}. \tag{F91}$$

The total pressure gradient along x-axis is:

$$\left(\frac{\partial \hat{p}}{\partial x}\right)_{fs} = \frac{\Delta x_1}{L_x}\left(\frac{\partial \hat{p}}{\partial x}\right)_f + \frac{\Delta x_2}{L_x}\left(\frac{\partial \hat{p}}{\partial x}\right)_s. \tag{F92}$$

Substitute Eqs. (F89)-(F91) into Eq. (F92):

$$-\frac{\hat{k}_{xy_{fs}}}{\hat{k}_{xx_{fs}}}\left(\frac{\partial \hat{p}}{\partial y}\right)_{fs} = \frac{\Delta x_1}{L_x}\left(-\frac{\hat{k}_{xy_f}}{\hat{k}_{xx_f}}\left(\frac{\partial \hat{p}}{\partial y}\right)_f\right) + \frac{\Delta x_2}{L_x}\left(-\frac{\hat{k}_{xy_s}}{\hat{k}_{xx_s}}\left(\frac{\partial \hat{p}}{\partial y}\right)_s\right). \tag{F93}$$

Since

$$\left(\frac{\partial \hat{p}}{\partial y}\right)_{fs} = \left(\frac{\partial \hat{p}}{\partial y}\right)_f = \left(\frac{\partial \hat{p}}{\partial y}\right)_s, \tag{F94}$$

Eq. (F93) can be expressed as follows:

$$\frac{\hat{k}_{xy_{fs}}}{\hat{k}_{xx_{fs}}} = \frac{\Delta x_1}{L_x}\frac{\hat{k}_{xy_f}}{\hat{k}_{xx_f}} + \frac{\Delta x_2}{L_x}\frac{\hat{k}_{xy_s}}{\hat{k}_{xx_s}}. \tag{F95}$$

Rearrange Eq. (F95) and substitute the rearranged equation into Eq. (F85):

$$\left(\frac{\Delta x_1 \hat{k}_{xy_f}\hat{k}_{xx_s} + \Delta x_2 \hat{k}_{xy_s}\hat{k}_{xx_f}}{L_x \hat{k}_{xx_f}\hat{k}_{xx_s}}\right)\left(\frac{\partial \hat{p}}{\partial y}\right)_{fs} = \frac{\Delta x_1}{L_x}\frac{\hat{k}_{xy_f}}{\hat{k}_{xx_f}}\left(\frac{\partial \hat{p}}{\partial y}\right)_f + \frac{\Delta x_2}{L_x}\frac{\hat{k}_{xy_s}}{\hat{k}_{xx_s}}\left(\frac{\partial \hat{p}}{\partial y}\right)_s. \tag{F96}$$

Solve Eq. (F96) for $\left(\frac{\partial \hat{p}}{\partial y}\right)_{fs}$:

$$\left(\frac{\partial \hat{p}}{\partial y}\right)_{fs} = \left(\frac{\Delta x_1 \hat{k}_{xy_f} \hat{k}_{xx_s}}{\Delta x_1 \hat{k}_{xy_f} \hat{k}_{xx_s} + \Delta x_2 \hat{k}_{xy_s} \hat{k}_{xx_f}}\right) \left(\frac{\partial \hat{p}}{\partial y}\right)_f + \left(\frac{\Delta x_2 \hat{k}_{xy_s} \hat{k}_{xx_f}}{\Delta x_1 \hat{k}_{xy_f} \hat{k}_{xx_s} + \Delta x_2 \hat{k}_{xy_s} \hat{k}_{xx_f}}\right) \left(\frac{\partial \hat{p}}{\partial y}\right)_s . \qquad (F97)$$

Based on Figure F-8, $\hat{v}_{x_f} = \hat{v}_{x_s}$. Thus, set Eq. (F72) equal to Eq. (F73):

$$\hat{k}_{xx_f} \left(\frac{\partial \hat{p}}{\partial x}\right)_f + \hat{k}_{xy_f} \left(\frac{\partial \hat{p}}{\partial y}\right)_f = \hat{k}_{xx_s} \left(\frac{\partial \hat{p}}{\partial x}\right)_s + \hat{k}_{xy_s} \left(\frac{\partial \hat{p}}{\partial y}\right)_s . \qquad (F98)$$

Eqs. (F75) and (F76) can be solved for $\left(\frac{\partial \hat{p}}{\partial y}\right)_f$ and $\left(\frac{\partial \hat{p}}{\partial y}\right)_s$, respectively, and substituted into Eq. (F98):

$$\hat{k}_{xx_f} \left(\frac{\partial \hat{p}}{\partial x}\right)_f + \hat{k}_{xy_f} \left(-\frac{\hat{k}_{yx_f}}{\hat{k}_{yy_f}}\right) \left(\frac{\partial \hat{p}}{\partial x}\right)_f = \hat{k}_{xx_s} \left(\frac{\partial \hat{p}}{\partial x}\right)_s + \hat{k}_{xy_s} \left(-\frac{\hat{k}_{yx_s}}{\hat{k}_{yy_s}}\right) \left(\frac{\partial \hat{p}}{\partial x}\right)_s . \qquad (F99)$$

Rearrange Eq. (F99) to solve for $\left(\frac{\partial \hat{p}}{\partial x}\right)_s$:

$$\left(\frac{\partial \hat{p}}{\partial x}\right)_s = \frac{\hat{k}_{x_{app_f}}}{\hat{k}_{x_{app_s}}} \left(\frac{\partial \hat{p}}{\partial x}\right)_f \qquad (F100)$$

where

$$\hat{k}_{x_{app_f}} = \left(\hat{k}_{xx_f} - \frac{\hat{k}_{xy_f} \hat{k}_{yx_f}}{\hat{k}_{yy_f}}\right) \qquad (F101)$$

$$\hat{k}_{x_{app_s}} = \left(\hat{k}_{xx_s} - \frac{\hat{k}_{xy_s} \hat{k}_{yx_s}}{\hat{k}_{yy_s}}\right) . \qquad (F102)$$

Substitute Eq. (F100) into Eq. (F81):

$$\left(\frac{\partial \hat{p}}{\partial x}\right)_{fs} = \frac{\Delta x_1}{L_x}\left(\frac{\partial \hat{p}}{\partial x}\right)_f + \frac{\Delta x_2}{L_x}\frac{\hat{k}_{x_{appf}}}{\hat{k}_{x_{appe}}}\left(\frac{\partial \hat{p}}{\partial x}\right)_f$$

$$= \left(\frac{\Delta x_1}{L_x} + \frac{\Delta x_2}{L_x}\frac{\hat{k}_{x_{appf}}}{\hat{k}_{x_{appe}}}\right)\left(\frac{\partial \hat{p}}{\partial x}\right)_f . \qquad (F103)$$

Substitute the expressions used in Eq. (F99) for $\left(\frac{\partial \hat{p}}{\partial y}\right)_f$ and $\left(\frac{\partial \hat{p}}{\partial y}\right)_s$ and Eq. (F100) into Eq. (F97):

$$\left(\frac{\partial \hat{p}}{\partial y}\right)_{fs} = \left(\frac{\Delta x_1 \hat{k}_{xy_f}\hat{k}_{xx_e}}{\Delta x_1 \hat{k}_{xy_f}\hat{k}_{xx_e} + \Delta x_2 \hat{k}_{xy_e}\hat{k}_{xx_f}}\right)\left[-\frac{\hat{k}_{yx_f}}{\hat{k}_{yy_f}}\left(\frac{\partial \hat{p}}{\partial x}\right)_f\right]$$

$$+\left(\frac{\Delta x_2 \hat{k}_{xy_e}\hat{k}_{xx_f}}{\Delta x_1 \hat{k}_{xy_f}\hat{k}_{xx_e} + \Delta x_2 \hat{k}_{xy_e}\hat{k}_{xx_f}}\right)\left[-\frac{\hat{k}_{yx_e}}{\hat{k}_{yy_e}}\frac{\hat{k}_{x_{appf}}}{\hat{k}_{x_{appe}}}\left(\frac{\partial \hat{p}}{\partial x}\right)_f\right]. \qquad (F104)$$

Divide Eq. (F104) by Eq. (F103) to yield:

$$\frac{\left(\frac{\partial \hat{p}}{\partial y}\right)_{fs}}{\left(\frac{\partial \hat{p}}{\partial x}\right)_{fs}} = \frac{-w1fs\frac{\hat{k}_{yx_f}}{\hat{k}_{yy_f}} - w2fs\left(\frac{\hat{k}_{x_{appf}}}{\hat{k}_{x_{appe}}}\right)\frac{\hat{k}_{yx_e}}{\hat{k}_{yy_e}}}{\left(\frac{\Delta x_1}{L_x} + \frac{\Delta x_2}{L_x}\frac{\hat{k}_{x_{appf}}}{\hat{k}_{x_{appe}}}\right)} \qquad (F105)$$

where

$$w1fs = \frac{\Delta x_1 \hat{k}_{xy_f}\hat{k}_{xx_e}}{\Delta x_1 \hat{k}_{xy_f}\hat{k}_{xx_e} + \Delta x_2 \hat{k}_{xy_e}\hat{k}_{xx_f}} \qquad (F106)$$

$$w2fs = \frac{\Delta x_2 \hat{k}_{xy_e}\hat{k}_{xx_f}}{\Delta x_1 \hat{k}_{xy_f}\hat{k}_{xx_e} + \Delta x_2 \hat{k}_{xy_e}\hat{k}_{xx_f}}. \qquad (F107)$$

II. "Local" pressure gradient ratios for injection along the y-axis:

Determination of $\frac{\left(\frac{\partial \hat{p}}{\partial x}\right)_z}{\left(\frac{\partial \hat{p}}{\partial y}\right)_t}$:

1. Isolate the first column of Figure F-1 as shown in Figure F-10.

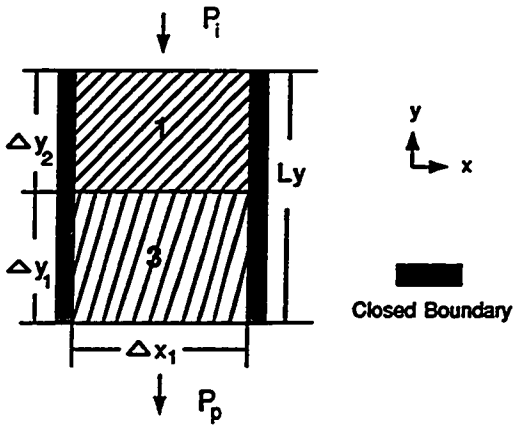

Fig. F-10: First Column of Figure F-1 (Injection Along y-axis).

Velocity components along the x-axis for blocks 1 and 3 are zero because of closed left and right boundaries:

$$v_{x_1} = -\frac{1}{\mu}\left(k_{xx_1}\left(\frac{\partial p}{\partial x}\right)_1 + k_{xy_1}\left(\frac{\partial p}{\partial y}\right)_1\right) = 0 \qquad (F108)$$

$$v_{x_3} = -\frac{1}{\mu}\left(k_{xx_3}\left(\frac{\partial p}{\partial x}\right)_3 + k_{xy_3}\left(\frac{\partial p}{\partial y}\right)_3\right) = 0. \qquad (F109)$$

Velocity component along the x-axis for blocks 1 and 3 combined is zero because of closed left and right boundaries:

$$\hat{v}_{x_f} = -\frac{1}{\mu}\left(\hat{k}_{xx_f}\left(\frac{\partial \hat{p}}{\partial x}\right)_f + \hat{k}_{xy_f}\left(\frac{\partial \hat{p}}{\partial y}\right)_f\right) = 0. \qquad (F110)$$

Velocity components along the y-axis for blocks 1 and 3:

$$v_{y_1} = -\frac{1}{\mu}\left(k_{yx_1}\left(\frac{\partial p}{\partial x}\right)_1 + k_{yy_1}\left(\frac{\partial p}{\partial y}\right)_1\right) \qquad (F111)$$

$$v_{y_3} = -\frac{1}{\mu}\left(k_{yx_3}\left(\frac{\partial p}{\partial x}\right)_3 + k_{yy_3}\left(\frac{\partial p}{\partial y}\right)_3\right). \qquad (F112)$$

Velocity component along the y-axis for blocks 1 and 3 combined:

$$\hat{v}_{y_f} = -\frac{1}{\mu}\left(\hat{k}_{yx_f}\left(\frac{\partial \hat{p}}{\partial x}\right)_f + \hat{k}_{yy_f}\left(\frac{\partial \hat{p}}{\partial y}\right)_f\right). \qquad (F113)$$

Rearrange Eqs. (F111)-(F113):

$$\left(\frac{\partial p}{\partial y}\right)_1 = -\frac{v_{y_1}\mu}{k_{yy_1}} - \frac{k_{yx_1}}{k_{yy_1}}\left(\frac{\partial p}{\partial x}\right)_1 \tag{F114}$$

$$\left(\frac{\partial p}{\partial y}\right)_3 = -\frac{v_{y_3}\mu}{k_{yy_3}} - \frac{k_{yx_3}}{k_{yy_3}}\left(\frac{\partial p}{\partial x}\right)_3 \tag{F115}$$

$$\left(\frac{\partial \hat{p}}{\partial y}\right)_f = -\frac{\hat{v}_{y_f}\mu}{\hat{k}_{yy_f}} - \frac{\hat{k}_{yx_f}}{\hat{k}_{yy_f}}\left(\frac{\partial \hat{p}}{\partial x}\right)_f . \tag{F116}$$

The total pressure gradient along the y-axis is expressed as:

$$\left(\frac{\partial \hat{p}}{\partial y}\right)_f = \frac{\Delta y_2}{L_y}\left(\frac{\partial p}{\partial y}\right)_1 + \frac{\Delta y_1}{L_y}\left(\frac{\partial p}{\partial y}\right)_3 \tag{F117}$$

and

$$\hat{v}_{y_f} = v_{y_1} = v_{y_3}. \tag{F118}$$

Use Eq. (F118) in Eqs. (F114)-(F116) which are substituted into Eq. (F117):

$$\begin{aligned}\frac{\hat{v}_{y_f}\mu}{\hat{k}_{yy_f}} + \frac{\hat{k}_{yx_f}}{\hat{k}_{yy_f}}\left(\frac{\partial \hat{p}}{\partial x}\right)_f =& \frac{\Delta y_2}{L_y}\left(\frac{\hat{v}_{y_f}\mu}{k_{yy_1}} + \frac{k_{yx_1}}{k_{yy_1}}\left(\frac{\partial p}{\partial x}\right)_1\right) \\ &+ \frac{\Delta y_1}{L_y}\left(\frac{\hat{v}_{y_f}\mu}{k_{yy_3}} + \frac{k_{yx_3}}{k_{yy_3}}\left(\frac{\partial p}{\partial x}\right)_3\right).\end{aligned} \tag{F119}$$

Rearrange Eq. (F119):

$$\begin{aligned}\frac{\hat{k}_{yx_f}}{\hat{k}_{yy_f}}\left(\frac{\partial \hat{p}}{\partial x}\right)_f =& \hat{v}_{y_f}\mu\left[\frac{\Delta y_2}{L_y k_{yy_1}} + \frac{\Delta y_1}{L_y k_{yy_3}} - \frac{1}{\hat{k}_{yy_f}}\right] \\ &+ \frac{\Delta y_2}{L_y}\frac{k_{yx_1}}{k_{yy_1}}\left(\frac{\partial p}{\partial x}\right)_1 + \frac{\Delta y_1}{L_y}\frac{k_{yx_3}}{k_{yy_3}}\left(\frac{\partial p}{\partial x}\right)_3.\end{aligned} \tag{F120}$$

No off-diagonal elements of the permeability tensor exist within the square brackets in Eq. (F120). From Eq. (C135) in Appendix C, it is seen that in the

absence of off-diagonal terms of the permeability tensors, Eq. (C135) reduces to:

$$\hat{k}_{yy_f} = \frac{L_y k_{yy_1} k_{yy_3}}{\Delta y_2 k_{yy_3} + \Delta y_1 k_{yy_1}}. \qquad (F121)$$

Using Eq. (F121), the expression within the square brackets in Eq. (F120) is zero and Eq. (F120) can be simplified to:

$$\frac{\hat{k}_{yx_f}}{\hat{k}_{yy_f}} \left(\frac{\partial \hat{p}}{\partial x}\right)_f = \frac{\Delta y_2}{L_y} \frac{k_{yx_1}}{k_{yy_1}} \left(\frac{\partial p}{\partial x}\right)_1 + \frac{\Delta y_1}{L_y} \frac{k_{yx_3}}{k_{yy_3}} \left(\frac{\partial p}{\partial x}\right)_3. \qquad (F122)$$

An expression for $\frac{\hat{k}_{yx_f}}{\hat{k}_{yy_f}}$ in Eq. (F122) in terms of local elements of the permeability tensors and system geometry is determined next.

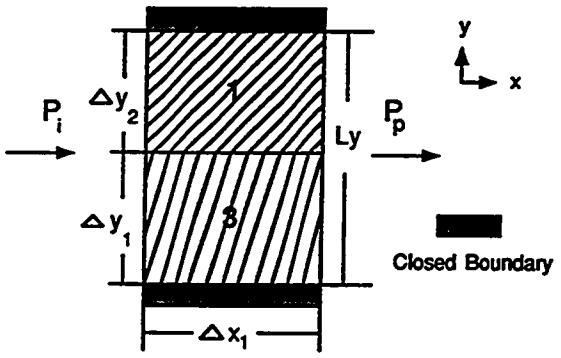

Fig. F-11: First Column of Figure F-1 (Injection Along x-axis).

From injection along the x-axis as in Figure F-11:

$$v_{y_1} = -\frac{1}{\mu}\left(k_{yx_1}\left(\frac{\partial p}{\partial x}\right)_1 + k_{yy_1}\left(\frac{\partial p}{\partial y}\right)_1\right) = 0 \qquad (F123)$$

$$v_{y_3} = -\frac{1}{\mu}\left(k_{yx_3}\left(\frac{\partial p}{\partial x}\right)_3 + k_{yy_3}\left(\frac{\partial p}{\partial y}\right)_3\right) = 0 \qquad (F124)$$

$$\hat{v}_{y_f} = -\frac{1}{\mu}\left(\hat{k}_{yx_f}\left(\frac{\partial \hat{p}}{\partial x}\right)_f + \hat{k}_{yy_f}\left(\frac{\partial \hat{p}}{\partial y}\right)_f\right) = 0. \qquad (F125)$$

Rearrange Eqs. (F123)-(F125):

$$\left(\frac{\partial p}{\partial y}\right)_1 = -\frac{k_{yx_1}}{k_{yy_1}}\left(\frac{\partial p}{\partial x}\right)_1 \qquad (F126)$$

$$\left(\frac{\partial p}{\partial y}\right)_3 = -\frac{k_{yx_3}}{k_{yy_3}}\left(\frac{\partial p}{\partial x}\right)_3 \qquad (F127)$$

$$\left(\frac{\partial \hat{p}}{\partial y}\right)_f = -\frac{\hat{k}_{yx_f}}{\hat{k}_{yy_f}}\left(\frac{\partial \hat{p}}{\partial x}\right)_f. \qquad (F128)$$

The total pressure gradient along y-axis is:

$$\left(\frac{\partial \hat{p}}{\partial y}\right)_f = \frac{\Delta y_2}{L_y}\left(\frac{\partial p}{\partial y}\right)_1 + \frac{\Delta y_1}{L_y}\left(\frac{\partial p}{\partial y}\right)_3. \qquad (F129)$$

Substitute Eqs. (F126)-(F128) into Eq. (F129):

$$-\frac{\hat{k}_{yx_f}}{\hat{k}_{yy_f}}\left(\frac{\partial \hat{p}}{\partial x}\right)_f = \frac{\Delta y_2}{L_y}\left(-\frac{k_{yx_1}}{k_{yy_1}}\left(\frac{\partial p}{\partial x}\right)_1\right) + \frac{\Delta y_1}{L_y}\left(-\frac{k_{yx_3}}{k_{yy_3}}\left(\frac{\partial p}{\partial x}\right)_3\right). \qquad (F130)$$

Since

$$\left(\frac{\partial \hat{p}}{\partial x}\right)_f = \left(\frac{\partial p}{\partial x}\right)_1 = \left(\frac{\partial p}{\partial x}\right)_3, \qquad (F131)$$

Eq. (F130) can be expressed as follows:

$$\frac{\hat{k}_{yx_f}}{\hat{k}_{yy_f}} = \frac{\Delta y_2}{L_y}\frac{k_{yx_1}}{k_{yy_1}} + \frac{\Delta y_1}{L_y}\frac{k_{yx_3}}{k_{yy_3}}. \qquad (F132)$$

Note that the sum of the coefficients of the local transverse pressure gradients in Eq. (F122) is equal to the right hand side of Eq. (F132).

Rearrange Eq. (F132) and substitute the rearranged equation into Eq. (F122):

$$\left(\frac{\Delta y_2 k_{yx_1} k_{yy_3} + \Delta y_1 k_{yx_3} k_{yy_1}}{L_y k_{yy_1} k_{yy_3}}\right)\left(\frac{\partial \hat{p}}{\partial x}\right)_f = \frac{\Delta y_2}{L_y}\frac{k_{yx_1}}{k_{yy_1}}\left(\frac{\partial p}{\partial x}\right)_1 + \frac{\Delta y_1}{L_y}\frac{k_{yx_3}}{k_{yy_3}}\left(\frac{\partial p}{\partial x}\right)_3. \quad (F133)$$

Solve Eq. (F133) for $\left(\frac{\partial \hat{p}}{\partial x}\right)_f$:

$$\left(\frac{\partial \hat{p}}{\partial x}\right)_f = \left(\frac{\Delta y_2 k_{yx_1} k_{yy_3}}{\Delta y_2 k_{yx_1} k_{yy_3} + \Delta y_1 k_{yx_3} k_{yy_1}}\right)\left(\frac{\partial p}{\partial x}\right)_1 + \left(\frac{\Delta y_1 k_{yx_3} k_{yy_1}}{\Delta y_2 k_{yx_1} k_{yy_3} + \Delta y_1 k_{yx_3} k_{yy_1}}\right)\left(\frac{\partial p}{\partial x}\right)_3. \quad (F134)$$

Based on Figure F-10, $v_{y_1} = v_{y_3}$. Thus, set Eq. (F111) equal to Eq. (F112):

$$k_{yx_1}\left(\frac{\partial p}{\partial x}\right)_1 + k_{yy_1}\left(\frac{\partial p}{\partial y}\right)_1 = k_{yx_3}\left(\frac{\partial p}{\partial x}\right)_3 + k_{yy_3}\left(\frac{\partial p}{\partial y}\right)_3. \quad (F135)$$

Eqs. (F108) and (F109) can be solved for $\left(\frac{\partial p}{\partial x}\right)_1$ and $\left(\frac{\partial p}{\partial x}\right)_3$, respectively, and substituted into Eq. (F135):

$$k_{yy_1}\left(\frac{\partial p}{\partial y}\right)_1 + k_{yx_1}\left(-\frac{k_{xy_1}}{k_{xx_1}}\right)\left(\frac{\partial p}{\partial y}\right)_1 = k_{yy_3}\left(\frac{\partial p}{\partial y}\right)_3 + k_{yx_3}\left(-\frac{k_{xy_3}}{k_{xx_3}}\right)\left(\frac{\partial p}{\partial y}\right)_3. \quad (F136)$$

Rearrange Eq. (F136) to solve for $\left(\frac{\partial p}{\partial y}\right)_3$:

$$\left(\frac{\partial p}{\partial y}\right)_3 = \frac{\hat{k}_{y_{app_1}}}{\hat{k}_{y_{app_3}}}\left(\frac{\partial p}{\partial y}\right)_1 \quad (F137)$$

where

$$\hat{k}_{y_{app_1}} = \left(k_{yy_1} - \frac{k_{xy_1} k_{yx_1}}{k_{xx_1}}\right) \quad (F138)$$

$$\hat{k}_{y_{app_3}} = \left(k_{yy_3} - \frac{k_{xy_3} k_{yx_3}}{k_{xx_3}} \right). \qquad (F139)$$

Substitute Eq. (F137) into Eq. (F117):

$$\begin{aligned} \left(\frac{\partial \hat{p}}{\partial y}\right)_f =& \frac{\Delta y_2}{L_y} \left(\frac{\partial p}{\partial y}\right)_1 + \frac{\Delta y_1}{L_y} \frac{\hat{k}_{y_{app_1}}}{\hat{k}_{y_{app_3}}} \left(\frac{\partial p}{\partial y}\right)_1 \\ =& \left(\frac{\Delta y_2}{L_y} + \frac{\Delta y_1}{L_y} \frac{\hat{k}_{y_{app_1}}}{\hat{k}_{y_{app_3}}} \right) \left(\frac{\partial p}{\partial y}\right)_1 . \end{aligned} \qquad (F140)$$

Substitute the expressions used in Eq. (F136) for $\left(\frac{\partial p}{\partial x}\right)_1$ and $\left(\frac{\partial p}{\partial x}\right)_3$ and Eq. (F137) into Eq. (F134):

$$\begin{aligned} \left(\frac{\partial \hat{p}}{\partial x}\right)_f =& \left(\frac{\Delta y_2 k_{yx_1} k_{yy_3}}{\Delta y_2 k_{yx_1} k_{yy_3} + \Delta y_1 k_{yx_3} k_{yy_1}} \right) \left[- \frac{k_{xy_1}}{k_{xx_1}} \left(\frac{\partial p}{\partial y}\right)_1 \right] \\ &+ \left(\frac{\Delta y_1 k_{yx_3} k_{yy_1}}{\Delta y_2 k_{yx_1} k_{yy_3} + \Delta y_1 k_{yx_3} k_{yy_1}} \right) \left[- \frac{k_{xy_3}}{k_{xx_3}} \frac{\hat{k}_{y_{app_1}}}{\hat{k}_{y_{app_3}}} \left(\frac{\partial p}{\partial y}\right)_1 \right]. \end{aligned} \qquad (F141)$$

Divide Eq. (F141) by Eq. (F140) to yield:

$$\frac{\left(\frac{\partial \hat{p}}{\partial x}\right)_f}{\left(\frac{\partial \hat{p}}{\partial y}\right)_f} = \frac{-w1f \frac{k_{xy_1}}{k_{xx_1}} - w2f \left(\frac{\hat{k}_{y_{app_1}}}{\hat{k}_{y_{app_3}}} \right) \frac{k_{xy_3}}{k_{xx_3}}}{\left(\frac{\Delta y_2}{L_y} + \frac{\Delta y_1}{L_y} \frac{\hat{k}_{y_{app_1}}}{\hat{k}_{y_{app_3}}} \right)} \qquad (F142)$$

where

$$w1f = \frac{\Delta y_2 k_{yx_1} k_{yy_3}}{\Delta y_2 k_{yx_1} k_{yy_3} + \Delta y_1 k_{yx_3} k_{yy_1}} \qquad (F143)$$

$$w2f = \frac{\Delta y_1 k_{yx_3} k_{yy_1}}{\Delta y_2 k_{yx_1} k_{yy_3} + \Delta y_1 k_{yx_3} k_{yy_1}}. \qquad (F144)$$

Determination of $\frac{\left(\frac{\partial \hat{p}}{\partial x}\right)_s}{\left(\frac{\partial \hat{p}}{\partial y}\right)_s}$:

2. Isolate the second column of Figure F-1 as shown in Figure F-12.

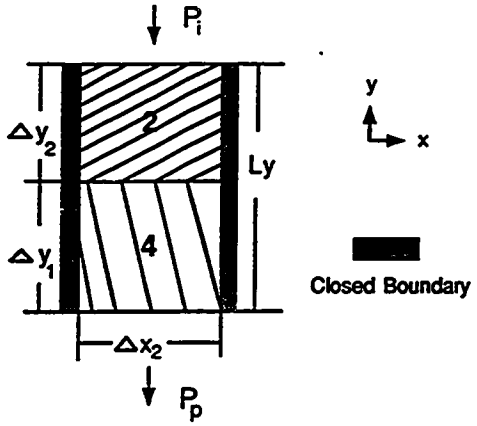

Fig. F-12: Second Column of Figure F-1 (Injection Along y-axis).

The derivation of $\frac{\left(\frac{\partial \hat{p}}{\partial x}\right)_s}{\left(\frac{\partial \hat{p}}{\partial y}\right)_s}$ is directly analogous to the derivation of $\frac{\left(\frac{\partial \hat{p}}{\partial x}\right)_f}{\left(\frac{\partial \hat{p}}{\partial y}\right)_f}$. Therefore, only the final expression is presented:

$$\frac{\left(\frac{\partial \hat{p}}{\partial x}\right)_s}{\left(\frac{\partial \hat{p}}{\partial y}\right)_s} = \frac{-w1s\frac{k_{xy_2}}{k_{xx_2}} - w2s\left(\frac{\hat{k}_{y_{app_2}}}{\hat{k}_{y_{app_4}}}\right)\frac{k_{xy_4}}{k_{xx_4}}}{\left(\frac{\Delta y_2}{L_y} + \frac{\Delta y_1}{L_y}\frac{\hat{k}_{y_{app_2}}}{\hat{k}_{y_{app_4}}}\right)} \qquad (F145)$$

where

$$w1s = \frac{\Delta y_2 k_{yx_2} k_{yy_4}}{\Delta y_2 k_{yx_2} k_{yy_4} + \Delta y_1 k_{yx_4} k_{yy_2}} \qquad (F146)$$

$$w2s = \frac{\Delta y_1 k_{yx_4} k_{yy_2}}{\Delta y_2 k_{yx_2} k_{yy_4} + \Delta y_1 k_{yx_4} k_{yy_2}}. \qquad (F147)$$

Determination of $\frac{\left(\frac{\partial \hat{p}}{\partial x}\right)_{s_1}}{\left(\frac{\partial \hat{p}}{\partial y}\right)_{s_1}}$:

3. Since the first and second columns are parallel with respect to the direction of flow, $\frac{\left(\frac{\partial \hat{p}}{\partial x}\right)_{f_2}}{\left(\frac{\partial \hat{p}}{\partial y}\right)_{f_2}}$ can be obtained from the following analysis using Figure F-13: Velocity components along the x-axis for the first and second columns are zero because of closed left and right boundaries:

$$\hat{v}_{x_f} = -\frac{1}{\mu}\left(\hat{k}_{xx_f}\left(\frac{\partial \hat{p}}{\partial x}\right)_f + \hat{k}_{xy_f}\left(\frac{\partial \hat{p}}{\partial y}\right)_f\right) = 0 \qquad (F148)$$

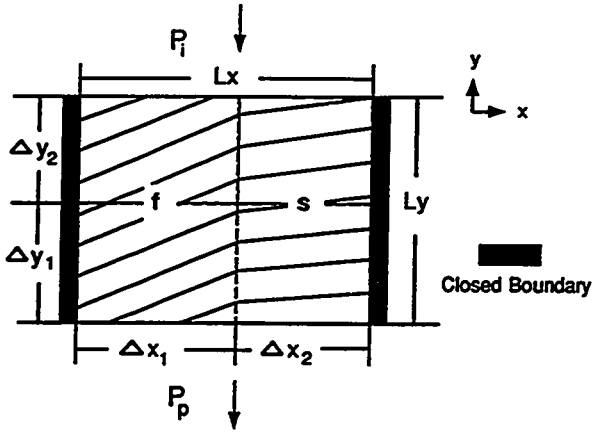

Fig. F-13: First and Second Columns of Figure F-1 (Injection Along y-axis).

$$\hat{v}_{x_s} = -\frac{1}{\mu}\left(\hat{k}_{xx_s}\left(\frac{\partial \hat{p}}{\partial x}\right)_s + \hat{k}_{xy_s}\left(\frac{\partial \hat{p}}{\partial y}\right)_s\right) = 0. \qquad (F149)$$

Velocity component along the x-axis for first and second columns combined are zero because of closed left and right boundaries:

$$\hat{v}_{x_{fs}} = -\frac{1}{\mu}\left(\hat{k}_{xx_{fs}}\left(\frac{\partial \hat{p}}{\partial x}\right)_{fs} + \hat{k}_{xy_{fs}}\left(\frac{\partial \hat{p}}{\partial y}\right)_{fs}\right) = 0. \qquad (F150)$$

Velocity components along the y-axis for the first and second columns:

$$\hat{v}_{y_f} = -\frac{1}{\mu}\left(\hat{k}_{yx_f}\left(\frac{\partial \hat{p}}{\partial x}\right)_f + \hat{k}_{yy_f}\left(\frac{\partial \hat{p}}{\partial y}\right)_f\right) \qquad (F151)$$

$$\hat{v}_{y_s} = -\frac{1}{\mu}\left(\hat{k}_{yx_s}\left(\frac{\partial \hat{p}}{\partial x}\right)_s + \hat{k}_{yy_s}\left(\frac{\partial \hat{p}}{\partial y}\right)_s\right). \qquad (F152)$$

Velocity component along the y-axis for first and second columns combined:

$$\hat{v}_{y_{fs}} = -\frac{1}{\mu}\left(\hat{k}_{yx_{fs}}\left(\frac{\partial \hat{p}}{\partial x}\right)_{fs} + \hat{k}_{yy_{fs}}\left(\frac{\partial \hat{p}}{\partial y}\right)_{fs}\right). \qquad (F153)$$

Rearrange Eqs. (F148)-(F150):

$$\left(\frac{\partial \hat{p}}{\partial x}\right)_f = -\frac{\hat{k}_{xy_f}}{\hat{k}_{xx_f}}\left(\frac{\partial \hat{p}}{\partial y}\right)_f \qquad (F154)$$

$$\left(\frac{\partial \hat{p}}{\partial x}\right)_s = -\frac{\hat{k}_{xy_s}}{\hat{k}_{xx_s}}\left(\frac{\partial \hat{p}}{\partial y}\right)_s \qquad (F155)$$

$$\left(\frac{\partial \hat{p}}{\partial x}\right)_{fs} = -\frac{\hat{k}_{xy_{fs}}}{\hat{k}_{xx_{fs}}}\left(\frac{\partial \hat{p}}{\partial y}\right)_{fs}. \qquad (F156)$$

The total pressure gradient along the x-axis is expressed as:

$$\left(\frac{\partial \hat{p}}{\partial x}\right)_{fs} = \frac{\Delta x_1}{L_x}\left(\frac{\partial \hat{p}}{\partial x}\right)_f + \frac{\Delta x_2}{L_x}\left(\frac{\partial \hat{p}}{\partial x}\right)_s. \qquad (F157)$$

Substitute Eqs. (F154)-(F156) into Eq. (F157):

$$-\frac{\hat{k}_{xy_{fs}}}{\hat{k}_{xx_{fs}}}\left(\frac{\partial \hat{p}}{\partial y}\right)_{fs} = \frac{\Delta x_1}{L_x}\left(-\frac{\hat{k}_{xy_f}}{\hat{k}_{xx_f}}\left(\frac{\partial \hat{p}}{\partial y}\right)_f\right) + \frac{\Delta x_2}{L_x}\left(-\frac{\hat{k}_{xy_s}}{\hat{k}_{xx_s}}\left(\frac{\partial \hat{p}}{\partial y}\right)_s\right). \qquad (F158)$$

The total pressure gradient along the y-axis is expressed as:

$$\left(\frac{\partial \hat{p}}{\partial y}\right)_{fs} = \left(\frac{\partial \hat{p}}{\partial y}\right)_f = \left(\frac{\partial \hat{p}}{\partial y}\right)_s. \qquad (F159)$$

Substitute Eq. (F159) into Eq. (F158) and cancel the pressure gradients:

$$-\frac{\hat{k}_{xy_{fs}}}{\hat{k}_{xx_{fs}}} = -\frac{\Delta x_1}{L_x}\frac{\hat{k}_{xy_f}}{\hat{k}_{xx_f}} - \frac{\Delta x_2}{L_x}\frac{\hat{k}_{xy_s}}{\hat{k}_{xx_s}}. \qquad (F160)$$

Eq. (F156) can be rearranged as follows:

$$\frac{\left(\frac{\partial \hat{p}}{\partial x}\right)_{fs}}{\left(\frac{\partial \hat{p}}{\partial y}\right)_{fs}} = -\frac{\hat{k}_{xy_{fs}}}{\hat{k}_{xx_{fs}}}. \qquad (F161)$$

Substitute Eq. (F161) into Eq. (F160):

$$\frac{\left(\frac{\partial \hat{p}}{\partial x}\right)_{fs}}{\left(\frac{\partial \hat{p}}{\partial y}\right)_{fs}} = -\frac{\Delta x_1}{L_x}\frac{\hat{k}_{xy_f}}{\hat{k}_{xx_f}} - \frac{\Delta x_2}{L_x}\frac{\hat{k}_{xy_s}}{\hat{k}_{xx_s}} \qquad (F162)$$

where $-\frac{\hat{k}_{xy_f}}{\hat{k}_{xx_f}} = \frac{\left(\frac{\partial \hat{p}}{\partial x}\right)_f}{\left(\frac{\partial \hat{p}}{\partial y}\right)_f}$ and $-\frac{\hat{k}_{xy_a}}{\hat{k}_{xx_a}} = \frac{\left(\frac{\partial \hat{p}}{\partial x}\right)_a}{\left(\frac{\partial \hat{p}}{\partial y}\right)_a}$ are given by Eqs. (F142) and (F145).

Determination of $\frac{\left(\frac{\partial \hat{p}}{\partial x}\right)_t}{\left(\frac{\partial \hat{p}}{\partial y}\right)_t}$:

4. Isolate the top layer of Figure F-1, i.e., combine blocks 1 and 2 as shown in Figure F-14.

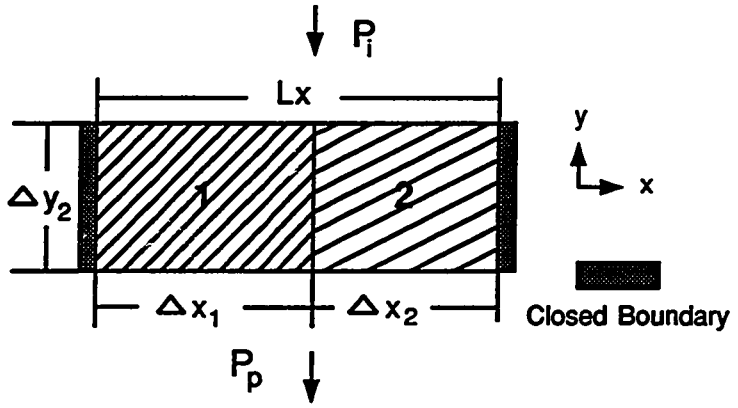

Fig. F-14: Top Layer of Figure F-1 (Injection Along y-axis).

Velocity components along the x-axis for blocks 1 and 2 are zero because of closed left and right boundaries:

$$v_{x_1} = -\frac{1}{\mu}\left(k_{xx_1}\left(\frac{\partial p}{\partial x}\right)_1 + k_{xy_1}\left(\frac{\partial p}{\partial y}\right)_1\right) = 0 \qquad (F163)$$

$$v_{x_2} = -\frac{1}{\mu}\left(k_{xx_2}\left(\frac{\partial p}{\partial x}\right)_2 + k_{xy_2}\left(\frac{\partial p}{\partial y}\right)_2\right) = 0. \qquad (F164)$$

Velocity component along the x-axis for blocks 1 and 2 combined is zero because of closed left and right boundaries:

$$\hat{v}_{x_t} = -\frac{1}{\mu}\left(\hat{k}_{xx_t}\left(\frac{\partial \hat{p}}{\partial x}\right)_t + \hat{k}_{xy_t}\left(\frac{\partial \hat{p}}{\partial y}\right)_t\right) = 0. \qquad (F165)$$

Velocity components along the y-axis for blocks 1 and 2:

$$v_{y_1} = -\frac{1}{\mu}\left(k_{yx_1}\left(\frac{\partial p}{\partial x}\right)_1 + k_{yy_1}\left(\frac{\partial p}{\partial y}\right)_1\right) \qquad (F166)$$

$$v_{y_2} = -\frac{1}{\mu}\left(k_{yx_2}\left(\frac{\partial p}{\partial x}\right)_2 + k_{yy_2}\left(\frac{\partial p}{\partial y}\right)_2\right). \qquad (F167)$$

Velocity component along the y-axis for blocks 1 and 2 combined:

$$\hat{v}_{y_t} = -\frac{1}{\mu}\left(\hat{k}_{yx_t}\left(\frac{\partial \hat{p}}{\partial x}\right)_t + \hat{k}_{yy_t}\left(\frac{\partial \hat{p}}{\partial y}\right)_t\right). \qquad (F168)$$

Rearrange Eqs. (F163)-(F165):

$$\left(\frac{\partial p}{\partial x}\right)_1 = -\frac{k_{xy_1}}{k_{xx_1}}\left(\frac{\partial p}{\partial y}\right)_1 \qquad (F169)$$

$$\left(\frac{\partial p}{\partial x}\right)_2 = -\frac{k_{xy_2}}{k_{xx_2}}\left(\frac{\partial p}{\partial y}\right)_2 \qquad (F170)$$

$$\left(\frac{\partial \hat{p}}{\partial x}\right)_t = -\frac{\hat{k}_{xy_t}}{\hat{k}_{xx_t}}\left(\frac{\partial \hat{p}}{\partial y}\right)_t. \qquad (F171)$$

The total pressure gradient along the x-axis is expressed as:

$$\left(\frac{\partial \hat{p}}{\partial x}\right)_t = \frac{\Delta x_1}{L_x}\left(\frac{\partial p}{\partial x}\right)_1 + \frac{\Delta x_2}{L_x}\left(\frac{\partial p}{\partial x}\right)_2. \qquad (F172)$$

Substitute Eqs. (F169)-(F171) into Eq. (F172):

$$-\frac{\hat{k}_{xy_t}}{\hat{k}_{xx_t}}\left(\frac{\partial \hat{p}}{\partial y}\right)_t = \frac{\Delta x_1}{L_x}\left(-\frac{k_{xy_1}}{k_{xx_1}}\left(\frac{\partial p}{\partial y}\right)_1\right) + \frac{\Delta x_2}{L_x}\left(-\frac{k_{xy_2}}{k_{xx_2}}\left(\frac{\partial p}{\partial y}\right)_2\right). \qquad (F173)$$

The total pressure gradient along the y-axis is expressed as:

$$\left(\frac{\partial \hat{p}}{\partial y}\right)_t = \left(\frac{\partial p}{\partial y}\right)_1 = \left(\frac{\partial p}{\partial y}\right)_2. \qquad (F174)$$

Substitute Eq. (F174) into Eq. (F173) and cancel the pressure gradients:

$$-\frac{\hat{k}_{xy_t}}{\hat{k}_{xx_t}} = -\frac{\Delta x_1}{L_x}\frac{k_{xy_1}}{k_{xx_1}} - \frac{\Delta x_2}{L_x}\frac{k_{xy_2}}{k_{xx_2}}. \qquad (F175)$$

Eq. (F171) can be rearranged as follows:

$$\frac{\left(\frac{\partial \hat{p}}{\partial x}\right)_t}{\left(\frac{\partial \hat{p}}{\partial y}\right)_t} = -\frac{\hat{k}_{xy_t}}{\hat{k}_{xx_t}}. \qquad (F176)$$

Substitute Eq. (F176) into Eq. (F175):

$$\frac{\left(\frac{\partial \hat{p}}{\partial x}\right)_t}{\left(\frac{\partial \hat{p}}{\partial y}\right)_t} = -\frac{\Delta x_1}{L_x}\frac{k_{xy_1}}{k_{xx_1}} - \frac{\Delta x_2}{L_x}\frac{k_{xy_2}}{k_{xx_2}}. \qquad (F177)$$

Determination of $\frac{\left(\frac{\partial \hat{p}}{\partial x}\right)_b}{\left(\frac{\partial \hat{p}}{\partial y}\right)_b}$:

5. Isolate the bottom layer of Figure F-1, i.e., combine blocks 3 and 4 as shown in Figure F-15.

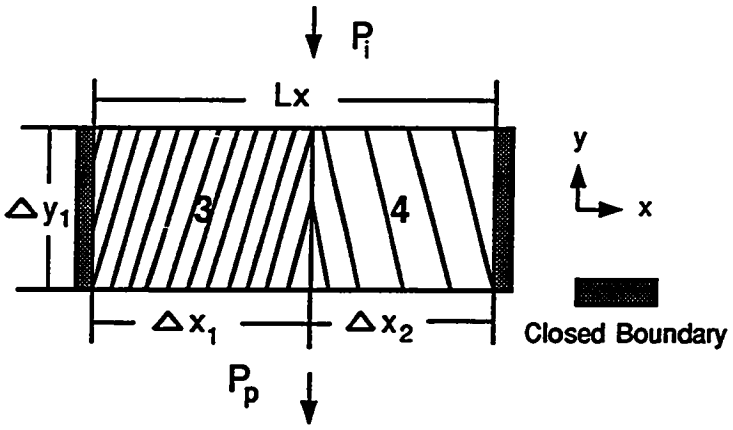

Fig. F-15: Bottom Layer of Figure F-1 (Injection Along y-axis).

The derivation of $\frac{\left(\frac{\partial \hat{p}}{\partial x}\right)_b}{\left(\frac{\partial \hat{p}}{\partial y}\right)_b}$ is directly analogous to the derivation of $\frac{\left(\frac{\partial \hat{p}}{\partial x}\right)_t}{\left(\frac{\partial \hat{p}}{\partial y}\right)_t}$. Therefore, only the final expression is presented:

$$\frac{\left(\frac{\partial \hat{p}}{\partial x}\right)_b}{\left(\frac{\partial \hat{p}}{\partial y}\right)_b} = -\frac{\Delta x_1}{L_x}\frac{k_{xy_3}}{k_{xx_3}} - \frac{\Delta x_2}{L_x}\frac{k_{xy_4}}{k_{xx_4}}. \qquad (F178)$$

Determination of $\frac{\left(\frac{\partial \hat{p}}{\partial x}\right)_{tb}}{\left(\frac{\partial \hat{p}}{\partial y}\right)_{tb}}$:

6. Since the top and bottom layers are in series with respect to the direction of flow, $\frac{\left(\frac{\partial \hat{p}}{\partial x}\right)_{tb}}{\left(\frac{\partial \hat{p}}{\partial y}\right)_{tb}}$ can be obtained from the following analysis using Figure F-16:

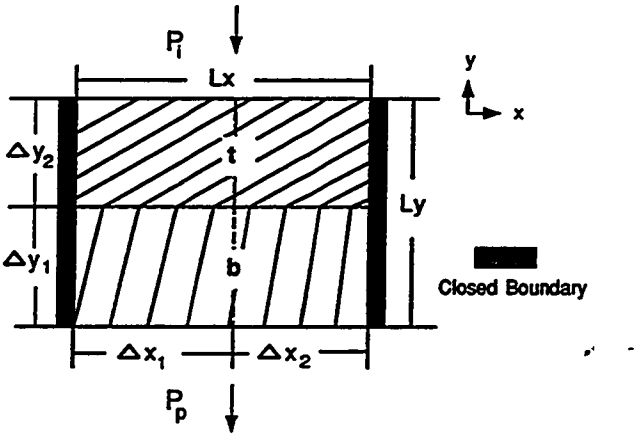

Fig. F-16: Top and Bottom Layers of Figure F-1 (Injection Along y-axis).

Velocity components along the x-axis for top and bottom layers are zero because of closed left and right boundaries:

$$\hat{v}_{x_t} = -\frac{1}{\mu}\left(\hat{k}_{xx_t}\left(\frac{\partial \hat{p}}{\partial x}\right)_t + \hat{k}_{xy_t}\left(\frac{\partial \hat{p}}{\partial y}\right)_t\right) = 0 \qquad (F179)$$

$$\hat{v}_{x_b} = -\frac{1}{\mu}\left(\hat{k}_{xx_b}\left(\frac{\partial \hat{p}}{\partial x}\right)_b + \hat{k}_{xy_b}\left(\frac{\partial \hat{p}}{\partial y}\right)_b\right) = 0. \qquad (F180)$$

Velocity component along the x-axis for top and bottom layers combined is zero because of closed left and right boundaries:

$$\hat{v}_{x_{tb}} = -\frac{1}{\mu}\left(\hat{k}_{xx_{tb}}\left(\frac{\partial \hat{p}}{\partial x}\right)_{tb} + \hat{k}_{xy_{tb}}\left(\frac{\partial \hat{p}}{\partial y}\right)_{tb}\right) = 0. \qquad (F181)$$

Velocity components along the y-axis for top and bottom layers:

$$\hat{v}_{y_t} = -\frac{1}{\mu}\left(\hat{k}_{yx_t}\left(\frac{\partial \hat{p}}{\partial x}\right)_t + \hat{k}_{yy_t}\left(\frac{\partial \hat{p}}{\partial y}\right)_t\right) \qquad (F182)$$

$$\hat{v}_{y_b} = -\frac{1}{\mu}\left(\hat{k}_{yx_b}\left(\frac{\partial \hat{p}}{\partial x}\right)_b + \hat{k}_{yy_b}\left(\frac{\partial \hat{p}}{\partial y}\right)_b\right). \qquad (F183)$$

Velocity component along the y-axis for top and bottom layers:

$$\hat{v}_{y_{tb}} = -\frac{1}{\mu}\left(\hat{k}_{yx_{tb}}\left(\frac{\partial \hat{p}}{\partial x}\right)_{tb} + \hat{k}_{yy_{tb}}\left(\frac{\partial \hat{p}}{\partial y}\right)_{tb}\right). \qquad (F184)$$

Rearrange Eqs. (F182)-(F184):

$$\left(\frac{\partial \hat{p}}{\partial y}\right)_t = -\frac{\hat{v}_{y_t}\mu}{\hat{k}_{yy_t}} - \frac{\hat{k}_{yx_t}}{\hat{k}_{yy_t}}\left(\frac{\partial \hat{p}}{\partial x}\right)_t \qquad (F185)$$

$$\left(\frac{\partial \hat{p}}{\partial y}\right)_b = -\frac{\hat{v}_{y_b}\mu}{\hat{k}_{yy_b}} - \frac{\hat{k}_{yx_b}}{\hat{k}_{yy_b}}\left(\frac{\partial \hat{p}}{\partial x}\right)_b \qquad (F186)$$

$$\left(\frac{\partial \hat{p}}{\partial y}\right)_{tb} = -\frac{\hat{v}_{y_{tb}}\mu}{\hat{k}_{yy_{tb}}} - \frac{\hat{k}_{yx_{tb}}}{\hat{k}_{yy_{tb}}}\left(\frac{\partial \hat{p}}{\partial x}\right)_{tb}. \qquad (F187)$$

The total pressure gradient along the y-axis is expressed as:

$$\left(\frac{\partial \hat{p}}{\partial y}\right)_{tb} = \frac{\Delta y_2}{L_y}\left(\frac{\partial \hat{p}}{\partial y}\right)_t + \frac{\Delta y_1}{L_y}\left(\frac{\partial \hat{p}}{\partial y}\right)_b \qquad (F188)$$

and

$$\hat{v}_{y_{tb}} = \hat{v}_{y_t} = \hat{v}_{y_b}. \qquad (F189)$$

Use Eq. (F189) in Eqs. (F185)-(F187) which are substituted into Eq. (F188):

$$\begin{aligned}\frac{\hat{v}_{y_{tb}}\mu}{\hat{k}_{yy_{tb}}} + \frac{\hat{k}_{yx_{tb}}}{\hat{k}_{yy_{tb}}}\left(\frac{\partial \hat{p}}{\partial x}\right)_{tb} =& \frac{\Delta y_2}{L_y}\left(\frac{\hat{v}_{y_{tb}}\mu}{\hat{k}_{yy_t}} + \frac{\hat{k}_{yx_t}}{\hat{k}_{yy_t}}\left(\frac{\partial \hat{p}}{\partial x}\right)_t\right) \\ &+ \frac{\Delta y_1}{L_y}\left(\frac{\hat{v}_{y_{tb}}\mu}{\hat{k}_{yy_b}} + \frac{\hat{k}_{yx_b}}{\hat{k}_{yy_b}}\left(\frac{\partial \hat{p}}{\partial x}\right)_b\right). \qquad (F190)\end{aligned}$$

Rearrange Eq. (F190):

$$\frac{\hat{k}_{yx_{tb}}}{\hat{k}_{yy_{tb}}}\left(\frac{\partial\hat{p}}{\partial x}\right)_{tb} = \hat{v}_{y_{tb}}\mu\left[\frac{\Delta y_2}{L_y\hat{k}_{yy_t}} + \frac{\Delta y_1}{L_y\hat{k}_{yy_b}} - \frac{1}{\hat{k}_{yy_{tb}}}\right] + \frac{\Delta y_2}{L_y}\frac{\hat{k}_{yx_t}}{\hat{k}_{yy_t}}\left(\frac{\partial\hat{p}}{\partial x}\right)_t + \frac{\Delta y_1}{L_y}\frac{\hat{k}_{yx_b}}{\hat{k}_{yy_b}}\left(\frac{\partial\hat{p}}{\partial x}\right)_b . \qquad (F191)$$

No off-diagonal elements of the permeability tensors exist within the square brackets of Eq. (F191). It can be shown that in the absence of off-diagonal elements, the two first terms within the square bracket in Eq. (F191) are equal to $\frac{1}{\hat{k}_{yy_{tb}}}$. Thus, Eq. (F191) can be reduced to:

$$\frac{\hat{k}_{yx_{tb}}}{\hat{k}_{yy_{tb}}}\left(\frac{\partial\hat{p}}{\partial x}\right)_{tb} = \frac{\Delta y_2}{L_y}\frac{\hat{k}_{yx_t}}{\hat{k}_{yy_t}}\left(\frac{\partial\hat{p}}{\partial x}\right)_t + \frac{\Delta y_1}{L_y}\frac{\hat{k}_{yx_b}}{\hat{k}_{yy_b}}\left(\frac{\partial\hat{p}}{\partial x}\right)_b . \qquad (F192)$$

An expression for $\frac{\hat{k}_{yx_{tb}}}{\hat{k}_{yy_{tb}}}$ in Eq. (F192) in terms of local elements of the permeability tensors and system geometry is determined next.

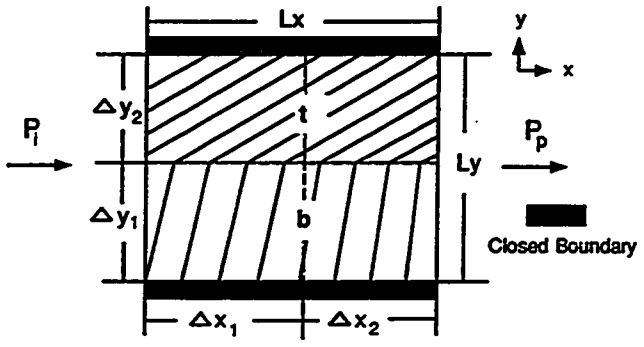

Fig. F-17: Top and Bottom Layers of Figure F-1 (Injection Along x-axis).

From injection along the x-axis as in Figure F-17:

$$\hat{v}_{y_t} = -\frac{1}{\mu}\left(\hat{k}_{yx_t}\left(\frac{\partial\hat{p}}{\partial x}\right)_t + \hat{k}_{yy_t}\left(\frac{\partial\hat{p}}{\partial y}\right)_t\right) = 0 \qquad (F193)$$

$$\hat{v}_{y_b} = -\frac{1}{\mu}\left(\hat{k}_{yx_b}\left(\frac{\partial\hat{p}}{\partial x}\right)_b + \hat{k}_{yy_b}\left(\frac{\partial\hat{p}}{\partial y}\right)_b\right) = 0 \qquad (F194)$$

$$\hat{v}_{y_{tb}} = -\frac{1}{\mu}\left(\hat{k}_{yx_{tb}}\left(\frac{\partial \hat{p}}{\partial x}\right)_{tb} + \hat{k}_{yy_{tb}}\left(\frac{\partial \hat{p}}{\partial y}\right)_{tb}\right) = 0. \qquad (F195)$$

Rearrange Eqs. (F193)-(F195):

$$\left(\frac{\partial \hat{p}}{\partial y}\right)_t = -\frac{\hat{k}_{yx_t}}{\hat{k}_{yy_t}}\left(\frac{\partial \hat{p}}{\partial x}\right)_t \qquad (F196)$$

$$\left(\frac{\partial \hat{p}}{\partial y}\right)_b = -\frac{\hat{k}_{yx_b}}{\hat{k}_{yy_b}}\left(\frac{\partial \hat{p}}{\partial x}\right)_b \qquad (F197)$$

$$\left(\frac{\partial \hat{p}}{\partial y}\right)_{tb} = -\frac{\hat{k}_{yx_{tb}}}{\hat{k}_{yy_{tb}}}\left(\frac{\partial \hat{p}}{\partial x}\right)_{tb}. \qquad (F198)$$

The total pressure gradient along y-axis is:

$$\left(\frac{\partial \hat{p}}{\partial y}\right)_{tb} = \frac{\Delta y_2}{L_y}\left(\frac{\partial \hat{p}}{\partial y}\right)_t + \frac{\Delta y_1}{L_y}\left(\frac{\partial \hat{p}}{\partial y}\right)_b. \qquad (F199)$$

Substitute Eqs. (F196)-(F198) into Eq. (F199):

$$-\frac{\hat{k}_{yx_{tb}}}{\hat{k}_{yy_{tb}}}\left(\frac{\partial \hat{p}}{\partial x}\right)_{tb} = \frac{\Delta y_2}{L_y}\left(-\frac{\hat{k}_{yx_t}}{\hat{k}_{yy_t}}\left(\frac{\partial \hat{p}}{\partial x}\right)_t\right) + \frac{\Delta y_1}{L_y}\left(-\frac{\hat{k}_{yx_b}}{\hat{k}_{yy_b}}\left(\frac{\partial \hat{p}}{\partial x}\right)_b\right). \qquad (F200)$$

Since

$$\left(\frac{\partial \hat{p}}{\partial x}\right)_{tb} = \left(\frac{\partial \hat{p}}{\partial x}\right)_t = \left(\frac{\partial \hat{p}}{\partial x}\right)_b, \qquad (F201)$$

Eq. (F200) can be expressed as follows:

$$\frac{\hat{k}_{yx_{tb}}}{\hat{k}_{yy_{tb}}} = \frac{\Delta y_2}{L_y}\frac{\hat{k}_{yx_t}}{\hat{k}_{yy_t}} + \frac{\Delta y_1}{L_y}\frac{\hat{k}_{yx_b}}{\hat{k}_{yy_b}}. \qquad (F202)$$

Rearrange Eq. (F202) and substitute the rearranged equation into Eq. (F192):

$$\left(\frac{\Delta y_2 \hat{k}_{yx_t}\hat{k}_{yy_b} + \Delta y_1 \hat{k}_{yx_b}\hat{k}_{yy_t}}{L_y \hat{k}_{yy_t}\hat{k}_{yy_b}}\right)\left(\frac{\partial \hat{p}}{\partial x}\right)_{tb} = \frac{\Delta y_2}{L_y}\frac{\hat{k}_{yx_t}}{\hat{k}_{yy_t}}\left(\frac{\partial \hat{p}}{\partial x}\right)_t + \frac{\Delta y_1}{L_y}\frac{\hat{k}_{yx_b}}{\hat{k}_{yy_b}}\left(\frac{\partial \hat{p}}{\partial x}\right)_b. \quad (F203)$$

Solve Eq. (F203) for $\left(\frac{\partial \hat{p}}{\partial x}\right)_{tb}$:

$$\left(\frac{\partial \hat{p}}{\partial x}\right)_{tb} = \left(\frac{\Delta y_2 \hat{k}_{yx_t}\hat{k}_{yy_b}}{\Delta y_2 \hat{k}_{yx_t}\hat{k}_{yy_b} + \Delta y_1 \hat{k}_{yx_b}\hat{k}_{yy_t}}\right)\left(\frac{\partial \hat{p}}{\partial x}\right)_t + \left(\frac{\Delta y_1 \hat{k}_{yx_b}\hat{k}_{yy_t}}{\Delta y_2 \hat{k}_{yx_t}\hat{k}_{yy_b} + \Delta y_1 \hat{k}_{yx_b}\hat{k}_{yy_t}}\right)\left(\frac{\partial \hat{p}}{\partial x}\right)_b. \quad (F204)$$

Based on Figure F-16, $\hat{v}_{y_t} = \hat{v}_{y_b}$. Thus, set Eq. (F182) equal to Eq. (F183):

$$\hat{k}_{yx_t}\left(\frac{\partial \hat{p}}{\partial x}\right)_t + \hat{k}_{yy_t}\left(\frac{\partial \hat{p}}{\partial y}\right)_t = \hat{k}_{yx_b}\left(\frac{\partial \hat{p}}{\partial x}\right)_b + \hat{k}_{yy_b}\left(\frac{\partial \hat{p}}{\partial y}\right)_b. \quad (F205)$$

Eqs. (F179) and (F180) can be solved for $\left(\frac{\partial \hat{p}}{\partial x}\right)_t$ and $\left(\frac{\partial \hat{p}}{\partial x}\right)_b$, respectively, and substituted into Eq. (F205):

$$\hat{k}_{yy_t}\left(\frac{\partial \hat{p}}{\partial y}\right)_t + \hat{k}_{yx_t}\left(-\frac{\hat{k}_{xy_t}}{\hat{k}_{xx_t}}\right)\left(\frac{\partial \hat{p}}{\partial y}\right)_t = \hat{k}_{yy_b}\left(\frac{\partial \hat{p}}{\partial y}\right)_b + \hat{k}_{yx_b}\left(-\frac{\hat{k}_{xy_b}}{\hat{k}_{xx_b}}\right)\left(\frac{\partial \hat{p}}{\partial y}\right)_b. \quad (F206)$$

Rearrange Eq. (F206) to solve for $\left(\frac{\partial \hat{p}}{\partial y}\right)_b$:

$$\left(\frac{\partial \hat{p}}{\partial y}\right)_b = \frac{\hat{k}_{y_{app_t}}}{\hat{k}_{y_{app_b}}}\left(\frac{\partial \hat{p}}{\partial y}\right)_t \quad (F207)$$

where

$$\hat{k}_{y_{app_t}} = \left(\hat{k}_{yy_t} - \frac{\hat{k}_{xy_t}\hat{k}_{yx_t}}{\hat{k}_{xx_t}} \right) \tag{F208}$$

$$\hat{k}_{y_{app_b}} = \left(\hat{k}_{yy_b} - \frac{\hat{k}_{xy_b}\hat{k}_{yx_b}}{\hat{k}_{xx_b}} \right). \tag{F209}$$

Substitute Eq. (F207) into Eq. (F188):

$$\begin{aligned}\left(\frac{\partial \hat{p}}{\partial y}\right)_{tb} &= \frac{\Delta y_2}{L_y}\left(\frac{\partial \hat{p}}{\partial y}\right)_t + \frac{\Delta y_1}{L_y}\frac{\hat{k}_{y_{app_t}}}{\hat{k}_{y_{app_b}}}\left(\frac{\partial \hat{p}}{\partial y}\right)_t \\ &= \left(\frac{\Delta y_2}{L_y} + \frac{\Delta y_1}{L_y}\frac{\hat{k}_{y_{app_t}}}{\hat{k}_{y_{app_b}}}\right)\left(\frac{\partial \hat{p}}{\partial y}\right)_t. \end{aligned} \tag{F210}$$

Substitute the expressions used in Eq. (F206) for $\left(\frac{\partial \hat{p}}{\partial x}\right)_t$ and $\left(\frac{\partial \hat{p}}{\partial x}\right)_b$ and Eq. (F207) into Eq. (F204):

$$\begin{aligned}\left(\frac{\partial \hat{p}}{\partial x}\right)_{tb} =& \left(\frac{\Delta y_2 \hat{k}_{yx_t}\hat{k}_{yy_b}}{\Delta y_2 \hat{k}_{yx_t}\hat{k}_{yy_b} + \Delta y_1 \hat{k}_{yx_b}\hat{k}_{yy_t}}\right)\left[-\frac{\hat{k}_{xy_t}}{\hat{k}_{xx_t}}\left(\frac{\partial \hat{p}}{\partial y}\right)_t\right] \\ &+ \left(\frac{\Delta y_1 \hat{k}_{yx_b}\hat{k}_{yy_t}}{\Delta y_2 \hat{k}_{yx_t}\hat{k}_{yy_b} + \Delta y_1 \hat{k}_{yx_b}\hat{k}_{yy_t}}\right)\left[-\frac{\hat{k}_{xy_b}}{\hat{k}_{xx_b}}\frac{\hat{k}_{y_{app_t}}}{\hat{k}_{y_{app_b}}}\left(\frac{\partial \hat{p}}{\partial y}\right)_t\right]. \end{aligned} \tag{F211}$$

Divide Eq. (F211) by Eq. (F210) to yield:

$$\frac{\left(\frac{\partial \hat{p}}{\partial x}\right)_{tb}}{\left(\frac{\partial \hat{p}}{\partial y}\right)_{tb}} = \frac{-w1tb\frac{\hat{k}_{xy_t}}{\hat{k}_{xx_t}} - w2tb\left(\frac{\hat{k}_{y_{app_t}}}{\hat{k}_{y_{app_b}}}\right)\frac{\hat{k}_{xy_b}}{\hat{k}_{xx_b}}}{\left(\frac{\Delta y_2}{L_y} + \frac{\Delta y_1}{L_y}\frac{\hat{k}_{y_{app_t}}}{\hat{k}_{y_{app_b}}}\right)} \tag{F212}$$

where

$$w1tb = \frac{\Delta y_2 \hat{k}_{yx_t}\hat{k}_{yy_b}}{\Delta y_2 \hat{k}_{yx_t}\hat{k}_{yy_b} + \Delta y_1 \hat{k}_{yx_b}\hat{k}_{yy_t}} \tag{F213}$$

$$w2tb = \frac{\Delta y_1 \hat{k}_{yx_b}\hat{k}_{yy_t}}{\Delta y_2 \hat{k}_{yx_t}\hat{k}_{yy_b} + \Delta y_1 \hat{k}_{yx_b}\hat{k}_{yy_t}}. \tag{F214}$$

From the above derivations, it can be observed that two-block effective permeabilities are needed to determine $\frac{\left(\frac{\partial \hat{p}}{\partial y}\right)_{fs}}{\left(\frac{\partial \hat{p}}{\partial x}\right)_{fs}}$ and $\frac{\left(\frac{\partial \hat{p}}{\partial x}\right)_{tb}}{\left(\frac{\partial \hat{p}}{\partial y}\right)_{tb}}$. Next, it will be shown how the elements of the two-block effective permeability of the first column, $\hat{k}_{xx_f}$, $\hat{k}_{xy_f}$, $\hat{k}_{yx_f}$, and $\hat{k}_{yy_f}$, are calculated.

From the derivations in Appendix C, the following equations can be stated:

$$\hat{k}_{x_{app_f}} = \hat{k}_{xx_f} - \frac{\hat{k}_{xy_f}\hat{k}_{yx_f}}{\hat{k}_{yy_f}} \qquad (F215)$$

$$\hat{k}_{y_{app_f}} = \hat{k}_{yy_f} - \frac{\hat{k}_{xy_f}\hat{k}_{yx_f}}{\hat{k}_{xx_f}} \qquad (F216)$$

$$\hat{k}_{xy_f} = -\hat{k}_{xx_f}\left(\frac{\partial \hat{p}}{\partial x}\right)_f \Big/ \left(\frac{\partial \hat{p}}{\partial y}\right)_f \qquad (F217)$$

$$\hat{k}_{yx_f} = -\hat{k}_{yy_f}\left(\frac{\partial \hat{p}}{\partial y}\right)_f \Big/ \left(\frac{\partial \hat{p}}{\partial x}\right)_f . \qquad (F218)$$

Eqs. (F215)-(F218) constitute four equations and four unknowns: $\hat{k}_{xx_f}$, $\hat{k}_{xy_f}$, $\hat{k}_{yx_f}$, and $\hat{k}_{yy_f}$ which can be obtained by solving these four equations simultaneously.

The final expressions for $\hat{k}_{xx_f}$ and $\hat{k}_{yy_f}$ are:

$$\hat{k}_{xx_f} = \frac{\hat{k}_{x_{app_f}}}{\left(1 - \left[\left(\frac{\partial \hat{p}}{\partial x}\right)_f \Big/ \left(\frac{\partial \hat{p}}{\partial y}\right)_f\right]\left[\left(\frac{\partial \hat{p}}{\partial y}\right)_f \Big/ \left(\frac{\partial \hat{p}}{\partial x}\right)_f\right]\right)} \qquad (F219)$$

$$\hat{k}_{yy_f} = \frac{\hat{k}_{y_{app_f}}}{\left(1 - \left[\left(\frac{\partial \hat{p}}{\partial x}\right)_f \Big/ \left(\frac{\partial \hat{p}}{\partial y}\right)_f\right]\left[\left(\frac{\partial \hat{p}}{\partial y}\right)_f \Big/ \left(\frac{\partial \hat{p}}{\partial x}\right)_f\right]\right)} . \qquad (F220)$$

Eq. (F219) is substituted into Eq. (F217) to solve for $\hat{k}_{xy_f}$, and Eq. (F220) is substituted into Eq. (F218) to solve for $\hat{k}_{yx_f}$.

The other three two-block effective permeability tensors are obtained in a similar manner.

The derivations shown in this appendix are essentially a variety of combinations of effective pressure gradient ratios for blocks in parallel and blocks in series.

It should be mentioned that special care should be taken in cases of series combination of pressure gradient ratios. If the signs of the off-diagonal permeability tensor elements are opposite for blocks in a series combination, a discontinuity exists. Physically, this means that there is a major difference in the direction of the principal axes of permeability from one block to another. For such cases, numerical experiments have shown that a weighted arithmetic average of the individual pressure gradient ratios may be used.